RAJ RAGHAVENDRA RAO
Power frequency electromagnetic field effects on APP695 transcription levels in differentiating human neuroblastoma cells.
(Under Direction of WILLIAM SSEMPA KISAALITA)

Epidemiological studies indicating a role for extremely low frequency electromagnetic fields (ELF-EMF) in the etiology of Alzheimer's disease (AD) provided an impetus for biological investigation. An in vitro approach was undertaken utilizing a human neuroblastoma (IMR-32), a model cell line in AD research. IMR-32 cells differentiated with 5-Bromo deoxy uridine were characterized with respect to morphological, biochemical (neuron specific enolase) and electrophysiological (resting membrane potential [V_m] development) differentiation markers. Biochemical and morphological differentiation markers were used to identify distinct differentiation ages for application as an experimental variable in future studies.

In order for an exposure system to constitute a uniform criterion across different experimental approaches, a controlled system for studying cellular responses to ELF-EMF exposure was designed and evaluated. The parameters considered for evaluation involved linear magnetic field distribution, compensation for microscope objective lens interference, heating effects of the coils, and harmonic contents of the signals. The system was found to be feasible for measuring real time biological changes (e.g., V_m) as well as for gene transcription studies, which involve longer exposure times traditionally conducted in cell culture incubators. An application of the system to study the effect of ELF-EMF on V_m in differentiating IMR-32 cells revealed a depolarization effect, attributed to a possible increase in Na^+-K^+-ATPase activity.

Northern analysis was used to evaluate the APP695 transcription levels in IMR-32 cells in response to power frequency (60 Hz) electromagnetic field exposure. Double-blind experiments were conducted in which IMR-32 cells were exposed to magnetic field intensities of 50, 100 or 200 μT (microtesla) for a period of four hours at the three ages of differentiation (2, 10, 16 days after incubation in differentiation medium). The results indicated that neither differentiation age nor magnetic field intensity had any effect on APP695 gene transcription in IMR-32 cells. These studies constitute a first step towards investigating the plausibility of an association between ELF-EMF exposure and AD manifestations at the cellular level.

INDEX WORDS: Alzheimer's disease, Differentiation, Neuron specific enolase, Confocal microscopy, Circular coil, Resting membrane potential.

POWER FREQUENCY ELECTROMAGNETIC FIELD EFFECTS ON APP695 TRANSCRIPTION LEVELS IN DIFFERENTIATING HUMAN NEUROBLASTOMA CELLS

by

RAJ RAGHAVENDRA RAO

BE, Birla Institute of Technology and Science, India, 1993

MSc, Birla Institute of Technology and Science, India, 1993

MS, University of Texas at San Antonio, 1996

A Dissertation Submitted to the Graduate Faculty

of The University of Georgia in Partial Fulfillment

of the

Requirements for the Degree

DOCTOR OF PHILOSOPHY

ATHENS, GEORGIA

2001

POWER FREQUENCY ELECTROMAGNETIC FIELD EFFECTS ON APP695 TRANSCRIPTION LEVELS IN DIFFERENTIATING HUMAN NEUROBLASTOMA CELLS

by

RAJ RAGHAVENDRA RAO

Approved:

Major Professor: Dr. William S. Kisaalita

Committee: Dr. Mark Eiteman
Dr. Jaroslava Halper
Dr. Charles Keith
Dr. Edward Law
Dr. Chi Thai

Electronic Version Approved:

Gordhan L. Patel
Dean of the Graduate School
The University of Georgia
August 2001

To my family for their love and support

ACKNOWLEDGEMENTS

*What a man knows is something, but what he does not know is immense…*Anonymous

I have always considered myself to be an intellectual vagrant, with an interest in wanting to know the trivial aspects of everything that life poses questions about. However, I have become more focussed about my research interests thanks largely due to the efforts of my major professor, Dr. William S. Kisaalita. He deserves immense thanks for taking me under his tutelage and providing excellent guidance and direction during the entire course of my Ph.D. He has always kept an open door and listened to all I had to tell him. I thank him for being a great friend. His calm nature and his advice, both on a personal and professional level have helped me weather many a tough situation.

I thank my committee members for their advice and critical reading of my dissertation. I sincerely thank Dr. Brahm Verma for his constant encouragement during the course of my stay here. I would also like to thank my fellow neurotics in the Cellular Bioengineering Laboratory for having made my stay an enjoyable experience. I especially thank Melissa Bishop and Dianne Stroman for their technical assistance.

I would also like to thank members of the Center for Molecular Bioengineering, especially Dr. Sundararaju, Dr. Sridhar and John March for their help and advice. Steve McDonald deserves sincere thanks for rendering help with the machine work on the exposure system. I also thank Steve Hilliard of the Cell Analysis Facility for technical assistance with the flow cytometer. Thanks are also due to Hongje Pan and David Isaacs in the Soft Tissue Center for their assistance in gene transcription experiments. I also extend my sincere thanks to Suparna Sarkar, Sripriya Rajaraman and Rajat Sapra for their help and advice. I would also like to thank all my friends and colleagues in the department for providing me help whenever necessary.

Love and thanks are due to my dear wife, Shilpa Iyer for her constant support and encouragement. My love and thanks to my family in India and Milwaukee for having always provided me their kind support and advice.

TABLE OF CONTENTS

Page

CHAPTER 1

INTRODUCTION

A large number of people living in today's highly industrialized world tend to question the subtle effects of routine exposures from their environmental surroundings. An example of such an exposure found in homes, offices and communities is electromagnetic fields. There is enormous interest among health professionals, government administrators and regulators, scientists and engineers, and the general public in the capability of electromagnetic field exposure to cause cancer (e.g., Galloni and Marino, 2000; Leman et al., 2001), reproductive abnormalities (e.g., Shaw, 2001; Cecconi et al., 2000) or neurological disorders (e.g., Johansen, 2000; Macias et al., 2000). It can be proudly said that modern science has been witness to enormous developments in identifying possible causes of diseases and developing combative therapies. However, scientists and engineers are widely divided as to the involvement of extremely low frequency (ELF) electromagnetic field (EMF) exposure in various disease processes. The principal reason is that although there is considerable research in the area, the resultant data are discordant for a variety of reasons (Jahn, 2000; Preece et al., 2000).

EPIDEMIOLOGICAL STUDIES

Ever since the epidemiological report (Wertheimer and Leeper, 1979) linking childhood leukemia and ELF-EMF exposure was published, many studies have followed up by focussing on the possible toxicological effects of power frequency (60 Hz) EMF's. Recent epidemiological studies have recently suggested a possible etiologic role for ELF-EMF exposure in the Alzheimer's disease (AD) process (Sobel et al., 1995; Schulte et al., 1996). Follow-up studies confirming or refuting the association between AD and ELF-EMF exposure are needed. AD is of extreme significance in the US since it impacts

millions of lives and more so as the proportion of elderly continues to increase (Sisodia, 1999).

EXPERIMENTAL APPROACHES

An important consideration in the development of an experimental approach is the appropriateness of the model/system to the factors involved in the disease process. Experimental approaches usually adopted beyond epidemiological analyses principally involve development of in vivo or in vitro systems for the study of specific and independent objectives related to factors that constitute the disease process. Biological investigation utilizing in vivo models have generally been guided by methods and end-points developed to assess the effects of drugs, chemicals, and ionizing radiation on the immune system, circulatory system, reproductive system, skeletal system and the nervous system (Portier and Wolfe, 1998). In vivo models focussing on effects on the nervous system have been used to study neurobehavioral (e.g. Orr et al., 1995; Kavaliers et al., 1996), neuropharmacological (e.g., Zecca et al., 1998), neurophysiological (NRC et al., 1997), and neurochemical (e.g., Margonato et al., 1995) effects of electromagnetic fields. Controlled laboratory studies have also been conducted with humans as experimental subjects in order to define dose metrics and response categories for epidemiological studies (e.g., Cohen et al., 1992; Doynov et al., 1998).

There is a general conception that a very large number of cellular components, cellular processes, and cellular systems can be affected by exposure to ELF-EMF. Most of the in vitro studies conducted have examined ELF-EMF effects on the cell membrane (e.g., Blackman et al., 1998; Griffin et al., 2000,), gene transcription (Lacy-Hulbert et al., 1998) and signal transduction (e.g., Shahidain et al., 2001). Studies specifically addressing the genotoxic effect of exposure to magnetic fields have also been pursued (McCann et al., 1998). While some studies were conducted with samples from animals exposed to EMF in vivo, most results have come from studies of cultured cells exposed in

vitro. One of the principal advantages of in vitro exposure is its precision, since the geometry and physical properties of the system can be well controlled.

EXPERIMENTAL STRATEGY

The in vitro approach adopted in this study was to utilize a human neuroblastoma (IMR-32), a model cell line in AD research, to study cellular effects due to ELF-EMF exposure. Specifically, we focussed on the amyloid precursor protein (APP), a key component in AD pathogenesis. The working hypothesis was that ELF-EMF exposure should alter the transcription of the amyloid precursor protein.

Our research is thus a preliminary attempt to generate evidence at the cellular level in support of previous epidemiological findings linking AD to ELF-EMF exposure in a dose-dependent manner. To test the hypothesis, work was divided into three components: two enabling and one hypothesis testing groups of experiments.

The first group of experiments involved the characterization of the in vitro differentiation of IMR-32 with respect to morphological, electrophysiological and biochemical markers. The second group of experiments involved the design and evaluation of a controlled ELF-EMF exposure system for studying real time responses. The system was evaluated with respect to parameters considered in ELF magnetic field exposure in vitro studies. These included linear magnetic field distribution, compensation for microscope objective lens interference, heating effects of the coils, and harmonic contents of the signals. In a third group of experiments, double-blind studies were conducted to elucidate the effects of varying magnetic field intensities on APP695 gene transcription levels. APP695 is an isoform of APP that is predominantly expressed in neurons.

SUMMARY OF RESULTS AND IMPACT

From the first group of experiments, three distinct differentiation ages were identified and were considered a key variable in the third group of experiments. Neither

the differentiation age nor the ELF-EMF intensity was found to have any effect on APP695 gene transcription levels in IMR-32 cells. Absence of ELF-EMF effect on APP695 gene transcription levels provides incentives to explore ELF-EMF effects on other factors implicated in AD pathogenesis. For example, it would be useful to consider the effects of ELF-EMF exposure on the activities of β- and γ-secretases and hence changes in amyloid-β (Aβ) protein production. These secretases are involved in the processing of APP in vivo and Aβ is one of the products of the secretase-catalyzed reactions. Knowledge of cellular responses due to ELF-EMF exposure will aid in the development of mechanistic studies aimed at products or processes to mitigate against undesirable exposure or to provide therapeutic/pharmacological value.

RELATION TO ONGOING WORK IN THE LABORATORY

The current thrust of work in the Cellular Bioengineering Laboratory is the development of cell-based systems for screening of new compounds with respect to toxicological or pharmacological activities (Hernandez and Kisaalita, 1996; Kisaalita and Bowen, 1996). The current focus is on neurodegenerative diseases, with a special emphasis on Alzheimer's disease. One of the minor motivations for testing the hypothesis in this study was the possibility of providing the basis for developing a cell-based system for screening for drugs against Alzheimer's disease.

REFERENCES

1. Blackman CF, Blanchard JP, Benane SG, House DE, Elder JA. (1998). Double blind test of magnetic field effects on neurite outgrowth. Bioelectromagnetics. 19 (4): 204-209.
2. Cecconi S, Gualtieri G, Di Bartolomeo A, Troiani G, Cifone MG, Canipari R. 2000. Evaluation of the effects of extremely low frequency electromagnetic fields on mammalian follicle development. Hum Reprod. 15(11): 2319-2325.

3. Cohen HD, Graham C, Cook MR, Phelps JW. (1992). ELF exposure facility for human testing. Bioelectromagnetics, 13, 169-182.
4. Doynov P, Cohen HD, Cook MR, Graham C. (1999). Test facility for human exposure to AC and DC magnetic fields. Bioelectromagnetics. 20(2): 101-111.
5. Galloni P, Marino C. (2000). Effects of 50 Hz magnetic field exposure on tumor experimental models. Bioelectromagnetics. 21(8): 608-614.
6. Griffin GD, Khalaf W, Hayden KE, Miller EJ, Dowray VR, Creekmore AL, Carruthers CW, Williams MW, Gailey PC. 2000. Power frequency magnetic field exposure and gap junctional communication in Clone 9 cells. Bioelectrochemistry 51(2): 117-123.
7. Hernandez, M., Kisaalita, W.S. (1996). Comparative evaluation of the susceptibility of neuronal (N1E-115) and non-neuronal (HeLa) cells to acetylsalicylic acid (ASA) cytotoxicity by confocal microscopy. Toxicology In Vitro. 10:447-453.
8. Jahn O. (2000). Electromagnetic fields: low dose exposure, current update. Int Arch Occup Environ Health. 73. Suppl: S1-3.
9. Johansen C. 2000. Exposure to electromagnetic fields and risk of central nervous system disease in utility workers. Epidemiology. 11(5): 539-543.
10. Kavaliers M, Ossenkopp K-P, Prato FS, Innes DGL, Galea LAM, Kinsella DM, Perrot-Sinal TS. (1996). Spatial learning in deer mice: sex differences and the effects of endogenous opioids and 60 Hz magnetic fields. Journal of Comparative Physiology 179: 715-724.
11. Kisaalita, W.S., Bowen, J.M. (1996). Effect of culture age on the susceptibility of differentiating neuroblastoma cells to retinoid cytotoxicity. Biotechnology & Bioengineering. 50:580-586.
12. Lacy-Hulbert A, Metcalfe JC, Hesketh R. (1998). Biological responses to electromagnetic fields. FASEB J, 12: 395-420.

13. Leman ES, Sisken BF, Zimmer S, Anderson KW. (2001). Studies of the interactions between melatonin and 2 Hz, 0.3 mT PEMF on the proliferation and invasion of human breast cancer cells. Bioelectromagnetics 22(3): 178-184.
14. Macias MY, Battocletti JH, Sutton CH, Pintar FA, Maiman DJ. 2000. Directed and enhanced neurite growth with pulsed magnetic field stimulation. Bioelectromagnetics. 21(4): 272-286.
15. Margonato V, Nicolini P, Conti R, Zecca, L, Veicsteinas A, Cerretelli P. (1995). Biologic effects of prolonged exposure to ELF electromagnetic fields in rats: II. 50 Hz magnetic fields. Bioelectromagnetics, 16, 343-355.
16. McCann J, Dietrich F, Rafferty C. (1998). The genotoxic potential of electric and magnetic fields - an update. Mutation Research. 411(1): 45-86.
17. NRC, Stevens CFCC, Savitz DAVC, Anderson LE, Driscoll DA, Gage FH, Garwin RL, Jelinski LW, Kelman BJ, Luben RA, Reiter RJ, Slovic P, Stolwijk JAJ, Stuchly MA, Wartenberg D, Waugh JS, Williams JR. (1997). Possible Health Effects of Exposure to Residential Electric and Magnetic Fields. National Academy Press: Washington DC.
18. Orr JL, Rogers WR, Smith HD. (1995). Exposure of baboons to combined 60 Hz electric and magnetic fields does not produce work stoppage or affect operant performance on a match-to-sample task. Bioelectromagnetics, 3, 61-70.
19. Portier CJ, Wolfe MS. (1998). Assessment of Health Effects from Exposure to Power-Line Frequency Electric and Magnetic Fields-Working Group Report. NIH Publication No. 98-3981.
20. Preece AW, Hand JW, Clarke RN. (2000). Power frequency electromagnetic fields and health. Where's the evidence? Phys Med Biol. 45(9): R139-154.
21. Schulte, P.A., Burnett, C.A., Boeniger, M.F., Johnson, J. (1996). Neurodegenerative diseases: Occupational Occurrence and Potential Risk Factors, 1982 through 1991. American Journal of Public Health. 86(9): 1281-1288.

22. Shahidain R, Mullins RD, Sisken JE. (2001). Calcium spiking activity and baseline calcium levels in ROS 17/2.8 cells exposed to extremely low frequency electromagnetic fields (ELF EMF). Int J Radiat Biol. 77(2): 241-248.
23. Shaw G. (2001). Adverse human reproductive outcomes and electromagnetic fields: A brief summary of the epidemiologic literature. Bioelectromagnetics 5: S5-S18.
24. Sisodia, S.S. (1999). Alzheimer's disease: perspectives for the new millennium. The J. Clinical Investigation 104, 1169-1170.
25. Sobel,E., Davanipour, Z., Sulkava, R., Erkinjuntti, T., Wikstrom, J., Henderson, H.W., Buckwalter, G., Bowman, J.D., Lee, P-J. (1995). Occupations with exposure to electromagnetic fields : A possible risk factor for Alzheimer's disease. American Journal of Epidemiology. 142(5): 515-524.
26. Zecca L, Mantegazza C, Margonato V, Cerretelli R, Caniatti M, Piva R, Dondi D, Hagino N. (1998). Biological effects of prolonged exposure to elf- electromagnetic fields in rats: III. 50 Hz electromagnetic fields. Bioelectromagnetics, 19, 57-66.

CHAPTER 2

LITERATURE REVIEW

ALZHEIMER'S DISEASE - FACTORS AND COMPONENTS

Alzheimer's disease (AD), the most common form of dementia occurring in mid-to-late life, is at the forefront of research as it is the fourth largest killer in the United States. It now affects more than 4 million individuals in the US and is increasing because of significant changes in life expectancy and demographic parameters (Sisodia, 1999). The etiology of the brain lesions associated with AD appears to be multifactorial (Tol, 1999). Factors that are possible components in the etiologic process are either genetic (Lippa, 1999; Munoz, 2000), environmental (Prince, 1998; Gauthier, 2000; De La Monte, 2000) or related to aging (Joseph et al., 2001).

The principal component of amyloid fibrils, a pathological hallmark of AD, is an amyloid protein (Masters, et al., 1985) which can be generated by the aberrant processing of a large membrane-bound glycoprotein, the amyloid-beta (Aβ) precursor protein (APP) (Selkoe, 1998). The transmembrane protein APP, expresses three major isoforms. The larger two isoforms consisting of 751 and 770 amino acid residues (APP751 and APP770, respectively) contain a Kunitz protease inhibitor (KPI) domain (Tanzi et al., 1988) and are ubiquitously expressed. The APP695 isoform, not containing the KPI domain, is predominantly expressed in neurons and is the most likely the source of most of the Aβ deposited in the central nervous system in patients with Alzheimer's disease. It has also been suggested that amyloid beta (Aβ) found in cerebral blood vessels, skin tissue, and elsewhere might come from a peripheral source and contribute to the AD pathogenesis (Selkoe, 2000).

Cleavage of the APPs in the membrane by β- and γ-secretase enzymes leads to the production of the Aβ protein (Sisodia, 2000). Although β-secretase has been identified, cloned and characterized (Vassar et al., 1999), the identity of γ-secretase is under intense scrutiny. This has been due to recent findings indicating that a new protein, nicastrin (Yu et al., 2000) associates with presenilins (Czech et al., 2000) and affects the γ-secretase processing of APP. Presenilins are thought to interact physically with APP and play a key role in the production of the Aβ protein.

EPIDEMIOLOGICAL STUDIES RELATING ELF-EMF AND AD

ELF-EMF exposure as a risk factor for AD or other dementias has been the subject of different epidemiological studies, summarized in Table 2.1. Results from three independent clinical studies have indicated an association between working in occupations with probable medium to high exposure to ELF (<300 Hz) electromagnetic fields and sporadic Alzheimer's disease (Sobel et al., 1995). Another study on occupational occurrence and potential risk factors has also indicated a link between electrical workers and AD (Schulte et al., 1996). Taken together, these studies have suggested the involvement of ELF-EMF as one of the environmental factors in the etiology or pathogenesis of AD. However, it is important to note that some of these studies had limitations. These included analyses in terms of diagnoses from death certificates (Savitz et al., 1998a; Savitz et al., 1998b) and different groups of cases and controls being used with some control groups including persons with other types of dementia (Sobel & Davanipour, 1996). There is thus a need for additional biological evidence to test the existence/absence of the relationship between ELF-EMF exposure and Alzheimer's disease.

Table 2.1. Alzheimer's disease and dementia in association with exposure to ELF-EMF (From NIH Publication #98-3981, 1998)

Reference; type of study; country	Study population	Comments
(Sobel et al.,1995); case-control; Finland and California (USA)	Two case series with sporadic AD, i.e. no cases in family (n=53 and 136), and one series with both sporadic and familial forms of AD (n=198). Controls had vascular dementia for one sporadic disease series (n=70) or were normal neighborhood subjects for the other (n=299); the series with both forms of AD had hospital controls with no neurological symptoms (n=106).	OR adjusted for age at onset, education, and social class. Exposures estimated by industrial hygienist for the reported primary occupation. First series had 90% agreement between clinical and autopsy diagnosis, and the second series had 98% agreement. The third series involved an older diagnosis scheme and had 82% agreement.
(Sobel et al., 1996); Case-control; California (USA)	326 clinic-based AD patients. 152 controls were cognitively impaired patients at the same clinic (excluding vascular dementia).	OR adjusted for age of onset, education, and gender. Exposure estimated by expert judgment from occupational history.
(Feychting et al., 1998); Case-control; Sweden	77 dementia cases (including 55 with AD) identified in Swedish twin study. Controls use twins without dementia. 2 control groups (228 and 238 subjects) formed to keep only one member of a twin pair in each group	OR adjusted for age of onset, education. and birth date. Exposure based on JEM constructed from occupational magnetic field measurements made 1988-92. Results for control group 2 are similar, e.g. dementia OR = 3.8 (1.4-10.2) for last job's TWA > 0.2 T.
(Johansen & Olsen, 1998); Cohort study; Denmark	Cohort of male employees of 99 Danish utility companies, 21236 total, 3540 deaths	SMR adjusted for age, education, and birth date. Magnetic fields in subject's first job from a JEM based on expert judgment and 24-h measurements.
(Savitz et al., 1998a); Cohort; USA	138905 men employed in 5 electric utilities followed for mortality 1950-86. 20068 deaths; 24 deaths for which AD was mentioned as an underlying cause of death and 56 for which it was mentioned as cause of death.	SMR adjusted for age, decade of death, race, class, retirement status, and solvent exposure. Magnetic field exposure based on company job records and JEM from full-shift measurements (Savitz et al. 1995).
(Savitz et al., 1998b); Cohort; USA	National Center for Health Statistics database of 25 states; 1931379 male deaths; 256 AD deaths. Schulte et al. (1996) analyzed AD risks by occupation with the same database.	MOR adjusted for age, year of death, social class, and race. Exposure is work in an electrical occupation as reported on death certificate.

RR, relative risk; OR, odds ratio; TWA, time-weighted average; JEM, job-exposure matrix; SMR, standardized mortality ratio; MOR, mortality odds ratio

ELF-EMF EFFECTS ON OTHER DISEASE PROCESSES

The focus of research in determining biological effects of electromagnetic fields has been to identify cellular responses to ELF-EMF, to develop a dose threshold for such interactions and use such information to formulate and test appropriate interaction mechanisms (Liburdy, 1995). Ever since the report (Wertheimer and Leeper, 1979) linking childhood leukemia and exposure to ELF-EMF was published, many studies followed attempting to study the possible toxicological effects of power frequency (60 Hz) EMF. Work in numerous laboratories has indicated that ELF-EMF may be capable of

causing biologic responses that could be associated with some of the disease processes in a causative manner. Most of the research at the cellular level has been carried out to determine the mechanisms by which ELF-EMF might promote cancer (e.g., Byus et al., 1987, Lyle et al., 1991, Tenforde, 1991, Litovitz et al., 1991, Cain et al., 1993, Liburdy et al., 1993, Loscher and Mevissen, 1995, Chen et al., 2000, Ansari and Hei, 2000). However, recent studies have disputed the link between ELF-EMF exposure and the risk of childhood acute lymphoblastic leukemia (Linet et al., 1997).

Other studies have focussed on factors related to disease resistance and have examined the effects of ELF-EMF on specific components of the immune system (Luster et al., 1993; House et al., 1996; Tremblay et al., 1996; Mevissen et al., 1998). Studies focussing on the effects on the nervous system have examined the perception of animals to the presence of electric and magnetic fields (NRC et al., 1997) and have found that animals tend to perceive electric fields better than magnetic fields at environmentally relevant values. Other studies have also focussed on the ability of power frequency fields to affect learning and memory tasks in animals (Coelho et al., 1995; Orr et al., 1995) and have found subtle or no changes on performance. Studies done on changes in neurotransmitters (Margonato et al., 1995) opiods (Lai & Carino, 1998) and endocrine factors (Burchard et al., 1996) have found that effects noted are extremely small. A number of reviews (Juutilainen & Lang, 1997; Huuskonen et al., 1998) published on the reproductive and developmental toxicity of EMF have shown some alterations in the development of embryos exposed to sinusoidal magnetic fields.

PHYSICAL INTERACTION MECHANISMS

Needless to say, there is a great interest in identifying the mechanism of interaction of ELF-EMF with biological systems. Many models have proposed to explain the effects of ELF-EMF exposure and most of these models have considered the plasma membrane as the principal site of interaction. These early membrane interaction models (Lin-Liu and Adey, 1982; Luben, 1991) proposed that EMFs modify the normal signal

processes in the membrane. The interaction of ELF-EMF with biological membranes could, in principle, lead to alterations in the already existing signaling process. Scientists have proposed a useful working mechanism in that the pericellular fields and currents induced by applied ELF-EMF could initiate electrochemical events within the cell membrane that are crucial components of the signal transduction and amplification process (Tenforde, 1993). These electrochemical events could then produce cytoplasmic second messengers that have the capacity of eliciting changes in the biosynthesis of macromolecules and causing alterations in cellular and eventually tissue function. Few of the many studies (Luben et al., 1982; Byus et al., 1984; Cain et al., 1987) seem to suggest the general mechanism of the sequence of events that lead to the ELF-EMF signal transduction and amplification at the cellular level (Tenforde, 1996).

Another interaction mechanism that has been proposed is an electrochemical model that involves alteration in enzyme activities that involve ELF-EMF induced changes (Blank and Goodman, 1988; Blank and Soo, 1990, 1992; Blank, 1992). These experiments were conducted with the integral membrane enzyme, Na^+/K^+/ATPase and the displacement of ions under the influence of ELF fields was observed. It has been suggested that ELF-EMF could interfere with or enhance enzyme activation by affecting the ion concentration that is available to the enzyme (Blank and Soo, 1989, 1992).

In other models, interaction mechanisms not involving the plasma membrane have been proposed. For example, a mechanism of alteration of chemical reaction rates due to ELF-EMF exposure has been proposed (Litovitz et al., 1992; Weaver and Astumian, 1992). It is hypothesized that different intensities and frequencies might differentially affect reaction rates and consequences could be observed subtly over time. Also, in a model based on the observation of specific ferromagnetic sites (magnetite) in insect and human tissue (Kirschvink et al., 1992), a mechanism for the direct interaction with magnetic fields has been proposed. Based on the observation of sharp, resonance features in response to specific combinations of frequency, intensity and duration of exposure, a cyclotron resonance model (Liboff, 1985; Liboff and McCleod, 1988)

incorporating the resonance frequency of free ions in a magnetic field has also been proposed as a possible mechanism.

TRANSDUCTION AND AMPLIFICATION

The understanding of how signals resulting from ELF-EMF/biological interactions are transduced is critical in our understanding of the pathways by which ELF-EMF influence membrane and cellular functions. A living cell tends to interact with its extracellular environment based on intricate biochemical pathways. The binding of a molecule of interest to a specific receptor on the membrane has the capacity of triggering a cascade of events, which in essence forms the signal transduction hypothesis. These events that lead to signal transduction and amplification via the production of second messengers like free Ca^{2+} and protein kinases regulate DNA transcription and protein biosynthesis (Alkon and Rasmussen, 1988; Luben, 1991). A single binding event can thus trigger amplification of signals, which could eventually lead to activation of certain genes and inhibition or activation of crucial proteins that may lead to disease processes.

Numerous studies have examined the effect of ELF-EMF on ion transport across membranes. Membrane potential alterations, which result from changes in mean channel conductances (Kandel et al., 1995) are the basis for all forms of sensory transduction. If one works on the assumption that ELF-EMF are transduced by mechanisms similar to transduction of other sensory stimuli, the ELF-EMF exposure might trigger changes in membrane potential. Studies on the effect of magnetic fields on Na^+ and K^+ transport (Teissie and Tsong, 1981; Serpersu and Tsong, 1983; Ikehara et al., 1998) seem to suggest that the enzyme Na^+/ K^+/ATPase extracts energy from the field and transduces it to transport K^+ or Na^+. These suggestions were based on observations of an enhanced transport against a concentration gradient in the presence of a magnetic field. Studies on chick myoblasts (Grandolfo et al., 1991) showed that field effects induced decreases in the conductivity and permittivity of cells, and this observation was interpreted as evidence for a decrease in transport of various ions. Studies examining the effects of

ELF-EMF on the Na^+/K^+/ATPase ion pump in membranes (Blank, 1992; Blank and Soo, 1992) have provided complex results, with either increases or decreases in enzyme activity depending on the level of K^+ and Na^+ ions in the medium. In other studies examining changes in membrane depolarizations, using a fluorescent potentiometric dye (Di-8-ANEPPS) (Patel and Poo, 1982), the investigators concluded that depolarization resulted in a localized activation of a voltage-dependent calcium channel, producing a transient influx of Ca^{2+}. A prevalent theme in most ELF-EMF exposure studies at the cellular level is altered ionized calcium (Ca^{2+}) flux (Blackman et al., 1988; Lyle et al, 1991; Liburdy, 1992; Walleczek and Budinger, 1992; Karabakhtsian et al., 1994; Fitzsimmons et al., 1994; Prasad et al., 1994; Garcia-Sancho et al., 1994; Lindström et al., 1995; Kenny et al., 1997; Mullins and Sisken, 2000; Shahidain et al., 2001).

A new postulate that moves away from the signal transduction hypothesis is the direct interaction of ELF-EMF with DNA based on evidence suggesting that it is possible for ELF-EMF to stimulate stress response by interacting directly with moving electrons in DNA (Blank, 1995; Blank and Soo, 1996, 1998; Blank and Goodman, 1999). Apparently the cell responds to ELF-EMF exposure in a manner analogous to that observed under conditions of cellular stress. For example, increases in transcripts for some heat shock genes in response to ELF-EMF exposure were observed (Goodman et al., 1992; Lin et al., 1997).

Early studies in which different cells were exposed to ELF-EMF pointed towards general changes (Goodman et al., 1983; Goodman and Henderson, 1986a,b, 1987; Phillips and McChesney, 1991) in gene transcription but did not address the more important issue of which specific genes were affected (Phillips, 1993). ELF-EMF effects on specific gene transcription (Phillips et al., 1992) showed an alteration in the transcription levels of histone H3 and p53 mRNA (Cantini et al., 1986), IGF-II (Fitzsimmons et al., 1992), β-actin, histone H2B, *v-myc* (Goodman et al., 1989), *c-fos* (Rao and Henderson, 1996) and *c-myc* (Lin et al., 1996; Morehouse and Owen, 2000). A relationship between increase in *c-myc* transcript levels, ELF-EMF and intracellular

calcium (Liburdy, 1992) has been experimentally observed. Other studies also show that 60 Hz electric fields tend to inhibit protein kinase-C (PKC) activity (Walter et al., 1997).

AD is thought by many to be intimately, if not causatively associated with the deposition of Aβ in the cerebral cortex and hippocampus of affected individuals. Aβ peptides are liberated from APP after cleavage of the APP in the membrane by β- and γ-secretase enzymes. It is reasonable to assume that over-expression of APP and/or secretases should lead to AD manifestations. In absence of any previous studies at the cellular level, it is plausible that ELF-EMF exposure contributes to AD pathogenesis by altering the transcription levels of APP695, the predominant isoform found in neurons.

APPROACHES FOR BIOLOGICAL INVESTIGATION

Scientific information can be obtained from different research disciplines with different experimental approaches, concerning completely different species of organisms, at widely varying levels of resolution, and the information can be put together into a unified body of knowledge. Testing of biological effects principally involve development of in vivo or in vitro systems for the study of specific independent objectives related to factors that constitute the disease process.

Although interactions of ELF-EMF with humans are of prime importance, many areas of biological investigation can be appropriately conducted with animal species. Biological investigation utilizing in vivo models have generally been guided by methods and end-points developed to assess the ELF-EMF effects on specific aspects of the immune system, circulatory system, reproductive system, skeletal system and the nervous system (Portier and Wolfe, 1998). Controlled laboratory studies have also been conducted with humans as experimental subjects in order to define dose metrics and response categories for epidemiological studies (e.g., Cohen et al., 1992; Doynov et al., 1998).

There is a general conception that a very large number of cellular components, cellular processes, and cellular systems can be affected by exposure to ELF-EMF. Most

of the in vitro studies conducted have examined its effect on the cell membrane (e.g., Blackman et al., 1998; Griffin et al., 2000), gene transcription (Lacy-Hulbert et al., 1998) and signal transduction (e.g., Wey, 2000). Studies specifically addressing the genotoxic effect of exposure to magnetic fields have also been pursued (McCann et al., 1998). While some studies were conducted with samples from animals exposed to EMF in vivo, most results have come from studies of cultured cells exposed in vitro. One of the principal advantages of in vitro exposure is its precision, since the geometry and physical properties of the system can be well controlled.

In vitro experiments can thus permit the testing of ELF-EMF exposure under controlled conditions, typically at doses well above those encountered in the environment. Studies of the genotoxic effect of such ELF-EMF exposure and effects on cell proliferation, alteration of signal transduction pathways, and modification of differentiation processes can serve to identify mechanisms with relevance to disease processes and other health end-points. Careful consideration must however be given to the range over which the 'dose' or intensity of ELF-EMF is varied, because unlike many chemical agents, ELF-EMF may have different mechanisms of field-cell coupling over different ranges of field intensities (Portier and Wolfe, 1998).

NEUROBLASTOMA CELLS AS TESTING SYSTEMS

Neuroblastomas are derived from malignant tumors originating from neural crest cells (Ishikawa, 1997). The neural crest is the thickened ectoderm around the edge of the embryonic neural plate. As the neural plate closes to form the neural tube, the neural crest cells are released from their position in the neural fold (Tosney, 1982). Although the neural fold consists of two additional cell types (the internally positioned neural tube cells and the epidermis of the skin), only the cells that migrate are called neural crest cells. The mechanism of release of the neural crest cells from the neural fold is still unknown. The advantages of using neuroblastomas in the development of testing systems include homogenous populations, immortality and versatility.

The rationale for development of neuroblastoma cell lines as testing systems is thus based on the premise that interference of any environmental agent with the integrity of excitable cell membranes usually causes serious impairment of the function of important organ systems and that such effects on the nervous system inevitably lead to alteration in impulse propagation (Kisaalita and Bowen, 1997). Impulse propagation involves the determination of cellular dynamic parameters, which will eventually form the basis of the cell-based testing system. Previous work in our laboratory has evaluated a differentiating murine neuroblastoma cell line (N1E-115) as a neural cell-based system for in vitro toxicology and efficacy testing (Hernandez, et al. 1996; Kisaalita and Bowen, 1997).

The neuroblastoma cell line of choice for this study, IMR-32, was established from an abdominal mass occurring in a 13-month-old Caucasian male (Tumilowicz et al., 1970), and is one of the many cell lines used in studies related to the stability of APP (Lahiri, 1993). Comparison of secreted APP immunoreactive bands from IMR-32 and PC12 (rat phaeochromocytoma cell line) cells suggested differences in APP processing between the cell lines. IMR-32 cells also have the capacity to form intracellular fibrillary material under certain tissue culture conditions (Ko et al., 1990). Neuronally differentiated human IMR-32 neuroblastoma cells can thus be used as a model cell line in some aspects of AD research (Neill et al., 1994). There is however a need to characterize IMR-32 in order to identify unique stages of differentiation. This is necessary because previous research in our laboratory (Kisaalita and Bowen, 1996) has shown that identification of unique differentiation stages helped identify exact time points where the cells could be most susceptible to toxicological agents.

EXPOSURE SYSTEMS FOR IN VITRO STUDIES

An electromagnetic field is composed of two components, the electric and the magnetic fields. The electric field is created by the presence of an electric charge, while the motion of electric charges creates a magnetic field. Exposure systems have been

designed for the study of ELF electromagnetic, uniform electric and magnetic fields over a wide range of frequencies (Bassen et al., 1992; Mullins et al., 1993). Several types of apparatus for generating uniform magnetic fields for in vitro studies have been described (Misakian et al., 1993). The most commonly used systems include circular or rectangular loops of wire of many turns. The critical factors that experimenters have tended to address when subjecting field-exposed and sham-exposed cultures are temperature, atmosphere, lighting levels and cycles and vibration from the field-generating apparatus. Design of experimental systems should focus on two criteria: first the magnetic fields must be well characterized, and second the apparatus should not exert any additional influence on the cells (Goodman et al., 1995).

Culture dishes are usually exposed to magnetic fields generated by placing them in a system of current-carrying coils. The magnetic field is parallel to the coil axis and is uniform near the axis and the center of the coil or coil system. A Helmholtz pair (Kraus, 1984) approximation has been used extensively by many investigators. The magnetic field at the center between the coils, can be calculated from the current in the coils as follows:

$$B = \mu IN/2\pi r$$

where B = magnetic flux density (T); I = current in the coils (A); N = number of loops; μ = permeability of the medium (H/m) and r = radius of the coil (m).

According to Faraday's Law, time varying magnetic fields can induce electric fields in any material and for a reasonably long, cylindrical body of radius r (Polk, 1986), the relationship between electric and magnetic fields can be expressed as follows:

$$E = \pi f B r$$

where E = induced electric field (V); B = magnetic flux density (T), f = frequency (Hz). Typically, the average electric field near the rim of a petri dish, with a radius of 3 cm, induced by a vertical 60 Hz, 100-μT magnetic field will be about 0.56×10^{-3} V/m, much lower than the 100 V/m external electric field in air (Polk, 1992).

In gene transcription studies, ELF-EMF have been generated by Helmholtz coils (Goodman et al., 1989; Lin et al., 1996), solenoids (Harrison et al., 1997) and a double-wound square 4-coil configuration (Saffer and Thurston, 1995). In other systems, square or rectangular coils (Kirschvink, 1992), sheets of currents in place of a coil (Gundersen et al., 1986; Miller et al., 1989), steel-cored electromagnet (Mullins et al., 1993) have been used.

Other considerations in the design of exposure systems involve the reduction of stray magnetic fields, especially when conducting experiments with sham-exposed cultures. Also of critical importance is to have identical configurations of coils for field-exposed and sham-exposed conditions. Use of controlled ELF-EMF exposure parameters with an identical exposure device will make it possible to study the relationship between ELF-EMF, membrane alterations and changes in gene transcription levels. This will aid in establishing dose-response relationships and appropriate physical interaction mechanisms.

OBJECTIVES

The overall aim of this research was to address the effects of extremely low frequency electromagnetic fields on the amyloid precursor protein in differentiating human neuroblastoma (IMR-32) cells. Our working hypothesis was that ELF-EMF exposure should alter the transcription of the amyloid precursor protein. To test this hypothesis we proposed:

Objective 1: To characterize human neuroblastoma (IMR-32) cells with respect to in vitro differentiation markers.

Objective 2: To design and evaluate a system for studying short real time and longer ELF-EMF exposure effects.

Objective 3: To determine the effects of ELF-EMF exposure on APP695 gene transcription levels in differentiating IMR-32 cells.

If successful, this study is expected to establish a new focus of cellular level investigation within the bioelectromagnetics field, which could lead to a better understanding of ELF-EMF interaction mechanisms and/or establishment of occupational exposure guidelines. Furthermore, positive results are expected to provide a basis for the development of a cell-based system for screening of drugs against AD-related pharmacological activities.

REFERENCES

1. Alkon, D.L. Rasmussen, H. (1988). A spatial-temporal model of cell activation. Science. 239: 998-1005.
2. Bassen H., Litovitz T., Penafiel M., Meister R. (1992). ELF in vitro exposure systems for inducing uniform electric and magnetic fields in cell culture media. Bioelectromagnetics, 13, 183-198.
3. Blackman, C.F., Benane, S.G., Elliot, D.J., House, D.E., Pollock, M.M. (1988). Influence of electromagnetic fields on the efflux of calcium ions from brain tissue in vitro: A three-model analysis consistent with the frequency response up to 510 Hz. Bioelectromagnetics 9:215-227.
4. Blank M. (1992). Na, K-ATPase function in alternating electric fields. FASEB J. 6: 2434-2438.
5. Blank M. (1995). Na/K-adenosine triphosphatase. Adv. Chem. 250: 339-348.
6. Blank M., Goodman R. (1988). An electrochemical model for the stimulation of biosynthesis by external electric fields. Bioelectrochem. Bioenerg. 19: 569-580.
7. Blank M., Soo L. (1989). The effects of alternating currents on Na, K-ATPase function. Bioelectrochem. Bioenerg. 22: 313-322.
8. Blank M., Soo L. (1990). Ion activation of the Na, K-ATPase in alternating currents. Bioelectrochem. Bioenerg. 24: 51-61.
9. Blank M., Soo L. (1992). The threshold for alternating current inhibition of the Na, K-ATPase. Bioelectromagnetics. 13: 329-333.
10. Blank M, Soo L. (1996). The threshold for Na, K-ATPase stimulation by electromagnetic fields. Bioelectrochem. Bioenerg. 40: 63-65.

11. Blank M., Soo L. (1998). Enhancement of cytochrome oxidase activity in 60 Hz magnetic fields. Bioelectrochem. Bioenerg. 45: 253-259.
12. Blank M., Goodman R. (1999). Electromagnetic fields may act directly on DNA, J. Cellular Biochem. 75: 369-374.
13. Brighton, C.T., McCluckey, W.P. (1988). Response of cultured bone cells to a capacitively coupled electric field: inhibition of cAMP response to parathyroid hormone. J.Orthopaedic Research 6: 567-571.
14. Brighton, C.T., Okereke, E., Pollack, S.R., Clark, C.C. (1992). In vitro bone-cell response to a capacitively coupled electric field: the role of field strength, pulse pattern and duty cycle. Clinical Orthopaedics and Related Research 285: 255-262.
15. Byus C.V., Lundak R.L., Fletcher R.M., Adey W.R. (1984). Alterations in protein kinase activity following exposure of cultured human lymphocytes to modulated microwave fields. Bioelectromagnetics. 5: 341-351.
16. Byus, C.V., Piper, S.E., Adey W.R. (1987). The effect of low-energy 60 Hz environmental electromagnetic fields upon the growth-related enzyme ornithine decarboxylase. Carcinogenesis. 8:1385-1389.
17. Cain C.D., Adey W.R., Luben R.A. (1987). Evidence that pulsed electromagnetic fields inhibit coupling of adenylate cyclase by parathyroid hormone in bone cells. J. Bone Min. Res. 2: 437-441.
18. Cain, C.D., Thomas, D.L., Adey, W.R. (1993). 60 Hz magnetic fields act as a co-promoter in focus formation of C3H/10T1/2 cells. Carcinogenesis. 14(2): 955-960.
19. Cantini, M., Cossarizza, A., Bersani, F., Cadossi, R., Ceccherelli, G., Tenconi, R., Gatti, C., Franceschi, R. (1986). Enhancing effect of low frequency pulsed electromagnetic fields on lectin induced human lymphocyte proliferation. Journal of Bioelectricity 5:91-104.
20. Czech C, Tremp G, Pradier L. (2000). Presenilins and Alzheimer's disease: biological functions and pathogenic mechanisms. Prog Neurobiol 60(4): 363-384
21. Czerska, E., Al-Barazi, H., Casamento, J., Davis, C., Elson, E., Ning, J., Swicord, M. (1991). Comparison of the effect of ELF fields on c-myc oncogene expression in normal and transformed human cells (abst). 13th Annual Meeting of the Bioelectromagnetics Society.

22. De la Monte SM, Luong T, Neely TR, Robinson D, Wands JR (2000). Mitochondrial DNA damage as a mechanism of cell loss in Alzheimer's disease. Lab Invest. 80(8): 1323-1335
23. Feychting, M., Forssen, U., Rutqvist, L.E. & Ahlbom, A. (1998). Magnetic fields and breast cancer in Swedish adults residing near high-voltage power lines. Epidemiology, 9, 392-397.
24. Fitzsimmons, R.J., Farley, J.R., Adey, W.R., Baylink, D.J. (1989). Frequency dependence of increased cell proliferation, in vitro, in exposures to a low-amplitude, low-frequency electric field: evidence for dependence on increased mitogen activity released into culture medium. J.Cellular Physiology 139: 586-591.
25. Fitzsimmons, R.J., Strong, D.D., Mohan, S., Baylink, D.J. (1992). Low-amplitude, low-frequency electric field-stimulated bone cell proliferation may in part be mediated by increased IGF-II release. J.Cellular Physiology. 150: 84-89.
26. Fitzsimmons, R.J., Ryaby, J.T., Magee, F.P., Baylink, D.J. (1994). Combined magnetic fields increased net calcium flux in bone cells. Calcified Tissue International 55: 376-380.
27. Fitzsimmons, R.J., Ryaby, J.T., Mohan, S., Magee, F.P., Baylink, D.J. (1995). Combined magnetic fields increase insulin-like growth factor II in TE-85 human osteosarcoma bone cell cultures. Endocrinology 136:3100-3106.
28. Garcia-Sancho, J., Montero,M., Alvarez, J., Fonteriz, R.I., Sanchez, A. (1994). Effects of extremely-low-frequency electromagnetic fields on ion transport in several mammalian cells. Bioelectromagnetics. 15:579-588.
29. Gauthier E, Fortier I, Courchesne F, Pepin P, Mortimer J, Gauvreau D. (2000) Aluminum forms in drinking water and risk of Alzheimer's disease Environ Res. 84(3): 234-246.
30. Goodman E.M., Greenebaum B., Marron, M.T. (1995). Effects of Electromagnetic Fields on Molecules and Cells. Intl. Rev. of Cytology. 158: 279-338.
31. Goodman, R., Bassett, C.A.L., Henderson, A.S. (1983). Pulsing electromagnetic fields induce cellular transcription. Science. 220:1283-1285.
32. Goodman, R., Henderson, A.S. (1986a). Some biological effects of electromagnetic fields. Bioelectrochem Bioenerg. 15:39-55.
33. Goodman, R., Henderson, A.S. (1986b). Sine waves enhance cellular transcription. Bioelectromagnetics. 7:23-29.

34. Goodman, R., Henderson, A.S. (1987). Stimulation of RNA synthesis in the salivary gland cells of Sciara coprophilia by an electromagnetic signal used for treatment of skeletal problems in horses. Journal of Bioelectricity. 6:37-47.
35. Goodman, R., Wei, L-X., Xu, J.C., Henderson, A. (1989). Exposure of human cells to low-frequency electromagnetic fields results in quantitative changes in transcripts. Biochim Biophys Acta. 1009:216-220.
36. Goodman, R., Shirley-Henderson, A. (1991). Transcription and translation in cells exposed to extremely low frequency electromagnetic fields. Bioelectrochem. Bioenerg. 25: 335-355.
37. Goodman, R., Weisbrot, D., Uluc, A., Henderson, A.S. (1992). Transcription in Drosophila melanogaster salivary gland cells is altered following exposure to low frequency electromagnetic fields: analysis of chromosome 3R. Bioelectromagnetics 13:111-118.
38. Goodman, R., Chizmadzhev Y., Henderson A.S. (1993). Electromagnetic fields and cells. J. Cell Biochem. 51: 436-441.
39. Grandolfo, M., Santini, M.T., Vecchia P., Bonincontro A., Camett C., Indovina P.L. (1991). Non-linear dependence of the dielectric properties of chick embryo myoblast membranes exposed to sinusoidal 50 Hz magnetic field. Int. J. Radiat. Biol. 60: 877-890.
40. Gundersen, R.M., Greenebaum B., Schaller M. (1986). Intracellular recording during magnetic field application to monitor neurotransmitter release events: Methods and preliminary results. Bioelectromagnetics 7: 271-282.
41. Hardy J (1997). Amyloid, the presenilins and Alzheimer's disease. Trends Neurosci 20:154-159.
42. Harrison, G.H., Balcer-Kubiczek, E.K., Shi, Z-M., Zhang, Y-F., McCready, W.A., Davis, C.C. (1997). Kinetics of gene expression following exposure to 60 Hz, 2mT magnetic fields in three human cell lines. Bioelectrochemistry and Bioenergetics 43:1-6.
43. Hernandez, M., Kisaalita, W.S. (1996). Comparative evaluation of the susceptibility of neuronal (N1E-115) and non-neuronal (HeLa) cells to acetylsalicylic acid (ASA) cytotoxicity by confocal microscopy. Toxicology In Vitro. 10:447-453.
44. Ishikawa S. 1977. Differentiation of human neuroblastoma cells in-vitro – morphological changes induced by dibutyryl cyclic AMP. Acta Path. Jap. 27: 697-711.

45. Johansen, C. & Olsen, J. (1998). Risk of cancer among Danish utility workers-A nationwide cohort study. American Journal of Epidemiology, 147, 548-555.
46. Joseph J, Shukitt-Hale B, Denisova NA, Martin A, Perry G, Smith MA. (2001). Copernicus revisited: amyloid beta in Alzheimer's disease. Neurobiol Aging. 22(1): 131-146.
47. Kandel E.R., Schwartz J.H., Jessell T.M. (eds). (1995). Essentials of neural science and behavior. Appleton and Lange, Norwalk, Connecticut.
48. Karabakhtsian, R., Broude, N., Shalts, N., Kochlatyi, S., Goodman, R., Henderson, A.S. (1994). Calcium is necessary in the cell response to EM fields. FEBS Letters. 349: 1-6.
49. Kenny, J.S., Kisaalita, W.S., Rowland, G., Thai, C., Foutz, T. (1997). Quantitative study of calcium uptake by tumorigenic bone (TE-85) and neuroblastoma x Glioma (NG108-15) cells exposed to extremely-low-frequency (ELF) electric fields. FEBS Letters. 414:343-348.
50. Kirschvink J.L. (1992). Uniform magnetic fields and double-wrapped coil systems: Improved techniques for the design of bioelectromagnetic experiments. Bioelectromagnetics 13: 401-411.
51. Kisaalita, W.S., Bowen, J.M. (1996). Effect of culture age on the susceptibility of differentiating neuroblastoma cells to retinoid cytotoxicity. Biotechnology & Bioengineering. 50:580-586.
52. Kisaalita, W.S., Bowen, J.M. (1997). Development of resting membrane potentials in differentiating murine neuroblastoma cells (N1E-115) evaluated by flow cytometry. Cytotechnology. 24: 201-212.
53. Ko, L-W., Sheu, K-F.R., Young, O., Thaler, H., Blass, J.P. (1990). Expression in cultured human neuroblastoma cells of epitopes associated with affected neurons in Alzheimer's disease. Am J Pathol. 136: 867-879.
54. Krause J.D. (1984). Electromagnetics. 3rd ed. McGraw Hill, New York.
55. Krause, D., Skowronski, W.J., Mullins, J.M., Nardone, R.M., Greene, J.J. (1991). Selective enhancement of gene expression by 60 Hz electromagnetic radiation. In Brighton, C.T., Pollack, S.R. (eds.): "Electromagnetics in Biology and Medicine". San Francisco: San Francisco Press, :133-138.

56. Lacy-Hulbert, A., Wilkins, R.C., Hesketh, T.R., Metcalfe, J.C. (1995). No Effect of 60 Hz Electromagnetic Fields on MYC or β-Actin Expression in Human Leukemic Cells. Radiation Research. 144:9-17.
57. Lahiri, D.K. (1993). The stability of β-amyloid precursor protein in nine different cell types. Biochemistry and Molecular Biology International. 29(5): 849-858.
58. Liboff A.R. (1985). Cyclotron resonance in membrane transport. In Interactions between electromagnetic fields and cells. A. Chiabara, C. Nicolini, H.P. Schwan, eds., Plenum Press, London, 281-296.
59. Liboff A.R. McCleod B.R. (1988). Kinetics of channelized membrane ions in magnetic fields. Bioelectromagnetics. 9: 39-51.
60. Liburdy, R.P. (1992b). Calcium signaling in lymphocytes and ELF fields: Evidence for an electric field metric and a site of interaction involving the calcium ion channel. FEBS Letters 301(1): 53-59.
61. Liburdy R.P. (1992c). ELF fields and the immune system: Signal transduction, calcium metabolism, and mitogenesis in lymphocytes with relevance to carcinogenesis, in Interaction mechanisms of low-level electromagnetic fields in living systems. ed., B. Norden and C.Ramel. : 217-239.
62. Liburdy, R.P., Sloma, T.R., Sokolic, R., Yaswen, P. (1993). ELF magnetic fields, breast cancer, and melatonin: 60 Hz fields block melatonin's oncostatic action on ER+breast cancer cell proliferation. J.Pineal Res. 14:89-97.
63. Liburdy, R.P. (1995). Cellular studies and interaction mechanisms of extremely low frequency fields. Radio Science. 30(1): 179-203.
64. Lin, H., Blank, M., Jin, M., Goodman, R. (1996). Electromagnetic field stimulation of biosynthesis: changes in c-myc transcript levels during continuous and intermittent exposures. Bioelectrochemistry and Bioenergetics. 39:215-220.
65. Lin H., Opler M., Head M., Blank M., Goodman R. Electromagnetic field exposure induces rapid, transitory heat shock factor activation in human cells, J. Cellular Biochem, 66 (1997) 482-488.
66. Linet, M.S., Hatch, E.E., Kleinerman, R.A., Robison, L.L., Kaune, W.T., Friedman, D.R., Severson, R.K., Haines, C.M., Hartstock, C.T., Niwa, S., Wacholder, S., Tarone, R.E.

(1997). Residential exposure to magnetic fields and acute lymphoblastic leukemia in children. The New England Journal of Medicine. 337(1): 1-7.

67. Lindström, E., Lindström, P., Berglund, A., Lundgren, E., Mild, K.H. (1995). Intracellular calcium oscillations in a T-cell line after exposure to extremely-low-frequency magnetic fields with variable frequencies and flux densities. Bioelectromagnetics 16:41-47.
68. Lippa CF. (1999). Familial Alzheimer's disease: genetic influences on the disease process (Review). Int J Mol Med. 4(5): 529-536
69. Litovitz, T.A., Krauss, D., Mullins, J.M. (1991). Effect of coherence time of the applied magnetic field on ornithine decarboxylase activity. Biochem Biophys.Res.Commun. 178: 862-865.
70. Loscher, W., Mevissen, M. (1995). Linear relationship between flux density and tumor co-promoting effect of prolonged magnetic field exposure in a breast cancer model. Cancer Letters 96:175-180.
71. Luben, R.A., Cain, C.D., Chen, M.C., Ronsen, D.M., Adey, W.R. (1982). Effects of electromagnetic stimuli on bone and bone cells in vitro: Inhibition of responses to parathyroid hormone by low-energy low-frequency fields. Proc. Natl. Acad. Sci. USA. 79: 4180-4184.
72. Luben, R.A. (1991). Effects of low-energy electromagnetic fields (pulsed and DC) on membrane signal transduction processes in biological systems. Health Phys. 61: 15-28.
73. Lyle, D.B., Wang, X., Ayotte, R.D., Sheppard, A.R., Adey, W.R. (1991). Calcium uptake by leukemic and normal T-lymphocytes exposed to low frequency magnetic fields. Bioelectromagnetics. 12:145-156.
74. Marron M.T., Greenbaum B., Swanson J.E., Goodman E.M. (1983). Cell surface effect of 60 Hz electromagnetic fields. Radiat. Res. 94: 217-220.
75. Marron M.T., Goodman E.M., Sharpe P.T., Greenbaum B. (1988). Low frequency electric and magnetic fields have different effects on the cell surface. FEBS Lett. 230: 13-16.
76. Masters, C.L., Simms, G., Weinman, N.A., Multhap, G., McDonald, B.L., Beyreuther, K. (1985). Amyloid plaque core protein in Alzheimer disease and Down syndrome. Proc. Natl. Acad. Sci. USA. 82: 4245-4249.

77. Miller D.L., Miller M.C., Kaune W.T. (1989). Addition of magnetic field capability to existing extremely low frequency electric field exposure systems. Bioelectromagnetics 10: 85-89.
78. Misakian M., Shephard A.R., Krause D., Frazier M.E., Miller, D.L. (1993). Biological, Physical and electrical parameters for in vitro studies with ELF magnetic and electric fields: A primer. Bioelectromagnetics Supplement 2: 1-73.
79. Mullins R.D., Sisken J.E., Hejase H.N., Sisken, B. (1993). Design and characterization of a system for exposure of cultured cells to extremely low frequency electric and magnetic fields over a wide range of field strengths. Bioelectromagnetics 14, 173-186.
80. Munoz DG, Feldman H. (2000). Causes of Alzheimer's disease. CMAJ. 162(1): 65-72
81. Nair I., Morgan M., Florig H. (1989). Power frequency electric and magnetic field exposure, effects, research and regulation. U.S. Congressional Office of Technology Assessment, Washington, DC.
82. Neill, D., Hughes, D., Edwardson, J.A., Rima, B.K., Allsop, D. (1994). Human IMR-32 neuroblastoma cells as a model cell line in Alzheimer's disease research. J. Neuroscience 39(4): 482-493.
83. Patel N.B., Poo M. (1982). Orientation of neurite outgrowth by extracellular electric fields. J. Neurosci. 2: 483-496.
84. Phillips, J.L., McChesney, L. (1991). Effect of 72 Hz pulsed magnetic field exposure on macromolecular synthesis in CCRF-CEM cells. Cancer Biochem Biophys 12:1-7.
85. Phillips, J.L., Haggren, W., Thomas, W.J., Ishida-Jones, T., Adey, W.R. (1992). Magnetic field-induced changes in specific gene transcription. Biochim Biophys Acta. 1132:140-144.
86. Phillips, J.L. (1993). Effects of Electromagnetic Field Exposure on Gene Transcription. Journal of Cellular Biochemistry. 51:381-386.
87. Prasad, A.V., Morton, W.M, Cox, C., Carstensen, E.L., Hoops, H., Brayman, A.A. (1994). A test of the influence of cyclotron resonance exposures on diatom mobility. Health Physics. 66(3): 305-312.
88. Prince M. (1998). Is chronic low-level lead exposure in early life an etiologic factor in Alzheimer's disease? Epidemiology. 9(6): 618-621

89. Rao, S., Henderson, A.S. (1996). Regulation of c-fos is Affected by Electromagnetic Fields. Journal of Cellular Biochemistry. 63:358-365.
90. Reese J.A., Jostes R.F., Frazier M.E. (1988). Exposure of mammalian cells to 60-Hz magnetic or electric fields: analysis for DNA single-strand breaks. Bioelectromagnetics 9(3): 237-247.
91. Rosenthal, M., Obe, G. (1989). Effects of 50-Hz electromagnetic fields on proliferation and on chromosomal alterations in human peripheral lymphocytes untreated or pretreated with chemical mutagens. Mutat. Res. 210: 329-335.
92. Saffer, J.D., Thurston, S.J. (1995). Short Exposures to 60 Hz Magnetic Fields do not alter MYC Expression in HL60 or Daudi Cells. Radiation Research. 144:18-25.
93. Savitz, D., Checkoway, H. & Loomis, D. (1998a). Magnetic field exposure and neurodegenerative disease mortality among electric utility workers. Epidemiology. 9:398-404.
94. Savitz, D., Loomis, D. & Chiu-Kit, T. (1998b). Electrical occupations and neurodegenerative disease: analysis of U.S. mortality data. Achives of Environmental Health, 53, 1-5.
95. Schulte, P.A., Burnett, C.A., Boeniger, M.F., Johnson, J. (1996). Neurodegenerative diseases: Occupational Occurrence and Potential Risk Factors, 1982 through 1991. American Journal of Public Health. 86(9): 1281-1288.
96. Selkoe DJ. (1998). The cell biology of beta-amyloid precursor protein and presenilin in Alzheimer's disease. Trends Cell Biol. 8(11): 447-453.
97. Selkoe DJ. (2000). The genetics and molecular pathology of Alzheimer's disease: roles of amyloid and the presenilins. Neurol Clin. 18(4): 903-922.
98. Serpersu, E.H., Tsong T.Y. (1983). Stimulation of a oubain-sensitive Rb^+ uptake in human erythrocytes with an external field. J. Membr. Biol. 74: 191-201.
99. Shoji, M., Golde T.E., Ghiso J., Cheung T.T., Estus S., Shaffer L.M., Cai X-D., McKay D.M., Tintner R., Frangione B., Younkin S.G. (1992). Production of the Alzheimer amyloid beta protein by normal proteolytic processing. Science 258: 126-129.
100. Sisodia, S.S. (1999). Alzheimer’s disease: perspectives for the new millennium. The J. Clinical Investigation 104, 1169-1170.

101. Sisodia, S.S. (2000). An accomplice for γ-secretase brought into focus. Science. 289: 2296-2297.

102. Sobel, E., Davanipour, Z. (1996). Electromagnetic field exposure may cause increased production of amyloid beta and eventually lead to Alzheimer's disease. Neurology 47: 1594-1600.

103. Sobel,E., Davanipour, Z., Sulkava, R., Erkinjuntti, T., Wikstrom, J., Henderson, H.W., Buckwalter, G., Bowman, J.D., Lee, P-J. (1995). Occupations with exposure to electromagnetic fields : A possible risk factor for Alzheimer's disease. American Journal of Epidemiology. 142(5): 515-524.

104. Stegemann S., Altman K.I., Muhlensiepen H., Feinendengen L.E. (1993). Influence of a stationary magnetic field on acetylcholinesterase in murine bone cells. Radiat. Environ. Biophys. 32: 65-72.

105. Tanzi, R.E., McClatchey, A.I., Lamperti, E.D., Villa-Komaroff, L., Gusella, J.F., Neve, R.L. (1988). Protease inhibitor domain encoded by an amyloid protein precursor mRNA associated with Alzheimer's disease. Nature. 331: 528-530.

106. Teissie, J., Tsong T.Y. (1981). Voltage modulation of Na^+/K^+ transport in human erythrocytes. J. Physiol. 77: 1043-1053.

107. Tenforde, T.S. (1991). Biological interactions of extremely-low-frequency electric and magnetic fields. Bioelectrochem. Bioenerg. 25:1-17.

108. Tenforde, T.S. (1993). Cellular and molecular pathways of extremely- low frequency electromagnetic field interactions with living systems. In: Electricity and Magnetism in Biology and Medicine, M. Blank, ed., San Francisco Press, San Francisco, CA. 1-8

109. Tenforde, T.S. (1996). Biological interaction of extremely low frequency electromagnetic fields. In: Biological effects of electric and magnetic fields, S. Ueno, ed, Plenum Press, New York.

110. Tol J, Roks G, Slooter AJ, van Duijn CM. (1999) Genetic and environmental factors in Alzheimer's disease. Rev Neurol (Paris). 155 Suppl 4: S10-16

111. Tosney KW. 1982. The segregation and early migration of cranial neural crest cells in avian embryo. Dev. Biol. 89: 13-24.

112. Tumilocwicz, J.J., Nichols, W.W., Cholon, J.J., Greene, A.E. (1970). Definition of a continuos human cell line derived from neuroblastoma. Cancer Res. 30: 2110-2118.

113. Vassar R, Bennett BD, Babu-Khan S, Kahn S, Mendiaz EA, Denis P, Teplow DB, Ross S, Amarante P, Loeloff R, Luo Y, Fisher S, Fuller J, Edenson S, Lile J, Jarosinski MA, Biere AL, Curran E, Burgess T, Louis JC, Collins F, Treanor J, Rogers G, Citron M. (1999). Beta-secretase cleavage of Alzheimer's amyloid precursor protein by the transmembrane aspartic protease BACE. Science. 286(5440): 735-41.

114. Walleczek, J., Budinger, T.F. (1992). Pulsed magnetic field effects on calcium signaling in lymphocytes: dependence on cell status and field intensity. FEBS Letters 314(3): 351-355.

115. Walter, R.J., Shtil, A.A., Roninson, I.B., Holian, O. (1997). 60-Hz Electric Fields Inhibit PKC Activity and Multidrug Resistance Gene (MDR1) Up-Regulation. Radiation Research. 147:369-375.

116. Yu G, Nishimura M, Arawaka S, Levitan D, Zhang L, Tandon A, Song YQ, Rogaeva E, Chen F, Kawarai T, Supala A, Levesque L, Yu H, Yang DS, Holmes E, Milman P, Liang Y, Zhang DM, Xu DH, Sato C, Rogaev E, Smith M, Janus C, Zhang Y, Aebersold R, Farrer LS, Sorbi S, Bruni A, Fraser P, St George-Hyslop P. (2000). Nicastrin modulates presenilin-mediated notch/glp-1 signal transduction and betaAPP processing. Nature 407:48-54.

CHAPTER 3

DEVELOPMENT OF A DISTINCT PHENOTYPE OF A HUMAN NEUROBLASTOMA (IMR-32) CELL LINE BY CHEMICAL CONTROL OF DIFFERENTIATION[1]

[1]Raj R. Rao and William S. Kisaalita. Submitted to Cytotechnology. 06/2001.

ABSTRACT

A human neuroblastoma cell line (IMR-32), when differentiated, mimics large projections of the human cerebral cortex and under certain tissue culture conditions, forms intracellular fibrillary material, commonly observed in brains of patients affected with Alzheimer's disease. Our interest is in using differentiated IMR-32 cells as an in vitro system for magnetic field exposure and integrative modeling studies. We have previously studied in vitro differentiation of murine neuroblastoma (N1E-115) cells with respect to resting membrane potential development. The purpose of this study was to extend our investigation to IMR-32 cells. Electrophysiological (resting membrane potential, V_m) and biochemical (neuron-specific enolase activity, NSE) measurements were taken every two days for a period of 16 days. A voltage-sensitive oxonol dye together with flow cytometry was used to measure relative changes in V_m. To rule out any effect due to mechanical cell detachment, V_m was indirectly measured with a slow potentiometric dye (Tetramethylrhodamine methyl ester) together with confocal digital imaging microscopy. NSE activity was measured by following the production of phosphoenolpyruvate from 2-phospho-D-glycerate at 240 nm. Our results indicate that in IMR-32, in vitro differentiation as characterized by an increase in NSE activity is not accompanied by resting membrane potential development. This finding suggests that pathways for morphological/biochemical and electrophysiological differentiation in IMR-32 cells exposed to 5-BrdU are independent of one another.

Key words: Neuron-specific enolase, Flow cytometry, Confocal microscopy, Resting membrane potential, Cellular engineering.

INTRODUCTION

The nervous system, due to its great diversity and intricate detail, presents a challenge to the field of neural tissue engineering. However, improvements in our understanding of the molecular control of differentiation will eventually pave the way for harnessing the differentiation potential of immature cells (Shamblott, et al. 1998; Thomson, et al. 1998). "Differentiation" of immature neural cells in vitro is normally associated with the cessation of cell division, extension of processes and increases in the expression of some neural-specific genes. Previous work in our laboratory has evaluated a differentiating murine neuroblastoma cell line (N1E-115) as a neural cell-based system for in vitro toxicology and efficacy testing (Hernandez, et al. 1996; Kisaalita and Bowen, 1996; Kisaalita and Bowen, 1997). In these studies, differentiation was characterized by resting membrane potential (V_m) development. The relative changes in V_m were measured by flow cytometry with the aid of a voltage-sensitive oxonol dye. For most cells of nervous system origin, low V_m characterizes exponentially growing cells and the transition from log to stationary phase is marked by a shift toward large V_m values.

Neuroblastomas are derived from malignant tumors originating from neural crest cells (Ishikawa, 1997). The neural crest is the thickened ectoderm around the edge of the embryonic neural plate. As the neural plate closes to form the neural tube, the neural crest cells are released from their position in the neural fold (Tosney, 1982). Although the neural fold consists of two additional cell types (the internally positioned neural tube cells and the epidermis of the skin), only the cells that migrate are called neural crest cells. The mechanism of release of the neural crest cells from the neural fold is still unknown. IMR-32 cells are a human neuroblastoma cell line (Tumilocwicz, et al. 1970) established from an abdominal mass occurring in a 13-month old Caucasian male. These cells can be made to express a differentiated phenotype using differentiating agents like 5-Bromo-deoxyuridine (BrdU).

Enolase, 2-phospho-D-glycerate hydrolyase (E.C.4.2.1.11), is a component of the glycolytic pathway and catalyzes the conversion of 2-phospho-D-glycerate to form

phosphoenolpyruvate, the only dehydration reaction in glycolysis. Three major tissue-specific isoforms of enolase have been identified in mammals. Gamma or neuron-specific enolase (NSE) is expressed primarily in neurons, beta or muscle-specific enolase is expressed in striated muscles, and alpha or nonneuronal enolase (NNE) is expressed in fetal or other cell types (Day, 1992). During cellular differentiation in vertebrates, expression of enolase is switched from the alpha to the beta form (Fletcher, et al. 1978), while there is a switch from the alpha to the gamma form in brain tissues (Schmechel, et al. 1980). An elevated expression of the alpha form is observed in neuroblastoma cell cultures (Marangos, et al. 1978). Since NSE is the major enolase isozyme in differentiated neurons and NNE is the major enolase form in non-differentiated neurons, elevated NSE serves as a marker for differentiation in neuroblastoma cells.

There is interest in our laboratory to investigate the biological effects of extremely low frequency magnetic fields at the cellular level with applications in Alzheimer's disease (AD) research (Sobel and Davanipour, 1996). The most desirable cell line with which to investigate such effects should mimic some if not all the complex neurochemical processing events associated with AD. In previous AD-related studies at the cellular level, amyloid precursor protein (APP)-transfected cells such as human embryonic kidney (293) (Esch, et al. 1990) and Chinese hamster ovary cells (Wang, et al. 1991) have been used. However, these transfected cell lines are less desirable because they are not of human neuronal origin and process APP abnormally (Fukuchi, et al. 1992). The aberrant processing of APP leads to the production of the amyloid protein (Kang et al. 1987), which is the principal component of amyloid fibrils, a pathological hallmark of AD (Masters, et al. 1985). The most commonly used non-transfected cells are neuronally differentiated PC-12 cells (Anderson, et al. 1991; Walsh, et al. 1994) which are of rat phaeochromocytoma origin. IMR-32 is more suitable because: when differentiated it mimics large projection neurons of the human cerebral cortex, is of human origin, large in size and has previously been used in studies related to the stability of the APP (Lahiri, 1993). Under specific tissue culture conditions (combination of

dibutryl cyclic AMP, nerve growth factor, gangliosides and sodium butyrate) these cells have been shown to form intracellular fibrillary material (Ko et al., 1990), commonly observed in brains of patients affected with AD.

The objective of the present study was to characterize differentiating IMR-32 neuroblastoma cells with respect to electrophysiological (V_m) and biochemical (NSE) differentiation markers as a first step towards our long-term goals. Our long-term goals involve the elucidation of the possible mechanism by which extremely low frequency magnetic field exposure may influence AD manifestations in vitro at the cellular and/or molecular level.

MATERIALS AND METHODS

Cell line and cell culture

Freely dividing IMR-32 cells (ATCC #127-CCL, Rockville, MD, U.S.A) were routinely cultured in 25 cm^2 flasks (Costar, Cambridge, MA) in 10 ml medium in 95% air and 5% CO_2 atmosphere at 37^oC and fed (i.e., refreshed the medium) at two day intervals. The growth medium comprised of Eagle Minimum Essential Medium and 10% heat-inactivated fetal bovine serum (FBS) with 2 mM L-glutamine and Earle's Balanced Salt Solution (BSS) adjusted to contain 1.5 g/L sodium bicarbonate, 0.1 mM non-essential amino acids, and 1.0 mM sodium pyruvate (Neill, et al., 1994). When confluent, the cells were detached by washing with trypsin solution preheated to 37^oC. The suspension was centrifuged (250xg, 10 min) and the cells were replated at 1 x 10^6 cells per 25 cm^2 T-flask. For induction of differentiation, cells were plated 2 days prior to the addition of differentiation medium. The differentiation medium comprised of Eagle Minimum Essential Medium with 2 mM L-glutamine and Earle's BSS adjusted to contain 1.5 g/L sodium bicarbonate, 0.1 mM non-essential amino acids, and 1.0 mM sodium pyruvate, 5% heat-inactivated FBS and 10 μM BrdU. The differentiation medium was refreshed once every two days.

Potentiometric dyes

The anionic oxonol dye, bis-(1,3-dibuytylbarbituric acid) trimethine oxonol (DiBa-C_4[3], Molecular Probes), was chosen for flow cytometry experiments since it is a probe with relatively low cell toxicity (Kohen and Hirschberg, 1989) that can reliably indicate the cell membrane potential without major contributions from the mitochondrial potential (Wilson and Chused, 1985). Cellular loading with DiBa-C_4[3] is a function of V_m. As cell depolarization occurs, dye loading increases, causing an increase in fluorescence intensity (Brashford, et al., 1985). Therefore low intensity reflects high V_m and vice versa. The oxonol used in this study has been reported to exhibit the highest voltage sensitivity of all oxonols (Bräuner, et al., 1984).

Tetramethylrhodamine methyl ester (TMRM; Molecular Probes) was chosen for the confocal digital imaging experiments for the following reasons: (1) it exhibits low non-specific binding and therefore readily displays reversible potential dependent uptake, (2) is not quenched when taken up by mitochondria and therefore cytoplasmic and mitochondrial fluorescence are readily distinguished, and (3) is non-toxic to most cells (Ehrenberg, et al. 1988; Emaus, et al. 1986).

Resting membrane potential determination by flow cytometry

A procedure previously used in our laboratory was followed (Kisaalita and Bowen, 1997). Cells were centrifuged (250xg, 10 min), resuspended at 0.5 x 10^6 cells/ml in a saline solution and incubated with 0.4 μM DiBa-C_4[3] and propidium iodide (20 μg/ml) dyes for 30 min at 37^{o}C. Flow cytometry analysis of the cell suspension was performed on the University of Georgia (UGA) Cell Analysis Facility's Beckman Coulter EPICS Elite Analyzer (Fullerton, CA). Forward-angle light scatter (FALS), side-light scatter (SSC), oxonol and propidium iodide signals/emissions were obtained in response to argon-ion laser excitation (488 nm) at 15 mW. Oxonol and propidium iodide (PI) emissions were measured after passage through a 525 nm band-pass and 610 nm long-pass filter respectively, using log amplification. Linear amplification was used for FALS and SSC signals, and acquisition was triggered on FALS. Unless otherwise stated, 10,000

events were counted at an approximate rate of 200 events per second. FALS was plotted against log PI fluorescence and regions were drawn around PI negative (live) and PI positive (dead) cells. Electronic gating was used to plot the oxonol fluorescence of viable cells.

Resting membrane potential determination by confocal microscopy

A modification of a procedure previously used in our laboratory was followed (Hernandez, et al. 1996). A confocal imaging system (PCM-2000, Nikon), equipped with high performance detection and control electronics was used. The imaging system was linked to an inverted (TE300, Nikon) microscope, equipped with a 60 X Apochromat, oil-immersion, high-numerical aperture (1.40) objective lens. The imaging system's helium/neon mixed gas laser (Green-HeNe) was used to excite the fluorescent dye at 543 nm, and emission scans were recorded through a 565 nm long pass filter as relative fluorescence intensities.

IMR-32 cells from culture flasks were replated in 35-mm glass bottom microwell dishes (Mattek, Ashland, MA), at a density of 3 x 10^5 cells/dish. Cultures were incubated overnight in growth medium, and the next day the growth medium was exchanged with differentiation medium. The incubation was terminated by removal of the medium, followed by washing of the cells with Hepes balanced salt solution (HBSS). The dish was filled with HBSS and 0.5 μM TMRM for V_m measurement. The sample was equilibrated at room temperature for 10 min and placed on the microscope stage. The GreenHeNe laser was focussed onto an appropriate focal plane of a single cell containing the fluorescent probe. The sample fluorescence was recorded and the image was digitized with 640x480 spatial and 8-bit intensity resolution via a frame grabber and stored. Cells were analyzed from two independent glass bottom microwell dishes.

Data analysis was performed with Compix SimplePCI 3.6 image analysis software package. Rectangular regions of interest (ROI) of approximately 2 μm^2 were defined via the image processor's cursor controls. An ROI was defined inside the cell in a region devoid of mitochondria. The same-size ROI was defined outside the cell, in a

region devoid of processes or any glowing debris. Fluorescence intensity histograms were generated for both the intracellular and extracellular ROIs. The ratio of the mean values of the fluorescent intensities measured from inside and outside the cell (Fl_i/Fl_o) is related to V_m by the Nernst equation:

$$V_m = -2.3\left(\frac{RT}{ZF}\right)\log_{10}\left(\frac{Fl_i}{Fl_o}\right)$$

where V_m is the resting membrane potential in mV, Z is the charge on the TMRM ion, F is the Faraday's constant, R is the ideal gas constant, and T is the absolute temperature. Fluorescence contributions from no-dye cell preparations were recorded and were used to correct Fl_i and Fl_o for background. The log of the ratio (Fl_i/Fl_o) was calculated and used as an indirect measure of the V_m.

Determination of neuron specific enolase activity

IMR-32 cells used for these experiments were seeded at a density of 10^8 cells in each T-75 flask. Differentiating cells from a T-75 flask were trypsinized and harvested by centrifugation (250xg, 10 min). The harvested cells were homogenized in 2 ml of 0.05% Triton X-100 in 10 mM Tris-HCl buffer (pH 7.4) containing 1 mM $MgSO_4$, for 4 hours at 37^{o}C. The homogenate was then centrifuged at 25,000xg for 20 min at 4^{o}C. Approximately 10^8 cells were used for each chromatographic experiment.

Enolase isozymes were separated by ion exchange chromatography and a modification of an earlier protocol (Odelstad, et al. 1981) was used. The sample containing protein was desalted on a Sephadex G-25 column and the two enolase fractions containing nonneural enolase (NNE) and neuron-specific enolase (NSE) were then separated by ion exchange chromatography on preswollen Diethylaminoethyl-Sephacel (Pharmacia) in 1.5 x 6 cm columns. The ion exchanger was equilibrated with 10 mM Tris-HCl buffer (pH 7.4) containing 1 mM $MgSO_4$. The sample was applied to the ion exchanger and washed with 10 ml of the column buffer. The column was subsequently washed with 10 ml of 0.2 M KCl and the adsorbed material was eluted by 30 ml of a linear gradient of 0.2-0.4 M KCl. The flow rate was 20 ml/h. All experiments

were conducted at 4°C. Fractions of approximately 1 ml were collected starting with the first column wash, and analyzed for enolase activity immediately after.

Enolase activity was determined by following the change in optical density at 240 nm. The total assay volume was 1 ml containing 50 mM Tris-HCl buffer (pH 7.4), 1.5 mM $MgSO_4$, 50 mM KCl, 1 mM 2-phospho-D-glycerate (sodium salt, Sigma) and 0.5 ml of sample. The reaction was carried out at 25°C. The substrate was added after the protein sample was equilibrated at room temperature. A linear absorbance increase of 0.1 at 240 nm was equivalent to the formation of 0.226 μM of phosphoenolpyruvate (Baranowski and Wolna, 1975). The activity was expressed in enzyme units per ml of sample. The NSE activity was calculated as a percentage of the total recovered enolase activity.

RESULTS AND DISCUSSION

Morphological differentiation

Morphological differentiation of neuronal cells is defined simply as the appearance of one (or more) neuritic processes longer than the somatic diameter (Mummery, et al., 1984). IMR-32 was treated with 10 μM BrdU and cell morphology was examined with a phase-contrast microscope. The dose of the differentiating agent was chosen after dose-response and time-course experiments (data not shown). Microscopic examination showed an alteration in the overall appearance of cultures and morphology of single cells after induction of differentiation. Differentiation caused IMR-32 cells to flatten and to extend long neuritic processes. Neurites were long, branched, strongly substratum-adherent, varicose and frequently interconnected after treatment. Scanning electron microscopy analysis (data not shown) also confirmed the development of a large network of neurites as shown in earlier related studies (Gotti, et al. 1987). In addition, cell bodies showed morphological alterations by becoming smaller and rounded after treatment. As differentiation progressed, the cultures produced less acid in comparison to the control and therefore required less media change, suggesting a marked decrease in cell division rate. This observation was also related to a decrease in cell

number with differentiation. As observed in Fig 3.1a-c, the fraction of cells bearing neurites increased with time. These observations are in agreement with previous results obtained in our laboratory with murine neuroblastoma N1E-115 cells (Kisaalita and Bowen, 1996). Cells also tended to form aggregates, which increased with time (Fig 3.1a-c).

Resting membrane potential development

A plot of FALS versus SSC revealed two cell populations (high- and low- FALS) (data not shown). FALS, one of the flow cytometry parameters, is defined as light of the same wavelength as the illuminating laser beam that is refracted as it passes through the cell so as to diverge from the original path of the laser beam by approximately 0.5^{o}. FALS is therefore a function of refractive index as well as the cross-sectional area. SSC is light of the same wavelength as the illuminating laser beam that bounces off cells in the orthogonal direction to the laser. The intensity of SSC is related to the roughness (sometimes referred to as irregularity or granularity) and internal components of the cell. One of the main advantages of flow cytometric techniques is that on-line plots of FALS and SSC identify cell subtypes based on differences in size, refractive index and surface granularity. As examined earlier in our laboratory (Kisaalita and Bowen, 1997), the relationship between FALS and PI fluorescence was used to separate or 'gate' viable cells (PI-negative) and dead/dying cells (PI-positive). As expected, the majority of PI-positive cells exhibited no oxonol fluorescence and therefore showed up in the lowest channel (10^{0}). The rest of the PI-positive cells that exhibited oxonol fluorescence were considered to be in the process of dying, since both dead and dying cells take up PI. A quantitative comparison of oxonol fluorescence histograms at different stages of differentiation was conducted on the viable PI-negative cells. From earlier studies (Kisaalita and Bowen, 1997), a shift of the histogram to the left is indicative of increase in V_m. Channel number is a flow cytometry term representing a millivolt signal from the PMT that corresponds to the dye fluorescence intensity. The oxonol fluorescence weighted channel number was used as a relative measure of the resting membrane

potential. The oxonol fluorescence weighted channel number (WCN) was calculated as follows:

$$WCN = \frac{\sum Channel \times Frequency}{\sum Frequency}$$

A plot of the oxonol fluorescence weighted channel number against differentiation/differentiating culture age (Fig. 3.2) revealed no change in V_m with culture age or differentiation state. This result is in direct contrast to previous results with N1E-115 cells (Kisaalita and Bowen, 1997), wherein three distinct regions of the differentiation profile (low V_m, rapid V_m rise and steady V_m) were observed. Although the exact V_m values were not determined by this flow cytometric technique, the results obtained are valuable in that the measurements were conducted on a large population of cells, which provides a more accurate indication of the V_m distribution within the culture.

To rule out the possibility that mechanical dislodging of cells had an effect on the observed flow cytometric measurements, changes in V_m for differentiated and undifferentiated cultures were compared using confocal microscopy. As shown in Fig. 3.3, TMRM stained the cell cytosol as well as intracellular organelles. The nuclear region was stained to a lesser extent, reflecting the absence of membranous organelles. Therefore, the measurement of fluorescence intensity inside the cells was made at these relatively darker, uniformly stained regions. Optical sections for image analysis were determined following published procedures (Hernandez, et al. 1996). The log of the ratio of the average fluorescence intensities inside and outside the cell was calculated. A comparison of $\log(Fl_i/Fl_o)$ histograms obtained from TMRM fluorescence for 2 & 16-day-old cultures is shown in Fig. 3.4. The nonparametric Mann-Whitney U test was used to test whether the V_m distributions of the two cultures were identical. The test was based on the null hypothesis H_0: the two histograms are identically distributed versus the alternative hypothesis H_1: the two histograms are not identically distributed. The p-value obtained (p=0.081), indicated that H_0 cannot be rejected at the 5% level, suggesting that there was no difference in resting membrane potential distribution between the 2 and 16-

day-old cultures. This confirmed the results obtained from flow cytometry and eliminated the possibility of interference due to mechanical cell dislodging.

The maintenance of the resting membrane potential of most cells is primarily determined by K^+ ions. The capacity of KCl to induce depolarization in IMR-32 cells has been previously reported by electrophysiological recordings (Gotti, et al. 1987). The V_m at which K^+ ions are in equilibrium (K^+ -Nernst potential) across the cell can be calculated from the Nernst equation. In studies with N1E-115 earlier in our laboratory (Kisaalita and Bowen, 1997), increasing extracellular potassium ($[K^+]_o$) resulted in the anticipated reduction in V_m, illustrated by the oxonol fluorescence's histogram's shift to the right or an increase in the fluorescence. In similar experiments with IMR-32 cells (data not shown), variation in the $[K^+]_o$ did not result in V_m changes, suggesting a poor development of K^+ currents or minimal K^+ permeability in BrdU differentiated IMR-32 cells.

The outward potassium currents, which are critical in the maintenance of the V_m include transient voltage-dependent currents (I_A); a non-inactivating current (I_M); slowly inactivating voltage-dependent currents (I_K), and a number of different calcium-dependent potassium currents. Earlier studies (Ginsborg, et al., 1991) showed that the outward current of the undifferentiated IMR-32 cell was predominantly found to be of the I_K type. Patch-clamp recordings of IMR-32 cells (Gotti, et al. 1987) have shown that certain K^+ currents are inactivated in undifferentiated and BrdU-differentiated cells, but not in dibutryl cyclic AMP-differentiated cells. The inactivation of the transient voltage dependent current (I_A) was observed in undifferentiated cells, while the steady calcium-dependent potassium current was inactivated in BrdU–treated cells. Based on the above studies and the observations reported herein, absence of V_m development in BrdU-differentiated IMR-32 cells has been attributed to the unbalanced development of K^+ currents.

Neuron specific enolase activity shift

The enolase activity shift was determined by fractionation of the cell extracts on DEAE Sephacel column followed by enzymatic activity assay of each chromatographic fraction at different differentiation stages of the cell culture. A typical enolase activity chromatogram (Fig. 3.5) indicates the two fractions typically obtained. As in previous work (Odelstad et al., 1981), the first major fraction corresponded to the NNE while the second minor fraction corresponded to the NSE, whose levels were used as the biochemical marker for differentiation. The enolase activity chromatogram also indicated that IMR-32 is deficient in the hybrid form as shown earlier (Marangos, et al. 1978). If present, the hybrid isozyme would have shown up during the 0.2 M KCl washing of the column. A plot of the %NSE against differentiation/differentiated culture age is shown in Fig. 3.6A while the rate of increase in %NSE after induction of differentiation is shown in Fig. 3.6B. The rate of increase in %NSE was calculated using the formula:

$$(\%\Delta NSE/days) = \left(\frac{\%NSE_n - \%NSE_m}{n-m} \right)$$

where *n* and *m* are the present day and the previous day of differentiation, respectively, under consideration. The relative amount of NSE increased with differentiation culture age and a rapid increase was observed in the rate of change of %NSE around the 10^{th} day of differentiation. The maximal relative NSE level came considerably later, reaching a near steady state after 14 days in culture. These results suggest three regions of the IMR-32 cells differentiation profile, i.e., 0-8, 8-14, and over 14 days, respectively, representing low NSE, rapid NSE rise and steady NSE levels respectively.

IMPLICATIONS FOR SUBSEQUENT STUDIES

Morphological development of cultured neuroblastomas along with their capability of neuritogenesis are commonly accepted indicators of neural differentiation. However, while these may be necessary, they may not be sufficient for all differentiated functions triggered by various agents. A more accurate approach may be to characterize

differentiated neuroblastoma cells with respect to both biochemical and electrophysiological markers. NSE is a unique neuronal biochemical marker in that it appears to be present in many, if not all, types of neurons. Neurotransmitter enzymes, on the other hand, are only present in restricted subsets of any given neuronal population (Marangos, et al. 1978). The identification of 3 phases in BrdU-differentiated IMR-32 cells as evaluated by relative NSE shift aids in the development of experiments aimed at studying the effects of neurotoxic agents at specific differentiation stages. One can expect to observe different responses to external stimuli in each of the 3 phases. It is also expected that the cells are likely to be most vulnerable to external neurotoxic agents in their dynamic state i.e., around the 10^{th} day of differentiation (Kisaalita and Bowen, 1996).

Cellular engineering is developing as an enterprising field and has been facilitated by rapid progress in molecular biology, molecular genetics and bioengineering. Proliferation and differentiation management of mammalian cells is a rapidly developing field and has potential scope to handle current and future challenges of human disease as therapy moves towards cell-based and genetic solutions in the next millennium.

The production of a distinct phenotype (by chemical control) observed in this study is consistent with recent work, where judicious choice of differentiating agents was associated with success in the production of dopaminergic and/or serotonergic phenotypes from embryonic stem cells (Dinsmore, et al. 1998; Hynes and Rosenthal, 1999; Lindvall, 1999). From a practical standpoint, control of in vitro differentiation is expected to be a critical component in the maturing of technologies for cell-based therapeutic and biotechnological applications. The ability to produce two distinct IMR-32 phenotypes (balanced *vs.* unbalanced K^+ channel development) offers a unique starting point for producing an integrative model of differentiation, similar to the one outlined for cardiac excitation (Rudy, 2000).

In conclusion, we have shown the presence of morphological and biochemical but no electrophysiological differentiation-associated changes in BrdU-differentiated IMR-32

cells. These results suggest that morphological changes are necessary but not sufficient for electrophysiological differentiation. It is also possible that electrophysiological and biochemical features of differentiation are independent of each other. The process of differentiation in IMR-32 cells may thus be a multistep phenomenon operating at different parallel levels, which in conjunction produce the complex features of differentiation. A better understanding and control of molecular mechanisms of differentiation is thus important for a complete solution for tissue engineering, cell-based therapies and other biotechnological applications.

ACKNOWLEDGEMENTS

This research was supported partly by a grant from the University of Georgia Research Foundation for the establishment of the Soft Tissue Center. The authors thank Steve Hilliard of the University of Georgia's Cell Analysis Facility for technical support. The authors also thank Suparna Sarkar and John March for critical reading of the manuscript. Mention of brand names is for information only and does not imply endorsement.

REFERENCES

Anderson JP, Esch FS, Keim PS, Sambamurti K, Leiberburg I & Robakis NK (1991) Exact cleavage site of Alzheimer amyloid precursor in neuronal PC12 cells. Neurosci Lett. 128:126-128.

Baranowski T & Wolna E (1975) Enolase from human muscle. Methods Enzymol . 42: 335-338.

Brashford CL, Alder GM, Gray MA, Micklem KJ, Taylor CC, Turek T & Pasternak CA (1985) Oxonol dyes as monitors of membrane potential of animal cells in monolayer culture and in suspension. J. Cell. Physiol. 123: 326-336.

Bräuner T, Hülser TF & Strasser RJ (1984) Comparative measurements of membrane potentials with microelectrodes and voltage-sensitive dyes. Biochim. Biophys. Acta . 771: 208-216.

Day INM (1992) Enolases and PGP 9.5 as tissue specific marker. Biochem Society Trans. 20: 637-642.

Dinsmore J, Ratliff J, Jacoby D, Wunderlich M & Lindberg C (1998) Embryonic stem cells as a model for studying regulation of cellular differentiation. Theriogenology. 49 (1): 145-151.

Ehrenberg B, Montana V, Wei MD, Wuskell JP & Loew LM (1988) Membrane potential can be determined in individual cells from the nernstian distribution of cationic dyes. Biophys J. 53(5): 785-794.

Emaus RK, Grunwald R & Lemasters JJ (1986) Rhodamine 123 as a probe of transmembrane potential in isolated rat-liver mitochondria: spectral and metabolic properties. Biochim Biophys Acta. 850 (3): 436-448.

Esch FS, Keim PS, Beattie EC, Blacher RW, Culwell AR, Oltersdorf T, McClure D & Ward PJ (1990) Cleavage of amyloid beta peptide during constitutive processing of its precursor. Science. 248(4959): 1122-1124.

Fletcher L, Rider CC, Taylor CB, Adamson ED, Luke BM, & Graham CF (1978) Enolase isozymes: Chromatographic and immunological characteristics of rat brain enolase. Biochim Biophys. Acta. 452: 245-252.

Fukuchi K-I, Kamino K, Deeb SS, Furlong CE, Sundstrom JA, Martin AC & Martin GM (1992) Expression of a carboxy-terminal region of the β-amyloid precursor protein in a heterogeneous culture of neuroblastoma cells: evidence for altered processing and selective neurotoxicicty. Mol Brain Res. 16:37-46.

Ginsborg B.L, Martin RJ & Patmore L (1991) On the sodium and potassium currents of a human neuroblastoma cell line. J Physiol (Lond), 434: 121-149.

Gotti C, Sher E, Cabrini D, Bondiolotti G, Wanke E, Mancinelli E & Clementi F (1987) Cholinergic receptors, ion channels, neurotransmitter synthesis, and neurite outgrowth are independently regulated during the in vitro differentiation of a human neuroblastoma cell line. Differentiation , 34 (2): 144-155.

Hernandez M, Kisaalita WS & Farmer MA (1996) Assessment of murine neuroblastoma (N1E-115) resting membrane potential by confocal microscopy. J. Fluorescence. 6(2):77-82.

Hynes M, Rosenthal A (1999) Specification of dopaminergic and serotonergic neurons in the vertebrate CNS. Curr Opin Neurobiol . 9 (1): 26-36.

Ishikawa S (1977) Differentiation of human neuroblastoma cells in-vitro – morphological changes induced by dibutyryl cyclic AMP. Acta Path. Jap. 27: 697-711.

Kang J, Lemaire HG, Unterback A, Salbaum JM, Masters CL, Grzeschik KH, Multhaup G, Beyreuther K & Muller-Hill B (1987) The precursor of Alzheimer's disease amyloid A4 protein resembles a cell-surface receptor. Nature. 325(6106): 733-736.

Kisaalita WS & Bowen JM (1996) Effect of culture age on the susceptibility of differentiating neuroblastoma cells to retinoid cytotoxicity. Biotech and Bioeng. 50:580-586.

Kisaalita WS & Bowen JM (1997) Development of resting membrane potentials in differentiating murine neuroblastoma cells (N1E-115) evaluated by flow cytometry. Cytotechnology. 24: 201-212.

Ko LW, Sheu KFR, Young O, Thaler H, Blass JP (1990) Expression in cultured human neuroblastoma cells of epitopes associated with affected neurons in Alzheimer's disease. Am J Pathol. 136: 867-879.

Kohen E & Hirschberg JA (1989) Cell structure and function by microspectrofluorometry. Academic Press, New York.

Lahiri DK (1993) The stability of β-amyloid precursor protein in nine different cell types. Biochem and Mol Bio Int. 29(5): 849-858.

Lindvall O (1999) Engineering neurons for Parkinson's disease. Nat Biotechnol. 17 (7): 635-636.

Marangos PJ, Goodwin FK, Parma AM, Leuter C & Trams E (1978) Neuron-specific protein (NSP) in neuroblastoma cells in relation to differentiation. Brain Res. 145:49-58.

Mummery CL, Van den Brink CE, Van der Saag PT & De Laat SW (1984) A short-term screening test for teratogens using differentiating neuroblastoma cells in vitro. Teratology , 29 (2): 271-279.

Neill D, Hughes D, Edwardson JA, Rima BK & Allsop D (1994) Human IMR-32 neuroblastoma cells as a model cell line in Alzheimer's disease research. J. Neuroscience.39(4): 482-493.

Odelstad L, Pahlman S, Nilsson K, Larsson E, Lackgren G, Johansson KE, Hjerten S & Grotte G (1981) Neuron-specific enolase in relation to differentiation in human neuroblastoma. Brain Res. 224 (1): 69-82.

Rudy Y (2000) From Genome to Physiome: Integrative Models of Cardiac Excitation. Annals of Biomedical Engineering. 28: 945-50.

Schmechel DE, Brightman MW & Marangos PJ (1980) Neurons switch from non-neuronal enolase to neuron-specific enolase during differentiation. Brain Res. 190:195-214.

Shamblott MJ, Axelman J, Wang S, Bugg EM, Littlefield JW, Donovan PJ, Blumenthal PD, Huggins GR & Gearhart JD (1998) Derivation of pluripotent stem cells from cultured human primordial germ cells [published erratum appears in Proc Natl Acad Sci USA 1999, 96(3): 1162] Proc Natl Acad Sci USA, 95 (23): 13726- 13731.

Sobel E & Davanipour Z (1996) Electromagnetic field exposure may cause increased production of amyloid beta and eventually lead to Alzheimer's disease. Neurology 47: 1594-1600.

Thomson JA, Itskovitz-Eldor J, Shapiro SS, Waknitz MA, Swiergiel JJ, Marshall VS & Jones JM (1998) Embryonic stem cell lines derived from human blastocysts [see comments] [published erratum appears in Science 1998; 282(5395): 1827]. Science , 282 (5391): 1145-1147.

Tosney KW (1982) The segregation and early migration of cranial neural crest cells in avian embryo. Dev. Biol. 89: 13-24.

Tumilocwicz JJ, Nichols WW, Cholon JJ & Greene AE (1970) Definition of a continuos human cell line derived from neuroblastoma. Cancer Res. 30: 2110-2118.

Walsh DM, Williams CH, Kennedy HE, Murphy G & Allsop D (1994) Gelatinase A not alpha-secretase? Nature 367:27-28.

Wang R, Meschia JF, Cotter RJ & Sisodia SS (1991) Secretion of the beta/A4 amyloid precursor protein. Identification of a cleavage site in cultured mammalian cells. J. Biol. Chem. 266(25): 16960-16964.

Wilson HA & Chused TM (1985) Lymphocyte membrane potentials and Ca2+-sensitive potassium channels described by oxonol dye fluorescence measurements. J.Cell. Physiol. 125:72-81.

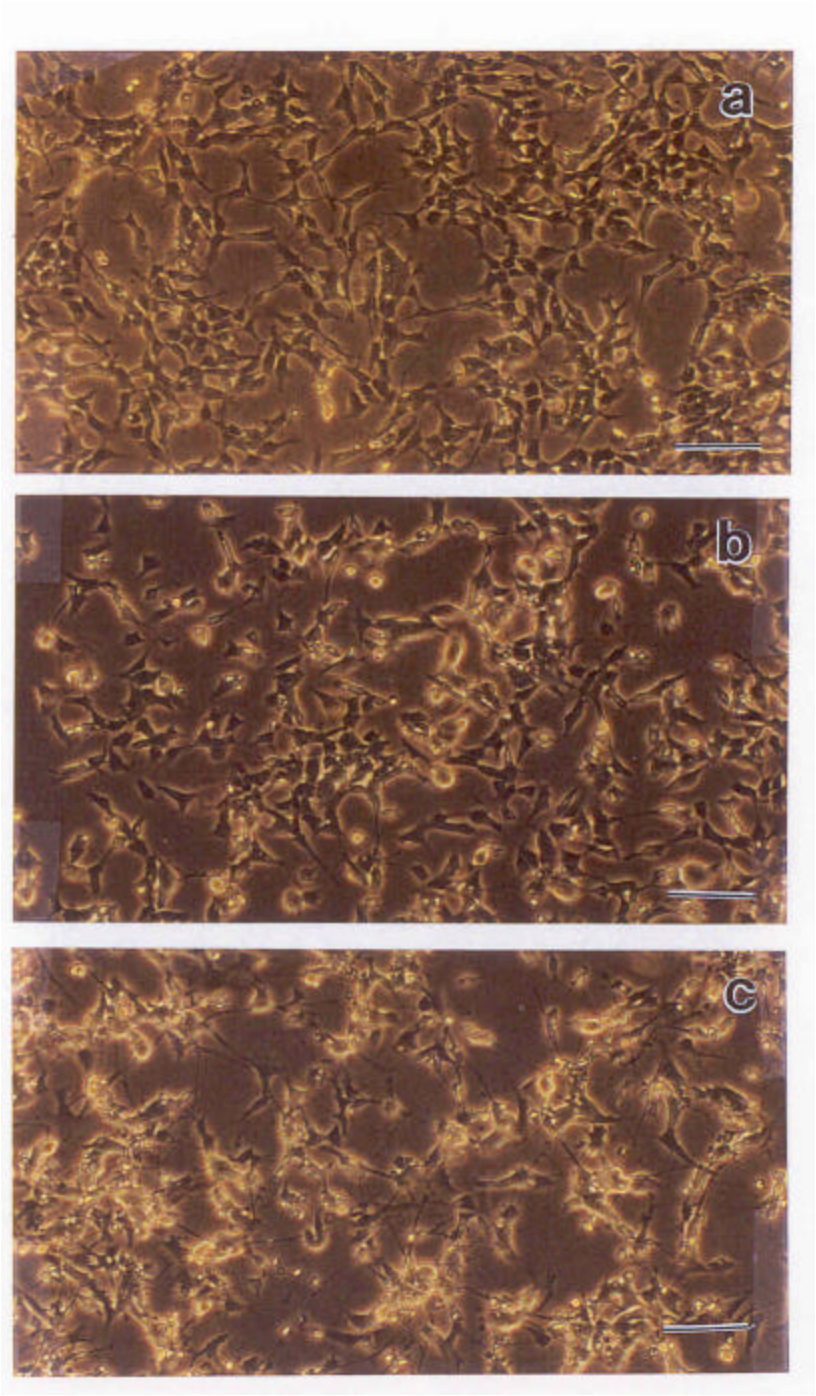

Figure 3.1. Phase contrast micrographs of IMR-32 cells after 0 (a), 4 (b) and 10(c) days of culture in differentiating medium (containing 10 µM 5-BrdU). Bars represent 100 µm.

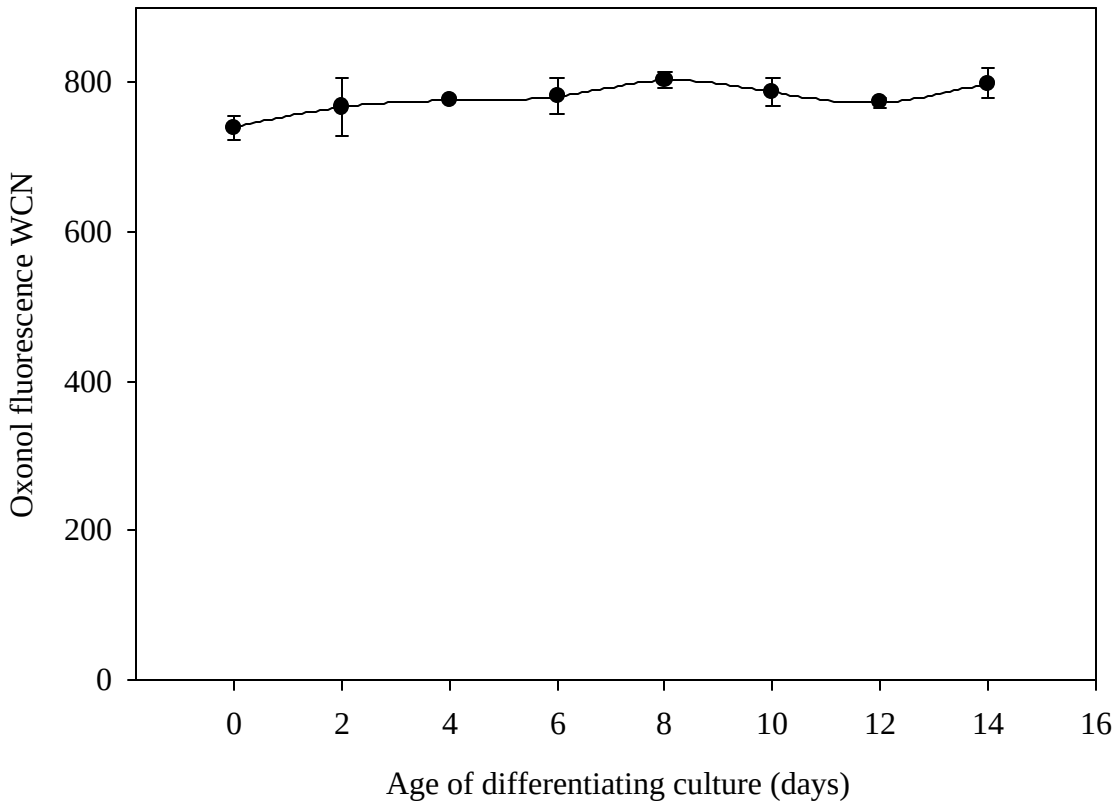

Figure 3.2. Resting membrane potential profile of IMR-32 cells based on oxonol fluorescence weighted channel number (WCN). Error bars represent standard error of the mean.

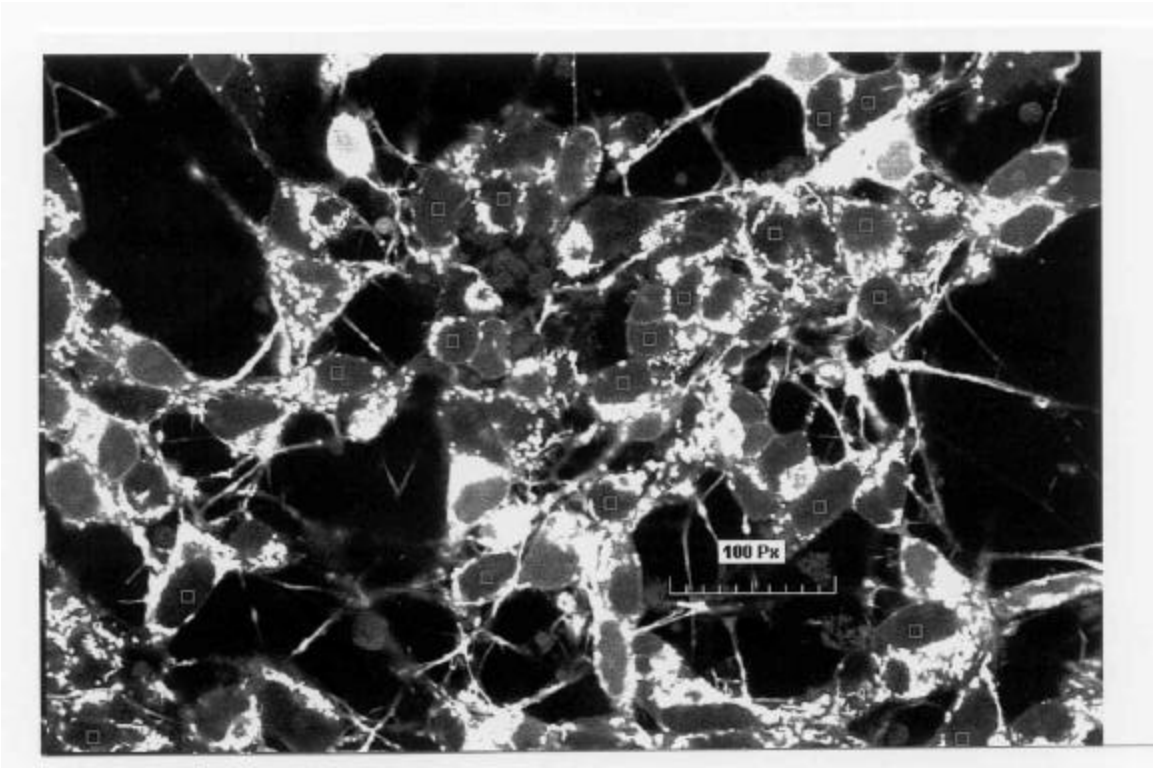

Figure 3.3. TMRM loaded IMR-32 cells. Nuclear regions (NR) exhibited lower and more uniform fluorescence and therefore were convenient for quantifying organelle-free cytoplasmic fluorescence. Squares represent regions of interest (ROI) used for measuring intracellular fluorescence intensity. The cells were loaded with 0.5 μM TMRM. 100 Pixels (Px) = 30 μm.

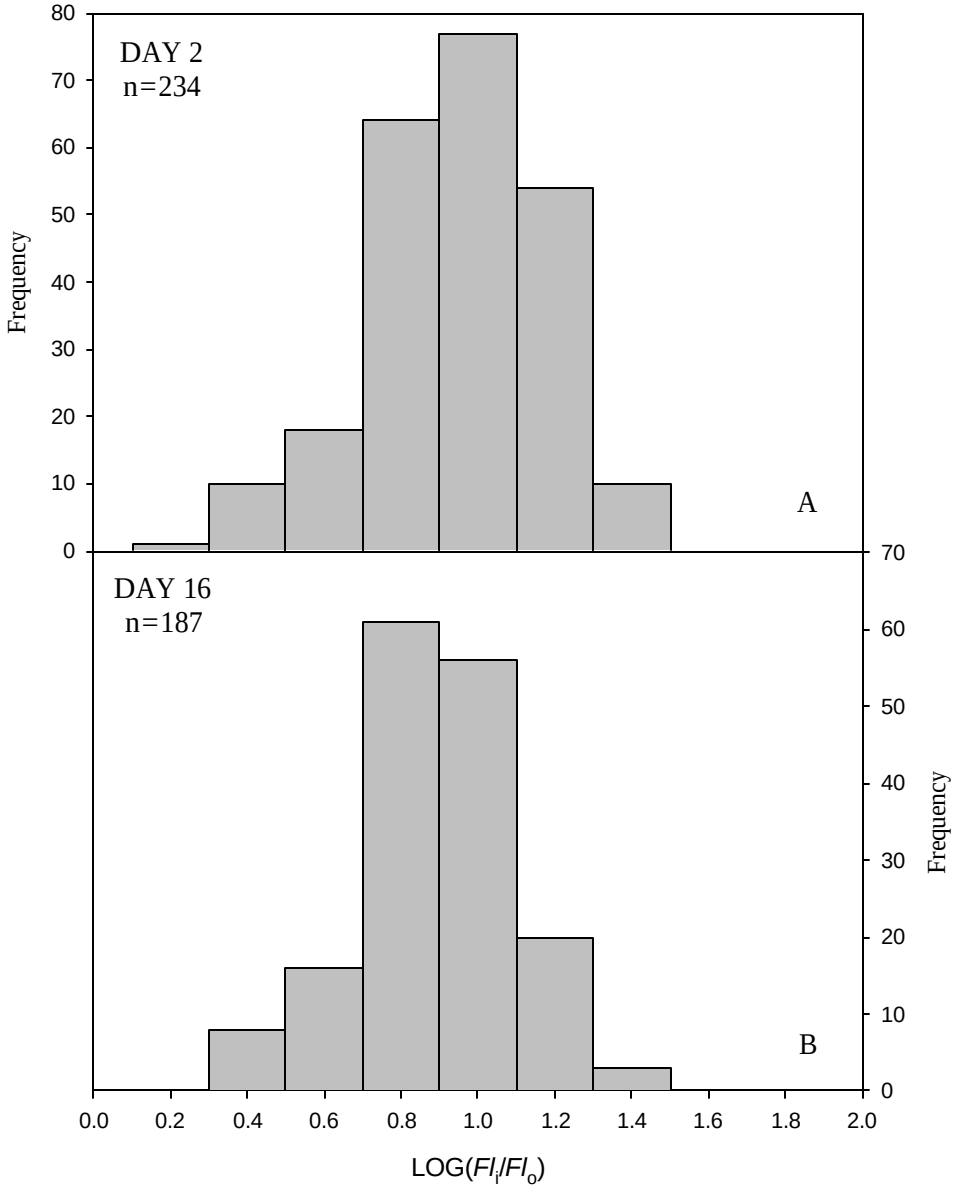

Figure 3.4. A comparison of histograms of the ratios (Fl_i/Fl_o) from Day 2 and Day 16 IMR-32 cells. Fluorescence intensities were measured by confocal microscopy. Mann-Whitney *U* comparison test returned a p-value of 0.081.

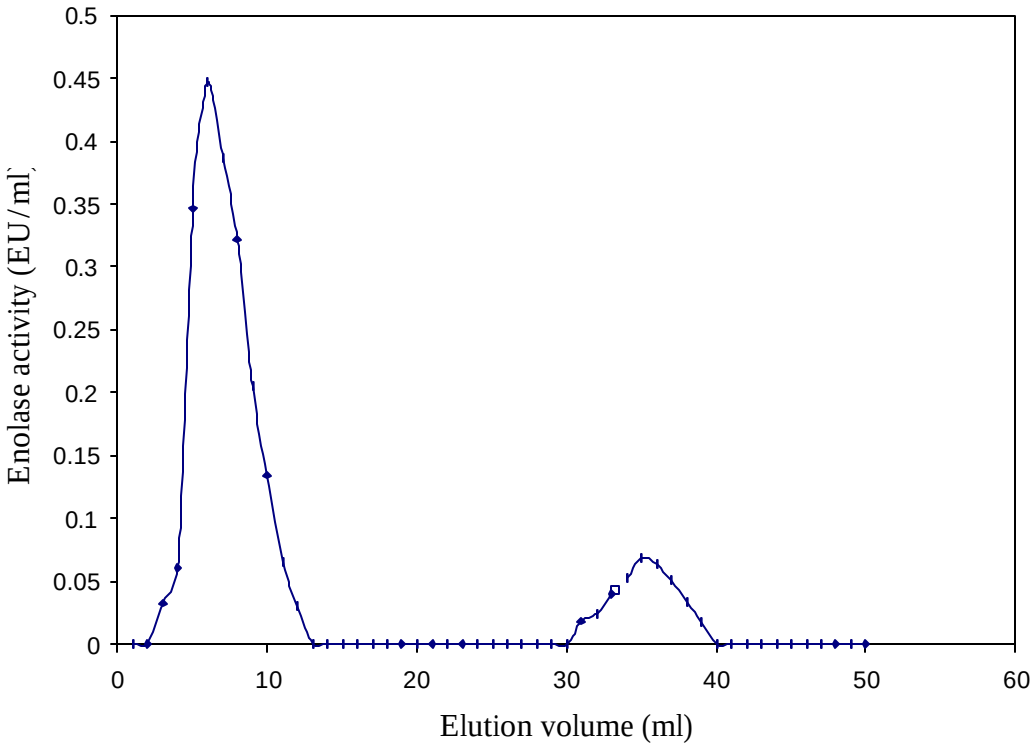

Figure 3.5. Typical chromatogram for the separation of enolase isozymes of 8-day old differentiated IMR-32 neuroblastoma cells by ion exchange chromatography on DEAE-Sephacel. Total enolase activity recovery after passage through the column was approximately 85%. The major and minor peaks correspond to NNE and NSE respectively.

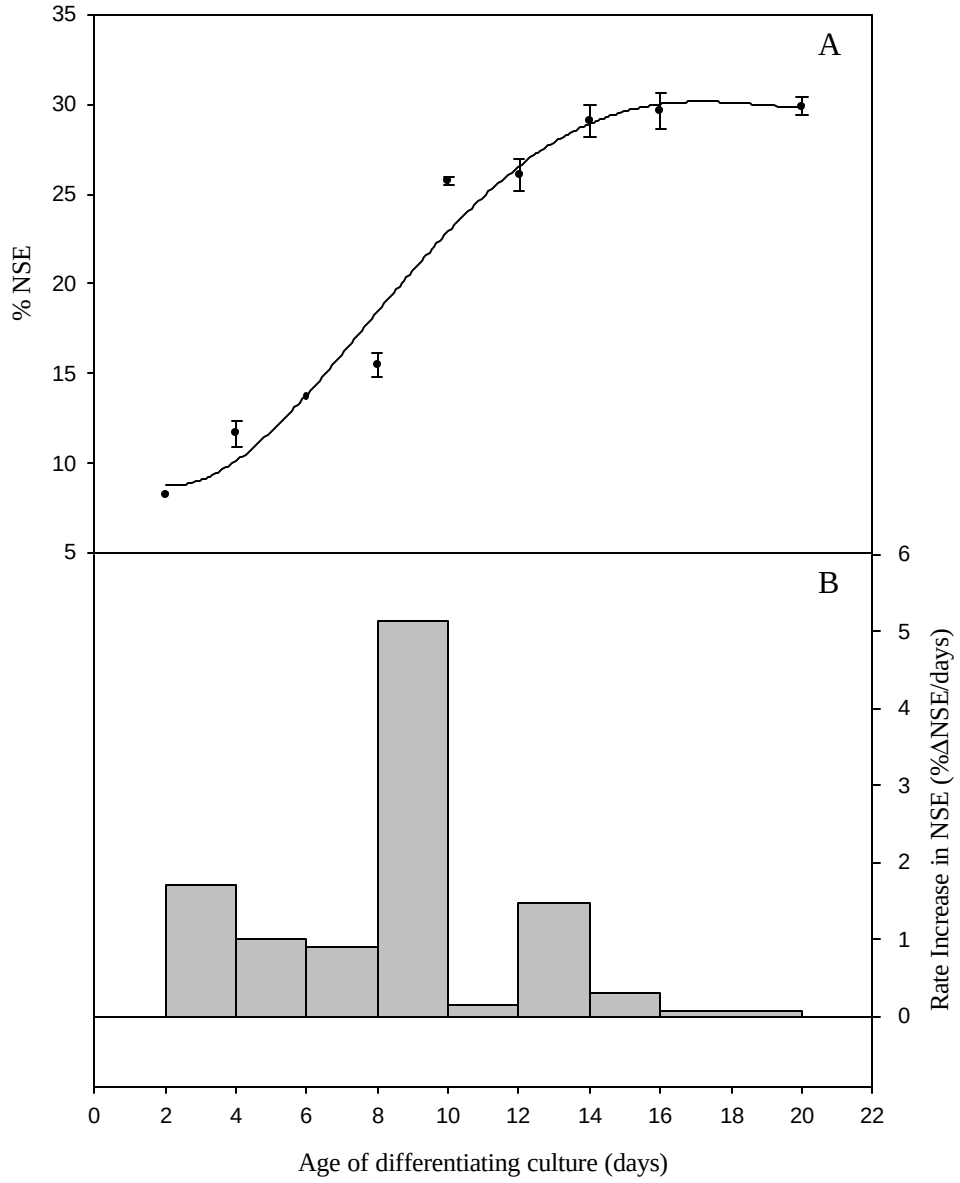

Figure 3.6. The relative level of NSE (A) and the rate change in the level of NSE (B) in IMR-32 cells after 5-BrdU treatment. The cells (10^8 cells /T75 flask) were treated with 10 μM 5-BrdU with medium changes every two days. Error bars correspond to standard error of the mean.

CHAPTER 4

DESIGN AND EVALUATION OF A CONTROLLED ELF-EMF EXPOSURE SYSTEM FOR INVESTIGATING REAL TIME RESPONSES IN VITRO[1]

[1]Raj R. Rao and William S. Kisaalita. To be submitted to Bioelectromagnetics.

ABSTRACT

To be able to correlate real time ion fluxes and gene transcription responses due to electromagnetic field exposure, we have devised an experimental system consisting of a pair of symmetric circular coils. This system can be used on an inverted microscope stage. The design of the system involves key components like a custom-made blinding switch box and a power amplifier. We report herein the evaluation of the exposure system with respect to parameters considered in ELF-EMF exposure for in vitro studies. These include linear magnetic field distribution, compensation for microscope objective lens interference, heating effects of the coils, and harmonic contents of the signals. We also report an application of the system in the study of the maintenance of resting membrane potential change in differentiated IMR-32 human neuroblastoma cells in response to power frequency magnetic field (200 μT) exposure.

KEYWORDS: Circular coils, Membrane Potential, Objective Interference, Harmonics

INTRODUCTION

Numerous studies have been undertaken during the past two decades to examine biological effects in cells exposed to extremely low frequency (ELF) electromagnetic fields (EMF). The biological mechanism and site of interaction of ELF-EMF have been of enormous interest. Studies have shown that ELF-EMF may be capable of causing biologic responses that could be associated with some of the disease processes in a causative manner. Most of the research at the cellular level has been carried out to determine the mechanisms by which ELF-EMF might promote cancer (e.g., Byus et al., 1987, Lyle et al., 1991, Tenforde, 1991, Litovitz et al., 1991, Cain et al., 1993, Liburdy et al., 1993, Loscher and Mevissen, 1995, Leman et al., 2001) or bone repair/cell proliferation (e.g., Luben et al., 1982, Brighton and McCluskey, 1988, Fitzsimmons et al., 1989, Fitzsimmons et al., 1992, Brighton et al., 1992, Fitzsimmons et al., 1994, & 1995, Matsumoto et al., 2000). Another prevalent theme in most ELF-EMF exposure studies at the cellular level is altered ionized calcium (Ca^{2+}) flux (Blackman et al., 1988; Lyle et al, 1991; Liburdy, 1992; Walleczek and Budinger, 1992; Karabakhtsian et al., 1994; Fitzsimmons et al., 1994; Prasad et al., 1994; Garcia-Sancho et al., 1994; Lindström et al., 1995; Kenny et al., 1997, Wey et al., 2000, Thompson et al., 2000).

Two independent interaction hypotheses have been proposed in the research that has been undertaken over the past two decades. The first and most prevalent working hypothesis is that the pericellular fields and currents induced by applied ELF fields could initiate electrochemical events within the cell membrane that are crucial components of the signal transduction and amplification process (Tenforde, 1993). These electrochemical events could then produce cytoplasmic second messengers that have the capacity of eliciting changes in the biosynthesis of macromolecules and causing alterations in cellular and eventually tissue function. Few of the many studies (Luben et al., 1982; Cain et al., 1987; Byus et al., 1984) seem to suggest the general mechanism of the sequence of events that lead to the ELF-EMF signal transduction and amplification at the cellular level (Tenforde, 1996). The second hypothesis that has been proposed is the

direct interaction of magnetic fields with DNA (Blank and Goodman, 1999). Evidence showing that it is possible for magnetic fields to stimulate stress responses by interacting directly with moving electrons in DNA has been published (Blank, 1995; Blank and Soo, 1996, 1998).

Exposure systems have been designed to study the effects of ELF electromagnetic fields over a wide range of frequencies (Mullins et al., 1993) and also for the induction of uniform electric and magnetic fields (Bassen et al., 1992). Several types of apparatus for generating uniform magnetic fields for in vitro studies have been described (Misakian et al., 1993). The most commonly used system uses circular or rectangular loops of wire of many turns. The critical factors that experimenters have tended to address when subjecting field-exposed and sham-exposed cultures are temperature, atmosphere, lighting levels and cycles, vibration from the field- generating apparatus. In addition, design of experimental systems has focussed on two criteria: first the magnetic fields must be well characterized, and second the apparatus should not exert any additional influence on the cells (Goodman et al., 1995). A Helmholtz pair (Kraus, 1984) approximation has been used extensively by many investigators. In gene transcription studies, ELF magnetic fields have been generated by Helmholtz coils (Lin et al., 1996; Goodman et al., 1989), solenoids (Harrison et al., 1997) and a double-wound square 4-coil configuration (Saffer and Thurston, 1995).

We describe herein a custom-made circular coil ELF magnetic field exposure system designed to serve dual purposes. The first purpose is to study real time changes in membrane alterations (membrane potential, ionic fluxes) and the second purpose is to study resultant downstream changes in gene transcription levels. Use of controlled ELF magnetic field exposure parameters with the identical exposure device will make it possible to study the relationship between ELF magnetic fields, membrane alterations and changes in gene transcription levels. Also, we report herein the exposure system characteristics with respect to parameters commonly considered in ELF magnetic field exposure system evaluation for in vitro studies. These include linear magnetic field

distribution, as well as changes in the nature of the distribution in the presence of a microscope objective lens, coil heating effects, and harmonic contents of the ELF magnetic field signals. We also report results of real time membrane potential changes in response to magnetic field exposure. Application of the system to monitor changes in gene transcription levels have been the subject of another study (Rao et al., 2001).

MATERIALS AND METHODS

Magnetic field exposure system

Extremely low frequency magnetic fields of controlled waveform and direction were generated by a pair of symmetric circular coils custom fabricated in the laboratory. The coils were wound around a PVC (dielectric constant = 1.4) bobbin. Details of the coils are given in Figure 4.1. The coils have a inner diameter of 2.75 in. (70 mm) and an outer diameter of 3.25 in. (83 mm). The vertical distance between the coils is 0.3125 in. (0.80 mm). The coils were driven by a sinusoidal signal from a function generator (LFG 1300S, Leader) and an in-house built class AB power amplifier. The amplifier has a frequency range of 5-100 Hz and a current range of 0-1 A. The magnetic field (B) at the center, between the coils, was measured with a F.W. Bell gaussmeter (Model 9550) and probe (Model T-99-253). The magnetic field intensity was adjusted by varying the coil current. A template was used to easily locate the exposed cell position in relation to the circular coil location. A custom-made blinding switch box was included to eliminate experimenter bias. The switch box is composed of three 8 pole, 6 position rotary switches (Electroswitch Inc., CA; Model # C4D0806N-A). Three front panel switch combinations were used to randomize exposure, sham and external coil activations. A schematic of the coils mounted on the stage of an inverted microscope (IX70, Olympus) is shown in Figure 4.2.

Measurement of ambient magnetic fields

The background AC magnetic field in the laboratory near the microscope and the background AC magnetic field inside the incubator were measured over a period of 4

hours using the F.W. Bell gaussmeter (Model 9550) and probe (Model T-99-253). The probe was placed in the center of the incubator close to the location of the exposure device.

Linear magnetic field mapping of the exposure system

The magnetic field levels across the coil were measured with a F.W. Bell gaussmeter (Model 9550) and probe (Model T-99-253). Since it was expected that the microscope objective lens would affect the magnetic field levels across the coil, experiments were carried out with the coil system on the microscope with the objective lens (Nikon Apo 60X, 1.40). The magnetic field levels across the coil system were also measured with the coil system located off the microscope. The mapping was conducted at 60 Hz with input current levels of 50, 100, 200, 300 and 500 mA.

Monitoring of heating effects

The heating in the system (difference between coil and room temperatures) due to current passing through the coils was measured using a Cole-Parmer Temperature and Humidity Logger Model # 91090-70. Measurements were made at the linear positions of 0, 12.5 and 25 mm from the center of the coil and at current levels of 50, 100, 300 and 500 mA, at 10-min. intervals over a period of 4 hours.

Measurement of harmonic contents

The harmonic content of a 60 Hz signal from the function generator was measured with a Onosokki CF 360 Portable Dual Channel FFT Analyzer at 15 Hz intervals. Measurements were made over a 4-hour period with input signals from the signal generator before and after amplification.

Cell line and culture conditions

Freely dividing IMR-32 cells (ATCC #127-CCL, Rockville, MD, U.S.A) were routinely cultured in 25 cm^2 flasks (Costar, Cambridge, MA) in 10 ml medium in 95% air and 5% CO_2 atmosphere at 37^oC and fed (i.e., refreshed the medium) at two day intervals. The growth medium comprised of Eagle Minimum Essential Medium with 2 mM L-glutamine and Earle's Balanced Salt Solution (BSS) adjusted to contain 1.5 g/L

sodium bicarbonate, 0.1 mM non-essential amino acids, and 1.0 mM sodium pyruvate, 10% heat-inactivated fetal bovine serum (FBS) (Neill et al., 1994). When confluent, the cells were detached by washing with trypsin solution preheated to 37^{o}C. The suspension was centrifuged (250xg, 10 min), and the cells were replated at 1 x 10^6 cells per 60mm plate. For induction of differentiation, cells were plated 2 days prior to the addition of differentiation medium. The differentiation medium comprised of Eagle Minimum Essential Medium with 2 mM L-glutamine and Earle's BSS adjusted to contain 1.5 g/L sodium bicarbonate, 0.1 mM non-essential amino acids, and 1.0 mM sodium pyruvate, 5% heat-inactivated FBS and 10 μM Bromo-deoxyuridine. The differentiation medium was refreshed once every two days. Before use in experiments, cells were exposed to differentiating medium for ten days. This age is characteristic of a maturing culture (Rao and Kisaalita, 2001).

Potentiometric dyes

Tetramethylrhodamine methyl ester (TMRM; Molecular Probes) was chosen for the measurement of membrane potential in our experiments for the following reasons: (1) it exhibits low non-specific binding and therefore readily displays reversible potential dependent uptake, (2) is not quenched when taken up by mitochondria and therefore cytoplasmic and mitochondrial fluorescence are readily distinguished, and (3) is non-toxic to most cells (Emaus, et al. 1986; Ehrenberg, et al. 1988).

Resting membrane potential determination by confocal microscopy

A modification of a protocol previously used in our laboratory was followed and details of this protocol have been published elsewhere (Rao and Kisaalita, 2001). Briefly, a confocal imaging system (PCM-2000, Nikon) equipped with high performance detection and control electronics was used. The imaging system's helium/neon mixed gas laser (Green-HeNe) was used to excite the fluorescent dye at 543 nm, and emission scans were recorded through a 565 nm long pass filter as relative fluorescence intensities.

IMR-32 cells from culture flasks were replated in 35-mm glass bottom microwell dishes (Mattek, Ashland, MA), at a density of 3 x 10^5 cells/dish. After subsequent

washes with HEPES-BSS (140 mM NaCl, 5 mM KCl, 1 mM $MgCl_2$, 1.8 mM $CaCl_2$, HEPES 10 mM, D-glucose 10 mM, pH 7.4), the dish was filled with the buffer and 0.5 μM TMRM. The sample fluorescence was recorded, and the image was digitized with 640x480 spatial and 8-bit intensity resolution via a frame grabber and stored. Cells were analyzed from at least two independent coverslips.

Rectangular regions of interest (ROI) of approximately 2 μm^2 were defined via the image processor's cursor controls. Fluorescence intensity histograms were generated for both the intracellular and extracellular ROIs. The ratio of the mean values of the fluorescent intensities measured from inside and outside the cell (Fl_i/Fl_o) is related to the resting membrane potential (V_m) by the modified Nernst equation:

$$V_m = -58 \log_{10} \left(\frac{Fl_i - B}{Fl_o - B} * \frac{D_o - B}{D_i - B} \right)$$

Fluorescence contribution from no-dye cell preparations (B) were recorded and were used to correct Fl_i and Fl_o for background. The ratio of the fluorescence intensity from inside and outside the cell (D_i/D_o) was also obtained with depolarized cells in valinomycin / high K^+ HEPES buffer and these values were used for correction for non-Nernstian binding (Ehrenberg et al., 1988).

ELF-EMF exposure conditions

Breysse et al., (1994) and Farag et al., (1998) have identified domestic ELF-EMF exposures at medium (predominant) and high (intermittent) levels of 0.2-1 and >100μT respectively. IMR-32 cells were exposed to a 60 Hz magnetic field intensity of 200 μT, considered well within practical limits. The choice of 60 Hz frequency was patterned after previous studies focussing on power-frequency magnetic fields.

Fluorescence intensities were measured for 60 minutes at 10-min intervals. Depolarization and/or hyperpolarization events in response to ionic disturbances are usually sustainable in time scales of minutes (e.g., Yamamoto et al., 1997). Given that TMRM is a slow response dye, and its equilibration time is in the order of minutes

(Farkas et al., 1989), the frequency of data collection (10-min intervals for 60 minutes) was considered adequate for capturing changes in V_m in response to ionic disturbances. The ability of the cells to respond to ELF-EMF in the presence of different membrane permeability modifying conditions was also studied. In the first condition (HEPES+TEA), cells were maintained in the HEPES-BSS containing 100 mM tetraethyl-ammonium chloride (TEA) (Sigma). In the second condition (HEPES +Cs^+), K^+ in HEPES-BSS was replaced with Cs^+. In the third condition (HEPES/Low Na^+/High K^+), cells were maintained in HEPES-BSS with high K^+ (50 mM) and low Na^+ (70 mM). TEA has been used in these studies as it is a well characterized K^+ channel blocker and a cholinergic antagonist. Cs^+ has been used in these studies since it not only blocks voltage-dependent potassium channels but also has been found to activate chloride channels (Hughes et al., 1987).

RESULTS AND DISCUSSION

Characterization of the exposure system

The maximum levels of the ambient ac magnetic field near the microscope and inside the incubator were 0.1 μT and were consistent with background levels measured by others (Davis et al., 1999). The dc magnetic field in the laboratory and inside the incubator was within the range 30-40 μT. The dc magnetic field level in the laboratory was not considered as one of the exposure parameters due to its constant value both near the microscope and in the incubator. The absence of stray ac fields from the incubator was noted.

The results from the linear magnetic field mapping are presented in Figures 4.3 and 4.4. The presence of the objective lens elicited an increase in the magnetic field level around the edges of the objective and the relative difference increased with current. In the absence of an objective, the exposure system elicited a bell-shaped magnetic field distribution across the coil (as shown in Figure 4.3) in accordance with minor variation with increased distance from the center (Misakian, 1993). As expected, the magnitude of

the field was directly proportional to the applied current. The relative difference in magnetic field levels at the center of the coils due to the presence of the objectives were found to change by 7.1, 4.3, 5.3, 4.9, 4.8% in response to current values of 50, 100, 200, 300 and 500 mA, respectively. The results from the linear magnetic field mapping of the coil at different currents indicates that under normal conditions, the magnetic field across the coil measured on the bottom plate is a direct measure of the input current, and the spatial distribution is maintained. The introduction of the objective lens on the microscope disrupts the spatial distribution of the magnetic field intensity with the major increase seen around the edges of the objective. For example, at the center of the coil the magnetic field difference in the presence and absence of the objective lens is linearly related to the input current (See Figure 4.5). The results presented in Figure 4.5 can be used to determine the amount of current adjustment required to compensate for the presence of the objective lens.

Figure 4.6 gives a summary of the temperature distribution with time at three different positions of the coil in response to different input currents. At an input current of 50 mA, there was no measurable temperature change. The coil heated up in response to input currents of 100, 300 and 500 mA. However, the magnetic field intensities in our experimental conditions were usually less than or equal to 200 μT (corresponding to input currents less than or equal to 50 mA).

The amplitude of harmonics was expressed as percentages of the 60 Hz signal (Figure 4.7). Since most electric power is generated at a frequency of 60 Hz, we were interested in studying the effects of magnetic fields generated at that particular frequency. The fundamental frequency (f_o) of 60 Hz and harmonic signals (15, 30, 45, 90, 120 Hz) were analyzed from the output of both the amplifier and the signal generator. The results indicated that 60 Hz is the fundamental frequency in both the outputs from the amplifier and the signal generator. The amplitude of the harmonics was of the order of 0.1-0.2% of the fundamental frequency which was an indication that the signal generator and the amplifier were suitable for exposure studies at 60 Hz. Blurring of edges of cells, which is

a characteristic of severe vibration, was not observed at all magnetic field intensities studied, suggesting that vibrations were minimal. Magnetic field levels decreased sharply with increasing distance from the coils (data not shown), suggesting that control and exposure experiments could be conducted simultaneously in the same incubator. This eliminated the need for a second incubator normally used in magnetic field exposure studies with large coil setups.

Biological application- membrane potential changes

Maintaining a steady V_m in nerve cells is dependent on highly coordinated processes involving passive and active ion transport across the cell membrane (Kandel, 1995). Disruption of any of these processes is expected to cause detectable changes in V_m. Since a prevalent theme in most ELF-EMF exposure studies is altered ion flux (Ca^{2+}, K^+, Na^+), V_m was considered a suitable end-point for a preliminary assessment of ELF-EMF effects. Average V_m values (n = 55-80) from different ionic conditions are presented in Figure 4.8a.

Under normal conditions (HEPES-BSS), the cells were in the depolarized state which is in agreement with earlier observations (Rao and Kisaalita, 2001) attributed to poor K^+ permeability development (Gotti et al., 1987). A V_m decreasing trend was observed, especially in the most depolarized conditions (Figure 4.8a). A similar trend was observed with cells examined twice at the beginning and the end of the 60-min interval, suggesting that photobleaching was not a factor. Further, photobleaching was completely ruled out based on absence of significant change in fluorescence intensity under depolarizing (high K^+/valinomycin) conditions (data not shown). The cause for this drop in V_m with time is currently unknown.

The contribution of different ions to the resting membrane potential can be quantified by the Goldman equation:

$$V_m = \left(\frac{RT}{F}\right)\ln\left(\frac{P_K\left[K^+\right]_o + P_{Na}\left[Na^+\right]_o + P_{Cl}\left[Cl^-\right]_i}{P_K\left[K^+\right]_i + P_{Na}\left[Na^+\right]_i + P_{Cl}\left[Cl^-\right]_o}\right)$$

Since the cells are in the depolarized state under normal buffer conditions, the permeability to Na^+ (P_{Na}) should be much higher than that for both Cl^- (P_{Cl}) and K^+ (P_K) (Kandel et al., 1995). Therefore, K^+ should have a minimal effect on the V_m, while Na^+ and Cl^- ions would be expected to be the major contributors to V_m in the IMR-32 phenotype in this study. As shown in Figure 8a, the order of depolarization was found as follows: (HEPES + Cs^+) > (HEPES) > (HEPES + TEA) > (HEPES- High $[K^+]_o$/Low $[Na^+]_o$). When TEA was added to the buffer, the cells were less depolarized in comparison to the normal buffer condition, which can be attributed to an increase in the extracellular Cl^- concentration (from 150.6 to 247 mM, See Table 4.1). When extracellular K^+ was replaced with Cs^+, the cells were even more depolarized and appeared more rounded in comparison to cells in normal buffer conditions. This observation is in agreement with studies previously conducted with C6 glioma and NG108-15 cells (Rouzaire-Dubois et al., 1999), where application of Cs^+ extracellularly depolarized cells. When the buffer conditions were changed to high $[K^+]_o$ and low $[Na^+]_o$ (See Table 4.1), the cells became less depolarized (hyperpolarized), which is predicable by the Goldman equation, if the P_K is assumed to be negligible.

Comparisons of the V_m values between ELF-EMF exposed and unexposed cells under different buffer conditions are shown in Figure 4.8b. The nonparametric Mann-Whitney U test was used to test whether the V_m distribution of the unexposed and exposed cultures, were identical. The test was based on the null hypothesis H_0: the two V_m distributions are identically distributed versus the alternative hypothesis H_1: the two V_m distributions are not identically distributed. A p-value< 0.05 obtained, indicating that a significant difference exists between the unexposed and exposed cells. A summary of the Mann-Whitney U test results are shown in Table 4.1. Under the buffer conditions of (HEPES + Cs^+), and (HEPES /Low Na^+/ High K^+) an ELF- EMF effect was observed in 83% (5/6) of the time points surveyed. Our results suggest a general depolarization ELF-EMF effect, predominantly observed under conditions of high $[K^+]_o$/low $[Na^+]_o$ and low $[K^+]_o$/high $[Na^+]_o$.

Other studies on the effect of magnetic fields on Na^+ and K^+ transport (Serpersu and Tsong, 1983; Ikehara et al., 1998) have suggested that the enzyme (Na^+/ K^+/ATPase) extracts energy from the field and transduces it through K^+ or Na^+ transport. These suggestions were based on observations of an enhanced transport against a concentration gradient in the presence of a magnetic field. Studies on chick myoblasts (Grandolfo et al., 1991) showed that field effects induced decreases in the conductivity and permeability of cells, and this was interpreted as evidence for a decrease in transport of various ions. Studies examining the effects of ELF-EMF on the Na^+/K^+/ATPase ion pump in membranes (Blank, 1995; Blank and Soo, 1996) have provided complex results, with either increases or decreases in enzyme activity depending on the level of K^+ and Na^+ ions in the medium. These studies concluded that ELF-EMF exposure could interfere or enhance enzyme activation by affecting the ion concentration that is immediately made available to the enzyme. Based on the Goldman equation, Na^+ permeability should play a significant role in depolarized cells. Since Na^+/K^+/ATPase is primarily responsible for Na^+ transport, depolarizing effects are likely to be mediated by increased Na^+/K^+/ATPase activity.

In conclusion, the exposure system in this study should be useful for measuring real time biological changes (e.g., membrane potential, ionic fluxes, pH) as well as gene transcription studies (Rao et al., 2001) which involve longer exposure times traditionally conducted in cell culture incubators. Furthermore, the system has been used to study the effect of ELF-EMF on the real time resting membrane potential of differentiated IMR-32 cells. The resultant depolarization effect suggests a possible interaction of ELF-EMF with Na^+/K^+/ATPase. More detailed studies are needed to confirm this interaction conclusively.

ACKNOWLEDGEMENTS

This research was supported partly by grants from the Georgia Research Alliance and the University of Georgia Research Foundation. The authors thank Steve McDonald

for machine work on the blind switch box and the amplifier. Mention of brand names is for information only and does not imply endorsement.

REFERENCES

Bassen H, Litovitz T, Penafiel M, Meister R. 1992. ELF in vitro exposure systems for inducing uniform electric and magnetic fields in cell culture media. Bioelectromagnetics, 13, 183-198.

Blackman CF, Benane SG, Elliot DJ, House DE, Pollock MM. 1988. Influence of electromagnetic fields on the efflux of calcium ions from brain tissue in vitro: A three-model analysis consistent with the frequency response up to 510 Hz. Bioelectromagnetics 9:215-227.

Blank M. 1995. Na/K-adenosine triphosphatase. Adv. Chem. 250: 339-348.

Blank M, Soo L. 1996. The threshold for Na, K-ATPase stimulation by electromagnetic fields. Bioelectrochem. Bioenerg. 40: 63-65.

Blank M, Soo L. 1998. Enhancement of cytochrome oxidase activity in 60 Hz magnetic fields. Bioelectrochem. Bioenerg. 45: 253-259.

Blank M, Goodman R. 1999. Electromagnetic fields may act directly on DNA, J. Cellular Biochem. 75: 369.

Brighton CT, McCluckey WP. 1988. Response of cultured bone cells to a capacitively coupled electric field: inhibition of cAMP response to parathyroid hormone. J.Orthopaedic Research 6: 567-571.

Breysse P, Lees P.S.J, McDiarmid M.A, Curbow B. 1994. ELF Magnetic Field Exposures in an Office Environment. Am. J. Ind. Med. 25: 177-185.

Brighton CT, Okereke E, Pollack SR, Clark CC. 1992. In vitro bone-cell response to a capacitively coupled electric field: the role of field strength, pulse pattern and duty cycle. Clinical Orthopaedics and Related Research 285: 255-262.

Byus CV, Lundak RL, Fletcher RM, Adey WR. 1984. Alterations in protein kinase activity following exposure of cultured human lymphocytes to modulated microwave fields. Bioelectromagnetics. 5: 341-351.

Byus CV, Piper SE, Adey WR. 1987. The effect of low-energy 60 Hz environmental

electromagnetic fields upon the growth-related enzyme ornithine decarboxylase. Carcinogenesis. 8:1385-1389.

Cain CD, Adey WR, Luben RA. 1987. Evidence that pulsed electromagnetic fields inhibit coupling of adenylate cyclase by parathyroid hormone in bone cells. J. Bone Min. Res. 2: 437-441.

Cain CD, Thomas DL, Adey WR. 1993. 60 Hz magnetic fields acts as a co-promoter in focus formation of C3H/10T1/2 cells. Carcinogenesis. 14(2): 955-960.

Davis CC, Barber I, Swicord ML. 1999. Food and Drug Administration Low-Level Extremely -Low Frequency Magnetic Field Exposure Facility. Bioelectromagnetics. 20: 203-215.

Ehrenberg B, Montana V, Wei MD, Wuskell JP, Loew LM. 1988. Membrane potential can be determined in individual cells from the nernstian distribution of cationic dyes. Biophys J. 53(5):785-794.

Emaus RK, Grunwald R, Lemasters JJ. 1986. Rhodamine 123 as a probe of transmembrane potential in isolated rat-liver mitochondria: spectral and metabolic properties. Biochim Biophys Acta. 850 (3): 436-448.

Farag AS, Dawoud MM, Selim SZ, Cheng TC, Marcus AM, Penn D. 1998. Electromagnetic fields in the home. Electric Power Systems Res. 45 73-89.

Fitzsimmons RJ, Farley JR, Adey WR, Baylink DJ. 1989. Frequency dependence of increased cell proliferation, in vitro, in exposures to a low-amplitude, low-frequency electric field: evidence for dependence on increased mitogen activity released into culture medium. J.Cellular Physiology 139: 586-591.

Fitzsimmons RJ, Strong DD, Mohan S, Baylink DJ. 1992. Low-amplitude, low-frequency electric field-stimulated bone cell proliferation may in part be mediated by increased IGF-II release. J.Cellular Physiology. 150: 84-89.

Fitzsimmons RJ, Ryaby JT, Magee FP, Baylink DJ. 1994. Combined magnetic fields increased net calcium flux in bone cells. Calcified Tissue International 55: 376-380.

Fitzsimmons RJ, Ryaby JT, Mohan S, Magee FP, Baylink DJ. 1995. Combined magnetic fields increase insulin-like growth factor II in TE-85 human osteosarcoma bone cell cultures. Endocrinology 136:3100-3106.

Garcia-Sancho J, Montero M, Alvarez J, Fonteriz RI, Sanchez A. 1994. Effects of extremely-low-

frequency electromagnetic fields on ion transport in several mammalian cells. Bioelectromagnetics. 15: 579-588.

Goodman R, Wei L-X, Xu JC, Henderson A. 1989. Exposure of human cells to low-frequency electromagnetic fields results in quantitative changes in transcripts. Biochim Biophys Acta. 1009:216-220.

Goodman EM, Greenebaum B, Marron MT. 1995. Effects of Electromagnetic Fields on Molecules and Cells. Intl. Rev. of Cytology. 158: 279-338.

Grandolfo M, Santini MT, Vecchia P, Bonincontro A, Camett C, Indovina PL. 1991. Non-linear dependence of the dielectric properties of chick embryo myoblast membranes exposed to sinusoidal 50 Hz magnetic field. Int. J. Radiat. Biol. 60: 877-890.

Harrison GH, Balcer-Kubiczek EK, Shi Z-M, Zhang Y-F, McCready WA, Davis CC. 1997. Kinetics of gene expression following exposure to 60 Hz, 2mT magnetic fields in three human cell lines. Bioelectrochem. Bioenerg. 43:1-6.

Hernandez M, Kisaalita WS, Farmer MA. 1996. Assessment of murine neuroblastoma (N1E-115) resting membrane potential by confocal microscopy. J. Fluorescence. 6(2):77-82.

Hughes D, McBurney RN, Smith SM, Zorec R. 1987. Cesium ions activate chloride channels in rat cultured spinal cord neuron. J. Physiol. 392: 231-251.

Ikehara T, Yamaguchi H, Miyamoto H. 1998. Effects of electromagnetic fields on membrane ion transport of cultured cells. J Med Invest 45(1-4): 47-56.

Kandel E.R., Schwartz J.H., Jessell T.M. (eds). (1995). Essentials of neural science and behavior. Appleton and Lange, Norwalk, Connecticut.

Karabakhtsian R, Broude N, Shalts N, Kochlatyi S, Goodman R, Henderson AS. 1994. Calcium is necessary in the cell response to EM fields. FEBS Letters. 349: 1-6.

Kenny JS, Kisaalita WS, Rowland G, Thai C, Foutz T. 1997. Quantitative study of calcium uptake by tumorigenic bone (TE-85) and neuroblastoma x Glioma (NG108-15) cells exposed to extremely-low-frequency (ELF) electric fields. FEBS Letters. 414:343-348.

Kisaalita WS, Bowen JM. 1996. Effect of culture age on the susceptibility of differentiating neuroblastoma cells to retinoid cytotoxicity. Biotech. Bioeng. 50: 580-.

Krause JD. 1984. Electromagnetics. 3rd ed. McGraw Hill, New York.

Liburdy RP. 1992. Calcium signaling in lymphocytes and ELF fields: Evidence for an electric

field metric and a site of interaction involving the calcium ion channel. FEBS Letters 301(1): 53-59.

Liburdy RP, Sloma TR, Sokolic R, Yaswen P. 1993. ELF magnetic fields, breast cancer, and melatonin: 60 Hz fields block melatonin's oncostatic action on ER+breast cancer cell proliferation. J.Pineal Res. 14:89-97.

Lin H, Blank M, Jin M, Goodman R. 1996. Electromagnetic field stimulation of biosynthesis: changes in c-myc transcript levels during continuous and intermittent exposures. Bioelectrochem. Bioenerg. 39:215-220.

Lindström E, Lindström P, Berglund A, Lundgren E, Mild KH. 1995. Intracellular calcium oscillations in a T-cell line after exposure to extremely-low-frequency magnetic fields with variable frequencies and flux densities. Bioelectromagnetics 16:41-47.

Litovitz TA, Krauss D, Mullins JM. 1991. Effect of coherence time of the applied magnetic field on ornithine decarboxylase activity. Biochem Biophys. Res. Commun. 178:862-865.

Loscher W, Mevissen M. 1995. Linear relationship between flux density and tumor co-promoting effect of prolonged magnetic field exposure in a breast cancer model. Cancer Letters 96:175-180.

Luben RA, Cain CD, Chen MC, Ronsen DM, Adey WR. 1982. Effects of electromagnetic stimuli on bone and bone cells in vitro: Inhibition of responses to parathyroid hormone by low-energy low-frequency fields. Proc. Natl. Acad. Sci. USA. 79: 4180-4184.

Lyle DB, Wang X, Ayotte RD, Sheppard AR, Adey WR. 1991. Calcium uptake by leukemic and normal T-lymphocytes exposed to low frequency magnetic fields. Bioelectromagnetics. 12:145-156.

Misakian M, Shephard AR, Krause D, Frazier ME, Miller DL. 1993. Biological, Physical and electrical parameters for in vitro studies with ELF magnetic and electric fields: A primer. Bioelectromagnetics Supplement 2: 1-73.

Mullins RD, Sisken JE, Hejase HN, Sisken B. 1993. Design and characterization of a system for exposure of cultured cells to extremely low frequency electric and magnetic fields over a wide range of field strengths. Bioelectromagnetics 14, 173-186.

Neill D, Hughes D, Edwardson JA, Rima BK, Allsop D. 1994. Human IMR-32 neuroblastoma cells as a model cell line in Alzheimer's disease research. J. Neuroscience.39(4): 482-493.

Prasad AV, Morton WM, Cox C, Carstensen EL, Hoops H, Brayman AA. 1994. A test of the influence of cyclotron resonance exposures on diatom mobility. Health Physics. 66(3):305-312.

Rao RR, Kisaalita WS. 2001. Development of a distinct phenotype of a human neuroblastoma (IMR-32) cell line by chemical control of differentiation, Cytotechnology. Submitted.

Rao RR, Halper J, Kisaalita WS. 2001. Effects of 60 Hz magnetic field exposure on APP695 transcription levels in differentiating human neuroblastoma cells. Bioelectrochem. Submitted.

Rouzaire-Dubois B, Milandri JB, Bostel S, Dubois JM. 2000. Control of cell proliferation by cell volume alterations in rat C6 glioma cells. Pflugers Arch 440(6): 881-8.

Saffer JD, Thurston SJ. 1995. Short Exposures to 60 Hz Magnetic Fields do not alter MYC Expression in HL60 or Daudi Cells. Radiation Research. 144:18-25.

Serpersu EH, Tsong TY. 1983. Stimulation of a oubain-sensitive Rb+ uptake in human erythrocytes with an external field. J. Membr. Biol. 74: 191-201.

Tenforde TS. 1991. Biological interactions of extremely-low-frequency electric and magnetic fields. Bioelectrochem. Bioenerg. 25:1-17.

Tenforde TS. 1993. Cellular and molecular pathways of extremely- low frequency electromagnetic field interactions with living systems. In: Electricity and Magnetism in Biology and Medicine, M. Blank, ed., San Francisco Press, San Francisco, CA. 1-8.

Tenforde TS. 1996. Biological interaction of extremely low frequency electromagnetic fields. In: Biological effects of electric and magnetic fields, S. Ueno, ed, Plenum Press, New York.

Walleczek J, Budinger TF. 1992. Pulsed magnetic field effects on calcium signaling in lymphocytes: dependence on cell status and field intensity. FEBS Letters 314(3):351-355.

Yamamoto S, Tanaka E, Shoji Y, Kudo Y, Inokuchi H, Higashi H. 1997. Factors that reverse the persistent depolarization produced by deprivation of oxygen and glucose in rat hippocampal CA1 neurons in vitro. J Neurophysiol. 78(2): 903-11.

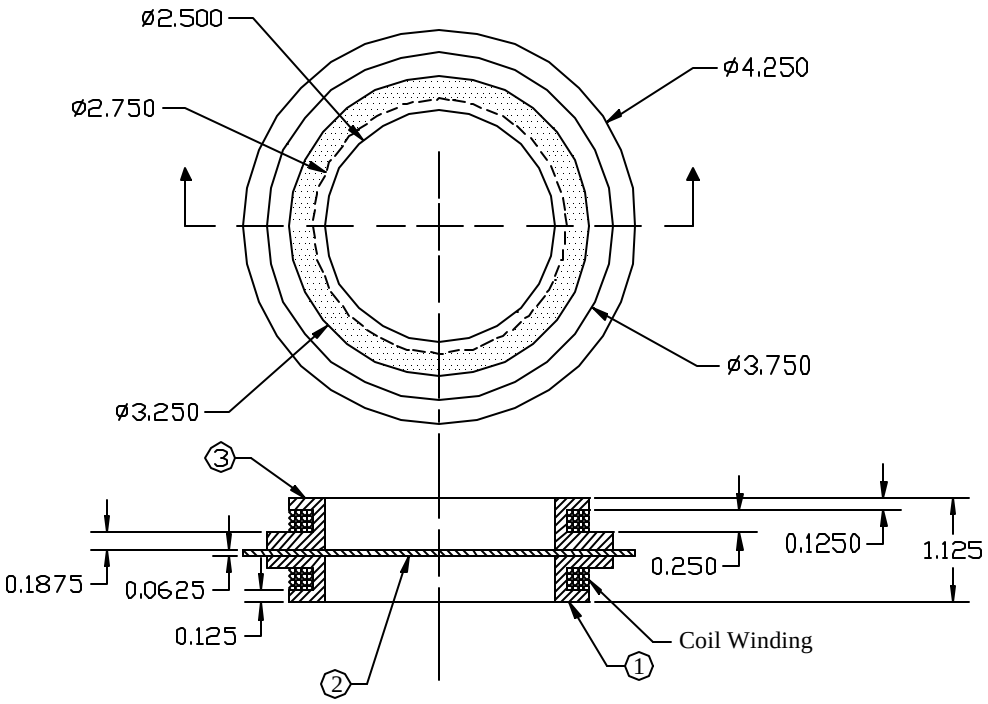

Figure 4.1. Scale drawings of circular coils showing (a) Top view of coil. (b) Side view of coil (***f*** - diameter; **1**- bottom coil; **2**- microscope stage; **3**- top coil; all dimensions in inches).

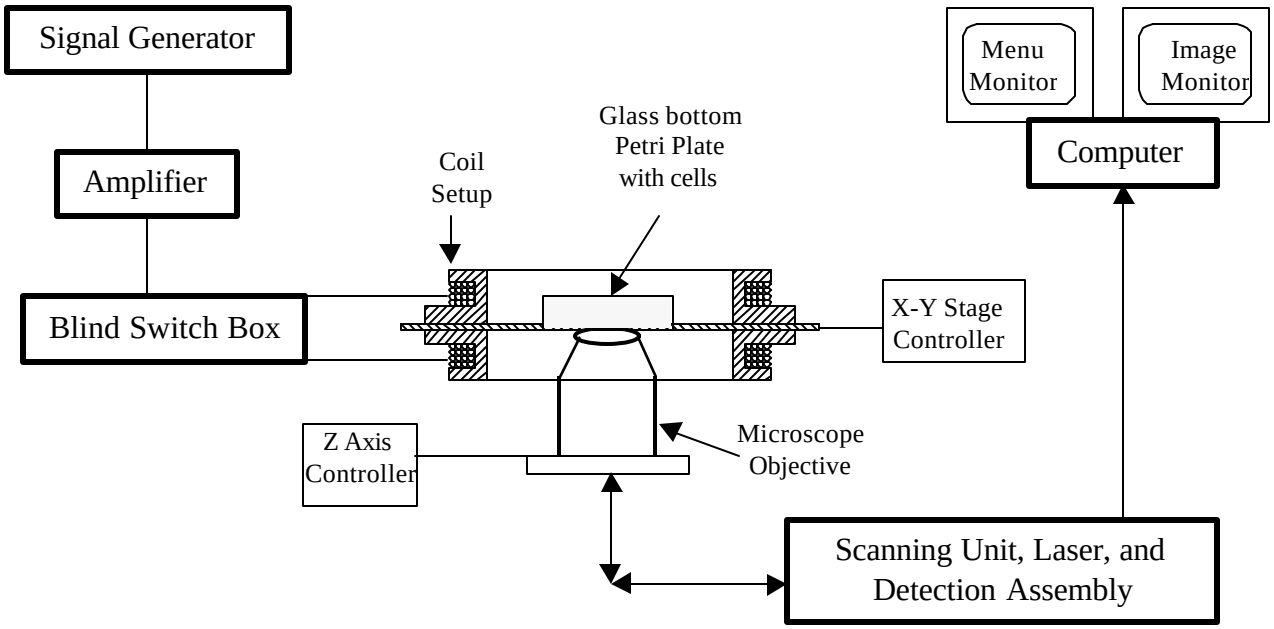

Figure 4.2. Schematic of the circular coil exposure apparatus mounted on the microscope.

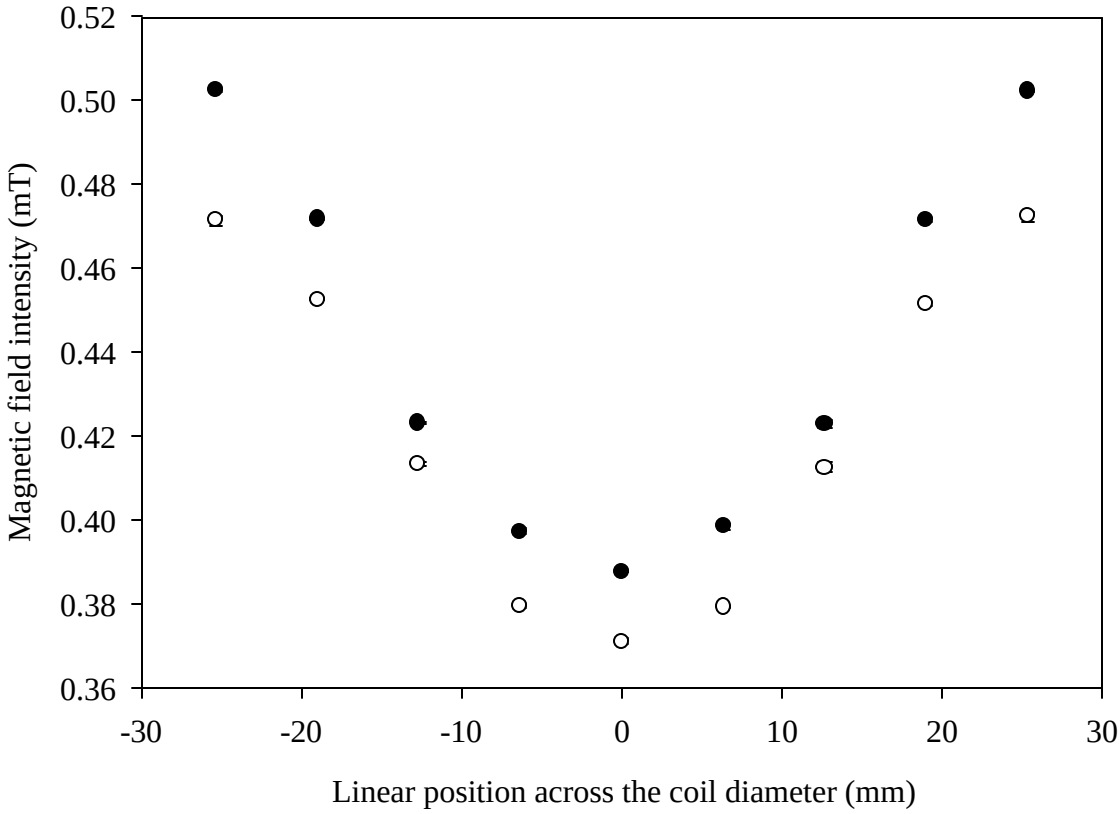

Figure 4.3. A typical linear magnetic field distribution of the coil setup without (•) and with (o) microscope objective lens, at a frequency of 60 Hz and an input current of 100 mA.

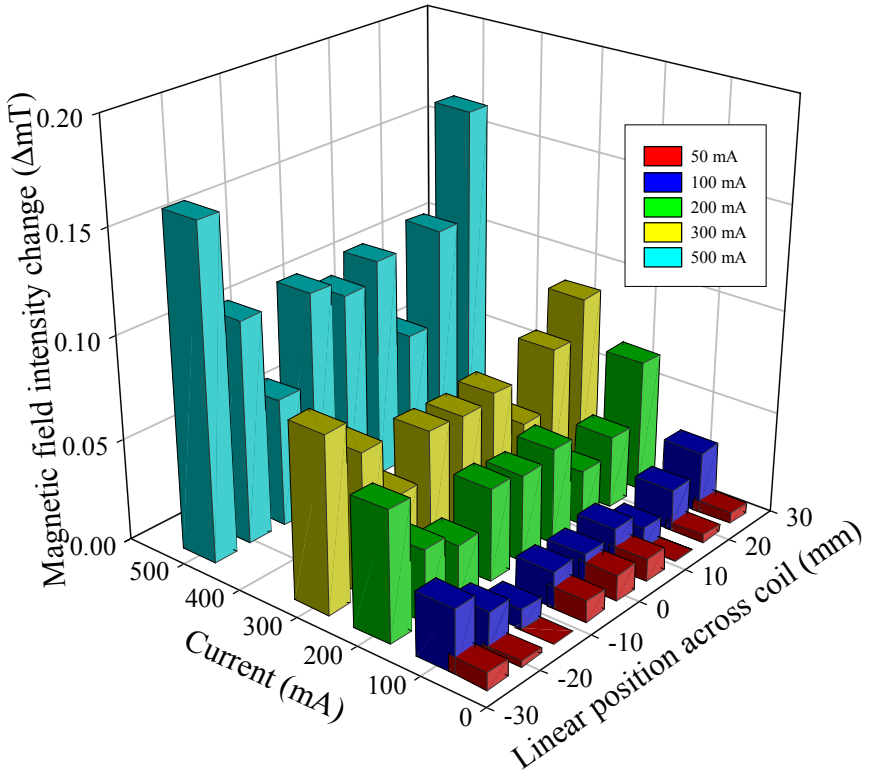

Figure 4.4. Magnetic field change due to microscope objective interference across the coil at different input currents at 60 Hz.

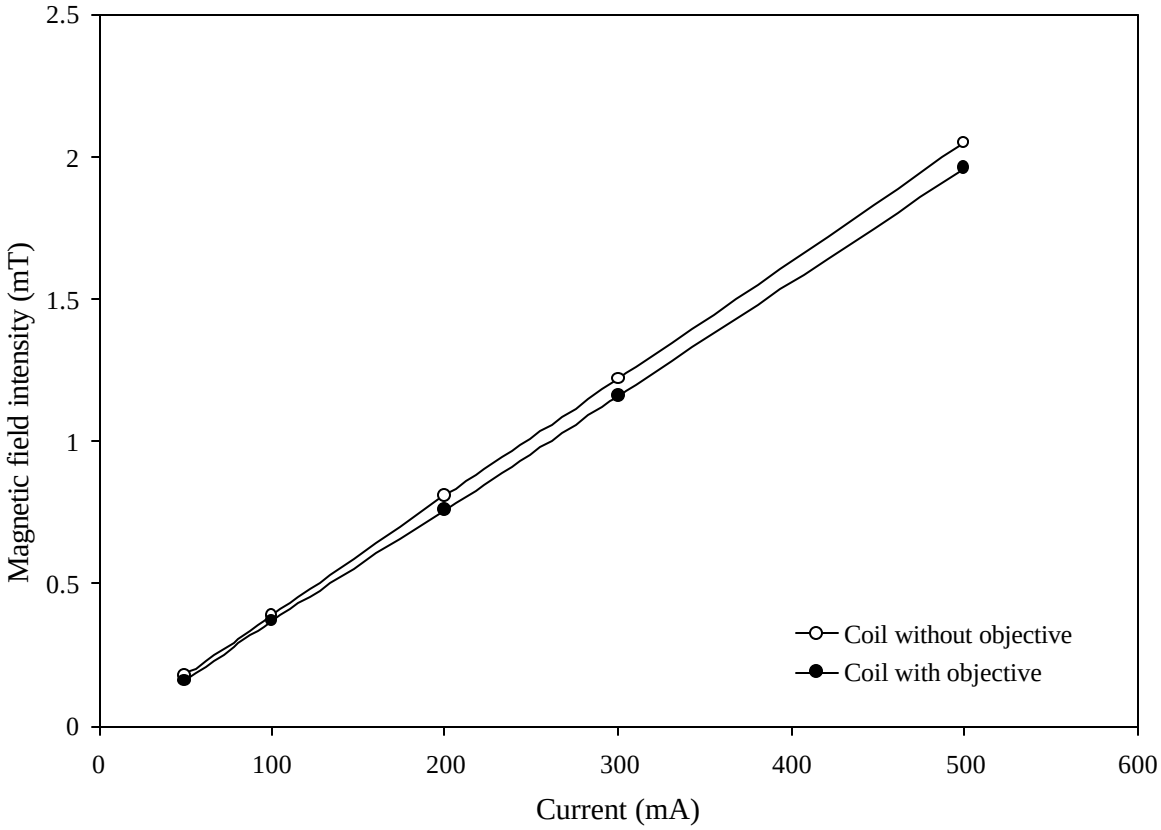

Figure 4.5**.** Change in magnetic field intensity at the center of the coil at different input currents at 60 Hz.

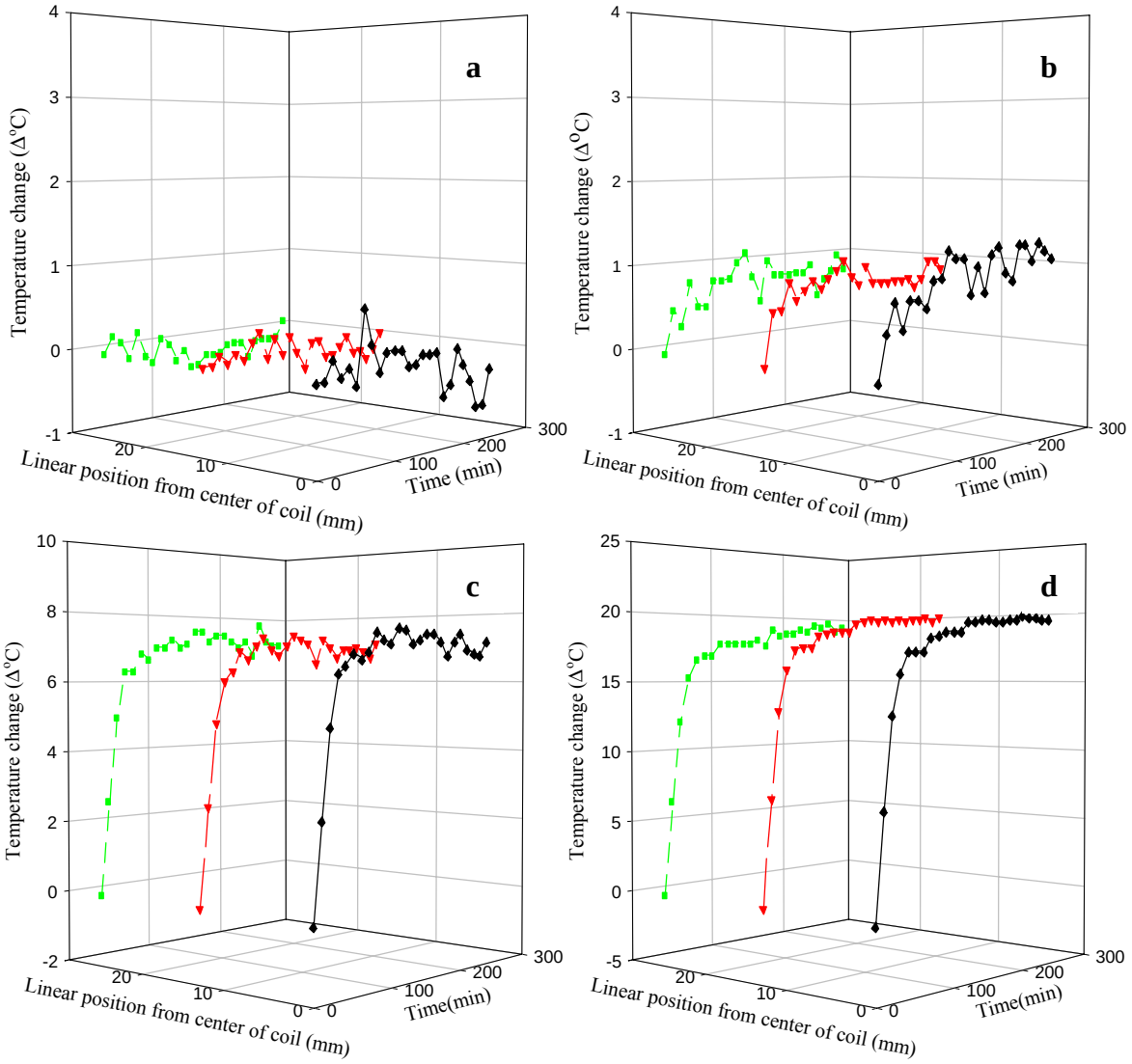

Figure 4.6**.** Temperature change (Coil- Room Temperature) in the coils at different currents and a constant frequency of 60 Hz over a 4 hour time period at three positions from the center of the coil. (**a**) Current = 50 mA. (**b**) Current = 100 mA. (**c**) Current = 300 mA. (**d**) Current = 500 mA.

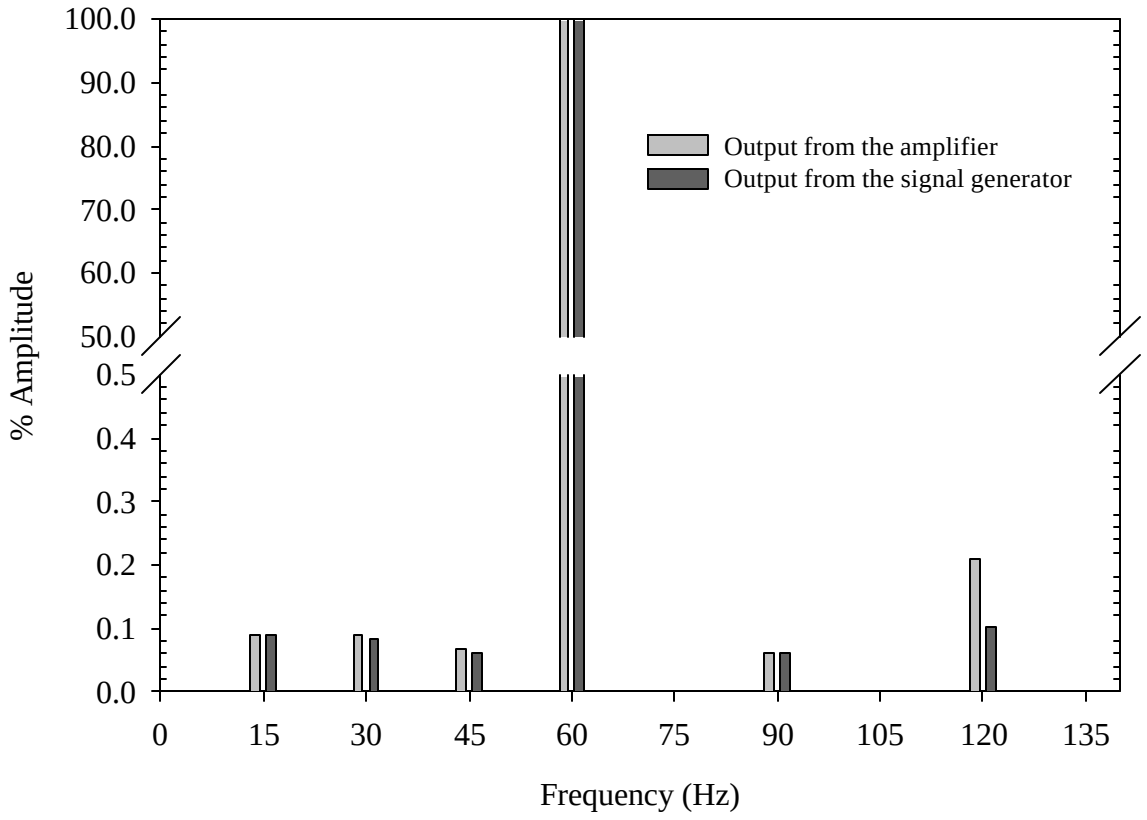

Figure 4.7. Harmonic content analysis of signal generator and amplifier at 60 Hz. Readings were averaged over a 4 hour time period.

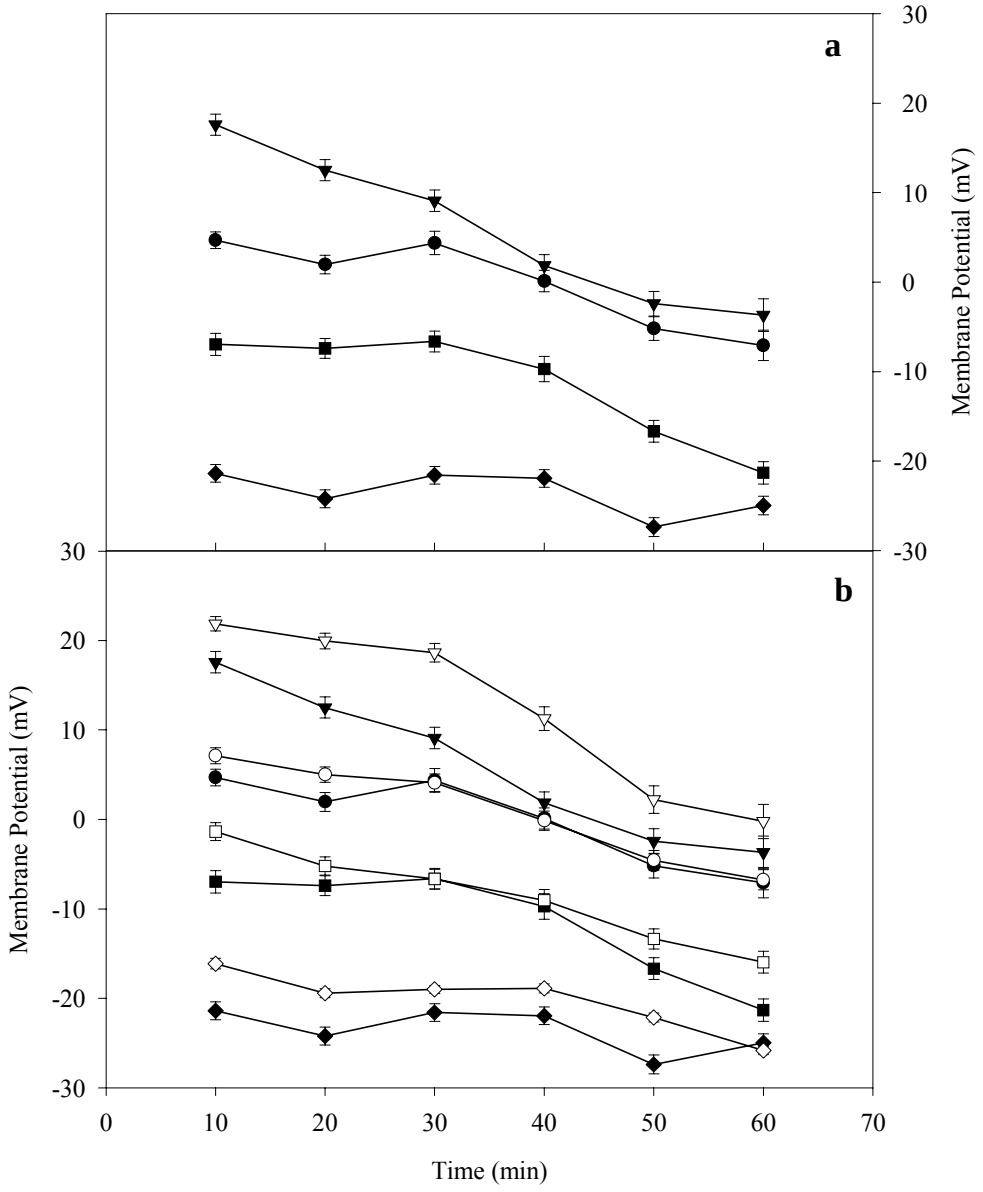

Figure 4.8. (a) Average resting membrane potentials (unexposed) from single IMR-32 cells loaded with 0.5 µM TMRM in different ionic environments. (b) Comparison of average resting membrane potentials between unexposed and exposed cells under different ionic environments. (▼- HEPES/Cs^+; ∇- HEPES/Cs^+ + ELF-EMF; ●- HEPES; ○- HEPES + ELF-EMF; ■- HEPES/TEA; □- HEPES/TEA + ELF-EMF; ♦- HEPES/Low Na^+/High K^+; ◊- HEPES/Low Na^+/High K^+ + ELF-EMF). Magnetic field intensity = 200 µT, 60 Hz. Error bars are standard error of the mean.

Table 4.1. Statistical comparison of V_m for ELF-EMF exposed (200 μT, 60 Hz) and unexposed cells.

Experimental Condition	**$[Na^+]_o$ (mM)**	**$[Cl^-]_o$ (mM)**	**T10**	**T20**	**T30**	**T40**	**T50**	**T60**
HEPES/Cs^+	140	150.6	0.008*	0*	0*	0*	0.016*	0.192
HEPES	140	150.6	0.024*	0.039*	0.946	0.68	0.401	0.608
HEPES/TEA	140	247	0.001*	0.112	0.984	0.582	0.031*	0.002*
HEPES/Low Na^+ /High K^+	70	125.6	0*	0*	0.028*	0.012*	0*	0.867

(*: p-value < 0.05 obtained, indicated that there was a significant difference between the unexposed and exposed cells).

CHAPTER 5

EFFECTS OF 60 HZ ELECTROMAGNETIC FIELD EXPOSURE ON APP695 TRANSCRIPTION LEVELS IN DIFFERENTIATING HUMAN NEUROBLASTOMA CELLS[1]

[1]Raj R. Rao, Jaroslava Halper and William S. Kisaalita. Submitted to Bioelectrochem. 06/2001.

ABSTRACT

Amyloid deposits derived from amyloid precursor proteins (APPs) have been implicated in the development of Alzheimer's disease (AD) pathogenesis. Among the three major APPs, the APP695 isoform is predominantly expressed in nervous tissue. Epidemiological studies have suggested that workers with primary occupation that are likely to have resulted in medium-to-high extremely low frequency (ELF) electromagnetic field (EMF) exposure are at increased risk of AD. The concept that ELF-EMF exposure might contribute to the AD pathogenesis merits attention. As a first step in investigating the possibility of an association between ELF-EMF exposure and AD at the cellular level, we have used differentiating IMR-32 neuroblastoma cells. In double-blind experiments, IMR-32 cells were exposed to magnetic field intensities of 50, 100 and 200 μT at a frequency of 60 Hz for a period of four hours at the three ages of differentiation (2, 10, 16 days after incubation in differentiation medium). We used a custom-made circular coil setup driven by a 60 Hz sinusoidal signal from a function generator and an in-house built power amplifier. Total RNA extracted from exposed cells was separated by agarose gel electrophoresis and transferred to a nylon membrane for northern hybridization. Digoxigenin-labeled APP695 RNA probes were used to detect changes in APP695 mRNA levels in response to ELF-EMF exposure. The results reported herein provided no support for any relationship between APP695 gene transcription and IMR-32 differentiation age as well as magnetic field exposure. This study constitutes a first step towards investigating the possibility of an association between ELF-EMF exposure and AD manifestations at the cellular level. Absence of ELF-EMF effect on APP695 gene transcription provides incentives to explore ELF-EMF effects on other factors implicated in AD pathogenesis, e.g., β- and γ- secretase activities.

KEYWORDS: ELF-EMF, Alzheimer's disease, Circular coil, IMR-32.

INTRODUCTION

There is a significant interest in the biological effects of power frequency (60 Hz) electromagnetic fields (EMF). Health professionals, government administrators and regulators, scientists and engineers, and the general public are interested in this health issue. The focus of research in this area at the cellular level is to identify cellular responses to EMF's, to develop a dose threshold for such interactions and use such information to formulate and test appropriate interaction mechanisms. Numerous studies have been undertaken during the past two decades to examine biological effects in cells exposed to extremely low frequency (ELF)-EMF's and the major interest has been to decipher the biological mechanism and site of interaction [1,2]. Several studies have demonstrated the possibility that a mechanism of interaction of the magnetic fields is through a direct reaction with DNA rather than through the generally accepted signal transduction cascade [3]. In these conditions the cell is responding to magnetic field exposure in a manner analogous to that observed under conditions of cellular stress such as an increase in transcripts for some heat shock genes [4,5]. Early studies in which different cells were exposed to EMF's pointed towards general changes in gene transcription [6-10] but did not address the more important issue of which specific genes were affected [11]. Specific mRNA level measurements in response to ELF-EMF exposure, showed an increase in levels of histone H3 and p53 mRNA [12], IGF-II [13], histone H2B, *v-myc* [14], *c-fos* [15] and *c-myc* [16]. However, these experiments have been difficult to replicate [17-20].

In epidemiological studies, workers with primary occupations that are likely to have resulted in medium-to-high ELF-EMF exposure are at increased risk of Alzheimer's disease (AD) [21,22]. Alzheimer's disease is one of the most serious health problems in the US, and its impact increases as the percentage of the elderly continues to increase. The etiology of the brain lesions associated with AD appears to be multifactorial [23]. Factors that are possible components in the etiologic process are either genetic [24-28], environmental [29-33], or related to aging [34,35]. AD is thought by many to be

intimately, if not causatively associated with the deposition of short β-amyloid (Aβ) peptides in the cerebral cortex and hippocampus of affected individuals [36]. These Aβ peptides are liberated from the β–amyloid precursor proteins (APPs) after cleavage of APPs in the membrane by β- and γ-secretase enzyme [37]. Among the three major APPs, the APP695 isoform is predominantly expressed in nervous tissue.

The concept that ELF-EMF exposure might contribute to the AD pathogenesis merits attention [38]. As a first step in investigating the possibility of an association between ELF-EMF exposure and AD at the cellular level, we have used differentiating IMR-32 neuroblastoma cells. When differentiated, IMR-32 cells mimic large projection neurons of the human cerebral cortex. IMR-32 cells are of human origin, large in size and have previously been used in studies related to the stability of APP [39]. Also, under specific tissue culture conditions (combination of dibutryl cyclic AMP, nerve growth factor, gangliosides and sodium butyrate) these cells have been shown to form intracellular fibrillary material [40], commonly observed in brains of patients affected with AD. We report herein on APP695 gene transcription after exposure of differentiating IMR-32 cells to ELF-EMF at intensities of 50, 100 and 200 μT.

MATERIALS & METHODS

Cell lines, reagents and culture conditions

Freely dividing IMR-32 cells (ATCC #127-CCL, Rockville, MD, U.S.A) were routinely cultured in 25 cm^2 flasks (Costar, Cambridge, MA) in 10 ml medium in 95% air and 5% CO_2 atmosphere at 37^oC and fed (i.e., refreshed the medium) at two day intervals. The growth medium comprised of Eagle Minimum Essential Medium with 2 mM L-glutamine and Earle's Balanced Salt Solution (BSS) adjusted to contain 1.5 g/L sodium bicarbonate, 0.1 mM non-essential amino acids, and 1.0 mM sodium pyruvate, 10% heat-inactivated fetal bovine serum (FBS) [41]. When confluent, the cells were detached by washing with trypsin solution preheated to 37^oC. The suspension was centrifuged (250xg, 10 min) and the cells were replated at 1 x 10^6 cells per 60-mm plate.

For induction of differentiation, cells were plated 2 days prior to the addition of differentiation medium. The differentiation medium comprised of Eagle Minimum Essential Medium with 2 mM L-glutamine and Earle's BSS adjusted to contain 1.5 g/L sodium bicarbonate, 0.1 mM non-essential amino acids, and 1.0 mM sodium pyruvate, 5% heat-inactivated FBS and 10 μM Bromo-deoxyuridine. The differentiation medium was refreshed once every two days.

Magnetic field exposure system

Details of the magnetic field exposure system are published elsewhere [42]. Briefly, the magnetic field was generated by a pair of symmetric circular coils, custom fabricated in the laboratory. The coils had an inner diameter of 2.75 in. (to accommodate 60 mm petri dishes) and an outer diameter of 3.25 in. The vertical distance between the coils was 0.3125 in. The coils were driven by a sinusoidal signal from a function generator (LFG 1300S, Leader) and an in-house built class AB power amplifier. The magnetic field (B) at the center, between the coils, was measured with a F.W. Bell gaussmeter (Model 9550) and probe (Model T-99-253). B was adjusted by varying the coil current. A custom-made blinding switch box was included to eliminate experimenter bias. The switch box was composed of three 8 pole, 6 position rotary switches (Electroswitch Inc., CA; Model # C4D0806N-A). Three front panel switch combinations were used to randomize exposure, sham and external coil activations.

Experimental conditions

The general experimental design involved differentiation age (3 levels), magnetic field intensity (3 levels) and exposure mode (field-exposed, sham-exposed and external coil activation).

Based on an earlier study involving the characterization of IMR-32 with neuron-specific enolase as a differentiation marker [43], three differentiation ages were selected : 2, 10, 16 days after incubation in differentiation medium. The second day represents undifferentiated (young) cells, the tenth day represents differentiating (maturing) cells and the sixteenth day represents fully differentiated (mature) cells. Differentiation age is

and important factor because previous studies in our laboratory have shown that the vulnerability of differentiating neuroblastoma cells to external stimuli is differentiation age-dependent [44].

Two studies [45,46] have evaluated the potential sources of ELF-EMF's and exposure levels in office and domestic environments. Based on these studies, the predominant medium values of 0.2-1 μT and the high intermittent values of >100 μT were identified. In this study, ELF-EMF exposure levels up to 200 μT were considered well within practical limits. The choice of 60 Hz frequency was based on the fact that most exposure studies have focussed on the possible adverse effects of power-frequency magnetic fields.

Several studies [47] have stressed the importance of the duration of the magnetic field exposure in the maintenance of steady state transcript levels. Short-term ELF-EMF exposures (minutes) produce short-lasting responses attributable to the inhibitory effect of the resultant non-specific synthesized proteins [16]. Studies addressing temperature as a stress factor have shown that the time required to cause an effect is reduced logarithmically with increasing temperature [48, 49]. It has thus been suggested that in continuously exposed cells, proteins specific to the stress are synthesized over long exposure times. Most of these studies have considered exposure periods of several hours (2-4 h) in order to maintain transcript levels [e.g., 50].

To minimize experimenter bias, a double blind approach was used. A custom-made blinding switch box was used to expose cells to magnetic fields in an unbiased manner. An example of blinding switch box setting is shown in Table 5.1. As revealed three exposure modes (field-exposed, sham-exposed and external coil activation) were made possible. After subjecting to different exposure modes, cells were washed twice with 1 ml of HEPES–BSS (140 mM NaCl, 5 mM KCl, 1 mM $MgCl_2$, 1.8 mM $CaCl_2$, HEPES 10 mM, D-glucose 10 mM, pH 7.4), and dislodged from the 60 mm dish using a cell scrapper. The cells were then centrifuged using the same buffer, and the pellets were snap-frozen in liquid nitrogen and stored at -70°C for later RNA isolation and processing.

Isolation and analysis of total RNA

Total RNA was extracted by following the manufacturer's protocols for monolayer cultures, using TRIzol™ reagent [51]. The integrity of the extracted RNA was ascertained by examination of 28S and 18S bands of ethidium-bromide-stained (1.2 %) agarose-formaldehyde gels. Samples were considered to be degraded if the 28S band was less intense than the 18S band. If any sample in a series was degraded, the experiment was repeated.

RNA samples (10-20 μg) were size-fractionated by electrophoresis in 1.2% agarose gels containing 6% formaldehyde and 1X MOPS (40V for 20 min; 60V for 3 h), followed by capillary blotting overnight from the formaldehyde gel to nylon membrane (Roche Molecular Biochemicals, Indianapolis, IN). Air-dried membranes were crosslinked by UV irradiation to immobilize the RNA using a UV Stratalinker (Stratagene, La Jolla, CA) on automatic setting. Membranes pre-hybridized in Dig-Easy Hyb solution (Roche Molecular Biochemicals, Indianapolis, IN) were hybridized at 60°C with digoxygenin-labeled APP695 and actin RNA probes. Conditions suggested in the kit for hybridization and washing of membranes were followed (Roche Molecular Biochemicals, Indianapolis, IN). Intensity of APP695 mRNA signal was obtained using the Digoxigenin chemiluminescent detection kit (Roche Molecular Bioechemicals, Indianapolis, IN).

Hybridization probes

In preparation for Northern hybridization experiments, DNA segments corresponding to a segment of APP695 was amplified by a RT-PCR reaction using the following pair of primers [52]:

Forward: 5′AATACGACTCACTATAGGGAGACACCACAGAGTCTGTGGAAG 3′;

Reverse: 5′CATACGATTTAGGTGACACTATAGAGGTGTCTCGAGATACTTGT 3′;

T7 RNA Polymerase (underlined) and SP6 RNA polymerase (underlined) sequences were incorporated into the forward and reverse primers respectively. These primers were synthesized at the Molecular Genetics Facility at the University of Georgia. Reverse

transcriptase-polymerase chain reaction (RT-PCR) was then conducted with Titan One tube RT-PCR system (Roche Biosciences) and evaluated by separation in a 1% agarose gel and staining with ethidium bromide.

The parameters for the RT-PCR were as follows: cDNA synthesis at 50^{o}C for 30 min, denaturation at 94^{o}C for 2 min; amplification cycle (denaturation at 94^{o}C for 0.5 min, annealing at 57^{o}C for 0.5 min, elongation at 68^{o}C for 0.75-4 min). PCR was run for 25 cycles with cycle elongation of 5 s for each cycle and a final elongation step at 68^{o}C for 7 min. The PCR product was purified by running the DNA in a 1.5 % low melting point agarose gel at 50V for 2 h, and the DNA bands were excised from agarose purified using a Supelco Wizard® minicolumn. The authenticity of the purified DNA was then verified by sequence analysis at the Molecular Genetics Facility, and digoxygenin-labeled APP695 RNA probes were prepared using the Digoxygenin labeling kit (Roche Biosciences). Genbank analysis showed that there was overall homology with existing sequences. Digoxygenin-labeled human actin probes were obtained from Roche Biosciences and were used as internal standards.

Evaluation of relative transcript levels

Our analysis allowed for possible treatment-induced variation of the transcript levels based on magnetic field strengths and differentiation time. In order to determine the amount of hybrids formed between the APP695 transcript and its probe, the X-ray films were analyzed by densitometry using the Expression 636 (Epson, Long Beach, CA) and the Quantity One, version 2 (BioRad Laboratories, Hercules, CA). Measurements of APP695 transcript levels were expressed as the ratio of APP695 to Actin (internal standard) for each experimental condition. Actin was used as an internal standard based on earlier studies showing no changes in actin transcript levels in response to magnetic field exposure [53]. A typical example of a northern blot output that is used for processing and analysis is shown in Fig. 5.1. The top row shows the levels of the APP695 mRNA elicited by hybridization with the APP695 RNA probe while the bottom row

shows the levels of the Actin mRNA elicited by hybridization with the digoxigenin-labeled human actin RNA probe.

The data were represented as the ratio of the experimental (E) signal to the control (C) signal [13]. The relative signal is a measure of the quantity (*E/C*)–1, where *E/C* is the mean ratio of experimental (exposed/sham/external coil) to control band density. (*E/C*)–1 is zero for no effect, positive or negative for increased or decreased mRNA signal levels, respectively. All the treatments of replicate ratios were examined with a two-tailed *t*-test to test the hypothesis that the ratio (*E/C*) is equal to unity.

RESULTS AND DISCUSSION

APP695 transcription level ratios [(*E/C*) –1] for a magnetic field intensity of 100 μT as a function of differentiation age are shown in Fig. 5.2. The largest variation among all the experimental conditions was a 23% decrease of APP695 relative signal. This variation was observed on the 10^{th} day of differentiation. In all the cases, there were no statistically significant ELF-EMF effects among the three experimental (exposed, sham and external coil) and control conditions at the three culture ages of differentiation. The results also showed that there was no change in APP695 transcription level with differentiation age. APP695 transcription level ratios [(*E/C*) –1] for all experimental conditions in 16-day old differentiated IMR-32 cells as a function of magnetic field strengths are shown in Fig. 5.3. In all the cases, there were no statistically significant ELF-EMF effect between the three experimental (exposed, sham and external coil) and control conditions at the three different magnetic field intensities. The results also showed that there was no change in APP695 transcription levels with increase in magnetic field strength.

Table 5.2 summarizes 27 different *t*-tests. Each block in Table 5.2 represents a test of the null hypothesis H_o: the mean APP695 relative transcription level for the respective experimental condition is equal to the value of unity (mean of the APP695 relative transcription level for the respective control condition) versus the alternative

hypothesis H_1: the mean APP695 relative transcription levels for the respective experimental condition is not equal to the value of unity; *p*-values for each test, are reported. A *p*-value greater than 0.05 indicated that the relative transcription levels for the experimental condition was not different from the control condition. Inspection of all the conditions show that all the 27 tests did not reject the null hypothesis at the 5% level, suggesting that there was no statistical difference between the experimental and the control conditions at different magnetic field intensities and ages of differentiation.

The results reported herein provided no support for any relationship between APP695 gene transcription and differentiation age as well as a continuos (4 h) magnetic field exposure. Our result is in contrast with a study in which ELF-EMF partially blocked the differentiation of erythroleukemia cells [54], revealed by both a decrease in percentage of cells containing hemoglobin and a relatively smaller decrease in telomerase activity in ELF-EMF exposed cells. The IMR-32 phenotype used in this study was differentiated with respect to morphological and biochemical but not electrophysiological end points [42]. More conclusive studies are needed with electrophysiologically differentiated cells (e.g., with respect to resting membrane potential development) [55].

This study constitutes a first step towards investigating the possibility of an association between ELF-EMF exposure and AD manifestations at the cellular level. Absence of ELF-EMF effect on APP695 gene transcription levels provides incentives to explore ELF-EMF effects on other factors implicated in AD pathogenesis. For example, it would be useful to consider the effects of ELF-EMF exposure on the enzyme activities of β- and γ-secretases [56]. Previous studies have shown that a possible interaction mechanism is an electrochemical model that involves alteration in enzyme activities that involve ELF-EMF field induced changes [57-59]. Results from previous studies have suggested that ELF-EMF fields could interfere or enhance enzyme activation by affecting the ion concentration available to the enzyme [60,61].

ACKNOWLEDGEMENTS

This research was supported partly by a grant from the University of Georgia Research Foundation for the establishment of the Soft Tissue Center. The authors thank Steve McDonald for fabrication of the blind switch box. Mention of brand names is for information only and does not imply endorsement. The authors also thank Suparna Sarkar and Hongje Pan for critical analysis.

REFERENCES

[1] M. Blank, R. Goodman, Do electromagnetic fields interact directly with DNA?, Bioelectromagnetics. 18 (1997) 111.

[2] T.S. Tenforde. Biological interaction of extremely low frequency electromagnetic fields. In: Biological effects of electric and magnetic fields, S. Ueno, ed, Plenum Press, New York. (1996) 23.

[3] M. Blank, R. Goodman, Electromagnetic fields may act directly on DNA, J. Cellular Biochem. 75 (1999) 369.

[4] R. Goodman, D. Weisbrot, A. Uluc, A.S. Henderson, Transcription in *Drosophila melanogaster* salivary gland cells is altered following exposure to low frequency electromagnetic fields: analysis of chromosome 3R. Bioelectromagnetics 13(1992)111.

[5] H. Lin, M. Opler, M. Head, M. Blank, R. Goodman, Electromagnetic field exposure induces rapid, transitory heat shock factor activation in human cells, J. Cellular Biochem, 66 (1997) 482.

[6] R. Goodman, C.A.L.Bassett, A.S. Henderson, Pulsing electromagnetic fields induce cellular transcription. *Science*. 220 (1983) 1283.

[7] J.L. Phillips, L. McChesney, Effect of 72 Hz pulsed magnetic field exposure on macromolecular synthesis in CCRF-CEM cells, Cancer Biochem. Biophys. 12 (1991) 1.

[8] R. Goodman, A.S. Henderson, Some biological effects of electromagnetic fields. Bioelectrochem Bioenerg. 15 (1986) 39.

[9] R. Goodman, A.S. Henderson, Sine waves enhance cellular transcription. Bioelectromagnetics. 7 (1986) 23.

[10] R. Goodman, A.S. Henderson, Stimulation of RNA synthesis in the salivary gland cells of *Sciara coprophilia* by an electromagnetic signal used for treatment of skeletal problems in horses. J. Bioelectricity. 6 (1987) 37.

[11] J.L. Phillips, Effects of Electromagnetic Field Exposure on Gene Transcription. J. Cellular Biochem. 51 (1993) 381.

[12] M. Cantini, A. Cossarizza, F. Bersani, R. Cadossi, G. Ceccherelli, R. Tenconi, C. Gatti, R. Franceschi, Enhancing effect of low frequency pulsed electromagnetic fields on lectin induced human lymphocyte proliferation. J. Bioelectricity 5 (1986) 91.

[13] R.J. Fitzsimmons, D.D. Strong, S. Mohan, D.J. Baylink, Low-amplitude, low-frequency electric field-stimulated bone cell proliferation may in part be mediated by increased IGF-II release. J. Cellular Physiol. 150(1992) 84.

[14] R. Goodman, L-X Wei, J.C. Xu, A. Henderson, Exposure of human cells to low-frequency electromagnetic fields results in quantitative changes in transcripts. Biochim Biophys Acta. 1009 (1989) 216.

[15] S. Rao, A.S. Henderson, Regulation of *c-fos* is affected by electromagnetic fields. J. Cellular Biochem. 63 (1996) 358.

[16] H. Lin, M. Blank, M. Jin, R. Goodman, Electromagnetic field stimulation of biosynthesis: changes in *c-myc* transcript levels during continuous and intermittent exposures. Bioelectrochem. Bioenerg. 39 (1996) 215.

[17] D. Krause, W.J. Skowronski, J.M. Mullins, R.M. Nardone, J.J. Greene, Selective enhancement of gene expression by 60 Hz electromagnetic radiation, in: C.T. Brighton, S.R. Pollack, (Eds.): Electromagnetics in Biology and Medicine. San Francisco: San Francisco Press, (1991) 133.

[18] A. Lacy-Hulbert, R.C. Wilkins, T.R. Hesketh, J.C. Metcalfe, (1995). No Effect of 60 Hz Electromagnetic Fields on *MYC* or β-Actin Expression in Human Leukemic Cells. Radiation Research. 144 (1995) 9.

[19] J.D. Saffer, S.J. Thurston, Short Exposures to 60 Hz Magnetic Fields do not alter *MYC* Expression in HL60 or Daudi Cells. Radiation Research. 144 (1995) 18.

[20] G.H. Harrison, E.K. Balcer-Kubiczek, Z-M. Shi, Y-F. Zhang, W.A. McCready, C.C. Davis. Kinetics of gene expression following exposure to 60 Hz, 2mT magnetic fields in three human cell lines. Bioelectrochem. Bioenerg. 43 (1997) 1.

[21] E. Sobel, Z. Davanipour, R. Sulkava, T. Erkinjuntti, J. Wikstrom, H.W. Henderson, G. Buckwalter, J.D. Bowman, P-J. Lee, Occupations with exposure to electromagnetic fields: A possible risk factor for Alzheimer's disease. American J. Epidemiology. 142 (1995) 515.

[22] E. Sobel, M. Dunn, Z. Davanipour, Z. Qian, H.C. Chui, Elevated risk of Alzheimer's disease among workers with likely electromagnetic field exposure, Neurology, 47 (1996) 1477.

[23] J.P. Blass, (1993). Metabolic alterations common in neural and non-neural cells in Alzheimer's disease. Hippocampus. 3 (1993) 45.

[24] S.S. Mirra, M.N. Hart, R.D. Terry, Making the diagnosis of Alzheimer's disease: a primer for practicing pathologists. Arch. Pathol. Lab. Med. 117 (1993) 132.

[25] A. Goate, M.C. Chartier-Harlin, M. Mullan, Segregation of a missense mutation in the amyloid precursor protein gene with familial Alzheimer's disease. Nature. 349 (1991) 704.

[26] R. Sherrington, E.I. Rogaev, Y. Liang, E.A. Rogaeva, G. Levesque, M. Ikeda, H. Chi, C. Lin, G. Li, K. Holman, Cloning of a gene bearing missense mutations in early-onset familial Alzheimer's disease. Nature. 375 (1995) 754.

[27] E. Levy-Lahad, W. Wasco, P. Poorkaj, D.M. Romano, J. Oshima, W.H. Pettingell, C.E. Yu, P.D. Jondro, S.D. Schmidt, K. Wang, Candidate gene for the chromosome I familial Alzheimer's disease locus. Science. 269 (1995) 973.

[28] C. Van Broeckhoven, Presenilins and Alzheimer's disease. Nature Genetics. 11 (1995) 230.

[29] W.A. Rocca, S. Bonaiuto, A. Lippi, Prevelance of clinically diagnosed Alzheimer's disease and other dementing disorders: a door-to-door survey in Appignano, Macerata Province, Italy. Neurology. 40 (1990) 626.

[30] J.D. Birchall, J.S. Chappel, Aluminum, chemical physiology, and Alzheimer's disease. Lancet. 2 (1988) 1008.

[31] C.N. Martyn, D.J.P. Barker, C. Osmond, Geographical relation between Alzheimer's disease and aluminum in drinking water. Lancet . 1 (1989) 59.

[32] A. Heyman, W.E. Wilkinson, J.A. Stafford, Alzheimer's disease: a study of epidemiological aspects. Ann Neurol. 15 (1984) 335.

[33] J.A. Edwardson, J.M. Candy, Aluminum and the pathogenesis of senile plaques in Alzheimer's disease, Down's syndrome, and chronic renal dialysis. Annals of Medicine. 21 (1989) 95.

[34] W.A. Rocca, L.A. Amaducci, B.S. Schenberg, (1986). Epidemiology of clinically diagnosed Alzheimer's disease. Ann Neurol 19 (1986) 415.

[35] J.P. Blass, E.P. Cherniak, M.E. Weksler, Theories of aging. In: E. Calkins, P.J. Davis, A.B. Ford, (Eds.) Practice of geriatrics. 2nd ed. New York: W.B. Saunders: (1992) 10.

[36] D.J. Selkoe, The cell biology of beta-amyloid precursor protein and presenilin in Alzheimer's disease. Trends Cell Biol. 8 (1998) 447.

[37] D.J. Selkoe, The genetics and molecular pathology of Alzheimer's disease: roles of amyloid and the presenilins. Neurol. Clin. 18 (2000) 903.

[38] E. Sobel, Z. Davanipour, Electromagnetic field exposure may cause increased production of amyloid beta and eventually lead to Alzheimer's disease. Neurology 47 (1996) 1594.

[39] D.K. Lahiri, The stability of β-amyloid precursor protein in nine different cell types. Biochemistry and Molecular Biology International. 29(5) (1993) 849.

[40] L.W. Ko, K.F. Sheu, O. Young, H. Thaler, J.P. Blass, Expression in cultured human neuroblastoma cells of epitopes associated with affected neurons in Alzheimer's disease. Am. J. Pathol. 136 (1990) 867.

[41] D. Neill, D. Hughes, J.A. Edwardson, B.K. Rima, D. Allsop, Human IMR-32 neuroblastoma cells as a model cell line in Alzheimer's disease research. J. Neuroscience.39 (1994) 482.

[42] R.R. Rao, W.S. Kisaalita, Design and evaluation of a dual-purpose experimental system for exposure of mammalian cells to extremely low frequency (ELF) magnetic fields, Bioelectromagnetics (2001) Submitted.

[43] R.R. Rao, W.S. Kisaalita, Development of a distinct phenotype of a human neuroblastoma (IMR-32) cell line by chemical control of differentiation, Cytotechnology. (2001) Submitted.

[44] W.S. Kisaalita, J.M Bowen, Effect of culture age on the susceptibility of differentiating neuroblastoma cells to retinoid cytotoxicity. Biotech. Bioeng. 50 (1996) 580.

[45] P. Breysse, P.S.J. Lees, M.A. McDiarmid, B. Curbow, ELF Magnetic Field Exposures in an Office Environment. Am. J. Ind. Med. 25 (1994) 177.

[46] A.S. Farag, M.M. Dawoud, S.Z. Selim, T.C. Cheng, A.M. Marcus, D. Penn, Electromagnetic fields in the home. Electric Power Systems Res. 45 (1998) 73.

[47] T. A. Litovitz, C.J. Montrose, W. Wang, Dose-response implications of the transient nature of electromagnetic field induced bioeffects: theoretical hypotheses and predictions, Bioelectromagnetics, Suppl.1 (1992) 237.

[48] J.M. Lary, D.L. Conover, P.H. Johnson, J.A. Burg, Teratogenicity of 27.12 MHz radiation in rats is related to duration of hyperthermic exposure, Bioelectromagnetics, 4 (1983) 249.

[49] M.A. Germain, W.S. Webster, M.J. Edwards, Hyperthermia as a teratogen: parameters determining hyperthermia-induced head defects in the rat. Teratology, 31 (1985) 265.

[50] D.A. Rodeberg, J.G. Meyer, G.F. Babcock, Heat shock response: presence and effects in burn patient neutrophils, J. Leukocyte Biol. 66 (1999) 773.

[51] Gibco BRL Life Technologies, TRIzol^{TM} Reagent. Doc. 3796, 1999.

[52] T.E. Golde, S. Estus, M. Usiak, L.H. Younkin, S.G. Younkin, Expression of beta amyloid protein precursor mRNAs: recognition of a novel alternatively spliced form and quantitation in Alzheimer's disease using PCR. Neuron. 4 (1990) 253.

[53] G.H. Harrison, E.K. Balcer-Kubiczek, Z-M. Shi, Y-F. Zhang, W.A. McCready, C.C. Davis, Kinetics of gene expression following exposure to 60 Hz, 2 mT magnetic fields in three human cell lines, Bioelectrochem. Bioenerg. 43 (1997) 1.

[54] G. Chen, B.L. Upham, W. Sun, C-C. Chang, E.J. Rothwell, K-M. Chen, H. Yamasaki, J.E. Trosko, Effect of Electromagnetic Field Exposure on Chemically Induced Differentiation of Friend Erythroleukemia Cells, Environ. Health. Perspect 108 (2000) 967.

[55] C. Gotti, E. Sher, D. Cabrini, G. Bondiolotti, E. Wanke, E. Mancinelli, F. Clementi, Cholinergic receptors, ion channels, neurotransmitter synthesis, and neurite outgrowth are independently regulated during the in vitro differentiation of a human neuroblastoma cell line. Differentiation, 34 (1987) 144.

[56] S.S. Sisodia, Alzheimer's disease: perspective for the new millennium, J. Clinical Investigation, 104 (1999) 1169.

[57] M. Blank, L. Soo, Enhancement of cytochrome oxidase activity in 60 Hz magnetic fields. Bioelectrochem. Bioenerg. 45 (1998) 253.

[58] M. Blank, L. Soo, The threshold for Na, K-ATPase stimulation by electromagnetic fields. Bioelectrochem. Bioenerg. 40 (1996) 63.

[59] M. Blank, R. Goodman, An electrochemical model for the stimulation of biosynthesis by external electric fields. Bioelectrochem. Bioenerg. 19 (1988) 569.

[60] M. Blank, L. Soo, The effects of alternating currents on Na, K-ATPase function. Bioelectrochem. Bioenerg. 22 (1989) 313.

[61] M. Blank, L. Soo, The threshold for alternating current inhibition of the Na, K-ATPase. Bioelectromagnetics. 13 (1992) 329.

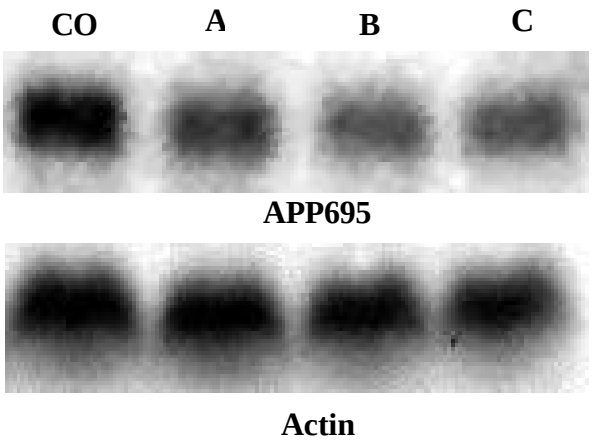

Figure 5.1. Northern blots for expression of APP695 in 10 day old BrdU-differentiated IMR-32 following a 4 hr magnetic field exposure at 200 μT. CO= Control; A= Exposed; B= Sham; C= External Coil.

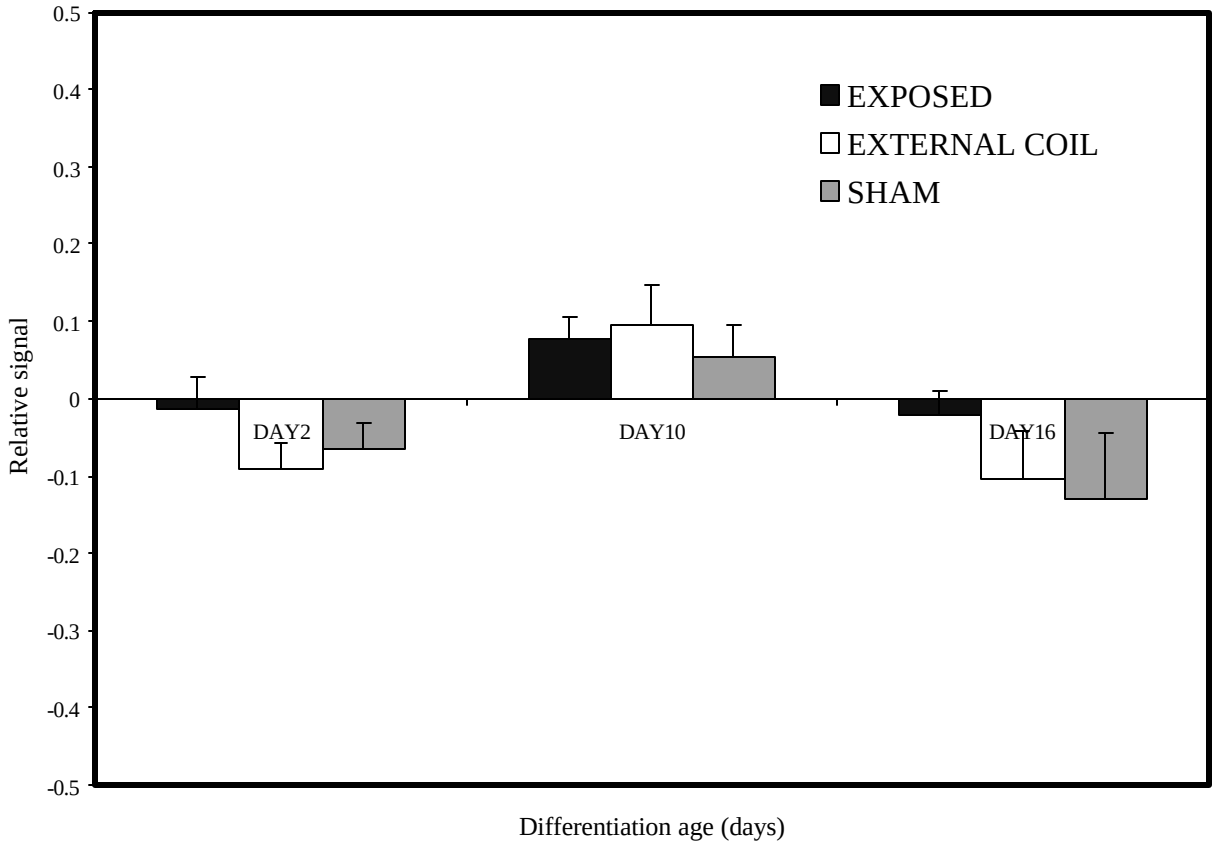

Figure 5.2. Mean expression of APP695 relative transcription (n=3) in BrdU-differentiated IMR-32 cells following 60 Hz magnetic field exposure (100 μT, 4 h). Error bars represent standard error of the mean.

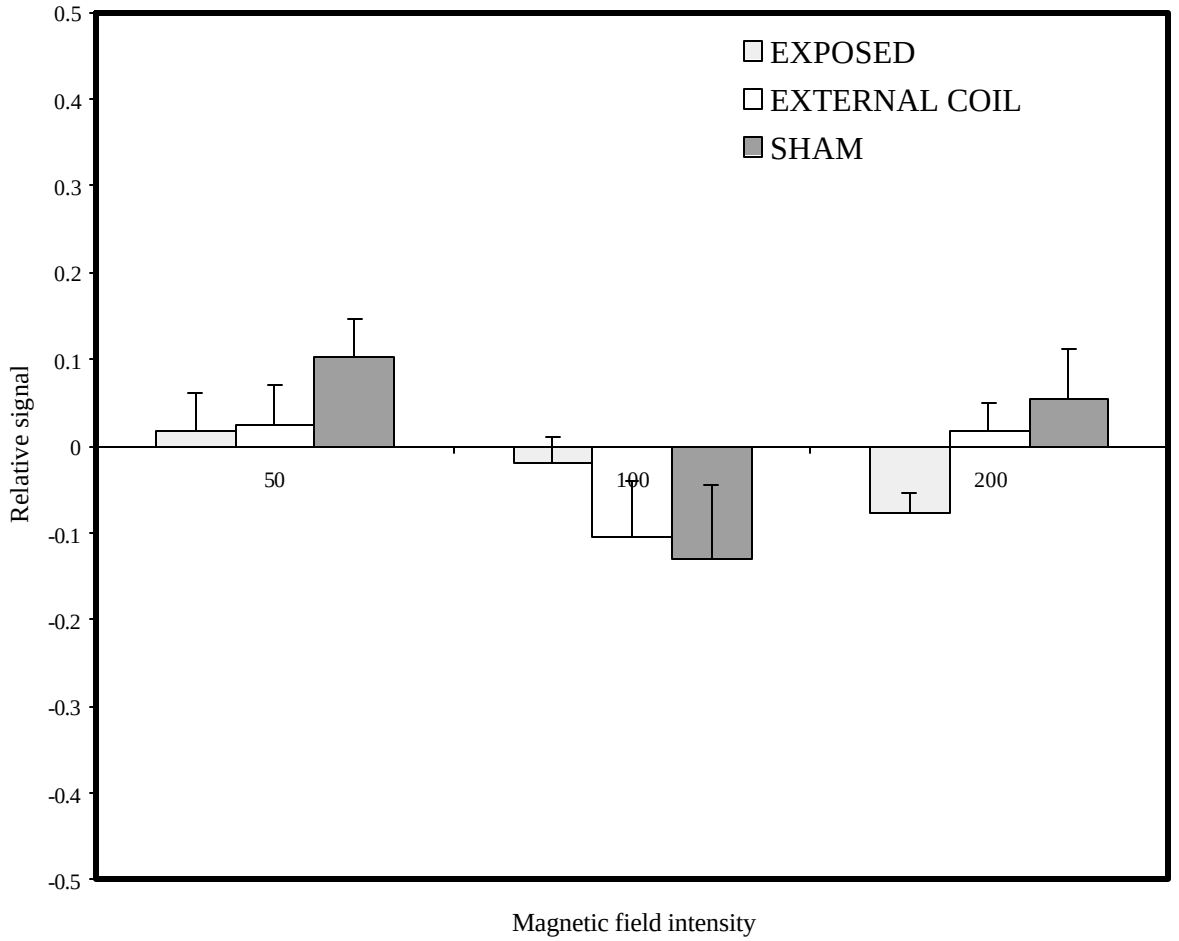

Figure 5.3. Mean expression of APP695 relative transcription (n=3) in 16-day old BrdU-differentiated IMR-32 cells following 60 Hz magnetic field exposure (4 h). Error bars represent standard error of the mean.

Table 5.1. An example of front panel switch combinations with corresponding exposure modes[a].

F1	F2	F3[c]	EXPOSURE MODE
0	0	0	EXP
0	1	0	SHAM
1	0	0	SHAM
1	1	0	EXP
X[b]	X	1	EXT

[a]Three internal rotary switches designated RS1, RS2 and RS3, control the "meaning" of the three front panel switches F1, F2 and F3. By changing RS switch setting, the front panel (F) switch meaning is altered. RS1 and RS2 control the polarity of the magnetic fields that are generated by the two coils to exposure (EXP) [current flowing in the same direction that magnetic fields from both coils are additive], sham-exposure (SHAM) [current flowing in opposite directions that magnetic fields from both coils cancel each other], and external coil activation: (EXT) [current flowing to an identical coil located more than 1m away from the biological specimen].

[b]X implies that the switch can take either the value of 0 or 1 without affecting the outcome.

[c]The setting of RS3 determines which one of the three front panel switches is to be the controller of the "External Coil/Exposure Coil" mode. (In our combination, F3 is the controller).

Table 5.2. Statistical comparison of control (unexposed) and exposed IMR-32 human neuroblastoma APP695 relative transcription levels. (EXP- Field- Exposed; SHAM- Sham- exposed; EXT- External coil activation)

50 μT								
Day 2	**Day 2**	**Day 2**	**Day 10**	**Day 10**	**Day 10**	**Day 16**	**Day 16**	**Day 16**
EXP	**SHAM**	**EXT**	**EXP**	**SHAM**	**EXT**	**EXP**	**SHAM**	**EXT**
0.2613[a]	0.1469	0.5466	0.3557	0.8595	0.9749	0.7289	0.5540	0.1458
don't rej. H_o	don't rej. H_o	don't rej. H_o	don't rej. H_o	don't rej. H_o	don't rej. H_o	don't rej. H_o	don't rej. H_o	don't rej. H_o
100 μT								
0.7636	0.1968	0.1165	0.1140	0.3234	0.2179	0.5639	0.2660	0.2391
don't rej. H_o	don't rej. H_o	don't rej. H_o	don't rej. H_o	don't rej. H_o	don't rej. H_o	don't rej. H_o	don't rej. H_o	don't rej. H_o
200 μT								
0.6842	0.6441	0.7298	0.2694	0.2471	0.4226	0.0735	0.4709	0.6446
don't rej. H_o	don't rej. H_o	don't rej. H_o	don't rej. H_o	don't rej. H_o	don't rej. H_o	don't rej. H_o	don't rej. H_o	don't rej. H_o

[a] p-values for t-test (p-value > 0.05 = don't reject H_o)

CHAPTER 6

CONCLUSIONS

The impetus behind this research was to take the first step towards testing the cellular effects of extremely low-frequency electromagnetic field exposure in the etiology of Alzheimer's disease. To achieve this, it was necessary to first characterize the experimental cellular model (IMR-32, human neuroblastoma) and magnetic field exposure systems. The study was thus conducted in three parts.

First, the in vitro differentiation of the human neuroblastoma cell line, IMR-32 was characterized with respect to morphological, electrophysiological (resting membrane potential) and biochemical (neuron specific enolase activity) markers. Results from these experiments supported the following conclusions:

1) IMR-32 exhibited in vitro differentiation based on morphological and biochemical but not electrophysiological markers (lack of V_m development).

2) With respect to the biochemical marker (neuron specific enolase activity), three differentiation ages were identified: undifferentiated (young: 0-8 days), differentiating (maturing: 8-14 days) and differentiated (mature: >14 days).

Second, a controlled ELF-EMF exposure system for investigating real time responses in vitro was designed and evaluated. Furthermore, the system was used to investigate the effects of ELF-EMF (200 μT, 60 Hz) on resting membrane potential in "maturing" (10 days) IMR-32 cells. Results from these experiments supported the following conclusions:

3) It is feasible to use the same exposure system for short exposure real time ionic flux studies and longer exposure gene transcription experiments.

4) ELF-EMF exposure depolarizes differentiating IMR-32 cells by probably interacting with the Na^+/K^+/ATPase pump.

Third, northern analysis was used to measure the APP695 mRNA transcription levels in differentiating IMR-32 cells exposed to power frequency electromagnetic fields (50-200 μT). Results from these experiments provided the following conclusions:

5) Differentiation age (young cells: 2 days, maturing cells: 10 days, differentiated cells: 16 days) had no effect on APP695 gene transcription in response to continuos (4 h) magnetic field exposure.

6) Increase in magnetic field intensity (50-200 μT) for a continuos (4 h) period had no effect on APP695 gene transcription in IMR-32 cells.

FUTURE DIRECTIONS

The studies conducted in this research have provided avenues to investigate further the plausible role of ELF-EMF in the etiology of AD. The development of the controlled experimental system for exposure studies makes it possible to pursue different in vitro experimental approaches. Studies with IMR-32 have demonstrated that characterization of neuroblastoma cells with respect to differentiation is very critical in developing unique experimental models, with which specific objectives could be addressed. The working hypothesis that ELF-EMF exposure might induce cellular effects related to AD pathogenesis needs further exploration, which may be accomplished through the following specific aims:

Specific Aim 1: Determine the differentiation profile with respect to morphological, biochemical and electrophysiological markers in IMR-32 cells with dibutryl cyclic AMP as the differentiating agent.

The purpose under this aim will be to confirm the development of an electrically excitable phenotype (low resting membrane potential) which might behave differently (compared to the present phenotype) when exposed to ELF-EMF under different ionic environments. The results obtained using the new excitable phenotype might be useful in the elucidation of physical interaction mechanisms related to ELF-EMF exposure.

Specific Aim 2: Determine the effect of ELF-EMF on changes in intracellular calcium ($[Ca^{2+}]_i$) in real time, in differentiating IMR-32 cells.

Since calcium is an important second messenger and may be involved in AD pathogenesis (Chen and Fernandez, 1999; Heinenger, 2000), it would be useful to study $[Ca^{2+}]_i$ changes in IMR-32 cells exposed to ELF-EMF. These experiments might provide insights into the question of whether ELF-EMF exposure affects AD 'manifestations' via Ca^{2+}-mediated signaling. Such data would offer a unique starting point for producing integrative models similar to the one outlined for cardiac excitation (Rudy, 2000).

Specific Aim 3: Determine the real time spatial and temporal changes in APP in response to ELF-EMF exposure using the circular coil setup.

Our laboratory is in the development stages of a transfected IMR-32, containing the APP in fusion with Green Fluorescence Protein (GFP). With the aid of the fluorescence signal from GFP, in conjunction with confocal microscopy, it will be possible to monitor spatial temporal APP changes in response to ELF-EMF exposure at the single cell level. This study has potential to provide evidence in support of the involvement of ELF-EMF in the etiology of AD pathogenesis at the protein processing level.

References

1. Chen M, Fernandez HL. (1999). The Alzheimer's plaques, tangles and memory deficits may have a common origin. Why is Ca^{2+} signal lower in the disease? Front Biosci 4:A9.
2. Heininger K. (2000). A unifying hypothesis of Alzheimer's disease. Causation and sequence of events. Rev Neurosci. 2000; 11 Spec No: 213.
3. Rudy Y. 2000. From Genome to Physiome: Integrative Models of Cardiac Excitation. Annals of Biomedical Engineering. 28: 945-50.

APPENDIX A

RAW DATA FOR CHAPTER 3

Table A1. Raw flow cytometry data for differentiating IMR-32 cells (Day 0, 1st replicate) used to generate Figure 3.2.

Channel #	*f*	Channel #	*f*	Channel #	*f*	Channel #	*f*	Channel #	*f*	Channel #	*f*
1	0	44	3	87	1	130	4	173	4	216	0
2	1	45	3	88	4	131	3	174	2	217	3
3	1	46	0	89	2	132	4	175	3	218	3
4	39	47	2	90	1	133	6	176	5	219	5
5	593	48	6	91	6	134	2	177	4	220	5
6	46	49	8	92	4	135	5	178	3	221	4
7	10	50	0	93	2	136	0	179	5	222	5
8	3	51	3	94	4	137	4	180	6	223	7
9	0	52	3	95	3	138	2	181	4	224	5
10	1	53	2	96	1	139	4	182	3	225	3
11	1	54	2	97	4	140	1	183	6	226	3
12	2	55	2	98	1	141	3	184	0	227	5
13	1	56	4	99	5	142	4	185	4	228	3
14	3	57	3	100	6	143	4	186	1	229	2
15	1	58	0	101	2	144	2	187	7	230	4
16	1	59	5	102	4	145	3	188	5	231	4
17	3	60	2	103	5	146	5	189	7	232	1
18	5	61	4	104	2	147	0	190	1	233	6
19	4	62	2	105	4	148	8	191	4	234	7
20	2	63	2	106	1	149	3	192	4	235	7
21	2	64	2	107	6	150	10	193	1	236	3
22	1	65	5	108	1	151	3	194	2	237	2
23	4	66	3	109	4	152	8	195	10	238	4
24	1	67	3	110	6	153	2	196	3	239	7
25	4	68	5	111	1	154	4	197	2	240	3
26	2	69	1	112	5	155	1	198	3	241	8
27	4	70	2	113	9	156	6	199	2	242	5
28	4	71	4	114	1	157	4	200	8	243	5
29	0	72	0	115	5	158	4	201	3	244	8
30	1	73	3	116	4	159	2	202	4	245	9
31	3	74	4	117	1	160	5	203	3	246	4
32	2	75	2	118	6	161	1	204	4	247	6
33	2	76	2	119	8	162	6	205	2	248	6
34	2	77	3	120	3	163	6	206	6	249	6
35	2	78	5	121	1	164	5	207	5	250	9
36	5	79	5	122	3	165	2	208	3	251	9
37	1	80	4	123	7	166	1	209	2	252	5
38	1	81	3	124	4	167	3	210	1	253	1
39	3	82	1	125	3	168	4	211	9	254	3
40	3	83	3	126	3	169	3	212	2	255	5
41	2	84	4	127	1	170	4	213	5	256	7
42	5	85	4	128	1	171	2	214	8	257	3
43	4	86	2	129	1	172	4	215	2	258	3

* Channel # and *f* represent oxonol fluorescence and frequency respectively.

Table A1. Continued.

Channel #	*f*	Channel #	*f*	Channel #	*f*	Channel #	*f*	Channel #	*f*	Channel #	*f*
259	10	302	6	345	10	388	7	431	9	474	4
260	7	303	4	346	5	389	7	432	9	475	5
261	5	304	3	347	7	390	9	433	11	476	4
262	4	305	3	348	9	391	6	434	10	477	7
263	7	306	6	349	6	392	7	435	7	478	14
264	9	307	6	350	2	393	8	436	7	479	9
265	2	308	7	351	12	394	8	437	8	480	8
266	7	309	4	352	5	395	12	438	7	481	9
267	5	310	4	353	5	396	5	439	6	482	4
268	2	311	7	354	2	397	6	440	8	483	5
269	3	312	6	355	5	398	8	441	14	484	6
270	3	313	7	356	5	399	13	442	7	485	8
271	4	314	7	357	11	400	10	443	7	486	1
272	7	315	7	358	6	401	7	444	8	487	6
273	12	316	8	359	6	402	10	445	8	488	7
274	9	317	5	360	6	403	13	446	6	489	9
275	6	318	4	361	6	404	8	447	6	490	6
276	3	319	7	362	7	405	7	448	8	491	16
277	3	320	7	363	9	406	8	449	12	492	11
278	3	321	7	364	7	407	7	450	5	493	11
279	4	322	7	365	7	408	12	451	3	494	8
280	2	323	7	366	6	409	3	452	6	495	9
281	6	324	3	367	8	410	4	453	13	496	13
282	2	325	3	368	5	411	7	454	4	497	9
283	2	326	9	369	6	412	10	455	11	498	7
284	2	327	9	370	8	413	7	456	10	499	7
285	2	328	7	371	7	414	3	457	7	500	4
286	5	329	9	372	7	415	5	458	7	501	12
287	5	330	7	373	4	416	6	459	9	502	10
288	5	331	5	374	9	417	3	460	12	503	10
289	12	332	6	375	4	418	11	461	8	504	9
290	6	333	8	376	7	419	8	462	6	505	9
291	6	334	6	377	13	420	6	463	9	506	12
292	10	335	3	378	7	421	6	464	6	507	4
293	8	336	6	379	10	422	9	465	9	508	7
294	3	337	8	380	5	423	8	466	6	509	10
295	6	338	3	381	6	424	6	467	5	510	12
296	4	339	10	382	4	425	6	468	9	511	7
297	6	340	9	383	6	426	9	469	4	512	9
298	3	341	10	384	3	427	7	470	9	513	13
299	10	342	6	385	7	428	11	471	5	514	16
300	4	343	5	386	5	429	5	472	2	515	6
301	3	344	12	387	10	430	6	473	8	516	13

Table A1. Continued.

Channel #	*f*	Channel #	*f*	Channel #	*f*	Channel #	*f*	Channel #	*f*	Channel #	*f*
517	11	560	8	603	15	646	3	689	9	732	14
518	4	561	2	604	7	647	4	690	13	733	11
519	9	562	7	605	7	648	13	691	10	734	18
520	10	563	7	606	10	649	7	692	8	735	9
521	7	564	5	607	8	650	12	693	9	736	14
522	14	565	6	608	6	651	9	694	10	737	11
523	12	566	6	609	4	652	5	695	8	738	12
524	12	567	10	610	7	653	10	696	6	739	17
525	10	568	9	611	5	654	9	697	17	740	14
526	10	569	9	612	3	655	8	698	8	741	15
527	7	570	7	613	6	656	9	699	10	742	12
528	6	571	4	614	12	657	7	700	11	743	9
529	7	572	10	615	6	658	8	701	8	744	14
530	6	573	6	616	8	659	6	702	10	745	14
531	11	574	11	617	6	660	4	703	6	746	13
532	7	575	4	618	2	661	7	704	8	747	16
533	6	576	4	619	9	662	11	705	6	748	16
534	9	577	7	620	6	663	7	706	16	749	15
535	10	578	4	621	4	664	7	707	11	750	12
536	11	579	7	622	8	665	8	708	7	751	17
537	9	580	11	623	15	666	5	709	16	752	14
538	7	581	2	624	8	667	9	710	14	753	21
539	0	582	9	625	9	668	5	711	6	754	19
540	12	583	7	626	13	669	5	712	7	755	14
541	6	584	5	627	6	670	9	713	12	756	24
542	8	585	11	628	7	671	7	714	9	757	15
543	9	586	7	629	4	672	11	715	10	758	19
544	12	587	8	630	9	673	7	716	12	759	13
545	9	588	8	631	11	674	7	717	9	760	18
546	11	589	8	632	9	675	9	718	15	761	17
547	11	590	7	633	4	676	6	719	11	762	16
548	6	591	8	634	3	677	5	720	17	763	17
549	11	592	10	635	5	678	9	721	9	764	13
550	9	593	6	636	7	679	3	722	8	765	16
551	11	594	5	637	6	680	13	723	9	766	23
552	7	595	2	638	7	681	11	724	15	767	22
553	7	596	6	639	13	682	13	725	9	768	16
554	4	597	3	640	8	683	9	726	9	769	15
555	9	598	6	641	13	684	9	727	8	770	16
556	6	599	8	642	7	685	9	728	17	771	24
557	7	600	7	643	1	686	6	729	16	772	25
558	11	601	6	644	13	687	9	730	8	773	13
559	6	602	11	645	5	688	10	731	7	774	18

Table A1. Continued.

Channel #	*f*	Channel #	*f*	Channel #	*f*	Channel #	*f*	Channel #	*f*	Channel #	*f*
775	16	818	26	861	13	904	16	947	27	990	10
776	15	819	14	862	27	905	22	948	21	991	6
777	17	820	16	863	31	906	16	949	19	992	10
778	17	821	17	864	24	907	29	950	17	993	7
779	19	822	23	865	20	908	21	951	10	994	9
780	19	823	15	866	16	909	9	952	14	995	7
781	25	824	19	867	17	910	19	953	13	996	7
782	33	825	28	868	19	911	15	954	17	997	4
783	9	826	21	869	31	912	20	955	20	998	8
784	14	827	24	870	19	913	15	956	13	999	4
785	18	828	19	871	23	914	26	957	18	1000	10
786	25	829	26	872	31	915	25	958	20	1001	10
787	27	830	29	873	30	916	21	959	14	1002	7
788	16	831	23	874	15	917	17	960	14	1003	6
789	15	832	16	875	17	918	21	961	20	1004	2
790	25	833	19	876	23	919	26	962	17	1005	6
791	17	834	21	877	19	920	22	963	13	1006	3
792	18	835	29	878	15	921	15	964	21	1007	5
793	21	836	29	879	14	922	21	965	18	1008	5
794	22	837	15	880	21	923	21	966	30	1009	2
795	19	838	23	881	11	924	21	967	11	1010	1
796	18	839	18	882	17	925	13	968	11	1011	0
797	21	840	28	883	25	926	15	969	18	1012	1
798	27	841	22	884	16	927	14	970	13	1013	3
799	19	842	23	885	13	928	21	971	9	1014	1
800	17	843	24	886	20	929	14	972	15	1015	1
801	20	844	22	887	17	930	15	973	12	1016	0
802	16	845	20	888	16	931	31	974	14	1017	0
803	31	846	29	889	20	932	19	975	11	1018	1
804	26	847	21	890	20	933	19	976	16	1019	0
805	14	848	20	891	15	934	25	977	9	1020	0
806	20	849	17	892	27	935	23	978	10	1021	1
807	18	850	27	893	14	936	23	979	7	1022	0
808	15	851	23	894	19	937	12	980	9	1023	0
809	22	852	21	895	14	938	20	981	6	1024	0
810	14	853	18	896	18	939	18	982	10		
811	21	854	28	897	19	940	29	983	3		
812	24	855	14	898	22	941	15	984	9		
813	14	856	15	899	20	942	16	985	11		
814	30	857	21	900	14	943	21	986	11		
815	19	858	15	901	15	944	19	987	7		
816	17	859	26	902	21	945	16	988	9		
817	24	860	13	903	16	946	22	989	4		

Table A2. Raw flow cytometry data for differentiating IMR-32 (Day 0, 2nd replicate) used to generate Figure 3.2.

Channel #	*f*	Channel #	*f*	Channel #	*f*	Channel #	*f*	Channel #	*f*	Channel #	*f*
1	0	44	0	87	0	130	2	173	1	216	0
2	0	45	0	88	0	131	0	174	0	217	0
3	0	46	0	89	0	132	0	175	1	218	0
4	0	47	0	90	1	133	0	176	0	219	0
5	17	48	1	91	0	134	0	177	0	220	0
6	13	49	0	92	0	135	1	178	0	221	0
7	6	50	0	93	0	136	0	179	0	222	0
8	1	51	0	94	0	137	0	180	0	223	0
9	0	52	0	95	0	138	1	181	0	224	1
10	0	53	0	96	0	139	0	182	0	225	0
11	0	54	0	97	0	140	0	183	0	226	0
12	1	55	1	98	0	141	0	184	0	227	1
13	0	56	0	99	0	142	0	185	0	228	1
14	0	57	1	100	0	143	0	186	1	229	1
15	0	58	1	101	0	144	0	187	0	230	0
16	0	59	0	102	0	145	1	188	0	231	0
17	0	60	0	103	0	146	0	189	0	232	1
18	0	61	0	104	0	147	0	190	0	233	1
19	0	62	0	105	0	148	0	191	0	234	0
20	0	63	0	106	0	149	0	192	0	235	1
21	0	64	0	107	1	150	1	193	1	236	0
22	0	65	0	108	0	151	0	194	0	237	0
23	1	66	0	109	0	152	0	195	1	238	0
24	1	67	0	110	0	153	0	196	2	239	0
25	0	68	0	111	0	154	0	197	0	240	0
26	0	69	1	112	0	155	0	198	0	241	0
27	0	70	0	113	0	156	0	199	0	242	0
28	0	71	0	114	0	157	0	200	0	243	1
29	0	72	0	115	0	158	0	201	0	244	0
30	0	73	0	116	0	159	0	202	0	245	0
31	0	74	0	117	0	160	0	203	0	246	0
32	0	75	0	118	0	161	0	204	1	247	1
33	0	76	0	119	0	162	0	205	0	248	1
34	0	77	0	120	0	163	0	206	1	249	2
35	0	78	0	121	0	164	0	207	1	250	2
36	0	79	0	122	0	165	0	208	1	251	0
37	0	80	1	123	1	166	0	209	1	252	0
38	0	81	0	124	0	167	2	210	0	253	0
39	0	82	0	125	1	168	0	211	1	254	0
40	0	83	0	126	0	169	0	212	0	255	1
41	1	84	1	127	0	170	0	213	0	256	0
42	0	85	0	128	0	171	1	214	0	257	1
43	0	86	0	129	0	172	0	215	1	258	0

* Channel # and *f* represent oxonol fluorescence and frequency respectively.

Table A2. Continued.

Channel #	*f*	Channel #	*f*	Channel #	*f*	Channel #	*f*	Channel #	*f*	Channel #	*f*
259	3	302	0	345	1	388	1	431	2	474	0
260	0	303	3	346	1	389	4	432	1	475	4
261	0	304	0	347	5	390	3	433	1	476	3
262	0	305	2	348	4	391	2	434	0	477	3
263	1	306	0	349	2	392	2	435	3	478	3
264	2	307	1	350	1	393	0	436	4	479	6
265	1	308	2	351	1	394	3	437	2	480	3
266	0	309	1	352	2	395	4	438	1	481	5
267	1	310	0	353	1	396	3	439	2	482	0
268	0	311	1	354	1	397	2	440	1	483	5
269	1	312	3	355	1	398	3	441	2	484	2
270	0	313	1	356	0	399	1	442	1	485	6
271	1	314	1	357	1	400	1	443	3	486	5
272	1	315	0	358	0	401	3	444	5	487	4
273	0	316	2	359	1	402	0	445	4	488	2
274	0	317	0	360	1	403	0	446	1	489	7
275	0	318	1	361	1	404	0	447	3	490	0
276	1	319	2	362	2	405	1	448	2	491	5
277	1	320	1	363	3	406	2	449	3	492	3
278	0	321	1	364	4	407	3	450	3	493	2
279	1	322	2	365	1	408	1	451	3	494	5
280	2	323	1	366	1	409	1	452	3	495	6
281	2	324	0	367	2	410	3	453	2	496	6
282	2	325	1	368	0	411	0	454	3	497	4
283	0	326	1	369	2	412	4	455	0	498	4
284	0	327	2	370	0	413	1	456	7	499	1
285	1	328	1	371	1	414	1	457	5	500	5
286	0	329	3	372	1	415	3	458	3	501	3
287	2	330	3	373	4	416	0	459	2	502	8
288	0	331	0	374	0	417	5	460	6	503	4
289	2	332	1	375	3	418	1	461	4	504	6
290	2	333	1	376	2	419	1	462	2	505	3
291	0	334	0	377	4	420	1	463	3	506	5
292	0	335	2	378	2	421	2	464	2	507	2
293	1	336	0	379	1	422	1	465	3	508	4
294	1	337	2	380	1	423	4	466	8	509	5
295	2	338	0	381	2	424	2	467	4	510	2
296	1	339	0	382	1	425	1	468	2	511	4
297	1	340	1	383	0	426	4	469	3	512	4
298	0	341	2	384	1	427	0	470	5	513	4
299	2	342	1	385	1	428	4	471	5	514	5
300	0	343	1	386	0	429	1	472	2	515	7
301	1	344	0	387	2	430	4	473	2	516	4

Table A2. Continued.

Channel #	*f*	Channel #	*f*	Channel #	*f*	Channel #	*f*	Channel #	*f*	Channel #	*f*
517	5	560	9	603	19	646	21	689	29	732	58
518	3	561	6	604	8	647	30	690	32	733	38
519	5	562	11	605	11	648	16	691	39	734	46
520	5	563	11	606	18	649	29	692	25	735	39
521	9	564	7	607	12	650	22	693	26	736	40
522	4	565	8	608	13	651	20	694	39	737	36
523	3	566	11	609	13	652	23	695	29	738	38
524	4	567	10	610	16	653	20	696	15	739	36
525	3	568	11	611	14	654	25	697	38	740	45
526	3	569	12	612	12	655	24	698	33	741	41
527	5	570	10	613	16	656	28	699	31	742	53
528	3	571	6	614	21	657	21	700	31	743	39
529	9	572	12	615	14	658	21	701	33	744	36
530	5	573	13	616	16	659	25	702	44	745	38
531	8	574	8	617	14	660	18	703	36	746	35
532	5	575	6	618	17	661	29	704	24	747	40
533	2	576	3	619	13	662	18	705	26	748	42
534	8	577	13	620	13	663	23	706	32	749	40
535	10	578	14	621	12	664	25	707	39	750	59
536	12	579	10	622	12	665	25	708	30	751	44
537	10	580	6	623	23	666	27	709	35	752	38
538	7	581	13	624	13	667	16	710	29	753	62
539	10	582	4	625	15	668	25	711	41	754	47
540	4	583	11	626	10	669	22	712	36	755	41
541	6	584	10	627	22	670	29	713	37	756	47
542	7	585	14	628	18	671	25	714	40	757	45
543	6	586	9	629	14	672	33	715	36	758	45
544	9	587	7	630	30	673	23	716	38	759	39
545	4	588	10	631	19	674	26	717	31	760	41
546	7	589	9	632	12	675	32	718	37	761	42
547	6	590	8	633	19	676	31	719	33	762	43
548	3	591	18	634	34	677	24	720	37	763	36
549	10	592	10	635	26	678	31	721	47	764	49
550	7	593	6	636	16	679	27	722	31	765	39
551	9	594	10	637	21	680	31	723	32	766	35
552	10	595	8	638	14	681	29	724	42	767	46
553	10	596	15	639	19	682	31	725	36	768	39
554	8	597	11	640	13	683	28	726	51	769	41
555	10	598	16	641	19	684	34	727	33	770	57
556	6	599	12	642	21	685	26	728	33	771	50
557	5	600	13	643	18	686	28	729	40	772	47
558	5	601	12	644	24	687	34	730	52	773	42
559	10	602	16	645	10	688	37	731	32	774	45

Table A2. Continued.

Channel #	*f*	Channel #	*f*	Channel #	*f*	Channel #	*f*	Channel #	*f*	Channel #	*f*
775	42	818	35	861	20	904	5	947	2	990	0
776	30	819	34	862	19	905	6	948	1	991	0
777	54	820	32	863	10	906	4	949	1	992	0
778	47	821	27	864	13	907	4	950	0	993	0
779	55	822	40	865	23	908	3	951	1	994	0
780	45	823	29	866	10	909	2	952	2	995	0
781	49	824	23	867	17	910	4	953	0	996	0
782	57	825	42	868	13	911	3	954	2	997	0
783	44	826	42	869	7	912	4	955	0	998	0
784	41	827	34	870	10	913	3	956	0	999	0
785	51	828	18	871	18	914	3	957	0	1000	0
786	46	829	27	872	17	915	2	958	1	1001	0
787	54	830	28	873	12	916	1	959	1	1002	0
788	49	831	30	874	8	917	6	960	0	1003	0
789	42	832	22	875	9	918	4	961	1	1004	0
790	57	833	35	876	9	919	3	962	0	1005	0
791	29	834	21	877	8	920	1	963	0	1006	0
792	41	835	41	878	14	921	3	964	0	1007	0
793	59	836	26	879	4	922	2	965	0	1008	0
794	38	837	23	880	9	923	0	966	0	1009	0
795	52	838	33	881	4	924	6	967	0	1010	0
796	43	839	21	882	12	925	1	968	0	1011	0
797	44	840	23	883	8	926	2	969	0	1012	0
798	42	841	30	884	5	927	3	970	0	1013	0
799	40	842	14	885	3	928	2	971	0	1014	0
800	38	843	30	886	11	929	3	972	0	1015	0
801	36	844	30	887	6	930	0	973	1	1016	0
802	40	845	28	888	8	931	0	974	0	1017	0
803	46	846	22	889	6	932	2	975	1	1018	0
804	44	847	17	890	6	933	3	976	0	1019	0
805	37	848	23	891	8	934	2	977	0	1020	0
806	49	849	17	892	6	935	1	978	1	1021	0
807	36	850	26	893	4	936	3	979	0	1022	0
808	40	851	21	894	6	937	2	980	0	1023	0
809	38	852	25	895	4	938	1	981	0	1024	0
810	30	853	16	896	6	939	0	982	0		
811	39	854	23	897	8	940	2	983	0		
812	36	855	19	898	7	941	0	984	0		
813	36	856	23	899	7	942	1	985	0		
814	57	857	19	900	6	943	0	986	0		
815	26	858	12	901	9	944	2	987	1		
816	33	859	26	902	5	945	1	988	1		
817	43	860	15	903	2	946	1	989	0		

Table A3. Raw flow cytometry data for differentiating IMR-32 cells (Day 0, 3rd replicate) used to generate Figure 3.2.

Channel #	*f*	Channel #	*f*	Channel #	*f*	Channel #	*f*	Channel #	*f*	Channel #	*f*
1	0	44	1	87	0	130	0	173	0	216	0
2	0	45	0	88	1	131	0	174	1	217	1
3	0	46	0	89	0	132	0	175	0	218	0
4	2	47	0	90	0	133	0	176	0	219	2
5	69	48	0	91	1	134	0	177	2	220	2
6	20	49	0	92	0	135	0	178	0	221	0
7	2	50	1	93	0	136	0	179	0	222	0
8	1	51	0	94	1	137	1	180	0	223	1
9	0	52	0	95	0	138	0	181	0	224	0
10	0	53	1	96	0	139	0	182	0	225	0
11	1	54	0	97	0	140	0	183	0	226	1
12	0	55	0	98	0	141	0	184	0	227	1
13	0	56	0	99	0	142	0	185	1	228	1
14	0	57	0	100	0	143	0	186	0	229	0
15	0	58	0	101	1	144	1	187	0	230	1
16	0	59	1	102	0	145	0	188	0	231	0
17	0	60	0	103	0	146	1	189	0	232	0
18	1	61	0	104	0	147	0	190	0	233	0
19	0	62	0	105	0	148	1	191	1	234	0
20	0	63	1	106	0	149	1	192	0	235	1
21	0	64	0	107	0	150	0	193	1	236	0
22	0	65	0	108	0	151	0	194	0	237	0
23	0	66	0	109	0	152	0	195	0	238	0
24	0	67	0	110	0	153	0	196	1	239	1
25	0	68	0	111	0	154	0	197	0	240	0
26	2	69	2	112	0	155	0	198	0	241	0
27	0	70	0	113	0	156	0	199	1	242	0
28	0	71	1	114	0	157	1	200	0	243	0
29	0	72	0	115	0	158	0	201	0	244	1
30	0	73	0	116	0	159	0	202	0	245	1
31	1	74	0	117	0	160	0	203	1	246	1
32	0	75	0	118	0	161	0	204	0	247	0
33	1	76	1	119	0	162	0	205	0	248	0
34	0	77	0	120	0	163	0	206	0	249	1
35	1	78	0	121	0	164	0	207	0	250	0
36	0	79	0	122	0	165	0	208	0	251	1
37	0	80	0	123	1	166	0	209	0	252	1
38	2	81	0	124	0	167	0	210	2	253	0
39	0	82	0	125	0	168	0	211	0	254	0
40	0	83	0	126	0	169	0	212	0	255	0
41	0	84	0	127	0	170	0	213	1	256	1
42	0	85	0	128	0	171	1	214	0	257	0
43	0	86	0	129	0	172	0	215	2	258	2

* Channel # and *f* represent oxonol fluorescence and frequency respectively.

Table A3. Continued.

Channel #	*f*	Channel #	*f*	Channel #	*f*	Channel #	*f*	Channel #	*f*	Channel #	*f*
259	0	302	0	345	0	388	2	431	2	474	2
260	0	303	0	346	0	389	1	432	1	475	1
261	0	304	0	347	2	390	0	433	1	476	1
262	0	305	0	348	0	391	2	434	3	477	3
263	0	306	0	349	1	392	1	435	3	478	2
264	0	307	1	350	1	393	2	436	0	479	2
265	0	308	1	351	1	394	0	437	3	480	5
266	1	309	0	352	0	395	2	438	0	481	4
267	0	310	1	353	1	396	5	439	2	482	3
268	1	311	1	354	1	397	0	440	1	483	4
269	1	312	1	355	0	398	1	441	1	484	6
270	1	313	2	356	0	399	0	442	1	485	1
271	0	314	0	357	0	400	1	443	3	486	2
272	0	315	0	358	0	401	4	444	3	487	5
273	0	316	0	359	0	402	0	445	3	488	3
274	0	317	0	360	2	403	1	446	1	489	5
275	0	318	0	361	2	404	2	447	1	490	1
276	0	319	0	362	2	405	4	448	0	491	4
277	1	320	0	363	0	406	1	449	1	492	2
278	0	321	2	364	0	407	1	450	1	493	1
279	1	322	1	365	2	408	0	451	5	494	2
280	0	323	0	366	1	409	1	452	1	495	2
281	1	324	0	367	0	410	4	453	2	496	3
282	0	325	0	368	1	411	2	454	1	497	2
283	2	326	0	369	1	412	0	455	6	498	2
284	0	327	3	370	1	413	2	456	0	499	2
285	0	328	1	371	1	414	0	457	1	500	3
286	0	329	0	372	1	415	1	458	0	501	2
287	2	330	1	373	0	416	1	459	3	502	3
288	1	331	0	374	0	417	1	460	1	503	4
289	0	332	0	375	3	418	1	461	1	504	6
290	0	333	3	376	2	419	3	462	3	505	3
291	1	334	0	377	1	420	0	463	3	506	3
292	1	335	0	378	2	421	1	464	0	507	2
293	2	336	0	379	1	422	1	465	3	508	3
294	1	337	0	380	2	423	2	466	3	509	4
295	0	338	0	381	0	424	1	467	4	510	4
296	0	339	0	382	1	425	0	468	1	511	1
297	0	340	2	383	0	426	6	469	1	512	6
298	1	341	2	384	2	427	0	470	1	513	2
299	0	342	0	385	4	428	4	471	5	514	3
300	0	343	4	386	2	429	2	472	3	515	5
301	0	344	0	387	0	430	2	473	1	516	2

Table A3. Continued.

Channel #	*f*	Channel #	*f*	Channel #	*f*	Channel #	*f*	Channel #	*f*	Channel #	*f*
517	4	560	4	603	12	646	8	689	19	732	31
518	1	561	3	604	6	647	12	690	18	733	29
519	2	562	3	605	8	648	11	691	28	734	34
520	6	563	3	606	5	649	13	692	15	735	24
521	1	564	2	607	9	650	11	693	23	736	25
522	4	565	3	608	9	651	14	694	21	737	41
523	5	566	2	609	8	652	10	695	17	738	37
524	4	567	5	610	5	653	16	696	22	739	43
525	3	568	8	611	3	654	15	697	24	740	23
526	7	569	5	612	8	655	18	698	17	741	37
527	1	570	4	613	8	656	6	699	25	742	40
528	6	571	7	614	4	657	25	700	25	743	26
529	4	572	3	615	8	658	12	701	21	744	24
530	4	573	5	616	4	659	12	702	19	745	41
531	3	574	5	617	11	660	9	703	17	746	33
532	5	575	6	618	16	661	10	704	25	747	47
533	1	576	4	619	7	662	14	705	27	748	32
534	3	577	2	620	3	663	17	706	19	749	40
535	6	578	1	621	9	664	7	707	30	750	40
536	3	579	4	622	5	665	16	708	20	751	43
537	3	580	3	623	12	666	12	709	24	752	28
538	3	581	3	624	8	667	10	710	24	753	39
539	1	582	6	625	9	668	10	711	39	754	40
540	4	583	5	626	12	669	11	712	20	755	34
541	4	584	6	627	8	670	14	713	19	756	27
542	6	585	5	628	9	671	18	714	28	757	37
543	7	586	4	629	8	672	16	715	29	758	30
544	3	587	8	630	8	673	17	716	23	759	38
545	4	588	3	631	8	674	11	717	32	760	30
546	4	589	9	632	3	675	19	718	25	761	30
547	5	590	3	633	11	676	14	719	22	762	34
548	4	591	9	634	11	677	9	720	36	763	45
549	2	592	11	635	6	678	15	721	30	764	35
550	4	593	6	636	9	679	13	722	19	765	35
551	2	594	9	637	6	680	17	723	34	766	30
552	1	595	6	638	13	681	17	724	32	767	34
553	5	596	4	639	8	682	16	725	17	768	40
554	5	597	6	640	11	683	14	726	37	769	29
555	5	598	7	641	14	684	12	727	23	770	42
556	3	599	5	642	6	685	23	728	38	771	47
557	7	600	9	643	4	686	20	729	25	772	42
558	5	601	8	644	7	687	18	730	40	773	44
559	2	602	8	645	9	688	15	731	36	774	37

Table A3. Continued.

Channel #	*f*	Channel #	*f*	Channel #	*f*	Channel #	*f*	Channel #	*f*	Channel #	*f*
775	38	818	47	861	31	904	11	947	3	990	2
776	36	819	51	862	37	905	12	948	8	991	3
777	44	820	39	863	32	906	11	949	3	992	2
778	46	821	48	864	33	907	17	950	2	993	1
779	51	822	50	865	39	908	8	951	7	994	0
780	44	823	45	866	35	909	17	952	3	995	4
781	45	824	47	867	51	910	23	953	4	996	1
782	40	825	40	868	21	911	17	954	5	997	1
783	47	826	52	869	37	912	8	955	5	998	0
784	33	827	60	870	52	913	9	956	1	999	0
785	44	828	58	871	39	914	14	957	7	1000	1
786	29	829	35	872	38	915	13	958	5	1001	0
787	37	830	51	873	34	916	11	959	1	1002	0
788	43	831	34	874	38	917	7	960	3	1003	0
789	40	832	40	875	39	918	12	961	7	1004	0
790	51	833	55	876	20	919	18	962	1	1005	0
791	34	834	50	877	29	920	7	963	4	1006	0
792	40	835	60	878	51	921	6	964	0	1007	0
793	42	836	40	879	29	922	13	965	2	1008	0
794	41	837	41	880	17	923	12	966	6	1009	0
795	53	838	45	881	34	924	7	967	2	1010	0
796	49	839	37	882	36	925	2	968	3	1011	0
797	34	840	55	883	28	926	10	969	4	1012	0
798	49	841	49	884	27	927	7	970	4	1013	0
799	43	842	41	885	26	928	9	971	1	1014	0
800	41	843	54	886	33	929	6	972	3	1015	0
801	35	844	53	887	16	930	8	973	0	1016	0
802	51	845	40	888	28	931	14	974	2	1017	0
803	55	846	51	889	19	932	10	975	2	1018	0
804	53	847	46	890	21	933	4	976	2	1019	0
805	33	848	37	891	22	934	8	977	1	1020	0
806	50	849	52	892	28	935	3	978	0	1021	0
807	45	850	53	893	19	936	10	979	1	1022	0
808	41	851	46	894	17	937	6	980	1	1023	0
809	26	852	34	895	20	938	3	981	1	1024	0
810	40	853	43	896	18	939	8	982	3		
811	47	854	46	897	19	940	5	983	1		
812	38	855	36	898	26	941	6	984	1		
813	40	856	49	899	14	942	8	985	3		
814	61	857	41	900	24	943	9	986	3		
815	35	858	40	901	15	944	2	987	0		
816	42	859	42	902	9	945	4	988	0		
817	45	860	42	903	20	946	3	989	0		

Table A4. Raw flow cytometry data for differentiating IMR-32 cells (Day 2, 1st replicate) used to generate Figure 3.2.

Channel #	*f*	Channel #	*f*	Channel #	*f*	Channel #	*f*	Channel #	*f*	Channel #	*f*
1	0	44	4	87	1	130	0	173	2	216	2
2	1	45	5	88	2	131	9	174	3	217	5
3	0	46	3	89	3	132	2	175	5	218	3
4	9	47	3	90	2	133	1	176	1	219	5
5	198	48	2	91	3	134	4	177	5	220	3
6	53	49	2	92	1	135	3	178	6	221	0
7	8	50	1	93	4	136	1	179	2	222	4
8	3	51	5	94	2	137	5	180	3	223	5
9	1	52	4	95	4	138	5	181	3	224	7
10	0	53	3	96	2	139	2	182	2	225	5
11	3	54	1	97	4	140	7	183	2	226	6
12	3	55	1	98	3	141	3	184	2	227	5
13	0	56	4	99	4	142	3	185	6	228	6
14	3	57	2	100	1	143	1	186	8	229	2
15	1	58	3	101	1	144	4	187	6	230	3
16	2	59	2	102	2	145	5	188	1	231	3
17	2	60	4	103	3	146	2	189	4	232	3
18	4	61	1	104	3	147	4	190	4	233	0
19	0	62	2	105	4	148	0	191	3	234	6
20	2	63	2	106	4	149	1	192	3	235	6
21	2	64	4	107	2	150	0	193	2	236	3
22	3	65	5	108	4	151	3	194	2	237	1
23	1	66	2	109	2	152	5	195	6	238	2
24	0	67	1	110	3	153	0	196	3	239	9
25	3	68	5	111	2	154	5	197	4	240	5
26	2	69	3	112	6	155	2	198	5	241	7
27	3	70	4	113	0	156	4	199	0	242	6
28	4	71	1	114	4	157	4	200	1	243	4
29	3	72	2	115	1	158	3	201	4	244	3
30	5	73	5	116	4	159	2	202	5	245	5
31	3	74	5	117	1	160	2	203	2	246	3
32	3	75	5	118	4	161	6	204	3	247	5
33	3	76	4	119	4	162	3	205	3	248	4
34	3	77	3	120	3	163	1	206	4	249	3
35	2	78	1	121	4	164	3	207	4	250	8
36	3	79	1	122	0	165	2	208	6	251	3
37	2	80	2	123	5	166	4	209	3	252	4
38	2	81	2	124	5	167	2	210	2	253	7
39	3	82	3	125	3	168	1	211	5	254	2
40	3	83	4	126	3	169	7	212	6	255	1
41	0	84	8	127	5	170	2	213	3	256	10
42	3	85	4	128	4	171	5	214	3	257	7
43	3	86	2	129	3	172	2	215	3	258	6

* Channel # and *f* represent oxonol fluorescence and frequency respectively.

Table A4. Continued.

Channel #	*f*	Channel #	*f*	Channel #	*f*	Channel #	*f*	Channel #	*f*	Channel #	*f*
259	7	302	7	345	11	388	5	431	9	474	4
260	5	303	9	346	6	389	8	432	12	475	9
261	6	304	6	347	5	390	8	433	8	476	13
262	7	305	10	348	11	391	9	434	10	477	11
263	2	306	4	349	7	392	9	435	5	478	10
264	8	307	7	350	2	393	14	436	4	479	8
265	9	308	3	351	6	394	7	437	10	480	10
266	3	309	8	352	10	395	5	438	6	481	12
267	5	310	5	353	3	396	6	439	9	482	10
268	8	311	5	354	9	397	9	440	4	483	10
269	4	312	6	355	13	398	4	441	6	484	8
270	0	313	9	356	6	399	7	442	9	485	9
271	8	314	4	357	8	400	8	443	8	486	7
272	6	315	4	358	8	401	10	444	11	487	10
273	2	316	9	359	7	402	9	445	11	488	7
274	5	317	6	360	5	403	8	446	7	489	15
275	6	318	6	361	9	404	8	447	11	490	5
276	5	319	12	362	5	405	7	448	7	491	9
277	8	320	6	363	11	406	5	449	6	492	10
278	3	321	6	364	12	407	6	450	7	493	14
279	4	322	6	365	7	408	9	451	12	494	9
280	5	323	10	366	4	409	10	452	7	495	13
281	9	324	5	367	7	410	10	453	12	496	10
282	6	325	10	368	4	411	5	454	9	497	10
283	4	326	2	369	11	412	9	455	5	498	7
284	10	327	8	370	6	413	10	456	11	499	9
285	6	328	13	371	6	414	8	457	9	500	13
286	10	329	9	372	7	415	8	458	5	501	10
287	2	330	4	373	14	416	5	459	8	502	7
288	8	331	1	374	8	417	3	460	7	503	8
289	4	332	6	375	7	418	9	461	11	504	8
290	8	333	6	376	8	419	12	462	12	505	7
291	8	334	5	377	4	420	2	463	8	506	16
292	6	335	10	378	7	421	6	464	6	507	16
293	6	336	6	379	8	422	4	465	12	508	12
294	7	337	6	380	9	423	10	466	8	509	5
295	5	338	6	381	1	424	3	467	10	510	5
296	4	339	4	382	5	425	10	468	13	511	13
297	4	340	5	383	9	426	10	469	10	512	8
298	2	341	2	384	8	427	12	470	3	513	12
299	9	342	9	385	7	428	4	471	7	514	6
300	5	343	6	386	10	429	9	472	12	515	7
301	4	344	8	387	10	430	9	473	12	516	7

Table A4. Continued.

Channel #	*f*	Channel #	*f*	Channel #	*f*	Channel #	*f*	Channel #	*f*	Channel #	*f*
517	7	560	9	603	6	646	6	689	17	732	11
518	5	561	8	604	9	647	9	690	15	733	31
519	5	562	9	605	7	648	11	691	19	734	22
520	8	563	8	606	6	649	14	692	19	735	25
521	5	564	8	607	6	650	12	693	13	736	26
522	12	565	7	608	7	651	13	694	15	737	28
523	7	566	6	609	15	652	8	695	9	738	21
524	11	567	4	610	4	653	14	696	19	739	32
525	8	568	12	611	6	654	9	697	19	740	18
526	10	569	11	612	13	655	13	698	18	741	23
527	6	570	12	613	8	656	14	699	20	742	23
528	5	571	7	614	3	657	9	700	16	743	24
529	11	572	9	615	3	658	13	701	21	744	22
530	13	573	12	616	5	659	9	702	21	745	26
531	8	574	12	617	11	660	13	703	25	746	32
532	8	575	12	618	4	661	11	704	15	747	22
533	8	576	9	619	7	662	11	705	14	748	26
534	6	577	8	620	4	663	11	706	15	749	19
535	7	578	9	621	11	664	13	707	21	750	29
536	12	579	10	622	11	665	12	708	19	751	43
537	13	580	7	623	4	666	9	709	11	752	23
538	4	581	11	624	15	667	11	710	19	753	24
539	7	582	4	625	7	668	13	711	21	754	20
540	12	583	5	626	7	669	7	712	25	755	38
541	6	584	8	627	9	670	20	713	23	756	31
542	8	585	7	628	6	671	13	714	22	757	31
543	7	586	9	629	14	672	12	715	25	758	26
544	11	587	9	630	14	673	13	716	23	759	28
545	10	588	10	631	6	674	10	717	20	760	19
546	13	589	12	632	7	675	17	718	25	761	20
547	10	590	9	633	8	676	17	719	19	762	30
548	5	591	9	634	6	677	16	720	26	763	24
549	10	592	4	635	11	678	20	721	22	764	23
550	7	593	9	636	12	679	14	722	25	765	20
551	6	594	2	637	11	680	14	723	26	766	18
552	5	595	2	638	15	681	14	724	14	767	29
553	8	596	5	639	12	682	21	725	22	768	29
554	13	597	7	640	14	683	10	726	29	769	36
555	4	598	6	641	13	684	22	727	20	770	38
556	5	599	11	642	7	685	20	728	23	771	24
557	9	600	6	643	9	686	13	729	29	772	25
558	9	601	5	644	6	687	15	730	23	773	19
559	8	602	10	645	19	688	15	731	30	774	26

Table A4. Continued.

Channel #	*f*	Channel #	*f*	Channel #	*f*	Channel #	*f*	Channel #	*f*	Channel #	*f*
775	29	818	27	861	18	904	16	947	3	990	0
776	18	819	27	862	27	905	8	948	2	991	0
777	35	820	29	863	17	906	17	949	5	992	1
778	29	821	21	864	9	907	18	950	9	993	1
779	31	822	28	865	22	908	18	951	2	994	0
780	28	823	25	866	13	909	18	952	3	995	0
781	24	824	19	867	19	910	19	953	3	996	1
782	24	825	17	868	27	911	10	954	3	997	1
783	16	826	30	869	23	912	7	955	4	998	0
784	24	827	25	870	27	913	13	956	3	999	1
785	28	828	20	871	25	914	9	957	4	1000	0
786	32	829	17	872	20	915	8	958	3	1001	0
787	28	830	26	873	19	916	10	959	2	1002	0
788	24	831	21	874	21	917	8	960	4	1003	0
789	20	832	27	875	20	918	11	961	3	1004	0
790	29	833	15	876	22	919	13	962	6	1005	3
791	15	834	27	877	19	920	8	963	3	1006	0
792	22	835	27	878	15	921	7	964	4	1007	0
793	21	836	22	879	23	922	9	965	0	1008	0
794	15	837	23	880	20	923	14	966	5	1009	0
795	33	838	29	881	20	924	12	967	3	1010	0
796	33	839	15	882	17	925	6	968	5	1011	0
797	33	840	24	883	16	926	15	969	1	1012	1
798	36	841	27	884	26	927	10	970	2	1013	0
799	29	842	16	885	15	928	11	971	4	1014	0
800	25	843	25	886	22	929	2	972	1	1015	0
801	25	844	24	887	18	930	6	973	1	1016	0
802	20	845	15	888	26	931	5	974	3	1017	0
803	31	846	26	889	19	932	9	975	0	1018	0
804	26	847	13	890	24	933	8	976	1	1019	0
805	17	848	15	891	21	934	4	977	0	1020	0
806	34	849	27	892	14	935	4	978	1	1021	0
807	20	850	13	893	17	936	6	979	0	1022	0
808	24	851	25	894	18	937	7	980	1	1023	0
809	33	852	15	895	13	938	2	981	0	1024	0
810	33	853	9	896	13	939	8	982	2		
811	20	854	16	897	19	940	4	983	0		
812	24	855	26	898	12	941	4	984	0		
813	18	856	25	899	20	942	4	985	0		
814	32	857	29	900	21	943	7	986	1		
815	20	858	14	901	12	944	5	987	0		
816	23	859	22	902	14	945	8	988	1		
817	23	860	17	903	15	946	3	989	0		

Table A5. Raw flow cytometry data for differentiating IMR-32 (Day 2, 2nd replicate) used to generate Figure 3.2.

Channel #	*f*	Channel #	*f*	Channel #	*f*	Channel #	*f*	Channel #	*f*	Channel #	*f*
1	0	44	0	87	0	130	0	173	0	216	0
2	0	45	0	88	0	131	0	174	0	217	0
3	0	46	0	89	0	132	0	175	1	218	0
4	0	47	1	90	0	133	0	176	0	219	0
5	10	48	0	91	0	134	0	177	0	220	0
6	15	49	0	92	0	135	0	178	0	221	0
7	0	50	0	93	0	136	0	179	0	222	0
8	0	51	0	94	0	137	0	180	1	223	0
9	0	52	0	95	0	138	0	181	0	224	0
10	0	53	0	96	0	139	0	182	0	225	0
11	0	54	0	97	0	140	0	183	0	226	1
12	0	55	0	98	0	141	0	184	0	227	0
13	0	56	0	99	0	142	0	185	0	228	0
14	0	57	0	100	0	143	0	186	0	229	0
15	0	58	0	101	0	144	0	187	0	230	0
16	0	59	0	102	0	145	0	188	0	231	0
17	0	60	0	103	0	146	0	189	0	232	0
18	0	61	0	104	0	147	0	190	0	233	0
19	0	62	0	105	0	148	0	191	0	234	0
20	1	63	0	106	0	149	0	192	0	235	0
21	0	64	0	107	0	150	0	193	0	236	0
22	0	65	0	108	0	151	0	194	0	237	1
23	0	66	0	109	0	152	0	195	0	238	2
24	0	67	0	110	0	153	0	196	0	239	0
25	0	68	0	111	0	154	0	197	0	240	0
26	0	69	0	112	0	155	0	198	0	241	0
27	0	70	0	113	0	156	0	199	0	242	0
28	0	71	0	114	0	157	0	200	0	243	0
29	0	72	0	115	0	158	0	201	0	244	0
30	0	73	0	116	0	159	0	202	0	245	0
31	0	74	0	117	0	160	0	203	0	246	0
32	0	75	0	118	0	161	1	204	0	247	0
33	0	76	0	119	0	162	0	205	0	248	0
34	0	77	0	120	0	163	0	206	0	249	0
35	0	78	0	121	0	164	0	207	0	250	0
36	0	79	0	122	0	165	0	208	0	251	0
37	0	80	0	123	0	166	0	209	0	252	0
38	0	81	0	124	0	167	0	210	0	253	0
39	0	82	0	125	0	168	0	211	0	254	0
40	0	83	0	126	0	169	0	212	0	255	0
41	0	84	0	127	0	170	0	213	0	256	0
42	0	85	0	128	0	171	0	214	0	257	0
43	0	86	0	129	0	172	0	215	0	258	0

* Channel # and *f* represent oxonol fluorescence and frequency respectively.

Table A5. Continued.

Channel #	*f*	Channel #	*f*	Channel #	*f*	Channel #	*f*	Channel #	*f*	Channel #	*f*
259	0	302	0	345	1	388	1	431	1	474	1
260	0	303	0	346	0	389	0	432	0	475	2
261	0	304	0	347	0	390	0	433	1	476	0
262	0	305	0	348	0	391	2	434	1	477	2
263	0	306	1	349	0	392	0	435	1	478	1
264	0	307	0	350	0	393	0	436	0	479	2
265	0	308	0	351	0	394	1	437	1	480	3
266	0	309	0	352	0	395	1	438	0	481	0
267	0	310	0	353	0	396	0	439	1	482	5
268	1	311	0	354	1	397	0	440	0	483	4
269	0	312	0	355	1	398	1	441	1	484	2
270	0	313	0	356	1	399	2	442	0	485	3
271	0	314	0	357	0	400	0	443	1	486	2
272	1	315	0	358	0	401	1	444	0	487	2
273	0	316	0	359	1	402	1	445	2	488	0
274	0	317	0	360	0	403	0	446	3	489	1
275	0	318	0	361	0	404	0	447	0	490	1
276	0	319	1	362	0	405	0	448	2	491	0
277	0	320	1	363	0	406	0	449	0	492	3
278	0	321	0	364	0	407	0	450	1	493	1
279	0	322	0	365	0	408	0	451	0	494	3
280	0	323	0	366	0	409	0	452	0	495	1
281	0	324	0	367	0	410	0	453	5	496	2
282	0	325	0	368	0	411	0	454	0	497	2
283	0	326	0	369	1	412	1	455	1	498	2
284	0	327	0	370	0	413	0	456	1	499	4
285	0	328	1	371	0	414	0	457	0	500	1
286	0	329	0	372	0	415	1	458	2	501	0
287	0	330	1	373	0	416	2	459	1	502	2
288	0	331	0	374	0	417	0	460	4	503	4
289	0	332	0	375	0	418	2	461	2	504	2
290	0	333	0	376	0	419	1	462	2	505	3
291	0	334	0	377	0	420	0	463	2	506	3
292	0	335	0	378	1	421	1	464	3	507	5
293	0	336	0	379	0	422	0	465	1	508	1
294	0	337	0	380	1	423	1	466	1	509	1
295	0	338	0	381	0	424	0	467	1	510	5
296	0	339	0	382	1	425	0	468	0	511	3
297	0	340	0	383	1	426	0	469	5	512	4
298	0	341	1	384	0	427	0	470	3	513	1
299	0	342	0	385	0	428	2	471	0	514	4
300	1	343	0	386	0	429	0	472	0	515	0
301	0	344	0	387	0	430	0	473	1	516	4

Table A5. Continued.

Channel #	*f*	Channel #	*f*	Channel #	*f*	Channel #	*f*	Channel #	*f*	Channel #	*f*
517	4	560	4	603	8	646	10	689	14	732	21
518	6	561	5	604	10	647	9	690	20	733	21
519	3	562	4	605	2	648	10	691	19	734	35
520	2	563	4	606	8	649	17	692	17	735	22
521	1	564	9	607	9	650	5	693	13	736	23
522	6	565	4	608	4	651	9	694	15	737	37
523	6	566	5	609	13	652	10	695	22	738	19
524	4	567	1	610	5	653	10	696	20	739	21
525	5	568	3	611	7	654	19	697	21	740	19
526	1	569	3	612	7	655	8	698	23	741	24
527	2	570	4	613	11	656	16	699	17	742	31
528	3	571	4	614	9	657	13	700	19	743	28
529	3	572	6	615	6	658	12	701	13	744	36
530	5	573	8	616	8	659	14	702	21	745	22
531	2	574	4	617	8	660	5	703	16	746	35
532	2	575	2	618	6	661	11	704	13	747	38
533	1	576	6	619	6	662	6	705	21	748	30
534	3	577	5	620	7	663	15	706	23	749	34
535	6	578	5	621	4	664	8	707	25	750	45
536	2	579	7	622	10	665	12	708	16	751	39
537	4	580	2	623	8	666	9	709	21	752	28
538	4	581	6	624	9	667	8	710	21	753	45
539	5	582	4	625	5	668	15	711	20	754	36
540	3	583	4	626	5	669	18	712	22	755	39
541	4	584	3	627	9	670	5	713	26	756	27
542	2	585	7	628	6	671	15	714	25	757	33
543	6	586	10	629	8	672	18	715	31	758	39
544	3	587	9	630	8	673	11	716	18	759	28
545	2	588	3	631	11	674	16	717	22	760	40
546	7	589	5	632	9	675	12	718	26	761	41
547	6	590	7	633	9	676	17	719	20	762	40
548	3	591	3	634	12	677	12	720	21	763	40
549	3	592	4	635	4	678	20	721	24	764	34
550	1	593	10	636	7	679	14	722	30	765	35
551	3	594	8	637	4	680	5	723	19	766	46
552	6	595	5	638	2	681	14	724	24	767	41
553	3	596	6	639	7	682	20	725	25	768	42
554	4	597	3	640	10	683	17	726	34	769	34
555	4	598	4	641	13	684	16	727	25	770	45
556	4	599	6	642	13	685	18	728	35	771	37
557	6	600	6	643	11	686	15	729	23	772	48
558	2	601	8	644	8	687	14	730	33	773	39
559	4	602	3	645	13	688	23	731	22	774	38

Table A5. Continued.

Channel #	*f*	Channel #	*f*	Channel #	*f*	Channel #	*f*	Channel #	*f*	Channel #	*f*
775	34	818	45	861	34	904	37	947	11	990	4
776	33	819	59	862	42	905	27	948	15	991	0
777	51	820	43	863	43	906	26	949	8	992	1
778	55	821	30	864	43	907	34	950	6	993	1
779	52	822	35	865	43	908	29	951	7	994	1
780	37	823	52	866	41	909	25	952	8	995	1
781	31	824	43	867	45	910	32	953	7	996	2
782	44	825	40	868	32	911	21	954	6	997	2
783	52	826	36	869	35	912	22	955	7	998	2
784	43	827	37	870	36	913	15	956	5	999	0
785	35	828	39	871	37	914	24	957	7	1000	0
786	43	829	29	872	39	915	22	958	4	1001	2
787	48	830	39	873	43	916	26	959	8	1002	1
788	48	831	44	874	33	917	21	960	4	1003	0
789	39	832	30	875	41	918	20	961	3	1004	1
790	55	833	52	876	38	919	20	962	6	1005	0
791	38	834	42	877	37	920	13	963	2	1006	0
792	42	835	45	878	42	921	28	964	4	1007	0
793	54	836	49	879	36	922	13	965	2	1008	0
794	30	837	35	880	32	923	20	966	7	1009	0
795	34	838	41	881	25	924	18	967	3	1010	0
796	52	839	43	882	29	925	14	968	2	1011	0
797	25	840	55	883	33	926	16	969	6	1012	0
798	50	841	54	884	42	927	17	970	5	1013	0
799	39	842	39	885	25	928	15	971	7	1014	0
800	44	843	36	886	37	929	19	972	7	1015	0
801	47	844	42	887	19	930	10	973	5	1016	0
802	53	845	35	888	26	931	15	974	1	1017	0
803	33	846	46	889	30	932	10	975	2	1018	0
804	35	847	38	890	27	933	14	976	3	1019	0
805	45	848	44	891	30	934	16	977	1	1020	0
806	43	849	55	892	31	935	14	978	2	1021	0
807	53	850	44	893	29	936	6	979	4	1022	0
808	38	851	51	894	46	937	18	980	3	1023	0
809	39	852	37	895	28	938	15	981	3	1024	0
810	48	853	45	896	29	939	12	982	3		
811	56	854	42	897	41	940	11	983	0		
812	53	855	40	898	36	941	4	984	1		
813	41	856	41	899	25	942	12	985	0		
814	50	857	30	900	24	943	13	986	2		
815	42	858	35	901	24	944	7	987	1		
816	44	859	48	902	32	945	11	988	1		
817	54	860	38	903	21	946	11	989	2		

Table A6. Raw flow cytometry data for differentiating IMR-32 (Day 2, 3rd replicate) used to generate Figure 3.2.

Channel #	*f*	Channel #	*f*	Channel #	*f*	Channel #	*f*	Channel #	*f*	Channel #	*f*
1	0	44	0	87	0	130	0	173	0	216	0
2	0	45	0	88	0	131	1	174	0	217	0
3	0	46	0	89	0	132	0	175	0	218	0
4	4	47	1	90	1	133	1	176	0	219	0
5	41	48	0	91	0	134	0	177	1	220	0
6	6	49	0	92	0	135	0	178	1	221	0
7	2	50	0	93	0	136	0	179	0	222	0
8	0	51	0	94	0	137	0	180	0	223	1
9	0	52	0	95	0	138	0	181	0	224	0
10	0	53	0	96	0	139	1	182	2	225	0
11	0	54	1	97	0	140	0	183	0	226	0
12	0	55	0	98	0	141	0	184	0	227	0
13	0	56	0	99	0	142	0	185	0	228	0
14	0	57	0	100	0	143	0	186	0	229	0
15	0	58	0	101	2	144	0	187	0	230	0
16	0	59	0	102	0	145	0	188	1	231	0
17	0	60	0	103	0	146	0	189	0	232	0
18	0	61	1	104	1	147	1	190	0	233	1
19	0	62	0	105	0	148	2	191	0	234	0
20	1	63	0	106	1	149	0	192	0	235	1
21	0	64	0	107	1	150	0	193	1	236	0
22	0	65	0	108	0	151	0	194	0	237	0
23	0	66	1	109	0	152	0	195	0	238	0
24	0	67	0	110	0	153	0	196	0	239	1
25	0	68	0	111	0	154	0	197	1	240	0
26	0	69	0	112	0	155	0	198	0	241	0
27	1	70	0	113	1	156	0	199	1	242	0
28	0	71	2	114	1	157	0	200	0	243	0
29	0	72	0	115	1	158	0	201	0	244	0
30	0	73	0	116	0	159	0	202	0	245	0
31	0	74	0	117	0	160	1	203	1	246	0
32	0	75	0	118	0	161	1	204	0	247	0
33	0	76	0	119	0	162	0	205	0	248	0
34	0	77	1	120	0	163	0	206	0	249	0
35	0	78	0	121	0	164	0	207	0	250	0
36	0	79	0	122	0	165	1	208	0	251	0
37	1	80	0	123	0	166	0	209	0	252	1
38	1	81	0	124	0	167	0	210	1	253	0
39	0	82	0	125	0	168	0	211	0	254	0
40	0	83	0	126	0	169	0	212	0	255	1
41	0	84	1	127	0	170	0	213	0	256	0
42	0	85	0	128	0	171	0	214	2	257	0
43	0	86	0	129	0	172	0	215	0	258	0

* Channel # and *f* represent oxonol fluorescence and frequency respectively.

Table A6. Continued.

Channel #	*f*	Channel #	*f*	Channel #	*f*	Channel #	*f*	Channel #	*f*	Channel #	*f*
259	1	302	0	345	0	388	1	431	1	474	4
260	0	303	1	346	0	389	1	432	1	475	2
261	0	304	1	347	1	390	1	433	1	476	0
262	1	305	0	348	1	391	0	434	0	477	2
263	0	306	0	349	0	392	1	435	0	478	4
264	1	307	0	350	0	393	0	436	0	479	3
265	0	308	0	351	0	394	1	437	2	480	7
266	0	309	0	352	0	395	1	438	1	481	1
267	1	310	0	353	0	396	1	439	1	482	3
268	0	311	1	354	2	397	0	440	1	483	2
269	0	312	0	355	0	398	2	441	1	484	2
270	0	313	0	356	0	399	0	442	0	485	1
271	1	314	0	357	1	400	2	443	3	486	0
272	0	315	1	358	1	401	0	444	0	487	2
273	1	316	0	359	0	402	1	445	2	488	2
274	1	317	0	360	0	403	1	446	1	489	1
275	0	318	0	361	0	404	0	447	1	490	3
276	0	319	1	362	0	405	1	448	1	491	2
277	0	320	0	363	2	406	1	449	1	492	1
278	0	321	0	364	0	407	0	450	0	493	3
279	0	322	0	365	0	408	0	451	0	494	2
280	0	323	0	366	0	409	1	452	2	495	2
281	0	324	1	367	0	410	1	453	1	496	2
282	0	325	0	368	1	411	1	454	1	497	3
283	0	326	0	369	1	412	1	455	0	498	3
284	1	327	0	370	0	413	2	456	1	499	3
285	0	328	0	371	1	414	2	457	0	500	1
286	0	329	0	372	1	415	0	458	0	501	2
287	0	330	0	373	1	416	0	459	3	502	5
288	0	331	0	374	0	417	1	460	3	503	0
289	0	332	0	375	0	418	1	461	0	504	2
290	0	333	0	376	0	419	0	462	2	505	1
291	0	334	0	377	0	420	2	463	3	506	1
292	0	335	1	378	1	421	0	464	1	507	3
293	0	336	0	379	0	422	1	465	0	508	1
294	1	337	1	380	0	423	0	466	3	509	2
295	1	338	2	381	0	424	1	467	1	510	2
296	0	339	0	382	1	425	0	468	4	511	1
297	0	340	0	383	0	426	0	469	1	512	3
298	0	341	0	384	0	427	1	470	1	513	2
299	0	342	0	385	0	428	2	471	0	514	2
300	0	343	0	386	0	429	0	472	0	515	1
301	0	344	1	387	0	430	2	473	1	516	3

Table A6. Continued.

Channel #	*f*	Channel #	*f*	Channel #	*f*	Channel #	*f*	Channel #	*f*	Channel #	*f*
517	1	560	2	603	3	646	7	689	8	732	14
518	1	561	2	604	7	647	7	690	14	733	22
519	0	562	3	605	3	648	7	691	10	734	22
520	4	563	6	606	9	649	6	692	15	735	8
521	2	564	1	607	9	650	10	693	14	736	28
522	3	565	3	608	6	651	10	694	22	737	10
523	4	566	1	609	2	652	6	695	13	738	26
524	5	567	1	610	3	653	5	696	17	739	21
525	2	568	2	611	5	654	7	697	15	740	16
526	3	569	3	612	3	655	7	698	12	741	21
527	4	570	5	613	5	656	5	699	15	742	25
528	2	571	2	614	4	657	3	700	7	743	32
529	4	572	6	615	3	658	6	701	20	744	11
530	2	573	3	616	2	659	10	702	17	745	18
531	4	574	1	617	7	660	10	703	13	746	29
532	8	575	6	618	9	661	8	704	14	747	23
533	1	576	3	619	6	662	8	705	12	748	18
534	6	577	8	620	6	663	8	706	15	749	19
535	2	578	1	621	4	664	7	707	11	750	22
536	1	579	3	622	4	665	10	708	20	751	24
537	3	580	3	623	9	666	6	709	9	752	27
538	2	581	1	624	3	667	10	710	14	753	29
539	3	582	3	625	8	668	9	711	13	754	30
540	4	583	3	626	3	669	5	712	19	755	11
541	6	584	5	627	0	670	6	713	22	756	19
542	2	585	3	628	3	671	11	714	12	757	19
543	3	586	3	629	5	672	11	715	17	758	21
544	2	587	5	630	11	673	8	716	11	759	16
545	2	588	6	631	1	674	9	717	19	760	25
546	3	589	5	632	9	675	8	718	21	761	21
547	0	590	3	633	5	676	9	719	14	762	25
548	1	591	2	634	5	677	11	720	22	763	35
549	2	592	7	635	6	678	11	721	11	764	22
550	5	593	3	636	7	679	3	722	21	765	28
551	1	594	3	637	3	680	7	723	18	766	31
552	1	595	4	638	7	681	4	724	21	767	16
553	2	596	4	639	4	682	5	725	11	768	22
554	2	597	10	640	5	683	15	726	12	769	21
555	2	598	2	641	5	684	7	727	12	770	25
556	3	599	4	642	4	685	12	728	18	771	28
557	5	600	5	643	6	686	17	729	19	772	33
558	7	601	3	644	7	687	6	730	22	773	27
559	1	602	4	645	5	688	13	731	18	774	27

Table A6. Continued.

Channel #	*f*	Channel #	*f*	Channel #	*f*	Channel #	*f*	Channel #	*f*	Channel #	*f*
775	33	818	34	861	42	904	55	947	29	990	7
776	22	819	45	862	58	905	34	948	20	991	4
777	31	820	35	863	30	906	39	949	15	992	10
778	27	821	37	864	40	907	46	950	17	993	6
779	34	822	36	865	49	908	41	951	23	994	11
780	33	823	41	866	44	909	38	952	8	995	8
781	28	824	30	867	49	910	44	953	16	996	12
782	36	825	40	868	42	911	36	954	16	997	7
783	39	826	31	869	41	912	51	955	26	998	5
784	24	827	44	870	47	913	42	956	26	999	4
785	32	828	40	871	42	914	50	957	13	1000	3
786	34	829	40	872	47	915	29	958	14	1001	3
787	25	830	52	873	58	916	48	959	17	1002	2
788	40	831	41	874	46	917	31	960	18	1003	2
789	27	832	35	875	50	918	38	961	13	1004	2
790	34	833	59	876	34	919	26	962	10	1005	1
791	32	834	39	877	41	920	35	963	19	1006	8
792	22	835	39	878	51	921	40	964	17	1007	2
793	31	836	44	879	50	922	37	965	23	1008	2
794	30	837	36	880	37	923	34	966	21	1009	2
795	36	838	52	881	43	924	36	967	21	1010	0
796	22	839	43	882	53	925	23	968	13	1011	1
797	33	840	38	883	51	926	36	969	18	1012	1
798	45	841	41	884	47	927	26	970	21	1013	0
799	26	842	38	885	45	928	27	971	18	1014	1
800	24	843	36	886	49	929	29	972	10	1015	0
801	20	844	51	887	33	930	24	973	16	1016	0
802	31	845	39	888	35	931	40	974	15	1017	0
803	37	846	57	889	51	932	28	975	12	1018	0
804	43	847	41	890	55	933	22	976	10	1019	0
805	27	848	29	891	49	934	31	977	10	1020	1
806	39	849	50	892	37	935	29	978	15	1021	0
807	31	850	33	893	46	936	21	979	7	1022	1
808	41	851	50	894	32	937	24	980	6	1023	0
809	43	852	38	895	42	938	30	981	9	1024	0
810	33	853	35	896	39	939	29	982	9		
811	35	854	40	897	39	940	28	983	8		
812	24	855	45	898	52	941	17	984	11		
813	27	856	50	899	43	942	19	985	11		
814	42	857	48	900	40	943	13	986	9		
815	39	858	43	901	46	944	17	987	9		
816	32	859	42	902	49	945	30	988	9		
817	42	860	45	903	44	946	22	989	4		

Table A7. Raw flow cytometry data for differentiating IMR-32 (Day 4, 1st replicate) used to generate Figure 3.2.

Channel #	*f*	Channel #	*f*	Channel #	*f*	Channel #	*f*	Channel #	*f*	Channel #	*f*
1	0	44	0	87	0	130	0	173	0	216	0
2	0	45	1	88	0	131	0	174	0	217	0
3	0	46	0	89	0	132	0	175	0	218	1
4	0	47	0	90	0	133	0	176	0	219	0
5	14	48	0	91	0	134	0	177	0	220	0
6	8	49	0	92	1	135	0	178	0	221	0
7	4	50	0	93	0	136	0	179	0	222	0
8	0	51	0	94	0	137	0	180	0	223	0
9	1	52	0	95	0	138	0	181	0	224	0
10	0	53	0	96	0	139	0	182	0	225	0
11	0	54	0	97	0	140	0	183	0	226	0
12	0	55	0	98	1	141	0	184	0	227	0
13	0	56	0	99	0	142	0	185	0	228	0
14	0	57	0	100	0	143	0	186	0	229	0
15	0	58	0	101	0	144	0	187	1	230	0
16	0	59	0	102	0	145	0	188	0	231	0
17	0	60	0	103	1	146	0	189	0	232	0
18	0	61	0	104	0	147	0	190	0	233	0
19	0	62	0	105	0	148	0	191	0	234	0
20	0	63	0	106	0	149	0	192	0	235	0
21	0	64	0	107	0	150	0	193	0	236	0
22	0	65	0	108	0	151	0	194	0	237	0
23	0	66	0	109	0	152	0	195	0	238	1
24	0	67	0	110	0	153	0	196	1	239	0
25	0	68	0	111	0	154	0	197	0	240	0
26	0	69	0	112	0	155	0	198	0	241	0
27	0	70	0	113	0	156	0	199	0	242	0
28	0	71	0	114	0	157	0	200	0	243	0
29	0	72	0	115	0	158	0	201	0	244	0
30	0	73	0	116	0	159	0	202	0	245	0
31	0	74	0	117	0	160	0	203	0	246	0
32	0	75	0	118	1	161	0	204	0	247	0
33	0	76	0	119	0	162	0	205	0	248	0
34	1	77	0	120	0	163	1	206	0	249	0
35	0	78	0	121	0	164	0	207	1	250	0
36	1	79	0	122	0	165	0	208	0	251	0
37	0	80	0	123	1	166	0	209	0	252	0
38	0	81	0	124	0	167	0	210	1	253	0
39	0	82	0	125	0	168	0	211	1	254	0
40	0	83	1	126	0	169	0	212	0	255	0
41	0	84	0	127	0	170	0	213	0	256	0
42	0	85	0	128	1	171	0	214	0	257	0
43	0	86	0	129	0	172	0	215	0	258	0

* Channel # and *f* represent oxonol fluorescence and frequency respectively.

Table A7. Continued.

Channel #	*f*	Channel #	*f*	Channel #	*f*	Channel #	*f*	Channel #	*f*	Channel #	*f*
259	0	302	0	345	0	388	0	431	1	474	1
260	1	303	0	346	1	389	2	432	0	475	2
261	0	304	0	347	0	390	2	433	1	476	1
262	0	305	0	348	0	391	1	434	0	477	0
263	0	306	0	349	0	392	0	435	0	478	2
264	0	307	0	350	2	393	0	436	1	479	1
265	0	308	0	351	0	394	1	437	1	480	1
266	0	309	1	352	0	395	0	438	2	481	3
267	1	310	1	353	0	396	1	439	1	482	5
268	0	311	0	354	1	397	1	440	1	483	1
269	0	312	0	355	0	398	1	441	3	484	0
270	0	313	0	356	0	399	1	442	2	485	1
271	0	314	0	357	0	400	1	443	4	486	2
272	0	315	0	358	0	401	0	444	2	487	0
273	1	316	1	359	0	402	0	445	3	488	2
274	0	317	0	360	0	403	1	446	0	489	3
275	0	318	0	361	1	404	1	447	2	490	6
276	0	319	0	362	1	405	0	448	3	491	1
277	0	320	0	363	1	406	2	449	2	492	3
278	0	321	0	364	0	407	0	450	1	493	3
279	0	322	1	365	0	408	1	451	3	494	2
280	0	323	1	366	0	409	1	452	1	495	1
281	1	324	1	367	1	410	2	453	3	496	3
282	0	325	0	368	1	411	3	454	1	497	2
283	0	326	1	369	0	412	0	455	3	498	3
284	0	327	0	370	2	413	1	456	1	499	6
285	0	328	1	371	1	414	1	457	4	500	5
286	0	329	0	372	1	415	2	458	1	501	0
287	0	330	1	373	0	416	0	459	3	502	6
288	0	331	1	374	2	417	0	460	1	503	3
289	0	332	0	375	0	418	0	461	3	504	2
290	0	333	1	376	0	419	2	462	5	505	1
291	0	334	1	377	0	420	1	463	3	506	1
292	0	335	1	378	0	421	1	464	1	507	2
293	0	336	0	379	2	422	0	465	2	508	6
294	1	337	1	380	0	423	4	466	2	509	1
295	1	338	0	381	2	424	0	467	3	510	1
296	2	339	0	382	0	425	2	468	2	511	2
297	0	340	0	383	1	426	0	469	4	512	0
298	0	341	1	384	2	427	0	470	2	513	3
299	0	342	0	385	1	428	1	471	4	514	4
300	0	343	0	386	0	429	0	472	1	515	1
301	0	344	0	387	2	430	3	473	0	516	1

Table A7. Continued.

Channel #	*f*	Channel #	*f*	Channel #	*f*	Channel #	*f*	Channel #	*f*	Channel #	*f*
517	3	560	4	603	9	646	13	689	11	732	38
518	2	561	9	604	12	647	10	690	20	733	21
519	0	562	4	605	5	648	7	691	19	734	32
520	3	563	3	606	6	649	12	692	10	735	21
521	0	564	3	607	6	650	15	693	27	736	33
522	1	565	5	608	11	651	15	694	15	737	30
523	2	566	4	609	5	652	16	695	12	738	32
524	2	567	1	610	7	653	13	696	20	739	30
525	1	568	7	611	12	654	14	697	15	740	31
526	4	569	6	612	10	655	12	698	19	741	36
527	1	570	3	613	6	656	16	699	22	742	38
528	5	571	3	614	8	657	12	700	24	743	37
529	6	572	5	615	9	658	11	701	16	744	29
530	2	573	4	616	10	659	18	702	23	745	36
531	4	574	2	617	9	660	20	703	19	746	37
532	2	575	4	618	9	661	5	704	18	747	34
533	2	576	6	619	13	662	28	705	31	748	44
534	0	577	7	620	9	663	7	706	30	749	41
535	3	578	7	621	11	664	14	707	17	750	32
536	3	579	12	622	11	665	13	708	25	751	34
537	4	580	3	623	10	666	8	709	18	752	33
538	3	581	4	624	8	667	15	710	24	753	35
539	3	582	4	625	5	668	12	711	28	754	33
540	5	583	7	626	9	669	12	712	18	755	40
541	6	584	8	627	9	670	13	713	20	756	23
542	4	585	3	628	10	671	17	714	20	757	28
543	0	586	6	629	9	672	20	715	28	758	39
544	3	587	4	630	9	673	21	716	32	759	39
545	5	588	9	631	12	674	29	717	30	760	27
546	4	589	4	632	9	675	19	718	28	761	45
547	2	590	3	633	10	676	11	719	27	762	35
548	2	591	6	634	9	677	20	720	17	763	34
549	2	592	5	635	14	678	25	721	23	764	59
550	3	593	8	636	14	679	18	722	30	765	30
551	3	594	4	637	11	680	13	723	26	766	36
552	1	595	6	638	10	681	12	724	26	767	28
553	3	596	5	639	8	682	15	725	20	768	39
554	1	597	10	640	12	683	24	726	40	769	34
555	1	598	5	641	14	684	13	727	27	770	49
556	2	599	6	642	14	685	14	728	27	771	47
557	6	600	3	643	11	686	22	729	24	772	36
558	3	601	8	644	9	687	20	730	24	773	37
559	7	602	9	645	8	688	20	731	27	774	54

Table A7. Continued.

Channel #	*f*	Channel #	*f*	Channel #	*f*	Channel #	*f*	Channel #	*f*	Channel #	*f*
775	45	818	57	861	40	904	23	947	2	990	1
776	35	819	54	862	38	905	22	948	3	991	1
777	62	820	42	863	33	906	13	949	5	992	1
778	47	821	49	864	33	907	24	950	10	993	0
779	43	822	41	865	37	908	12	951	4	994	0
780	43	823	39	866	35	909	18	952	5	995	0
781	41	824	50	867	31	910	15	953	4	996	0
782	45	825	53	868	37	911	11	954	4	997	0
783	47	826	54	869	32	912	19	955	1	998	1
784	34	827	51	870	47	913	13	956	5	999	0
785	40	828	51	871	46	914	12	957	1	1000	0
786	45	829	56	872	30	915	17	958	3	1001	0
787	45	830	65	873	52	916	19	959	2	1002	0
788	43	831	41	874	36	917	8	960	3	1003	0
789	43	832	53	875	47	918	9	961	2	1004	0
790	53	833	54	876	34	919	13	962	2	1005	0
791	59	834	54	877	24	920	9	963	2	1006	0
792	45	835	45	878	38	921	10	964	4	1007	0
793	50	836	46	879	32	922	12	965	3	1008	0
794	47	837	37	880	40	923	13	966	1	1009	0
795	46	838	48	881	29	924	10	967	1	1010	0
796	39	839	51	882	31	925	8	968	1	1011	1
797	36	840	41	883	29	926	7	969	4	1012	0
798	38	841	51	884	27	927	14	970	1	1013	0
799	39	842	36	885	31	928	9	971	2	1014	0
800	38	843	51	886	39	929	10	972	2	1015	0
801	49	844	40	887	28	930	9	973	0	1016	0
802	41	845	51	888	25	931	10	974	2	1017	0
803	53	846	41	889	22	932	6	975	0	1018	0
804	48	847	48	890	28	933	4	976	1	1019	0
805	38	848	44	891	29	934	11	977	1	1020	0
806	48	849	44	892	22	935	3	978	1	1021	0
807	35	850	41	893	26	936	1	979	0	1022	0
808	48	851	36	894	27	937	8	980	1	1023	0
809	35	852	42	895	17	938	6	981	0	1024	0
810	43	853	38	896	10	939	5	982	1		
811	41	854	42	897	31	940	9	983	0		
812	28	855	43	898	28	941	6	984	0		
813	31	856	44	899	22	942	6	985	0		
814	49	857	39	900	25	943	5	986	0		
815	48	858	38	901	30	944	7	987	0		
816	47	859	45	902	29	945	11	988	1		
817	46	860	44	903	21	946	2	989	0		

Table A8. Raw flow cytometry data for differentiating IMR-32 cells (Day 4, 2nd replicate) used to generate Figure 3.2.

Channel #	*f*	Channel #	*f*	Channel #	*f*	Channel #	*f*	Channel #	*f*	Channel #	*f*
1	0	44	0	87	0	130	0	173	0	216	0
2	0	45	0	88	0	131	0	174	0	217	0
3	0	46	0	89	0	132	0	175	0	218	0
4	1	47	0	90	0	133	0	176	0	219	0
5	15	48	0	91	0	134	0	177	0	220	0
6	5	49	1	92	0	135	0	178	1	221	0
7	2	50	1	93	0	136	0	179	1	222	1
8	2	51	0	94	0	137	0	180	0	223	0
9	0	52	0	95	0	138	0	181	0	224	0
10	0	53	0	96	0	139	0	182	0	225	0
11	0	54	0	97	0	140	0	183	0	226	0
12	1	55	0	98	0	141	1	184	0	227	0
13	0	56	0	99	0	142	0	185	0	228	0
14	0	57	0	100	0	143	0	186	0	229	0
15	0	58	0	101	0	144	0	187	0	230	0
16	0	59	0	102	0	145	0	188	0	231	0
17	0	60	0	103	0	146	0	189	0	232	0
18	0	61	0	104	0	147	0	190	0	233	0
19	0	62	0	105	0	148	0	191	0	234	0
20	0	63	0	106	0	149	0	192	0	235	1
21	0	64	0	107	0	150	0	193	1	236	0
22	0	65	0	108	0	151	0	194	0	237	0
23	0	66	0	109	0	152	0	195	0	238	0
24	0	67	0	110	0	153	0	196	0	239	0
25	0	68	0	111	0	154	0	197	0	240	1
26	0	69	0	112	0	155	0	198	0	241	0
27	0	70	0	113	0	156	0	199	0	242	0
28	0	71	0	114	0	157	0	200	1	243	0
29	0	72	0	115	0	158	0	201	0	244	0
30	0	73	0	116	0	159	1	202	0	245	0
31	0	74	0	117	0	160	0	203	0	246	0
32	0	75	0	118	0	161	0	204	0	247	0
33	0	76	0	119	0	162	0	205	0	248	0
34	0	77	0	120	0	163	0	206	1	249	0
35	0	78	0	121	0	164	0	207	0	250	0
36	0	79	0	122	0	165	0	208	1	251	0
37	0	80	0	123	0	166	0	209	0	252	0
38	0	81	0	124	0	167	0	210	0	253	0
39	0	82	0	125	2	168	0	211	0	254	0
40	0	83	0	126	0	169	0	212	0	255	0
41	0	84	0	127	0	170	0	213	0	256	0
42	0	85	0	128	0	171	0	214	0	257	0
43	0	86	0	129	0	172	2	215	0	258	0

* Channel # and *f* represent oxonol fluorescence and frequency respectively.

Table A8. Continued.

Channel #	*f*	Channel #	*f*	Channel #	*f*	Channel #	*f*	Channel #	*f*	Channel #	*F*
259	0	302	0	345	0	388	0	431	0	474	2
260	0	303	0	346	0	389	0	432	0	475	3
261	0	304	0	347	0	390	1	433	2	476	1
262	0	305	0	348	0	391	0	434	1	477	0
263	0	306	0	349	0	392	0	435	0	478	3
264	0	307	0	350	0	393	0	436	0	479	0
265	0	308	1	351	0	394	1	437	1	480	1
266	0	309	0	352	0	395	1	438	0	481	2
267	0	310	1	353	1	396	0	439	0	482	0
268	0	311	0	354	0	397	0	440	2	483	4
269	0	312	0	355	0	398	0	441	1	484	2
270	0	313	0	356	0	399	1	442	0	485	0
271	0	314	0	357	0	400	0	443	0	486	2
272	0	315	0	358	0	401	0	444	0	487	0
273	0	316	0	359	0	402	0	445	0	488	1
274	0	317	0	360	0	403	2	446	1	489	1
275	2	318	0	361	1	404	1	447	1	490	3
276	0	319	0	362	1	405	1	448	0	491	1
277	0	320	0	363	1	406	1	449	0	492	3
278	0	321	0	364	0	407	1	450	1	493	0
279	0	322	0	365	0	408	2	451	0	494	4
280	0	323	0	366	0	409	0	452	1	495	2
281	0	324	0	367	1	410	1	453	3	496	1
282	0	325	0	368	0	411	0	454	1	497	2
283	0	326	0	369	0	412	0	455	0	498	1
284	0	327	0	370	0	413	1	456	0	499	4
285	0	328	0	371	0	414	1	457	0	500	2
286	0	329	0	372	1	415	0	458	1	501	0
287	0	330	1	373	1	416	0	459	1	502	2
288	0	331	0	374	0	417	0	460	0	503	1
289	0	332	0	375	1	418	0	461	1	504	1
290	0	333	0	376	2	419	0	462	1	505	1
291	0	334	0	377	0	420	1	463	0	506	1
292	0	335	0	378	1	421	0	464	1	507	2
293	0	336	0	379	0	422	0	465	0	508	0
294	0	337	0	380	0	423	2	466	2	509	1
295	0	338	0	381	0	424	1	467	1	510	2
296	0	339	0	382	0	425	0	468	0	511	1
297	1	340	0	383	1	426	1	469	0	512	2
298	0	341	1	384	0	427	3	470	0	513	0
299	0	342	1	385	0	428	1	471	1	514	4
300	0	343	0	386	3	429	0	472	3	515	2
301	0	344	0	387	1	430	1	473	1	516	1

Table A8. Continued.

Channel #	*f*	Channel #	*f*	Channel #	*f*	Channel #	*f*	Channel #	*f*	Channel #	*f*
517	3	560	7	603	6	646	8	689	25	732	19
518	3	561	6	604	3	647	6	690	22	733	31
519	3	562	2	605	9	648	9	691	24	734	37
520	0	563	4	606	11	649	12	692	24	735	32
521	3	564	5	607	13	650	19	693	21	736	24
522	2	565	4	608	9	651	18	694	21	737	40
523	0	566	6	609	3	652	11	695	24	738	32
524	3	567	6	610	7	653	12	696	14	739	40
525	3	568	1	611	11	654	13	697	22	740	41
526	1	569	6	612	7	655	8	698	23	741	52
527	3	570	7	613	8	656	10	699	19	742	37
528	6	571	5	614	12	657	10	700	21	743	35
529	3	572	6	615	7	658	15	701	16	744	38
530	2	573	3	616	5	659	22	702	24	745	37
531	2	574	2	617	10	660	15	703	21	746	33
532	2	575	3	618	10	661	15	704	23	747	42
533	0	576	4	619	9	662	13	705	28	748	47
534	4	577	5	620	1	663	9	706	27	749	35
535	3	578	6	621	6	664	9	707	27	750	44
536	6	579	5	622	9	665	13	708	28	751	40
537	1	580	4	623	8	666	15	709	23	752	32
538	1	581	3	624	10	667	16	710	34	753	52
539	7	582	7	625	12	668	15	711	20	754	50
540	5	583	4	626	7	669	14	712	19	755	53
541	1	584	4	627	13	670	18	713	26	756	43
542	1	585	6	628	15	671	7	714	23	757	28
543	2	586	5	629	12	672	19	715	36	758	56
544	2	587	8	630	8	673	12	716	32	759	30
545	3	588	3	631	11	674	21	717	23	760	38
546	2	589	2	632	15	675	19	718	30	761	41
547	2	590	2	633	7	676	8	719	22	762	39
548	1	591	8	634	6	677	13	720	33	763	43
549	0	592	5	635	15	678	15	721	33	764	46
550	1	593	5	636	11	679	16	722	30	765	57
551	3	594	6	637	7	680	23	723	27	766	45
552	4	595	6	638	13	681	22	724	35	767	37
553	3	596	12	639	6	682	23	725	26	768	41
554	6	597	8	640	10	683	28	726	31	769	44
555	2	598	10	641	15	684	24	727	37	770	41
556	6	599	4	642	11	685	26	728	30	771	51
557	5	600	9	643	9	686	27	729	28	772	48
558	5	601	5	644	12	687	14	730	26	773	50
559	3	602	10	645	8	688	13	731	31	774	46

Table A8. Continued.

Channel #	*f*	Channel #	*f*	Channel #	*f*	Channel #	*f*	Channel #	*f*	Channel #	*f*
775	50	818	47	861	43	904	19	947	10	990	1
776	31	819	45	862	32	905	14	948	5	991	0
777	60	820	47	863	31	906	10	949	4	992	0
778	53	821	40	864	34	907	21	950	3	993	1
779	58	822	51	865	39	908	16	951	7	994	1
780	49	823	45	866	35	909	15	952	5	995	0
781	38	824	39	867	29	910	15	953	3	996	0
782	65	825	50	868	27	911	11	954	6	997	2
783	42	826	39	869	32	912	15	955	11	998	0
784	40	827	56	870	34	913	23	956	3	999	2
785	50	828	34	871	26	914	18	957	3	1000	0
786	47	829	54	872	19	915	17	958	1	1001	0
787	48	830	52	873	25	916	19	959	3	1002	0
788	42	831	46	874	21	917	12	960	3	1003	0
789	56	832	41	875	34	918	14	961	8	1004	0
790	54	833	50	876	34	919	20	962	1	1005	1
791	54	834	32	877	28	920	12	963	5	1006	0
792	60	835	41	878	32	921	13	964	1	1007	0
793	45	836	42	879	19	922	10	965	0	1008	0
794	47	837	30	880	27	923	15	966	3	1009	0
795	41	838	52	881	17	924	7	967	3	1010	0
796	50	839	45	882	22	925	7	968	1	1011	0
797	41	840	33	883	28	926	6	969	0	1012	1
798	50	841	52	884	20	927	8	970	5	1013	0
799	39	842	32	885	30	928	12	971	5	1014	0
800	46	843	39	886	19	929	17	972	2	1015	0
801	53	844	39	887	27	930	10	973	0	1016	0
802	47	845	27	888	24	931	15	974	1	1017	0
803	54	846	52	889	24	932	12	975	0	1018	0
804	60	847	41	890	17	933	4	976	0	1019	0
805	33	848	36	891	24	934	9	977	1	1020	0
806	48	849	37	892	24	935	6	978	1	1021	0
807	54	850	32	893	14	936	9	979	1	1022	0
808	45	851	36	894	25	937	7	980	2	1023	0
809	37	852	43	895	21	938	5	981	0	1024	1
810	43	853	35	896	30	939	9	982	1		
811	63	854	50	897	18	940	4	983	0		
812	38	855	25	898	18	941	12	984	1		
813	42	856	37	899	19	942	11	985	2		
814	67	857	38	900	24	943	8	986	1		
815	44	858	28	901	23	944	5	987	1		
816	54	859	28	902	24	945	2	988	2		
817	43	860	31	903	13	946	4	989	0		

Table A9. Raw flow cytometry data for differentiating IMR-32 (Day 6, 1st replicate) used to generate Figure 3.2.

Channel #	*f*	Channel #	*f*	Channel #	*f*	Channel #	*f*	Channel #	*f*	Channel #	*f*
1	0	44	0	87	0	130	0	173	0	216	0
2	0	45	0	88	0	131	0	174	0	217	0
3	0	46	0	89	0	132	0	175	0	218	0
4	0	47	0	90	0	133	0	176	0	219	0
5	12	48	0	91	0	134	0	177	0	220	0
6	7	49	1	92	0	135	1	178	0	221	0
7	4	50	0	93	0	136	0	179	0	222	0
8	0	51	0	94	0	137	0	180	1	223	0
9	0	52	0	95	0	138	0	181	0	224	0
10	0	53	0	96	0	139	0	182	0	225	0
11	0	54	0	97	0	140	0	183	0	226	0
12	0	55	0	98	0	141	0	184	0	227	0
13	0	56	0	99	0	142	0	185	0	228	0
14	0	57	0	100	0	143	0	186	0	229	0
15	0	58	0	101	0	144	0	187	0	230	0
16	1	59	0	102	0	145	0	188	0	231	0
17	0	60	0	103	0	146	0	189	0	232	0
18	0	61	0	104	0	147	0	190	0	233	0
19	0	62	0	105	0	148	0	191	0	234	0
20	0	63	0	106	0	149	0	192	0	235	0
21	0	64	0	107	0	150	0	193	0	236	0
22	0	65	0	108	0	151	0	194	0	237	1
23	0	66	0	109	0	152	0	195	0	238	0
24	0	67	0	110	0	153	0	196	0	239	0
25	0	68	0	111	0	154	0	197	0	240	0
26	0	69	0	112	0	155	0	198	0	241	0
27	0	70	0	113	0	156	0	199	0	242	0
28	0	71	0	114	0	157	0	200	0	243	0
29	0	72	0	115	0	158	0	201	0	244	0
30	0	73	0	116	0	159	0	202	0	245	0
31	0	74	0	117	0	160	0	203	0	246	0
32	0	75	0	118	0	161	0	204	0	247	0
33	0	76	0	119	0	162	0	205	0	248	0
34	0	77	0	120	0	163	0	206	0	249	0
35	0	78	0	121	0	164	0	207	0	250	0
36	0	79	0	122	0	165	0	208	0	251	1
37	0	80	0	123	0	166	0	209	0	252	0
38	0	81	0	124	0	167	0	210	0	253	0
39	0	82	0	125	1	168	0	211	0	254	0
40	0	83	0	126	0	169	0	212	1	255	0
41	0	84	0	127	0	170	0	213	0	256	0
42	0	85	0	128	0	171	0	214	0	257	0
43	0	86	0	129	0	172	0	215	0	258	1

* Channel # and *f* represent oxonol fluorescence and frequency respectively.

Table A9. Continued.

Channel #	*f*	Channel #	*f*	Channel #	*f*	Channel #	*f*	Channel #	*f*	Channel #	*F*
259	0	302	0	345	0	388	0	431	1	474	1
260	0	303	0	346	0	389	0	432	0	475	0
261	0	304	0	347	0	390	0	433	1	476	0
262	0	305	1	348	0	391	0	434	1	477	0
263	0	306	0	349	0	392	0	435	1	478	2
264	0	307	0	350	0	393	1	436	0	479	0
265	0	308	0	351	0	394	1	437	0	480	3
266	0	309	0	352	1	395	0	438	0	481	2
267	0	310	0	353	0	396	0	439	0	482	1
268	1	311	0	354	0	397	1	440	1	483	0
269	0	312	0	355	0	398	0	441	0	484	4
270	0	313	0	356	0	399	1	442	0	485	0
271	0	314	0	357	0	400	0	443	0	486	1
272	0	315	0	358	0	401	2	444	0	487	0
273	0	316	0	359	0	402	0	445	0	488	1
274	1	317	0	360	0	403	0	446	0	489	3
275	0	318	0	361	0	404	1	447	0	490	1
276	0	319	0	362	0	405	0	448	1	491	0
277	0	320	0	363	0	406	0	449	1	492	2
278	0	321	0	364	0	407	1	450	1	493	3
279	0	322	1	365	0	408	2	451	1	494	0
280	0	323	0	366	0	409	0	452	1	495	1
281	0	324	0	367	1	410	0	453	0	496	0
282	0	325	0	368	0	411	0	454	0	497	2
283	0	326	0	369	0	412	0	455	0	498	1
284	0	327	0	370	0	413	0	456	1	499	0
285	0	328	0	371	0	414	2	457	0	500	0
286	0	329	0	372	0	415	1	458	1	501	1
287	0	330	0	373	1	416	0	459	1	502	0
288	1	331	0	374	1	417	0	460	1	503	1
289	0	332	0	375	0	418	1	461	1	504	0
290	0	333	0	376	0	419	0	462	0	505	0
291	0	334	1	377	0	420	1	463	1	506	0
292	0	335	0	378	0	421	1	464	0	507	1
293	0	336	0	379	0	422	0	465	1	508	1
294	0	337	1	380	0	423	0	466	0	509	4
295	0	338	0	381	0	424	1	467	1	510	0
296	0	339	0	382	0	425	0	468	0	511	0
297	0	340	0	383	0	426	0	469	0	512	1
298	0	341	0	384	0	427	0	470	1	513	0
299	0	342	0	385	1	428	0	471	0	514	2
300	0	343	0	386	0	429	1	472	0	515	3
301	0	344	0	387	0	430	0	473	2	516	0

Table A9. Continued.

Channel #	*f*	Channel #	*f*	Channel #	*f*	Channel #	*f*	Channel #	*f*	Channel #	*f*
517	1	560	2	603	2	646	5	689	11	732	21
518	1	561	2	604	2	647	5	690	13	733	21
519	1	562	3	605	2	648	7	691	13	734	32
520	2	563	3	606	4	649	8	692	9	735	23
521	0	564	4	607	6	650	5	693	13	736	28
522	1	565	0	608	2	651	10	694	11	737	20
523	0	566	1	609	7	652	5	695	14	738	26
524	4	567	4	610	4	653	10	696	4	739	27
525	1	568	2	611	6	654	9	697	12	740	23
526	2	569	1	612	2	655	7	698	11	741	19
527	4	570	4	613	6	656	2	699	22	742	30
528	2	571	1	614	4	657	7	700	13	743	26
529	3	572	3	615	4	658	7	701	13	744	26
530	0	573	3	616	3	659	10	702	14	745	19
531	0	574	1	617	4	660	6	703	19	746	25
532	1	575	3	618	4	661	7	704	8	747	44
533	0	576	4	619	7	662	10	705	19	748	33
534	1	577	4	620	7	663	4	706	12	749	22
535	1	578	1	621	9	664	11	707	20	750	22
536	2	579	3	622	3	665	13	708	13	751	36
537	1	580	2	623	3	666	6	709	16	752	25
538	2	581	1	624	6	667	6	710	21	753	32
539	0	582	2	625	5	668	9	711	18	754	26
540	0	583	0	626	11	669	7	712	16	755	32
541	0	584	3	627	11	670	10	713	23	756	36
542	2	585	4	628	7	671	9	714	19	757	31
543	2	586	0	629	4	672	7	715	22	758	41
544	1	587	5	630	8	673	5	716	21	759	37
545	4	588	3	631	6	674	9	717	14	760	30
546	2	589	2	632	3	675	11	718	25	761	34
547	2	590	3	633	8	676	11	719	23	762	48
548	2	591	5	634	2	677	5	720	14	763	47
549	3	592	3	635	4	678	11	721	17	764	37
550	1	593	4	636	4	679	11	722	19	765	27
551	0	594	0	637	6	680	11	723	22	766	32
552	1	595	4	638	5	681	8	724	15	767	35
553	1	596	1	639	5	682	10	725	15	768	41
554	1	597	6	640	5	683	15	726	25	769	33
555	2	598	5	641	5	684	9	727	16	770	38
556	2	599	8	642	8	685	10	728	21	771	39
557	0	600	4	643	12	686	16	729	21	772	31
558	0	601	3	644	6	687	15	730	25	773	36
559	2	602	7	645	5	688	12	731	28	774	49

Table A9. Continued.

Channel #	*f*	Channel #	*f*	Channel #	*f*	Channel #	*f*	Channel #	*f*	Channel #	*f*
775	27	818	50	861	43	904	20	947	8	990	0
776	30	819	50	862	41	905	32	948	8	991	0
777	44	820	64	863	51	906	23	949	8	992	0
778	42	821	49	864	43	907	32	950	14	993	2
779	43	822	57	865	59	908	24	951	8	994	0
780	40	823	41	866	58	909	22	952	5	995	2
781	55	824	63	867	63	910	32	953	2	996	1
782	56	825	54	868	33	911	15	954	6	997	0
783	42	826	65	869	49	912	25	955	5	998	0
784	48	827	68	870	51	913	21	956	2	999	1
785	43	828	53	871	42	914	19	957	1	1000	0
786	37	829	45	872	48	915	17	958	7	1001	0
787	49	830	53	873	56	916	26	959	3	1002	1
788	57	831	51	874	50	917	12	960	4	1003	0
789	37	832	44	875	35	918	19	961	0	1004	0
790	43	833	67	876	55	919	14	962	4	1005	0
791	52	834	51	877	42	920	26	963	3	1006	1
792	44	835	47	878	40	921	18	964	4	1007	0
793	47	836	58	879	38	922	19	965	4	1008	0
794	48	837	38	880	41	923	17	966	3	1009	0
795	56	838	69	881	30	924	11	967	4	1010	0
796	49	839	60	882	40	925	10	968	2	1011	0
797	53	840	51	883	57	926	18	969	3	1012	0
798	61	841	53	884	39	927	13	970	5	1013	0
799	38	842	48	885	48	928	15	971	3	1014	0
800	52	843	50	886	36	929	19	972	3	1015	0
801	46	844	57	887	34	930	18	973	0	1016	0
802	54	845	50	888	38	931	24	974	4	1017	0
803	34	846	64	889	41	932	20	975	0	1018	0
804	43	847	51	890	51	933	7	976	2	1019	0
805	41	848	53	891	33	934	9	977	1	1020	0
806	61	849	67	892	30	935	15	978	1	1021	0
807	44	850	61	893	37	936	11	979	1	1022	0
808	52	851	59	894	26	937	13	980	0	1023	0
809	70	852	67	895	34	938	9	981	2	1024	0
810	51	853	40	896	23	939	16	982	1		
811	60	854	57	897	30	940	4	983	1		
812	66	855	47	898	36	941	10	984	0		
813	60	856	42	899	29	942	4	985	0		
814	58	857	41	900	31	943	13	986	3		
815	58	858	57	901	29	944	9	987	3		
816	57	859	63	902	31	945	8	988	1		
817	52	860	50	903	29	946	4	989	0		

Table A10. Raw flow cytometry data for differentiating IMR-32 (Day 6, 2nd replicate) used to generate Figure 3.2.

Channel #	*f*	Channel #	*f*	Channel #	*f*	Channel #	*f*	Channel #	*f*	Channel #	*f*
1	0	44	0	87	0	130	0	173	0	216	0
2	0	45	0	88	0	131	0	174	0	217	0
3	0	46	0	89	0	132	0	175	0	218	0
4	3	47	0	90	0	133	0	176	0	219	0
5	15	48	0	91	0	134	0	177	0	220	0
6	5	49	0	92	0	135	0	178	0	221	0
7	2	50	0	93	0	136	0	179	1	222	0
8	0	51	0	94	1	137	0	180	0	223	0
9	0	52	0	95	0	138	0	181	0	224	0
10	0	53	0	96	0	139	0	182	0	225	0
11	0	54	1	97	0	140	0	183	0	226	0
12	0	55	0	98	0	141	0	184	0	227	0
13	0	56	0	99	1	142	0	185	0	228	0
14	0	57	0	100	0	143	0	186	0	229	0
15	0	58	0	101	0	144	0	187	0	230	0
16	0	59	0	102	0	145	0	188	0	231	0
17	0	60	0	103	0	146	0	189	0	232	0
18	0	61	0	104	0	147	0	190	0	233	0
19	0	62	0	105	0	148	0	191	0	234	1
20	0	63	0	106	0	149	0	192	0	235	0
21	0	64	0	107	0	150	0	193	0	236	0
22	0	65	0	108	0	151	1	194	0	237	0
23	0	66	0	109	0	152	0	195	0	238	0
24	0	67	0	110	0	153	0	196	0	239	0
25	0	68	0	111	0	154	0	197	0	240	0
26	0	69	1	112	0	155	0	198	0	241	0
27	0	70	0	113	0	156	0	199	0	242	0
28	0	71	0	114	0	157	0	200	0	243	0
29	0	72	0	115	0	158	0	201	0	244	0
30	0	73	0	116	0	159	0	202	0	245	0
31	0	74	0	117	0	160	0	203	0	246	0
32	0	75	0	118	0	161	0	204	0	247	0
33	0	76	0	119	0	162	0	205	0	248	0
34	0	77	0	120	0	163	0	206	0	249	0
35	0	78	0	121	0	164	0	207	0	250	0
36	0	79	0	122	0	165	0	208	1	251	0
37	0	80	0	123	0	166	0	209	0	252	0
38	0	81	0	124	0	167	0	210	0	253	0
39	0	82	0	125	0	168	1	211	0	254	0
40	0	83	0	126	0	169	0	212	0	255	0
41	0	84	0	127	0	170	0	213	0	256	0
42	0	85	0	128	0	171	0	214	1	257	0
43	0	86	0	129	0	172	1	215	0	258	0

* Channel # and *f* represent oxonol fluorescence and frequency respectively.

Table A10. Continued.

Channel #	*f*	Channel #	*f*	Channel #	*f*	Channel #	*f*	Channel #	*f*	Channel #	*F*
259	1	302	0	345	0	388	1	431	1	474	0
260	0	303	0	346	0	389	0	432	1	475	0
261	0	304	0	347	1	390	0	433	1	476	1
262	0	305	0	348	0	391	0	434	0	477	0
263	0	306	0	349	0	392	0	435	1	478	0
264	0	307	0	350	3	393	1	436	1	479	3
265	0	308	0	351	0	394	0	437	2	480	1
266	0	309	0	352	0	395	0	438	0	481	5
267	0	310	0	353	0	396	2	439	3	482	3
268	0	311	0	354	0	397	0	440	0	483	1
269	0	312	0	355	0	398	1	441	0	484	4
270	0	313	0	356	0	399	2	442	0	485	1
271	1	314	0	357	0	400	1	443	0	486	0
272	0	315	0	358	0	401	0	444	2	487	3
273	0	316	0	359	0	402	1	445	2	488	4
274	0	317	0	360	0	403	0	446	1	489	0
275	0	318	0	361	1	404	0	447	1	490	2
276	0	319	0	362	0	405	0	448	2	491	2
277	0	320	0	363	1	406	0	449	2	492	2
278	0	321	0	364	0	407	0	450	2	493	2
279	0	322	0	365	0	408	0	451	2	494	1
280	0	323	0	366	1	409	1	452	2	495	1
281	0	324	0	367	1	410	2	453	2	496	0
282	0	325	0	368	0	411	2	454	3	497	4
283	0	326	0	369	1	412	1	455	3	498	4
284	1	327	1	370	0	413	0	456	3	499	4
285	0	328	0	371	0	414	1	457	2	500	2
286	0	329	0	372	1	415	0	458	1	501	3
287	0	330	0	373	0	416	2	459	0	502	2
288	1	331	0	374	0	417	0	460	1	503	2
289	0	332	0	375	0	418	0	461	0	504	3
290	0	333	0	376	0	419	0	462	0	505	3
291	0	334	0	377	0	420	1	463	3	506	4
292	0	335	1	378	0	421	2	464	2	507	0
293	1	336	2	379	1	422	1	465	1	508	1
294	0	337	0	380	1	423	0	466	2	509	2
295	0	338	1	381	1	424	2	467	2	510	5
296	0	339	1	382	1	425	0	468	1	511	3
297	0	340	0	383	0	426	0	469	0	512	6
298	0	341	0	384	0	427	4	470	1	513	3
299	0	342	1	385	1	428	0	471	1	514	5
300	0	343	2	386	2	429	1	472	1	515	3
301	0	344	0	387	1	430	0	473	3	516	3

Table A10. Continued.

Channel #	*f*	Channel #	*f*	Channel #	*f*	Channel #	*f*	Channel #	*f*	Channel #	*f*
517	2	560	2	603	11	646	12	689	32	732	37
518	2	561	5	604	11	647	19	690	24	733	32
519	0	562	6	605	9	648	14	691	27	734	31
520	3	563	11	606	11	649	13	692	24	735	36
521	3	564	12	607	15	650	24	693	13	736	33
522	3	565	5	608	8	651	19	694	35	737	40
523	2	566	3	609	16	652	16	695	29	738	47
524	1	567	4	610	8	653	13	696	19	739	45
525	2	568	7	611	15	654	19	697	33	740	37
526	2	569	7	612	8	655	20	698	25	741	39
527	1	570	6	613	9	656	19	699	32	742	44
528	3	571	7	614	10	657	19	700	23	743	39
529	0	572	5	615	6	658	24	701	28	744	52
530	1	573	7	616	5	659	16	702	24	745	45
531	1	574	6	617	10	660	16	703	22	746	46
532	0	575	6	618	15	661	14	704	19	747	46
533	3	576	4	619	14	662	13	705	27	748	46
534	1	577	5	620	10	663	9	706	32	749	39
535	1	578	9	621	11	664	16	707	29	750	42
536	4	579	7	622	8	665	23	708	24	751	38
537	5	580	5	623	9	666	14	709	23	752	54
538	8	581	6	624	9	667	26	710	41	753	45
539	4	582	8	625	16	668	18	711	36	754	45
540	2	583	3	626	15	669	21	712	38	755	51
541	3	584	5	627	16	670	10	713	44	756	42
542	5	585	7	628	14	671	15	714	31	757	47
543	2	586	7	629	10	672	23	715	47	758	49
544	5	587	7	630	11	673	25	716	40	759	57
545	4	588	6	631	14	674	24	717	27	760	44
546	2	589	11	632	10	675	16	718	31	761	46
547	6	590	9	633	13	676	21	719	31	762	62
548	6	591	8	634	7	677	16	720	32	763	49
549	7	592	5	635	11	678	38	721	32	764	56
550	3	593	8	636	16	679	24	722	25	765	47
551	2	594	5	637	11	680	25	723	29	766	50
552	3	595	9	638	19	681	19	724	37	767	50
553	4	596	6	639	12	682	21	725	32	768	51
554	3	597	17	640	17	683	16	726	56	769	37
555	4	598	7	641	12	684	24	727	41	770	50
556	1	599	3	642	13	685	22	728	40	771	51
557	4	600	13	643	11	686	23	729	44	772	44
558	4	601	8	644	13	687	27	730	50	773	47
559	8	602	7	645	13	688	27	731	32	774	50

Table A10. Continued.

Channel #	*f*	Channel #	*f*	Channel #	*f*	Channel #	*f*	Channel #	*f*	Channel #	*f*
775	53	818	49	861	25	904	13	947	2	990	1
776	47	819	46	862	22	905	14	948	1	991	1
777	63	820	42	863	21	906	13	949	3	992	0
778	47	821	32	864	34	907	9	950	0	993	0
779	47	822	43	865	20	908	12	951	2	994	0
780	55	823	35	866	19	909	9	952	0	995	1
781	40	824	43	867	26	910	11	953	3	996	0
782	51	825	42	868	24	911	9	954	0	997	0
783	54	826	54	869	24	912	7	955	3	998	0
784	47	827	40	870	23	913	5	956	1	999	0
785	52	828	41	871	28	914	9	957	0	1000	0
786	41	829	42	872	20	915	6	958	2	1001	0
787	47	830	29	873	25	916	12	959	0	1002	0
788	52	831	37	874	16	917	3	960	3	1003	0
789	51	832	39	875	20	918	6	961	4	1004	0
790	64	833	46	876	12	919	8	962	1	1005	0
791	32	834	47	877	19	920	8	963	0	1006	0
792	47	835	29	878	16	921	10	964	3	1007	0
793	39	836	30	879	18	922	8	965	1	1008	0
794	57	837	27	880	18	923	6	966	0	1009	0
795	51	838	32	881	14	924	6	967	2	1010	0
796	34	839	31	882	19	925	4	968	3	1011	0
797	60	840	32	883	25	926	9	969	2	1012	0
798	54	841	28	884	22	927	3	970	1	1013	0
799	25	842	36	885	20	928	6	971	2	1014	0
800	35	843	24	886	34	929	8	972	0	1015	0
801	53	844	27	887	25	930	4	973	0	1016	0
802	55	845	32	888	11	931	9	974	0	1017	0
803	43	846	45	889	14	932	2	975	0	1018	0
804	53	847	33	890	16	933	1	976	0	1019	0
805	42	848	27	891	20	934	9	977	0	1020	0
806	51	849	30	892	10	935	4	978	0	1021	0
807	50	850	36	893	20	936	5	979	1	1022	0
808	45	851	27	894	16	937	4	980	0	1023	0
809	45	852	32	895	12	938	4	981	0	1024	0
810	47	853	31	896	17	939	3	982	0		
811	53	854	28	897	16	940	8	983	0		
812	46	855	16	898	11	941	3	984	1		
813	46	856	26	899	16	942	4	985	0		
814	51	857	25	900	24	943	2	986	0		
815	50	858	23	901	7	944	3	987	0		
816	41	859	32	902	8	945	4	988	0		
817	45	860	36	903	12	946	1	989	0		

Table A11. Raw flow cytometry data for differentiating IMR-32 (Day 8, 1st replicate) used to generate Figure 3.2.

Channel #	*f*	Channel #	*f*	Channel #	*f*	Channel #	*f*	Channel #	*f*	Channel #	*f*
1	0	44	0	87	0	130	4	173	4	216	5
2	0	45	0	88	3	131	2	174	2	217	2
3	0	46	3	89	1	132	2	175	1	218	0
4	12	47	1	90	0	133	3	176	1	219	2
5	157	48	0	91	1	134	0	177	2	220	2
6	31	49	0	92	3	135	1	178	6	221	3
7	4	50	3	93	0	136	2	179	0	222	1
8	0	51	1	94	4	137	1	180	1	223	3
9	1	52	2	95	2	138	0	181	2	224	5
10	3	53	1	96	5	139	1	182	1	225	5
11	0	54	3	97	1	140	1	183	2	226	0
12	2	55	1	98	1	141	2	184	1	227	5
13	1	56	0	99	3	142	0	185	2	228	3
14	2	57	1	100	3	143	1	186	4	229	2
15	2	58	1	101	1	144	0	187	2	230	3
16	0	59	3	102	0	145	1	188	1	231	4
17	1	60	1	103	0	146	2	189	2	232	1
18	1	61	2	104	0	147	2	190	4	233	4
19	3	62	2	105	0	148	1	191	1	234	1
20	0	63	1	106	2	149	0	192	2	235	3
21	1	64	1	107	0	150	1	193	4	236	4
22	0	65	1	108	0	151	0	194	4	237	1
23	0	66	2	109	1	152	1	195	1	238	2
24	0	67	0	110	0	153	0	196	1	239	2
25	2	68	2	111	0	154	1	197	3	240	2
26	1	69	1	112	3	155	2	198	5	241	6
27	4	70	1	113	1	156	3	199	2	242	0
28	0	71	2	114	2	157	5	200	4	243	5
29	1	72	1	115	0	158	2	201	3	244	2
30	1	73	1	116	3	159	1	202	2	245	2
31	0	74	1	117	1	160	6	203	7	246	3
32	1	75	5	118	3	161	3	204	5	247	4
33	2	76	0	119	1	162	0	205	4	248	3
34	2	77	2	120	0	163	0	206	2	249	5
35	3	78	1	121	1	164	3	207	3	250	2
36	1	79	1	122	1	165	1	208	1	251	2
37	1	80	1	123	0	166	1	209	1	252	1
38	2	81	0	124	1	167	1	210	1	253	1
39	1	82	1	125	0	168	1	211	2	254	1
40	0	83	1	126	0	169	3	212	3	255	3
41	1	84	1	127	1	170	6	213	0	256	1
42	1	85	1	128	4	171	3	214	3	257	3
43	2	86	1	129	1	172	4	215	0	258	5

* Channel # and *f* represent oxonol fluorescence and frequency respectively.

Table A11. Continued.

Channel #	*f*	Channel #	*f*	Channel #	*f*	Channel #	*f*	Channel #	*f*	Channel #	*F*
259	3	302	3	345	3	388	2	431	2	474	4
260	1	303	1	346	3	389	4	432	3	475	4
261	4	304	2	347	1	390	2	433	3	476	6
262	2	305	3	348	3	391	2	434	4	477	6
263	2	306	3	349	2	392	2	435	3	478	2
264	2	307	4	350	1	393	5	436	6	479	3
265	2	308	2	351	3	394	1	437	9	480	3
266	2	309	4	352	2	395	5	438	2	481	4
267	0	310	4	353	3	396	2	439	5	482	3
268	0	311	4	354	2	397	2	440	3	483	9
269	4	312	4	355	5	398	3	441	6	484	0
270	1	313	6	356	4	399	4	442	5	485	3
271	6	314	2	357	3	400	3	443	2	486	1
272	0	315	2	358	1	401	5	444	3	487	3
273	2	316	2	359	2	402	2	445	4	488	4
274	2	317	1	360	4	403	3	446	0	489	3
275	1	318	3	361	2	404	5	447	4	490	4
276	5	319	1	362	2	405	3	448	4	491	6
277	5	320	4	363	2	406	2	449	2	492	2
278	6	321	4	364	5	407	4	450	3	493	2
279	2	322	1	365	0	408	3	451	3	494	6
280	4	323	4	366	5	409	7	452	7	495	4
281	5	324	4	367	7	410	8	453	3	496	3
282	3	325	4	368	3	411	1	454	2	497	3
283	3	326	2	369	4	412	6	455	3	498	9
284	2	327	4	370	3	413	4	456	1	499	8
285	2	328	1	371	5	414	7	457	8	500	4
286	4	329	3	372	5	415	5	458	1	501	6
287	2	330	0	373	1	416	2	459	5	502	8
288	1	331	7	374	4	417	3	460	8	503	1
289	3	332	2	375	3	418	4	461	2	504	2
290	3	333	5	376	2	419	0	462	1	505	2
291	2	334	5	377	1	420	2	463	4	506	2
292	1	335	2	378	3	421	3	464	5	507	3
293	1	336	3	379	5	422	2	465	4	508	2
294	1	337	2	380	4	423	4	466	4	509	6
295	2	338	4	381	1	424	5	467	3	510	4
296	2	339	4	382	4	425	3	468	4	511	1
297	4	340	5	383	4	426	3	469	7	512	4
298	3	341	6	384	3	427	5	470	2	513	6
299	5	342	4	385	2	428	6	471	5	514	8
300	2	343	4	386	7	429	3	472	4	515	2
301	1	344	4	387	1	430	3	473	2	516	4

Table A11. Continued.

Channel #	*f*	Channel #	*f*	Channel #	*f*	Channel #	*f*	Channel #	*f*	Channel #	*f*
517	3	560	5	603	5	646	8	689	5	732	17
518	7	561	4	604	4	647	5	690	14	733	17
519	5	562	2	605	6	648	6	691	7	734	20
520	6	563	6	606	5	649	5	692	11	735	11
521	8	564	5	607	5	650	2	693	12	736	9
522	5	565	3	608	3	651	4	694	13	737	18
523	5	566	2	609	5	652	7	695	15	738	13
524	6	567	5	610	5	653	8	696	7	739	21
525	3	568	7	611	6	654	6	697	5	740	16
526	3	569	8	612	2	655	6	698	9	741	19
527	3	570	9	613	4	656	5	699	8	742	21
528	6	571	4	614	5	657	5	700	12	743	13
529	7	572	4	615	6	658	5	701	4	744	14
530	5	573	7	616	5	659	9	702	9	745	17
531	4	574	3	617	3	660	6	703	9	746	13
532	1	575	2	618	5	661	5	704	8	747	19
533	2	576	4	619	2	662	8	705	9	748	18
534	5	577	5	620	4	663	5	706	8	749	12
535	3	578	9	621	5	664	6	707	10	750	21
536	6	579	3	622	5	665	6	708	8	751	14
537	4	580	5	623	7	666	6	709	7	752	15
538	3	581	3	624	3	667	6	710	9	753	25
539	3	582	1	625	2	668	6	711	8	754	28
540	2	583	3	626	4	669	5	712	9	755	22
541	3	584	4	627	3	670	4	713	5	756	23
542	3	585	3	628	5	671	10	714	6	757	12
543	3	586	8	629	2	672	6	715	9	758	19
544	1	587	6	630	2	673	8	716	8	759	19
545	4	588	3	631	4	674	7	717	7	760	17
546	3	589	6	632	2	675	10	718	11	761	20
547	6	590	6	633	2	676	7	719	8	762	21
548	5	591	4	634	4	677	1	720	6	763	17
549	6	592	5	635	7	678	5	721	13	764	23
550	6	593	8	636	6	679	8	722	10	765	14
551	11	594	4	637	4	680	6	723	17	766	19
552	3	595	7	638	5	681	9	724	6	767	22
553	5	596	4	639	5	682	4	725	9	768	24
554	12	597	6	640	8	683	4	726	15	769	22
555	5	598	2	641	9	684	9	727	11	770	26
556	7	599	5	642	8	685	8	728	14	771	17
557	2	600	0	643	4	686	9	729	10	772	29
558	5	601	2	644	6	687	6	730	14	773	23
559	8	602	4	645	0	688	5	731	13	774	26

Table A11. Continued.

Channel #	*f*	Channel #	*f*	Channel #	*f*	Channel #	*f*	Channel #	*f*	Channel #	*f*
775	20	818	49	861	33	904	36	947	6	990	1
776	27	819	49	862	65	905	34	948	9	991	1
777	28	820	47	863	42	906	33	949	9	992	1
778	25	821	50	864	55	907	29	950	6	993	1
779	30	822	54	865	51	908	26	951	4	994	0
780	22	823	51	866	47	909	27	952	12	995	0
781	28	824	40	867	56	910	25	953	9	996	0
782	38	825	51	868	42	911	28	954	10	997	0
783	29	826	47	869	52	912	27	955	5	998	0
784	19	827	58	870	70	913	26	956	9	999	1
785	23	828	57	871	45	914	29	957	5	1000	1
786	31	829	49	872	45	915	12	958	3	1001	0
787	31	830	54	873	54	916	32	959	8	1002	0
788	28	831	35	874	54	917	25	960	3	1003	1
789	31	832	49	875	43	918	17	961	4	1004	0
790	39	833	45	876	45	919	24	962	3	1005	0
791	34	834	45	877	36	920	19	963	7	1006	0
792	37	835	64	878	48	921	18	964	4	1007	0
793	28	836	40	879	36	922	25	965	4	1008	0
794	40	837	55	880	40	923	25	966	6	1009	1
795	39	838	57	881	45	924	24	967	8	1010	0
796	21	839	48	882	33	925	12	968	2	1011	0
797	30	840	36	883	43	926	15	969	3	1012	0
798	31	841	51	884	49	927	22	970	2	1013	0
799	37	842	55	885	30	928	13	971	5	1014	0
800	26	843	56	886	43	929	16	972	6	1015	0
801	38	844	52	887	43	930	18	973	3	1016	0
802	45	845	51	888	36	931	19	974	3	1017	0
803	33	846	50	889	35	932	16	975	0	1018	0
804	39	847	59	890	52	933	7	976	2	1019	0
805	41	848	44	891	27	934	17	977	1	1020	0
806	38	849	54	892	34	935	11	978	2	1021	0
807	44	850	48	893	30	936	9	979	0	1022	0
808	41	851	58	894	34	937	13	980	0	1023	0
809	47	852	41	895	35	938	10	981	1	1024	0
810	44	853	45	896	31	939	8	982	0		
811	38	854	53	897	50	940	12	983	1		
812	31	855	49	898	46	941	4	984	1		
813	42	856	53	899	31	942	15	985	1		
814	40	857	59	900	29	943	4	986	1		
815	30	858	48	901	36	944	4	987	0		
816	38	859	65	902	35	945	12	988	0		
817	61	860	44	903	28	946	11	989	0		

Table A12. Raw flow cytometry data for differentiating IMR-32 (Day 8, 2nd replicate) used to generate Figure 3.2.

Channel #	*f*	Channel #	*f*	Channel #	*f*	Channel #	*f*	Channel #	*f*	Channel #	*f*
1	0	44	0	87	0	130	0	173	0	216	0
2	0	45	0	88	0	131	0	174	0	217	0
3	0	46	0	89	0	132	0	175	0	218	0
4	0	47	1	90	0	133	0	176	0	219	0
5	6	48	0	91	0	134	0	177	0	220	0
6	8	49	0	92	0	135	0	178	0	221	0
7	2	50	0	93	0	136	0	179	0	222	0
8	1	51	0	94	0	137	0	180	0	223	0
9	0	52	0	95	0	138	0	181	0	224	0
10	0	53	0	96	0	139	0	182	0	225	0
11	0	54	0	97	0	140	0	183	0	226	0
12	0	55	0	98	0	141	0	184	0	227	0
13	0	56	0	99	0	142	0	185	1	228	0
14	0	57	0	100	0	143	0	186	0	229	0
15	0	58	0	101	0	144	0	187	0	230	0
16	0	59	0	102	1	145	0	188	0	231	0
17	0	60	0	103	0	146	0	189	0	232	0
18	0	61	0	104	0	147	0	190	0	233	0
19	0	62	0	105	0	148	1	191	0	234	0
20	0	63	0	106	0	149	0	192	0	235	0
21	0	64	0	107	0	150	0	193	0	236	0
22	0	65	0	108	0	151	0	194	0	237	0
23	0	66	0	109	0	152	0	195	0	238	0
24	0	67	0	110	0	153	0	196	0	239	0
25	0	68	0	111	0	154	0	197	0	240	0
26	0	69	0	112	0	155	0	198	0	241	0
27	0	70	0	113	0	156	1	199	0	242	0
28	0	71	0	114	0	157	0	200	0	243	0
29	0	72	0	115	0	158	0	201	0	244	0
30	0	73	0	116	0	159	0	202	0	245	0
31	0	74	0	117	0	160	0	203	0	246	0
32	0	75	0	118	0	161	0	204	0	247	0
33	0	76	0	119	0	162	0	205	0	248	0
34	0	77	0	120	0	163	0	206	0	249	0
35	0	78	0	121	0	164	0	207	0	250	0
36	0	79	0	122	0	165	0	208	0	251	0
37	0	80	0	123	0	166	0	209	0	252	0
38	0	81	0	124	0	167	0	210	0	253	0
39	0	82	0	125	0	168	0	211	0	254	0
40	0	83	0	126	0	169	0	212	0	255	0
41	0	84	0	127	0	170	0	213	0	256	0
42	0	85	0	128	0	171	0	214	0	257	0
43	0	86	0	129	0	172	0	215	0	258	0

* Channel # and *f* represent oxonol fluorescence and frequency respectively.

Table A12. Continued.

Channel #	*f*	Channel #	*f*	Channel #	*f*	Channel #	*f*	Channel #	*f*	Channel #	*F*
259	0	302	0	345	0	388	0	431	0	474	2
260	1	303	0	346	1	389	0	432	0	475	1
261	0	304	0	347	1	390	0	433	1	476	0
262	0	305	0	348	0	391	0	434	0	477	1
263	0	306	0	349	0	392	1	435	1	478	1
264	0	307	0	350	0	393	1	436	1	479	2
265	0	308	0	351	0	394	0	437	0	480	1
266	0	309	0	352	0	395	0	438	0	481	0
267	0	310	0	353	2	396	0	439	0	482	0
268	0	311	0	354	0	397	0	440	1	483	2
269	0	312	0	355	0	398	0	441	0	484	0
270	0	313	0	356	0	399	2	442	0	485	0
271	0	314	0	357	0	400	0	443	0	486	0
272	0	315	0	358	0	401	0	444	0	487	0
273	0	316	0	359	0	402	0	445	1	488	0
274	0	317	0	360	0	403	1	446	0	489	0
275	0	318	0	361	1	404	1	447	0	490	0
276	0	319	0	362	1	405	1	448	0	491	0
277	0	320	0	363	0	406	0	449	0	492	0
278	0	321	0	364	0	407	0	450	1	493	1
279	0	322	0	365	0	408	0	451	0	494	1
280	0	323	0	366	0	409	0	452	2	495	1
281	0	324	0	367	0	410	0	453	0	496	0
282	0	325	0	368	0	411	0	454	2	497	1
283	0	326	0	369	0	412	0	455	1	498	0
284	0	327	0	370	0	413	1	456	1	499	0
285	0	328	0	371	0	414	0	457	1	500	1
286	0	329	0	372	0	415	1	458	0	501	1
287	0	330	0	373	0	416	1	459	1	502	0
288	0	331	0	374	0	417	1	460	0	503	1
289	0	332	0	375	0	418	0	461	1	504	1
290	0	333	0	376	0	419	0	462	0	505	3
291	0	334	0	377	1	420	0	463	0	506	1
292	0	335	0	378	0	421	0	464	2	507	1
293	0	336	0	379	0	422	1	465	0	508	2
294	0	337	0	380	1	423	0	466	1	509	2
295	0	338	0	381	0	424	0	467	1	510	3
296	0	339	0	382	0	425	0	468	0	511	2
297	0	340	0	383	0	426	0	469	0	512	1
298	0	341	0	384	0	427	0	470	0	513	1
299	0	342	1	385	1	428	0	471	1	514	0
300	0	343	0	386	0	429	0	472	1	515	0
301	0	344	1	387	0	430	1	473	2	516	3

Table A12. Continued.

Channel #	*f*	Channel #	*f*	Channel #	*f*	Channel #	*f*	Channel #	*f*	Channel #	*f*
517	1	560	0	603	6	646	6	689	9	732	20
518	0	561	2	604	3	647	7	690	10	733	22
519	0	562	2	605	3	648	7	691	12	734	21
520	0	563	1	606	3	649	6	692	10	735	22
521	2	564	3	607	2	650	8	693	10	736	17
522	2	565	3	608	3	651	11	694	15	737	16
523	2	566	0	609	3	652	9	695	8	738	17
524	1	567	1	610	6	653	5	696	15	739	22
525	0	568	0	611	4	654	5	697	11	740	25
526	2	569	0	612	3	655	3	698	16	741	18
527	1	570	2	613	6	656	4	699	13	742	30
528	4	571	3	614	0	657	7	700	6	743	24
529	3	572	2	615	5	658	6	701	10	744	28
530	2	573	2	616	4	659	9	702	13	745	26
531	0	574	2	617	2	660	7	703	10	746	24
532	2	575	1	618	5	661	9	704	19	747	23
533	1	576	1	619	8	662	3	705	14	748	23
534	0	577	3	620	4	663	11	706	21	749	11
535	3	578	1	621	5	664	7	707	13	750	28
536	1	579	5	622	4	665	5	708	13	751	24
537	0	580	2	623	4	666	4	709	14	752	24
538	3	581	3	624	3	667	20	710	11	753	39
539	1	582	1	625	5	668	7	711	11	754	37
540	2	583	6	626	8	669	11	712	16	755	34
541	0	584	1	627	6	670	7	713	17	756	28
542	1	585	2	628	5	671	11	714	14	757	24
543	1	586	2	629	7	672	9	715	17	758	26
544	2	587	5	630	4	673	3	716	15	759	33
545	0	588	1	631	4	674	2	717	12	760	38
546	2	589	3	632	8	675	5	718	21	761	28
547	7	590	3	633	5	676	7	719	21	762	32
548	0	591	2	634	8	677	5	720	11	763	26
549	0	592	2	635	5	678	9	721	14	764	32
550	2	593	3	636	5	679	11	722	11	765	29
551	1	594	5	637	6	680	9	723	19	766	33
552	0	595	1	638	8	681	9	724	17	767	35
553	1	596	9	639	2	682	7	725	12	768	35
554	0	597	0	640	8	683	8	726	13	769	34
555	1	598	8	641	5	684	9	727	16	770	39
556	2	599	3	642	2	685	9	728	17	771	33
557	1	600	3	643	6	686	7	729	17	772	41
558	2	601	3	644	4	687	10	730	17	773	40
559	1	602	1	645	4	688	14	731	18	774	32

Table A12. Continued.

Channel #	*f*	Channel #	*f*	Channel #	*f*	Channel #	*f*	Channel #	*f*	Channel #	*f*
775	34	818	65	861	42	904	39	947	9	990	0
776	34	819	46	862	70	905	30	948	8	991	2
777	44	820	40	863	56	906	31	949	8	992	1
778	44	821	48	864	57	907	28	950	7	993	3
779	41	822	56	865	68	908	31	951	6	994	0
780	42	823	74	866	63	909	26	952	3	995	2
781	29	824	49	867	70	910	23	953	4	996	0
782	56	825	61	868	62	911	29	954	10	997	0
783	36	826	58	869	56	912	27	955	8	998	1
784	43	827	71	870	49	913	24	956	10	999	0
785	35	828	56	871	48	914	23	957	5	1000	0
786	35	829	51	872	47	915	23	958	10	1001	2
787	48	830	69	873	47	916	25	959	3	1002	0
788	34	831	50	874	62	917	21	960	3	1003	0
789	28	832	50	875	54	918	17	961	5	1004	0
790	68	833	70	876	57	919	17	962	3	1005	0
791	43	834	51	877	42	920	19	963	3	1006	1
792	41	835	69	878	53	921	18	964	4	1007	0
793	44	836	63	879	40	922	24	965	2	1008	0
794	43	837	52	880	52	923	21	966	3	1009	0
795	43	838	82	881	27	924	25	967	3	1010	0
796	48	839	53	882	61	925	21	968	4	1011	0
797	53	840	53	883	36	926	16	969	3	1012	0
798	55	841	58	884	33	927	14	970	3	1013	0
799	40	842	59	885	44	928	7	971	6	1014	0
800	41	843	69	886	47	929	16	972	3	1015	0
801	47	844	54	887	48	930	7	973	1	1016	0
802	54	845	52	888	42	931	14	974	2	1017	0
803	40	846	70	889	60	932	13	975	2	1018	0
804	45	847	55	890	45	933	21	976	2	1019	0
805	46	848	38	891	43	934	15	977	2	1020	0
806	57	849	73	892	42	935	16	978	0	1021	1
807	44	850	56	893	33	936	13	979	0	1022	0
808	59	851	61	894	43	937	11	980	1	1023	0
809	48	852	60	895	31	938	10	981	2	1024	0
810	39	853	61	896	30	939	12	982	0		
811	49	854	72	897	36	940	8	983	1		
812	35	855	49	898	31	941	17	984	3		
813	38	856	62	899	39	942	7	985	1		
814	50	857	54	900	42	943	11	986	2		
815	57	858	56	901	34	944	12	987	1		
816	55	859	56	902	38	945	7	988	0		
817	63	860	53	903	25	946	14	989	2		

Table A13. Raw flow cytometry data for differentiating IMR-32 (Day 8, 3rd replicate) used to generate Figure 3.2.

Channel #	*f*	Channel #	*f*	Channel #	*f*	Channel #	*f*	Channel #	*f*	Channel #	*f*
1	0	44	0	87	0	130	0	173	0	216	0
2	0	45	0	88	0	131	0	174	1	217	0
3	0	46	0	89	0	132	0	175	0	218	0
4	0	47	0	90	0	133	0	176	0	219	0
5	7	48	0	91	0	134	0	177	0	220	0
6	3	49	0	92	0	135	0	178	0	221	0
7	0	50	0	93	0	136	0	179	0	222	0
8	0	51	0	94	0	137	0	180	0	223	0
9	0	52	0	95	0	138	0	181	0	224	0
10	0	53	0	96	0	139	0	182	0	225	0
11	0	54	0	97	0	140	0	183	0	226	0
12	0	55	0	98	0	141	0	184	0	227	0
13	0	56	0	99	0	142	0	185	0	228	0
14	0	57	0	100	0	143	0	186	0	229	0
15	0	58	0	101	0	144	0	187	0	230	0
16	0	59	0	102	0	145	0	188	0	231	0
17	0	60	0	103	0	146	0	189	0	232	0
18	0	61	0	104	0	147	0	190	0	233	0
19	0	62	0	105	0	148	0	191	0	234	0
20	0	63	0	106	0	149	0	192	1	235	0
21	0	64	0	107	0	150	0	193	0	236	0
22	0	65	0	108	0	151	0	194	0	237	0
23	0	66	0	109	0	152	0	195	0	238	0
24	0	67	0	110	0	153	0	196	1	239	0
25	0	68	0	111	0	154	0	197	0	240	0
26	0	69	0	112	0	155	0	198	0	241	0
27	0	70	0	113	0	156	0	199	0	242	0
28	0	71	0	114	0	157	0	200	0	243	0
29	0	72	0	115	0	158	0	201	1	244	1
30	0	73	0	116	0	159	0	202	0	245	0
31	0	74	0	117	0	160	0	203	0	246	0
32	0	75	0	118	0	161	0	204	0	247	0
33	0	76	0	119	0	162	0	205	0	248	0
34	0	77	0	120	0	163	0	206	0	249	0
35	0	78	0	121	0	164	0	207	0	250	0
36	0	79	0	122	0	165	0	208	0	251	0
37	0	80	0	123	0	166	0	209	0	252	2
38	0	81	0	124	0	167	0	210	0	253	0
39	0	82	0	125	0	168	0	211	0	254	0
40	0	83	0	126	0	169	1	212	0	255	0
41	0	84	0	127	0	170	0	213	0	256	0
42	0	85	0	128	0	171	0	214	0	257	1
43	0	86	0	129	0	172	0	215	0	258	0

* Channel # and *f* represent oxonol fluorescence and frequency respectively.

Table A13. Continued.

Channel #	*f*	Channel #	*f*	Channel #	*f*	Channel #	*f*	Channel #	*f*	Channel #	*F*
259	1	302	0	345	0	388	0	431	0	474	1
260	0	303	0	346	0	389	0	432	0	475	1
261	0	304	0	347	0	390	0	433	0	476	1
262	0	305	0	348	0	391	0	434	1	477	1
263	0	306	0	349	0	392	0	435	0	478	1
264	0	307	0	350	0	393	0	436	1	479	1
265	0	308	0	351	0	394	1	437	1	480	1
266	0	309	1	352	0	395	0	438	0	481	3
267	0	310	0	353	0	396	0	439	0	482	0
268	0	311	0	354	1	397	0	440	1	483	1
269	0	312	0	355	0	398	0	441	1	484	0
270	0	313	0	356	0	399	0	442	0	485	0
271	0	314	0	357	0	400	0	443	0	486	2
272	0	315	0	358	0	401	0	444	2	487	1
273	0	316	0	359	0	402	0	445	0	488	0
274	0	317	0	360	1	403	2	446	0	489	0
275	0	318	0	361	0	404	1	447	0	490	0
276	0	319	0	362	1	405	0	448	0	491	1
277	0	320	0	363	0	406	0	449	1	492	0
278	0	321	0	364	0	407	0	450	0	493	0
279	0	322	0	365	0	408	0	451	0	494	2
280	0	323	0	366	0	409	0	452	2	495	0
281	0	324	0	367	0	410	0	453	1	496	0
282	0	325	0	368	0	411	0	454	0	497	2
283	0	326	0	369	0	412	0	455	0	498	2
284	0	327	0	370	0	413	1	456	0	499	0
285	0	328	0	371	0	414	0	457	1	500	0
286	0	329	0	372	0	415	0	458	0	501	2
287	0	330	0	373	0	416	0	459	0	502	1
288	0	331	0	374	0	417	0	460	1	503	1
289	0	332	0	375	0	418	0	461	0	504	1
290	0	333	1	376	0	419	0	462	0	505	3
291	0	334	1	377	0	420	1	463	0	506	0
292	0	335	0	378	0	421	0	464	1	507	0
293	0	336	0	379	0	422	1	465	0	508	1
294	0	337	0	380	0	423	0	466	0	509	0
295	0	338	0	381	0	424	0	467	0	510	0
296	0	339	0	382	1	425	1	468	0	511	0
297	0	340	0	383	0	426	1	469	0	512	3
298	0	341	0	384	0	427	0	470	0	513	2
299	0	342	0	385	0	428	0	471	1	514	2
300	0	343	0	386	1	429	1	472	1	515	2
301	0	344	0	387	0	430	0	473	2	516	1

Table A13. Continued.

Channel #	*f*	Channel #	*f*	Channel #	*f*	Channel #	*f*	Channel #	*f*	Channel #	*f*
517	0	560	0	603	4	646	4	689	10	732	18
518	1	561	0	604	0	647	6	690	13	733	29
519	1	562	0	605	4	648	7	691	11	734	21
520	1	563	4	606	1	649	6	692	7	735	18
521	0	564	1	607	2	650	8	693	9	736	21
522	1	565	4	608	5	651	6	694	20	737	26
523	1	566	2	609	1	652	3	695	15	738	15
524	0	567	1	610	2	653	10	696	9	739	12
525	0	568	2	611	5	654	6	697	12	740	32
526	0	569	2	612	3	655	7	698	25	741	22
527	1	570	2	613	2	656	6	699	20	742	24
528	0	571	4	614	2	657	7	700	10	743	22
529	2	572	1	615	2	658	8	701	13	744	22
530	0	573	4	616	1	659	3	702	14	745	15
531	0	574	1	617	6	660	7	703	14	746	38
532	0	575	3	618	3	661	6	704	25	747	22
533	2	576	7	619	4	662	8	705	21	748	23
534	1	577	3	620	3	663	13	706	21	749	27
535	0	578	2	621	6	664	11	707	15	750	31
536	2	579	2	622	5	665	9	708	22	751	30
537	3	580	2	623	4	666	7	709	15	752	23
538	1	581	2	624	2	667	6	710	15	753	25
539	1	582	1	625	4	668	9	711	20	754	23
540	0	583	3	626	5	669	2	712	26	755	20
541	3	584	3	627	7	670	5	713	16	756	29
542	2	585	1	628	1	671	10	714	12	757	25
543	1	586	1	629	8	672	8	715	15	758	28
544	2	587	4	630	1	673	9	716	17	759	29
545	1	588	4	631	4	674	11	717	16	760	32
546	3	589	1	632	9	675	7	718	18	761	22
547	0	590	0	633	4	676	10	719	20	762	23
548	2	591	3	634	4	677	6	720	20	763	33
549	1	592	3	635	6	678	7	721	24	764	31
550	3	593	6	636	9	679	13	722	18	765	32
551	0	594	2	637	7	680	10	723	20	766	38
552	0	595	3	638	5	681	16	724	17	767	22
553	2	596	3	639	3	682	12	725	17	768	31
554	5	597	2	640	6	683	14	726	22	769	29
555	0	598	4	641	7	684	10	727	20	770	40
556	1	599	1	642	4	685	6	728	19	771	45
557	0	600	2	643	11	686	6	729	19	772	34
558	2	601	3	644	4	687	8	730	21	773	31
559	1	602	1	645	7	688	10	731	21	774	42

Table A13. Continued.

Channel #	*f*	Channel #	*f*	Channel #	*f*	Channel #	*f*	Channel #	*f*	Channel #	*f*
775	32	818	46	861	60	904	25	947	13	990	2
776	27	819	47	862	74	905	41	948	8	991	4
777	34	820	60	863	63	906	25	949	7	992	2
778	30	821	44	864	66	907	28	950	7	993	2
779	37	822	68	865	61	908	20	951	11	994	0
780	45	823	51	866	53	909	24	952	8	995	1
781	33	824	61	867	56	910	36	953	7	996	3
782	36	825	37	868	66	911	34	954	3	997	0
783	32	826	55	869	59	912	20	955	5	998	2
784	33	827	56	870	64	913	25	956	7	999	0
785	42	828	54	871	59	914	26	957	7	1000	1
786	27	829	39	872	48	915	27	958	2	1001	1
787	44	830	65	873	55	916	26	959	5	1002	2
788	39	831	51	874	50	917	30	960	2	1003	0
789	28	832	55	875	58	918	32	961	5	1004	1
790	39	833	64	876	47	919	22	962	10	1005	0
791	34	834	51	877	42	920	32	963	10	1006	0
792	38	835	51	878	62	921	28	964	6	1007	1
793	40	836	63	879	46	922	14	965	3	1008	0
794	42	837	48	880	40	923	38	966	8	1009	0
795	37	838	79	881	35	924	20	967	6	1010	0
796	42	839	57	882	58	925	19	968	3	1011	0
797	47	840	57	883	48	926	19	969	3	1012	0
798	50	841	56	884	43	927	18	970	4	1013	0
799	48	842	51	885	45	928	9	971	5	1014	0
800	47	843	67	886	50	929	19	972	3	1015	0
801	51	844	55	887	64	930	24	973	2	1016	0
802	44	845	54	888	49	931	10	974	4	1017	0
803	35	846	74	889	43	932	10	975	5	1018	0
804	44	847	56	890	37	933	16	976	3	1019	0
805	35	848	55	891	31	934	19	977	2	1020	0
806	49	849	61	892	45	935	13	978	3	1021	0
807	58	850	80	893	38	936	12	979	4	1022	0
808	38	851	69	894	54	937	13	980	5	1023	0
809	39	852	50	895	25	938	10	981	3	1024	0
810	42	853	48	896	31	939	14	982	1		
811	48	854	57	897	35	940	7	983	1		
812	44	855	54	898	48	941	9	984	3		
813	53	856	53	899	38	942	14	985	1		
814	42	857	75	900	41	943	6	986	3		
815	33	858	60	901	33	944	12	987	5		
816	36	859	52	902	27	945	10	988	1		
817	44	860	52	903	39	946	18	989	0		

Table A14. Raw flow cytometry data for differentiating IMR-32 (Day 10, 1st replicate) used to generate Figure 3.2.

Channel #	*f*	Channel #	*f*	Channel #	*f*	Channel #	*f*	Channel #	*f*	Channel #	*f*
1	0	44	1	87	4	130	0	173	0	216	2
2	1	45	1	88	3	131	2	174	1	217	1
3	0	46	2	89	1	132	0	175	0	218	1
4	11	47	1	90	2	133	1	176	0	219	2
5	186	48	0	91	2	134	3	177	2	220	2
6	16	49	0	92	1	135	0	178	3	221	0
7	1	50	0	93	0	136	1	179	0	222	1
8	0	51	1	94	0	137	3	180	2	223	3
9	0	52	1	95	2	138	3	181	1	224	3
10	1	53	0	96	1	139	0	182	1	225	2
11	3	54	1	97	0	140	1	183	3	226	0
12	0	55	1	98	0	141	0	184	3	227	5
13	2	56	2	99	1	142	3	185	1	228	3
14	0	57	2	100	1	143	1	186	1	229	1
15	2	58	1	101	0	144	1	187	3	230	0
16	1	59	0	102	3	145	0	188	0	231	0
17	1	60	0	103	1	146	2	189	0	232	1
18	0	61	2	104	1	147	1	190	0	233	5
19	2	62	0	105	0	148	0	191	2	234	3
20	0	63	1	106	1	149	2	192	3	235	1
21	0	64	1	107	3	150	1	193	3	236	2
22	1	65	0	108	1	151	0	194	1	237	1
23	0	66	1	109	0	152	1	195	1	238	3
24	1	67	0	110	3	153	1	196	0	239	2
25	0	68	2	111	1	154	4	197	4	240	5
26	0	69	1	112	1	155	1	198	4	241	0
27	1	70	2	113	0	156	2	199	1	242	4
28	3	71	4	114	0	157	1	200	2	243	1
29	0	72	1	115	1	158	4	201	1	244	1
30	1	73	1	116	1	159	1	202	3	245	2
31	0	74	3	117	3	160	3	203	1	246	2
32	2	75	3	118	2	161	1	204	1	247	2
33	1	76	0	119	0	162	2	205	1	248	0
34	1	77	0	120	2	163	3	206	1	249	3
35	4	78	1	121	2	164	2	207	1	250	1
36	0	79	0	122	0	165	0	208	0	251	3
37	2	80	1	123	1	166	2	209	0	252	4
38	2	81	1	124	3	167	3	210	1	253	2
39	1	82	1	125	1	168	2	211	3	254	1
40	0	83	1	126	0	169	1	212	2	255	2
41	0	84	3	127	1	170	2	213	2	256	3
42	1	85	2	128	2	171	1	214	1	257	2
43	0	86	1	129	2	172	1	215	2	258	2

* Channel # and *f* represent oxonol fluorescence and frequency respectively.

Table A14. Continued.

Channel #	*f*	Channel #	*f*	Channel #	*f*	Channel #	*f*	Channel #	*f*	Channel #	*F*
259	3	302	3	345	2	388	2	431	0	474	6
260	3	303	4	346	5	389	3	432	7	475	6
261	2	304	4	347	3	390	3	433	2	476	2
262	0	305	0	348	5	391	3	434	1	477	6
263	2	306	5	349	1	392	3	435	4	478	3
264	1	307	1	350	4	393	3	436	0	479	5
265	1	308	3	351	4	394	4	437	3	480	11
266	4	309	5	352	6	395	3	438	6	481	3
267	3	310	2	353	3	396	3	439	4	482	3
268	3	311	4	354	2	397	3	440	2	483	1
269	4	312	1	355	2	398	1	441	3	484	1
270	2	313	7	356	2	399	2	442	7	485	2
271	3	314	1	357	1	400	3	443	1	486	3
272	0	315	4	358	4	401	2	444	5	487	5
273	2	316	4	359	1	402	3	445	3	488	3
274	1	317	1	360	3	403	6	446	3	489	2
275	3	318	3	361	3	404	2	447	1	490	6
276	4	319	2	362	3	405	1	448	0	491	2
277	1	320	2	363	4	406	9	449	6	492	2
278	1	321	1	364	3	407	4	450	2	493	6
279	2	322	4	365	3	408	2	451	7	494	9
280	1	323	1	366	5	409	2	452	4	495	4
281	3	324	0	367	2	410	3	453	6	496	6
282	0	325	3	368	6	411	4	454	3	497	5
283	3	326	2	369	4	412	7	455	2	498	6
284	4	327	3	370	4	413	2	456	2	499	6
285	3	328	4	371	4	414	2	457	0	500	4
286	3	329	3	372	2	415	6	458	3	501	1
287	4	330	2	373	4	416	3	459	4	502	4
288	2	331	4	374	4	417	3	460	2	503	4
289	1	332	2	375	1	418	5	461	2	504	3
290	2	333	0	376	4	419	4	462	4	505	5
291	4	334	2	377	1	420	4	463	7	506	5
292	1	335	3	378	1	421	3	464	3	507	4
293	2	336	2	379	4	422	6	465	1	508	1
294	0	337	2	380	0	423	3	466	3	509	6
295	4	338	0	381	4	424	3	467	0	510	3
296	0	339	1	382	0	425	8	468	1	511	3
297	3	340	6	383	3	426	3	469	3	512	4
298	2	341	2	384	4	427	4	470	1	513	6
299	7	342	2	385	2	428	6	471	3	514	4
300	2	343	2	386	3	429	2	472	7	515	7
301	5	344	1	387	0	430	1	473	5	516	0

Table A14. Continued.

Channel #	*f*	Channel #	*f*	Channel #	*f*	Channel #	*f*	Channel #	*f*	Channel #	*f*
517	3	560	9	603	7	646	7	689	13	732	17
518	2	561	6	604	5	647	4	690	4	733	10
519	3	562	7	605	3	648	5	691	12	734	15
520	3	563	4	606	10	649	11	692	10	735	12
521	3	564	7	607	5	650	7	693	11	736	16
522	6	565	5	608	5	651	3	694	4	737	15
523	6	566	8	609	4	652	2	695	12	738	5
524	5	567	6	610	7	653	5	696	6	739	13
525	2	568	8	611	6	654	7	697	6	740	9
526	5	569	4	612	5	655	9	698	10	741	12
527	7	570	2	613	5	656	9	699	16	742	17
528	2	571	4	614	6	657	6	700	16	743	15
529	6	572	6	615	3	658	14	701	7	744	18
530	2	573	6	616	5	659	5	702	14	745	17
531	7	574	4	617	3	660	6	703	9	746	21
532	5	575	3	618	6	661	6	704	11	747	23
533	6	576	3	619	11	662	11	705	10	748	18
534	5	577	8	620	5	663	4	706	15	749	18
535	7	578	7	621	5	664	8	707	13	750	17
536	2	579	6	622	5	665	10	708	11	751	17
537	3	580	4	623	6	666	12	709	8	752	20
538	5	581	3	624	7	667	7	710	15	753	17
539	3	582	6	625	6	668	4	711	10	754	20
540	3	583	2	626	5	669	4	712	17	755	25
541	6	584	7	627	4	670	8	713	9	756	23
542	3	585	3	628	6	671	7	714	8	757	20
543	1	586	3	629	5	672	4	715	11	758	17
544	6	587	5	630	4	673	9	716	15	759	14
545	9	588	5	631	6	674	6	717	9	760	19
546	4	589	6	632	10	675	12	718	17	761	12
547	10	590	5	633	1	676	5	719	12	762	23
548	2	591	0	634	4	677	10	720	9	763	18
549	3	592	7	635	4	678	7	721	9	764	20
550	2	593	1	636	8	679	6	722	10	765	28
551	6	594	6	637	6	680	7	723	9	766	26
552	3	595	2	638	9	681	8	724	9	767	24
553	7	596	6	639	9	682	8	725	7	768	13
554	2	597	4	640	11	683	10	726	12	769	26
555	7	598	10	641	7	684	10	727	10	770	33
556	8	599	4	642	12	685	8	728	12	771	31
557	5	600	7	643	10	686	8	729	17	772	19
558	3	601	4	644	5	687	9	730	13	773	19
559	5	602	5	645	4	688	13	731	6	774	28

Table A14. Continued.

Channel #	*f*	Channel #	*f*	Channel #	*f*	Channel #	*f*	Channel #	*f*	Channel #	*f*
775	23	818	40	861	37	904	30	947	17	990	1
776	14	819	39	862	62	905	34	948	2	991	1
777	19	820	48	863	60	906	34	949	6	992	4
778	18	821	40	864	42	907	28	950	6	993	0
779	25	822	37	865	42	908	28	951	9	994	3
780	27	823	44	866	60	909	33	952	9	995	3
781	17	824	36	867	42	910	26	953	10	996	1
782	32	825	41	868	48	911	36	954	12	997	0
783	29	826	50	869	38	912	42	955	7	998	1
784	25	827	55	870	56	913	25	956	7	999	1
785	24	828	48	871	57	914	27	957	4	1000	1
786	26	829	35	872	52	915	31	958	7	1001	0
787	34	830	45	873	55	916	30	959	9	1002	0
788	19	831	38	874	62	917	20	960	9	1003	1
789	27	832	43	875	35	918	22	961	8	1004	0
790	28	833	41	876	42	919	25	962	8	1005	1
791	33	834	50	877	42	920	23	963	4	1006	2
792	29	835	64	878	42	921	20	964	6	1007	0
793	44	836	38	879	38	922	23	965	3	1008	0
794	32	837	48	880	35	923	14	966	11	1009	1
795	31	838	45	881	37	924	22	967	4	1010	0
796	29	839	52	882	47	925	13	968	4	1011	0
797	30	840	45	883	46	926	24	969	8	1012	0
798	30	841	53	884	45	927	15	970	9	1013	0
799	41	842	39	885	33	928	13	971	9	1014	0
800	32	843	53	886	44	929	13	972	7	1015	0
801	41	844	45	887	46	930	14	973	7	1016	0
802	39	845	48	888	40	931	28	974	5	1017	0
803	29	846	54	889	33	932	22	975	4	1018	0
804	45	847	46	890	35	933	11	976	6	1019	0
805	19	848	42	891	46	934	23	977	2	1020	0
806	37	849	66	892	42	935	21	978	3	1021	0
807	30	850	47	893	33	936	10	979	4	1022	0
808	32	851	48	894	50	937	20	980	2	1023	0
809	34	852	46	895	25	938	9	981	0	1024	0
810	43	853	37	896	39	939	21	982	2		
811	47	854	47	897	31	940	10	983	1		
812	41	855	33	898	33	941	11	984	1		
813	52	856	46	899	32	942	13	985	3		
814	38	857	63	900	36	943	12	986	1		
815	36	858	53	901	36	944	13	987	0		
816	41	859	59	902	42	945	14	988	2		
817	49	860	52	903	49	946	7	989	5		

Table A15. Raw flow cytometry data for differentiating IMR-32 (Day 10, 2nd replicate) used to generate Figure 3.2.

Channel #	*f*	Channel #	*f*	Channel #	*f*	Channel #	*f*	Channel #	*f*	Channel #	*f*
1	0	44	0	87	0	130	0	173	0	216	0
2	0	45	0	88	0	131	0	174	0	217	0
3	0	46	0	89	0	132	0	175	0	218	0
4	0	47	0	90	0	133	0	176	0	219	0
5	2	48	0	91	0	134	0	177	0	220	0
6	6	49	0	92	0	135	0	178	0	221	0
7	3	50	0	93	0	136	0	179	0	222	0
8	0	51	0	94	0	137	0	180	0	223	0
9	0	52	0	95	0	138	0	181	0	224	0
10	0	53	0	96	0	139	0	182	0	225	0
11	0	54	0	97	0	140	0	183	0	226	0
12	0	55	0	98	0	141	0	184	0	227	0
13	0	56	0	99	0	142	0	185	0	228	0
14	0	57	0	100	0	143	0	186	0	229	0
15	0	58	0	101	0	144	0	187	0	230	0
16	0	59	0	102	0	145	0	188	1	231	0
17	0	60	0	103	0	146	0	189	0	232	0
18	0	61	0	104	0	147	0	190	0	233	0
19	0	62	0	105	0	148	0	191	0	234	0
20	1	63	0	106	0	149	0	192	0	235	0
21	0	64	0	107	0	150	0	193	0	236	0
22	0	65	0	108	0	151	0	194	0	237	0
23	0	66	0	109	0	152	0	195	0	238	0
24	0	67	0	110	0	153	0	196	0	239	0
25	0	68	0	111	0	154	0	197	0	240	0
26	0	69	0	112	0	155	0	198	0	241	1
27	1	70	0	113	0	156	0	199	0	242	0
28	0	71	0	114	0	157	0	200	0	243	0
29	0	72	0	115	0	158	0	201	0	244	0
30	0	73	0	116	0	159	0	202	0	245	0
31	0	74	0	117	0	160	0	203	0	246	0
32	0	75	0	118	0	161	0	204	0	247	0
33	0	76	0	119	0	162	0	205	0	248	0
34	0	77	0	120	0	163	0	206	0	249	0
35	0	78	0	121	0	164	0	207	0	250	0
36	0	79	0	122	0	165	0	208	0	251	0
37	0	80	0	123	0	166	0	209	0	252	0
38	0	81	0	124	0	167	0	210	0	253	0
39	0	82	1	125	0	168	0	211	0	254	0
40	0	83	0	126	0	169	0	212	0	255	0
41	0	84	0	127	0	170	0	213	0	256	0
42	0	85	0	128	0	171	0	214	0	257	0
43	0	86	0	129	0	172	0	215	0	258	0

* Channel # and *f* represent oxonol fluorescence and frequency respectively.

Table A15. Continued.

Channel #	*f*	Channel #	*f*	Channel #	*f*	Channel #	*f*	Channel #	*f*	Channel #	*f*
259	0	302	0	345	0	388	0	431	0	474	0
260	0	303	0	346	0	389	0	432	0	475	0
261	0	304	0	347	0	390	0	433	0	476	1
262	0	305	0	348	0	391	0	434	0	477	0
263	0	306	0	349	0	392	0	435	0	478	0
264	0	307	0	350	0	393	0	436	0	479	0
265	0	308	0	351	0	394	0	437	0	480	1
266	0	309	0	352	0	395	0	438	1	481	0
267	0	310	0	353	0	396	0	439	0	482	0
268	0	311	0	354	0	397	0	440	1	483	0
269	0	312	0	355	0	398	0	441	0	484	0
270	0	313	0	356	0	399	0	442	0	485	0
271	0	314	0	357	0	400	0	443	0	486	1
272	0	315	0	358	0	401	0	444	0	487	0
273	0	316	0	359	0	402	0	445	0	488	1
274	0	317	0	360	0	403	0	446	0	489	0
275	1	318	0	361	0	404	0	447	0	490	0
276	0	319	0	362	0	405	0	448	0	491	0
277	0	320	0	363	1	406	0	449	0	492	0
278	0	321	1	364	0	407	0	450	0	493	0
279	0	322	0	365	0	408	0	451	0	494	1
280	0	323	0	366	0	409	0	452	1	495	0
281	0	324	0	367	0	410	0	453	0	496	0
282	0	325	0	368	0	411	0	454	0	497	0
283	0	326	0	369	0	412	0	455	0	498	1
284	0	327	0	370	0	413	0	456	0	499	1
285	0	328	0	371	0	414	0	457	0	500	0
286	0	329	0	372	0	415	0	458	0	501	0
287	0	330	0	373	0	416	1	459	0	502	0
288	0	331	0	374	0	417	1	460	0	503	1
289	0	332	0	375	1	418	0	461	0	504	1
290	0	333	0	376	0	419	0	462	0	505	1
291	0	334	0	377	0	420	0	463	1	506	1
292	0	335	0	378	0	421	0	464	0	507	1
293	0	336	0	379	0	422	0	465	0	508	0
294	0	337	0	380	1	423	1	466	0	509	3
295	0	338	0	381	1	424	0	467	0	510	0
296	0	339	0	382	0	425	0	468	0	511	1
297	0	340	0	383	0	426	0	469	0	512	1
298	0	341	0	384	0	427	0	470	1	513	3
299	0	342	0	385	0	428	0	471	1	514	0
300	0	343	0	386	0	429	1	472	0	515	0
301	0	344	0	387	0	430	1	473	1	516	0

Table A15. Continued.

Channel #	*f*	Channel #	*f*	Channel #	*f*	Channel #	*f*	Channel #	*f*	Channel #	*f*
517	0	560	0	603	0	646	5	689	7	732	14
518	1	561	2	604	3	647	8	690	9	733	20
519	0	562	1	605	3	648	8	691	15	734	21
520	1	563	0	606	4	649	3	692	10	735	22
521	2	564	1	607	1	650	8	693	9	736	23
522	1	565	2	608	4	651	5	694	6	737	21
523	2	566	2	609	3	652	3	695	8	738	16
524	2	567	1	610	3	653	1	696	10	739	21
525	0	568	2	611	3	654	11	697	9	740	22
526	0	569	1	612	4	655	2	698	18	741	14
527	0	570	0	613	0	656	6	699	13	742	25
528	0	571	2	614	3	657	7	700	11	743	21
529	1	572	1	615	2	658	5	701	18	744	21
530	0	573	2	616	3	659	11	702	7	745	17
531	0	574	3	617	1	660	5	703	8	746	20
532	1	575	0	618	1	661	6	704	5	747	18
533	0	576	1	619	7	662	6	705	10	748	31
534	1	577	1	620	4	663	10	706	15	749	28
535	2	578	3	621	1	664	6	707	13	750	20
536	2	579	3	622	2	665	4	708	7	751	31
537	2	580	0	623	4	666	7	709	14	752	15
538	0	581	2	624	7	667	3	710	11	753	25
539	3	582	3	625	2	668	4	711	7	754	27
540	1	583	0	626	7	669	6	712	10	755	26
541	0	584	1	627	3	670	5	713	15	756	23
542	1	585	0	628	3	671	6	714	12	757	20
543	3	586	2	629	1	672	7	715	18	758	36
544	0	587	1	630	3	673	7	716	10	759	37
545	1	588	1	631	3	674	7	717	11	760	21
546	2	589	1	632	3	675	12	718	19	761	29
547	1	590	4	633	3	676	9	719	16	762	23
548	1	591	3	634	9	677	3	720	17	763	36
549	0	592	3	635	2	678	7	721	19	764	30
550	2	593	1	636	5	679	9	722	12	765	32
551	1	594	1	637	3	680	6	723	17	766	30
552	3	595	2	638	4	681	19	724	14	767	31
553	0	596	1	639	4	682	12	725	18	768	38
554	0	597	4	640	7	683	4	726	21	769	34
555	1	598	1	641	8	684	11	727	17	770	46
556	1	599	4	642	7	685	8	728	16	771	45
557	2	600	1	643	6	686	7	729	14	772	23
558	0	601	2	644	4	687	7	730	15	773	31
559	2	602	2	645	4	688	7	731	9	774	29

Table A15. Continued.

Channel #	*f*	Channel #	*f*	Channel #	*f*	Channel #	*f*	Channel #	*f*	Channel #	*f*
775	36	818	58	861	58	904	30	947	6	990	1
776	31	819	64	862	68	905	34	948	10	991	0
777	40	820	79	863	42	906	35	949	10	992	2
778	42	821	46	864	61	907	36	950	11	993	2
779	41	822	82	865	52	908	29	951	6	994	2
780	35	823	48	866	56	909	28	952	8	995	1
781	48	824	61	867	59	910	38	953	7	996	1
782	31	825	62	868	44	911	26	954	10	997	4
783	32	826	51	869	47	912	29	955	1	998	2
784	39	827	71	870	66	913	28	956	4	999	3
785	30	828	66	871	51	914	17	957	7	1000	2
786	36	829	45	872	45	915	24	958	3	1001	1
787	59	830	68	873	63	916	27	959	4	1002	1
788	30	831	66	874	50	917	14	960	3	1003	1
789	44	832	55	875	50	918	20	961	4	1004	0
790	51	833	74	876	56	919	27	962	5	1005	1
791	39	834	55	877	49	920	19	963	9	1006	0
792	49	835	73	878	62	921	24	964	8	1007	1
793	45	836	76	879	50	922	20	965	6	1008	1
794	50	837	61	880	51	923	21	966	9	1009	0
795	54	838	68	881	48	924	22	967	2	1010	0
796	36	839	57	882	57	925	12	968	4	1011	0
797	38	840	57	883	55	926	15	969	6	1012	0
798	47	841	74	884	55	927	16	970	4	1013	0
799	48	842	49	885	23	928	12	971	3	1014	0
800	47	843	68	886	45	929	15	972	3	1015	0
801	47	844	61	887	48	930	10	973	2	1016	0
802	46	845	55	888	28	931	18	974	5	1017	0
803	45	846	86	889	45	932	16	975	2	1018	0
804	50	847	62	890	46	933	13	976	1	1019	1
805	51	848	75	891	48	934	14	977	2	1020	0
806	45	849	68	892	42	935	10	978	2	1021	0
807	62	850	66	893	42	936	9	979	3	1022	1
808	49	851	53	894	41	937	12	980	1	1023	0
809	55	852	52	895	43	938	10	981	4	1024	0
810	58	853	51	896	39	939	16	982	7		
811	58	854	71	897	42	940	8	983	4		
812	53	855	57	898	42	941	5	984	3		
813	54	856	62	899	29	942	10	985	5		
814	47	857	66	900	25	943	12	986	6		
815	70	858	61	901	27	944	14	987	0		
816	58	859	53	902	35	945	9	988	1		
817	67	860	61	903	25	946	4	989	1		

Table A16. Raw flow cytometry data for differentiating IMR-32 (Day 10, 3rd replicate) used to generate Figure 3.2.

Channel #	*f*	Channel #	*f*	Channel #	*f*	Channel #	*f*	Channel #	*f*	Channel #	*f*
1	0	44	0	87	0	130	0	173	0	216	0
2	0	45	0	88	0	131	0	174	0	217	0
3	0	46	0	89	0	132	0	175	0	218	0
4	0	47	0	90	0	133	0	176	0	219	0
5	2	48	0	91	0	134	0	177	0	220	0
6	1	49	0	92	0	135	0	178	0	221	0
7	0	50	0	93	0	136	0	179	0	222	0
8	1	51	0	94	0	137	0	180	0	223	0
9	0	52	0	95	0	138	0	181	0	224	0
10	0	53	0	96	0	139	0	182	0	225	0
11	0	54	0	97	1	140	0	183	0	226	0
12	0	55	0	98	0	141	0	184	0	227	1
13	0	56	0	99	0	142	0	185	0	228	0
14	0	57	0	100	0	143	0	186	0	229	0
15	0	58	0	101	0	144	0	187	0	230	0
16	0	59	0	102	0	145	0	188	0	231	0
17	0	60	0	103	0	146	0	189	0	232	0
18	0	61	0	104	0	147	0	190	0	233	0
19	0	62	0	105	0	148	0	191	0	234	0
20	0	63	0	106	0	149	0	192	0	235	0
21	0	64	0	107	0	150	0	193	0	236	0
22	0	65	0	108	0	151	0	194	0	237	0
23	0	66	0	109	0	152	1	195	0	238	0
24	0	67	0	110	0	153	0	196	0	239	0
25	0	68	0	111	0	154	0	197	0	240	0
26	0	69	0	112	0	155	0	198	0	241	0
27	0	70	0	113	0	156	0	199	0	242	0
28	0	71	0	114	0	157	0	200	0	243	0
29	0	72	0	115	0	158	0	201	0	244	0
30	0	73	0	116	0	159	0	202	0	245	0
31	0	74	0	117	0	160	0	203	1	246	0
32	0	75	0	118	0	161	0	204	0	247	0
33	0	76	0	119	0	162	0	205	0	248	0
34	0	77	0	120	0	163	0	206	0	249	0
35	0	78	0	121	0	164	0	207	0	250	0
36	0	79	0	122	0	165	0	208	0	251	0
37	0	80	0	123	0	166	0	209	0	252	0
38	0	81	0	124	0	167	0	210	0	253	0
39	0	82	0	125	0	168	0	211	0	254	0
40	0	83	0	126	0	169	0	212	0	255	0
41	0	84	0	127	0	170	0	213	0	256	1
42	0	85	0	128	0	171	0	214	0	257	0
43	0	86	0	129	0	172	0	215	0	258	0

* Channel # and *f* represent oxonol fluorescence and frequency respectively.

Table A16. Continued.

Channel #	*f*	Channel #	*f*	Channel #	*f*	Channel #	*f*	Channel #	*f*	Channel #	*f*
259	0	302	0	345	0	388	0	431	0	474	0
260	0	303	0	346	0	389	0	432	0	475	0
261	0	304	0	347	0	390	1	433	0	476	2
262	0	305	0	348	0	391	0	434	0	477	0
263	0	306	0	349	0	392	0	435	0	478	1
264	0	307	1	350	0	393	0	436	0	479	1
265	0	308	0	351	0	394	0	437	1	480	1
266	0	309	0	352	0	395	0	438	0	481	2
267	0	310	0	353	0	396	0	439	0	482	3
268	0	311	0	354	0	397	0	440	0	483	0
269	0	312	0	355	0	398	0	441	1	484	2
270	0	313	0	356	0	399	0	442	0	485	1
271	0	314	0	357	0	400	0	443	0	486	1
272	0	315	0	358	0	401	0	444	0	487	0
273	0	316	0	359	0	402	1	445	0	488	0
274	0	317	0	360	0	403	0	446	3	489	2
275	0	318	1	361	0	404	0	447	2	490	0
276	0	319	0	362	0	405	0	448	2	491	3
277	0	320	0	363	0	406	0	449	0	492	2
278	0	321	0	364	0	407	0	450	1	493	3
279	1	322	0	365	0	408	0	451	2	494	3
280	0	323	1	366	1	409	0	452	0	495	2
281	0	324	0	367	0	410	1	453	0	496	1
282	0	325	0	368	0	411	0	454	1	497	0
283	0	326	0	369	1	412	2	455	0	498	4
284	0	327	0	370	0	413	0	456	2	499	2
285	0	328	0	371	0	414	0	457	0	500	0
286	0	329	0	372	0	415	1	458	2	501	0
287	0	330	1	373	0	416	1	459	3	502	0
288	0	331	0	374	1	417	0	460	0	503	2
289	0	332	0	375	0	418	1	461	0	504	2
290	0	333	0	376	0	419	0	462	1	505	1
291	0	334	0	377	1	420	1	463	1	506	1
292	0	335	0	378	0	421	0	464	0	507	1
293	0	336	1	379	0	422	0	465	1	508	2
294	1	337	0	380	0	423	0	466	0	509	1
295	0	338	0	381	0	424	0	467	0	510	0
296	0	339	0	382	0	425	1	468	0	511	1
297	0	340	0	383	0	426	0	469	2	512	0
298	0	341	0	384	0	427	1	470	1	513	1
299	0	342	1	385	0	428	0	471	0	514	1
300	1	343	1	386	0	429	0	472	1	515	1
301	0	344	0	387	0	430	2	473	2	516	4

Table A16. Continued.

Channel #	*f*	Channel #	*f*	Channel #	*f*	Channel #	*f*	Channel #	*f*	Channel #	*f*
517	0	560	4	603	8	646	16	689	36	732	38
518	2	561	4	604	8	647	13	690	31	733	34
519	3	562	7	605	7	648	14	691	25	734	47
520	1	563	6	606	8	649	13	692	34	735	43
521	1	564	5	607	9	650	9	693	17	736	40
522	3	565	7	608	9	651	12	694	19	737	52
523	1	566	7	609	15	652	18	695	27	738	41
524	1	567	4	610	9	653	17	696	25	739	55
525	0	568	2	611	9	654	27	697	28	740	50
526	2	569	4	612	10	655	18	698	33	741	48
527	3	570	7	613	14	656	19	699	21	742	39
528	4	571	2	614	5	657	20	700	28	743	47
529	2	572	6	615	16	658	10	701	16	744	47
530	3	573	2	616	14	659	18	702	26	745	39
531	0	574	4	617	9	660	18	703	26	746	65
532	1	575	10	618	12	661	18	704	23	747	62
533	2	576	0	619	13	662	16	705	33	748	45
534	1	577	4	620	16	663	18	706	34	749	49
535	2	578	5	621	7	664	17	707	30	750	61
536	1	579	4	622	8	665	19	708	27	751	46
537	1	580	11	623	16	666	21	709	33	752	46
538	2	581	5	624	6	667	18	710	39	753	37
539	4	582	5	625	11	668	28	711	29	754	64
540	4	583	8	626	10	669	27	712	23	755	54
541	3	584	7	627	16	670	20	713	34	756	46
542	2	585	5	628	11	671	24	714	38	757	45
543	8	586	6	629	6	672	13	715	32	758	59
544	6	587	6	630	11	673	22	716	39	759	50
545	3	588	9	631	9	674	27	717	23	760	46
546	3	589	10	632	14	675	18	718	39	761	41
547	3	590	9	633	9	676	17	719	34	762	56
548	4	591	4	634	13	677	21	720	42	763	55
549	2	592	8	635	15	678	21	721	32	764	58
550	6	593	5	636	13	679	29	722	30	765	43
551	7	594	8	637	14	680	17	723	40	766	49
552	1	595	6	638	20	681	22	724	37	767	54
553	7	596	4	639	8	682	25	725	40	768	50
554	1	597	10	640	17	683	33	726	48	769	61
555	6	598	11	641	18	684	24	727	39	770	58
556	3	599	7	642	8	685	19	728	46	771	63
557	10	600	4	643	17	686	20	729	40	772	60
558	0	601	8	644	14	687	29	730	39	773	47
559	2	602	8	645	20	688	20	731	55	774	55

Table A16. Continued.

Channel #	*f*	Channel #	*f*	Channel #	*f*	Channel #	*f*	Channel #	*f*	Channel #	*f*
775	72	818	54	861	16	904	4	947	0	990	0
776	49	819	43	862	29	905	5	948	0	991	1
777	62	820	52	863	24	906	5	949	2	992	0
778	61	821	45	864	19	907	6	950	0	993	0
779	70	822	45	865	29	908	7	951	1	994	0
780	54	823	30	866	19	909	4	952	1	995	0
781	51	824	47	867	14	910	4	953	0	996	0
782	69	825	47	868	26	911	3	954	0	997	0
783	52	826	46	869	23	912	5	955	1	998	0
784	65	827	52	870	11	913	5	956	0	999	0
785	56	828	52	871	17	914	5	957	0	1000	0
786	53	829	34	872	10	915	6	958	2	1001	0
787	69	830	49	873	25	916	6	959	2	1002	0
788	38	831	34	874	19	917	5	960	0	1003	0
789	38	832	33	875	16	918	6	961	1	1004	0
790	59	833	46	876	19	919	1	962	0	1005	0
791	56	834	28	877	16	920	1	963	0	1006	0
792	52	835	51	878	26	921	4	964	0	1007	0
793	61	836	44	879	18	922	4	965	1	1008	0
794	50	837	37	880	16	923	4	966	0	1009	0
795	53	838	44	881	11	924	3	967	0	1010	0
796	53	839	28	882	13	925	1	968	1	1011	0
797	32	840	32	883	20	926	1	969	0	1012	0
798	64	841	26	884	15	927	2	970	0	1013	0
799	65	842	35	885	11	928	0	971	0	1014	0
800	43	843	39	886	10	929	2	972	0	1015	0
801	55	844	23	887	19	930	2	973	0	1016	0
802	47	845	33	888	13	931	2	974	0	1017	0
803	50	846	29	889	9	932	2	975	0	1018	0
804	59	847	36	890	13	933	4	976	0	1019	0
805	52	848	35	891	10	934	4	977	0	1020	0
806	50	849	32	892	4	935	2	978	0	1021	0
807	44	850	28	893	11	936	0	979	0	1022	0
808	35	851	35	894	18	937	0	980	0	1023	0
809	54	852	32	895	9	938	2	981	0	1024	0
810	49	853	27	896	11	939	1	982	0		
811	51	854	36	897	7	940	2	983	0		
812	47	855	23	898	3	941	2	984	0		
813	52	856	24	899	7	942	1	985	0		
814	40	857	26	900	16	943	1	986	0		
815	42	858	17	901	6	944	3	987	1		
816	51	859	25	902	10	945	0	988	0		
817	44	860	25	903	12	946	1	989	0		

Table A17. Raw flow cytometry data for differentiating IMR-32 (Day 12, 1st replicate) used to generate Figure 3.2.

Channel #	*f*	Channel #	*f*	Channel #	*f*	Channel #	*f*	Channel #	*f*	Channel #	*f*
1	0	44	1	87	2	130	2	173	3	216	2
2	1	45	3	88	2	131	1	174	2	217	1
3	0	46	1	89	1	132	3	175	2	218	3
4	42	47	0	90	1	133	6	176	2	219	2
5	728	48	4	91	0	134	1	177	5	220	5
6	25	49	2	92	0	135	5	178	2	221	7
7	4	50	0	93	4	136	2	179	3	222	3
8	2	51	0	94	3	137	3	180	4	223	1
9	1	52	0	95	1	138	2	181	2	224	3
10	0	53	2	96	1	139	3	182	2	225	3
11	1	54	0	97	1	140	3	183	2	226	4
12	1	55	0	98	1	141	5	184	1	227	4
13	0	56	2	99	4	142	3	185	2	228	5
14	1	57	0	100	1	143	3	186	3	229	2
15	0	58	0	101	1	144	1	187	5	230	3
16	1	59	4	102	0	145	1	188	3	231	0
17	2	60	2	103	3	146	0	189	1	232	1
18	1	61	1	104	4	147	3	190	5	233	2
19	2	62	2	105	4	148	2	191	3	234	2
20	3	63	0	106	3	149	2	192	2	235	1
21	0	64	0	107	2	150	1	193	1	236	4
22	2	65	5	108	3	151	1	194	5	237	1
23	1	66	2	109	0	152	0	195	4	238	2
24	0	67	3	110	2	153	4	196	4	239	1
25	2	68	1	111	0	154	1	197	2	240	1
26	3	69	0	112	2	155	3	198	6	241	3
27	1	70	0	113	2	156	1	199	1	242	2
28	0	71	2	114	0	157	3	200	1	243	1
29	3	72	0	115	3	158	4	201	6	244	3
30	1	73	1	116	2	159	1	202	4	245	3
31	1	74	1	117	2	160	5	203	3	246	4
32	1	75	0	118	1	161	0	204	3	247	2
33	1	76	0	119	0	162	5	205	3	248	0
34	2	77	1	120	5	163	3	206	2	249	2
35	0	78	4	121	2	164	1	207	1	250	0
36	1	79	2	122	1	165	5	208	4	251	2
37	3	80	3	123	4	166	1	209	3	252	1
38	1	81	2	124	3	167	3	210	5	253	4
39	2	82	0	125	2	168	2	211	3	254	4
40	1	83	2	126	0	169	2	212	5	255	6
41	0	84	3	127	1	170	2	213	3	256	3
42	2	85	0	128	2	171	2	214	1	257	5
43	1	86	0	129	1	172	3	215	5	258	2

* Channel # and *f* represent oxonol fluorescence and frequency respectively.

Table A17. Continued.

Channel #	*f*	Channel #	*f*	Channel #	*f*	Channel #	*f*	Channel #	*f*	Channel #	*f*
259	3	302	1	345	8	388	5	431	3	474	4
260	0	303	4	346	4	389	4	432	4	475	4
261	7	304	6	347	3	390	7	433	6	476	3
262	5	305	1	348	2	391	8	434	8	477	3
263	6	306	6	349	3	392	5	435	6	478	5
264	3	307	2	350	9	393	6	436	6	479	6
265	6	308	10	351	4	394	2	437	6	480	2
266	3	309	2	352	3	395	6	438	3	481	1
267	2	310	1	353	10	396	9	439	4	482	3
268	1	311	3	354	5	397	4	440	4	483	9
269	4	312	3	355	6	398	5	441	7	484	2
270	5	313	3	356	8	399	2	442	1	485	3
271	5	314	7	357	6	400	4	443	5	486	8
272	2	315	4	358	6	401	7	444	8	487	5
273	3	316	6	359	5	402	3	445	4	488	5
274	2	317	4	360	2	403	1	446	5	489	6
275	8	318	4	361	6	404	6	447	9	490	4
276	2	319	4	362	1	405	4	448	5	491	7
277	5	320	2	363	7	406	6	449	5	492	5
278	6	321	3	364	8	407	4	450	5	493	4
279	5	322	2	365	8	408	4	451	4	494	7
280	4	323	6	366	4	409	6	452	6	495	2
281	3	324	6	367	5	410	2	453	4	496	5
282	5	325	3	368	2	411	6	454	9	497	4
283	2	326	4	369	4	412	3	455	3	498	3
284	10	327	8	370	5	413	8	456	8	499	4
285	1	328	4	371	4	414	7	457	3	500	5
286	4	329	4	372	6	415	9	458	7	501	8
287	3	330	5	373	3	416	2	459	5	502	6
288	2	331	3	374	6	417	5	460	6	503	6
289	4	332	5	375	11	418	6	461	7	504	8
290	2	333	3	376	4	419	2	462	5	505	7
291	3	334	7	377	6	420	6	463	6	506	7
292	8	335	7	378	2	421	6	464	1	507	2
293	4	336	1	379	8	422	8	465	5	508	5
294	6	337	4	380	4	423	5	466	4	509	0
295	6	338	5	381	7	424	9	467	7	510	3
296	2	339	8	382	4	425	4	468	7	511	4
297	11	340	3	383	3	426	6	469	6	512	5
298	5	341	8	384	6	427	7	470	4	513	8
299	7	342	3	385	2	428	5	471	5	514	3
300	12	343	2	386	3	429	5	472	4	515	5
301	2	344	4	387	4	430	5	473	4	516	3

Table A17. Continued.

Channel #	*f*	Channel #	*f*	Channel #	*f*	Channel #	*f*	Channel #	*f*	Channel #	*f*
517	6	560	11	603	10	646	10	689	8	732	12
518	6	561	6	604	8	647	9	690	8	733	6
519	2	562	5	605	4	648	4	691	7	734	8
520	4	563	9	606	4	649	11	692	6	735	16
521	6	564	4	607	1	650	3	693	10	736	12
522	3	565	6	608	0	651	6	694	16	737	12
523	6	566	5	609	5	652	8	695	2	738	10
524	6	567	3	610	6	653	2	696	7	739	17
525	7	568	10	611	10	654	3	697	7	740	9
526	4	569	6	612	9	655	6	698	3	741	10
527	6	570	5	613	3	656	8	699	5	742	12
528	3	571	1	614	6	657	5	700	11	743	7
529	3	572	1	615	3	658	4	701	12	744	8
530	6	573	4	616	9	659	7	702	11	745	8
531	6	574	3	617	5	660	4	703	4	746	12
532	4	575	5	618	5	661	6	704	6	747	11
533	3	576	7	619	5	662	9	705	12	748	15
534	6	577	2	620	3	663	4	706	16	749	13
535	2	578	4	621	6	664	8	707	7	750	11
536	7	579	5	622	4	665	5	708	10	751	11
537	6	580	4	623	4	666	6	709	6	752	8
538	4	581	1	624	6	667	8	710	6	753	10
539	3	582	7	625	4	668	10	711	9	754	10
540	3	583	6	626	9	669	15	712	5	755	18
541	6	584	8	627	6	670	4	713	7	756	17
542	7	585	10	628	4	671	6	714	8	757	18
543	3	586	4	629	2	672	5	715	9	758	16
544	7	587	6	630	6	673	3	716	6	759	10
545	8	588	6	631	5	674	7	717	8	760	11
546	6	589	7	632	4	675	8	718	8	761	15
547	5	590	7	633	4	676	9	719	6	762	21
548	3	591	4	634	5	677	11	720	9	763	14
549	3	592	5	635	6	678	6	721	10	764	10
550	5	593	6	636	9	679	4	722	14	765	15
551	3	594	8	637	2	680	8	723	9	766	9
552	6	595	7	638	6	681	2	724	10	767	22
553	7	596	9	639	5	682	6	725	5	768	13
554	5	597	4	640	4	683	11	726	14	769	12
555	3	598	6	641	3	684	8	727	11	770	21
556	7	599	8	642	6	685	8	728	10	771	19
557	6	600	7	643	6	686	4	729	8	772	12
558	7	601	12	644	12	687	8	730	6	773	10
559	4	602	8	645	6	688	6	731	13	774	16

Table A17. Continued.

Channel #	*f*	Channel #	*f*	Channel #	*f*	Channel #	*f*	Channel #	*f*	Channel #	*f*
775	14	818	32	861	42	904	34	947	11	990	7
776	13	819	30	862	45	905	47	948	12	991	1
777	15	820	35	863	41	906	30	949	9	992	2
778	13	821	27	864	37	907	45	950	18	993	3
779	25	822	33	865	31	908	24	951	13	994	1
780	24	823	40	866	43	909	27	952	6	995	4
781	13	824	34	867	41	910	35	953	14	996	4
782	24	825	29	868	31	911	28	954	7	997	3
783	26	826	42	869	35	912	19	955	7	998	2
784	21	827	33	870	40	913	25	956	9	999	2
785	20	828	37	871	43	914	30	957	8	1000	2
786	20	829	36	872	34	915	36	958	8	1001	0
787	24	830	29	873	48	916	16	959	6	1002	2
788	27	831	27	874	40	917	20	960	5	1003	1
789	19	832	38	875	31	918	26	961	7	1004	1
790	25	833	50	876	57	919	23	962	9	1005	1
791	23	834	35	877	39	920	25	963	11	1006	0
792	11	835	43	878	34	921	34	964	15	1007	1
793	17	836	38	879	39	922	22	965	7	1008	0
794	22	837	29	880	48	923	26	966	8	1009	2
795	19	838	33	881	40	924	26	967	11	1010	1
796	24	839	38	882	41	925	22	968	8	1011	0
797	31	840	41	883	51	926	24	969	9	1012	0
798	19	841	50	884	46	927	26	970	13	1013	0
799	20	842	37	885	38	928	21	971	6	1014	0
800	23	843	41	886	46	929	23	972	8	1015	2
801	25	844	35	887	28	930	18	973	8	1016	1
802	31	845	32	888	44	931	24	974	9	1017	0
803	26	846	30	889	30	932	22	975	3	1018	0
804	31	847	33	890	40	933	13	976	5	1019	0
805	22	848	31	891	43	934	15	977	10	1020	0
806	32	849	44	892	39	935	18	978	5	1021	0
807	23	850	28	893	29	936	12	979	6	1022	0
808	28	851	35	894	50	937	14	980	3	1023	0
809	24	852	37	895	39	938	12	981	5	1024	0
810	25	853	46	896	29	939	26	982	1		
811	24	854	42	897	24	940	8	983	2		
812	37	855	43	898	40	941	12	984	3		
813	26	856	48	899	33	942	8	985	3		
814	24	857	39	900	30	943	13	986	3		
815	26	858	33	901	24	944	12	987	1		
816	30	859	44	902	34	945	19	988	6		
817	28	860	40	903	33	946	7	989	5		

Table A18. Raw flow cytometry data for differentiating IMR-32 (Day 12, 2nd replicate) used to generate Figure 3.2.

Channel #	*f*	Channel #	*f*	Channel #	*f*	Channel #	*f*	Channel #	*f*	Channel #	*f*
1	0	44	0	87	0	130	0	173	0	216	0
2	0	45	0	88	0	131	0	174	0	217	0
3	0	46	0	89	0	132	0	175	0	218	0
4	0	47	0	90	0	133	0	176	0	219	0
5	2	48	0	91	0	134	0	177	0	220	1
6	4	49	0	92	0	135	0	178	0	221	1
7	0	50	0	93	0	136	0	179	0	222	0
8	0	51	0	94	0	137	0	180	0	223	0
9	0	52	0	95	0	138	0	181	0	224	0
10	0	53	0	96	0	139	0	182	0	225	0
11	0	54	0	97	0	140	0	183	0	226	0
12	0	55	0	98	0	141	0	184	0	227	0
13	0	56	1	99	0	142	0	185	0	228	0
14	0	57	0	100	0	143	0	186	0	229	0
15	0	58	0	101	0	144	0	187	0	230	0
16	0	59	0	102	0	145	0	188	0	231	0
17	0	60	0	103	0	146	0	189	0	232	0
18	0	61	0	104	0	147	0	190	0	233	0
19	0	62	0	105	0	148	0	191	0	234	0
20	0	63	0	106	0	149	0	192	0	235	0
21	0	64	0	107	0	150	0	193	0	236	0
22	0	65	0	108	0	151	0	194	0	237	0
23	0	66	0	109	0	152	0	195	0	238	0
24	0	67	0	110	0	153	0	196	0	239	0
25	0	68	0	111	0	154	0	197	0	240	0
26	0	69	0	112	0	155	0	198	0	241	0
27	0	70	0	113	0	156	0	199	0	242	0
28	0	71	0	114	0	157	0	200	0	243	0
29	0	72	1	115	0	158	0	201	0	244	0
30	0	73	0	116	0	159	0	202	0	245	0
31	0	74	0	117	0	160	0	203	0	246	0
32	0	75	0	118	0	161	0	204	0	247	0
33	1	76	0	119	0	162	0	205	0	248	0
34	0	77	0	120	0	163	0	206	0	249	0
35	0	78	0	121	0	164	0	207	0	250	0
36	0	79	0	122	0	165	0	208	0	251	0
37	0	80	0	123	0	166	0	209	0	252	0
38	0	81	0	124	0	167	0	210	0	253	0
39	0	82	0	125	0	168	0	211	0	254	0
40	0	83	0	126	0	169	0	212	0	255	0
41	0	84	0	127	0	170	0	213	0	256	0
42	0	85	0	128	0	171	0	214	0	257	0
43	0	86	0	129	0	172	0	215	0	258	0

* Channel # and *f* represent oxonol fluorescence and frequency respectively.

Table A18. Continued.

Channel #	*f*	Channel #	*f*	Channel #	*f*	Channel #	*f*	Channel #	*f*	Channel #	*f*
259	0	302	0	345	0	388	1	431	1	474	0
260	0	303	0	346	0	389	0	432	0	475	0
261	0	304	0	347	0	390	0	433	0	476	2
262	0	305	0	348	0	391	0	434	1	477	0
263	0	306	0	349	0	392	0	435	0	478	1
264	0	307	0	350	0	393	0	436	0	479	0
265	0	308	0	351	1	394	0	437	1	480	0
266	0	309	0	352	0	395	0	438	0	481	1
267	0	310	0	353	0	396	0	439	1	482	0
268	0	311	0	354	0	397	0	440	0	483	1
269	0	312	0	355	0	398	0	441	0	484	0
270	0	313	0	356	0	399	0	442	1	485	0
271	0	314	0	357	0	400	0	443	0	486	1
272	0	315	0	358	0	401	1	444	0	487	0
273	0	316	0	359	0	402	0	445	0	488	1
274	0	317	0	360	0	403	0	446	0	489	1
275	0	318	0	361	0	404	0	447	2	490	0
276	0	319	0	362	0	405	0	448	1	491	1
277	0	320	0	363	0	406	0	449	1	492	1
278	0	321	0	364	0	407	0	450	0	493	0
279	0	322	0	365	0	408	0	451	0	494	0
280	0	323	0	366	1	409	0	452	0	495	0
281	0	324	0	367	0	410	0	453	0	496	1
282	1	325	0	368	0	411	0	454	0	497	0
283	0	326	0	369	0	412	0	455	1	498	1
284	0	327	0	370	1	413	0	456	0	499	0
285	0	328	0	371	0	414	0	457	0	500	0
286	0	329	0	372	0	415	1	458	0	501	2
287	0	330	0	373	0	416	0	459	1	502	0
288	1	331	0	374	0	417	0	460	0	503	2
289	0	332	1	375	0	418	0	461	0	504	1
290	0	333	0	376	0	419	0	462	1	505	0
291	0	334	0	377	0	420	0	463	0	506	0
292	0	335	0	378	0	421	0	464	0	507	2
293	0	336	0	379	0	422	0	465	0	508	1
294	0	337	0	380	0	423	0	466	0	509	2
295	0	338	0	381	0	424	0	467	0	510	0
296	0	339	0	382	0	425	0	468	0	511	2
297	0	340	0	383	0	426	0	469	0	512	0
298	0	341	0	384	0	427	1	470	0	513	1
299	0	342	0	385	0	428	1	471	0	514	3
300	0	343	0	386	1	429	0	472	0	515	2
301	0	344	1	387	0	430	0	473	1	516	2

Table A18. Continued.

Channel #	*f*	Channel #	*f*	Channel #	*f*	Channel #	*f*	Channel #	*f*	Channel #	*f*
517	2	560	1	603	4	646	12	689	23	732	33
518	3	561	5	604	4	647	8	690	17	733	29
519	1	562	3	605	7	648	12	691	19	734	44
520	2	563	3	606	6	649	10	692	20	735	30
521	1	564	3	607	0	650	8	693	15	736	38
522	0	565	0	608	7	651	5	694	27	737	33
523	0	566	3	609	2	652	10	695	18	738	29
524	5	567	2	610	6	653	4	696	18	739	47
525	1	568	2	611	4	654	6	697	22	740	31
526	1	569	3	612	9	655	12	698	18	741	48
527	1	570	1	613	7	656	9	699	17	742	54
528	2	571	4	614	6	657	11	700	28	743	44
529	1	572	2	615	6	658	6	701	24	744	37
530	1	573	3	616	6	659	14	702	34	745	44
531	1	574	1	617	13	660	14	703	36	746	53
532	0	575	4	618	8	661	9	704	21	747	45
533	1	576	9	619	5	662	10	705	30	748	38
534	0	577	3	620	10	663	7	706	33	749	47
535	0	578	3	621	11	664	10	707	24	750	56
536	1	579	5	622	5	665	18	708	23	751	43
537	1	580	4	623	3	666	9	709	21	752	45
538	2	581	6	624	4	667	13	710	22	753	62
539	5	582	3	625	4	668	16	711	28	754	37
540	2	583	1	626	9	669	13	712	17	755	43
541	0	584	6	627	8	670	10	713	22	756	58
542	0	585	1	628	8	671	11	714	29	757	55
543	3	586	4	629	4	672	13	715	28	758	54
544	0	587	3	630	9	673	18	716	26	759	46
545	0	588	5	631	12	674	13	717	24	760	39
546	1	589	7	632	5	675	8	718	36	761	55
547	1	590	5	633	6	676	10	719	29	762	60
548	2	591	4	634	7	677	13	720	18	763	57
549	2	592	3	635	7	678	18	721	30	764	52
550	2	593	5	636	7	679	11	722	40	765	44
551	1	594	5	637	10	680	11	723	40	766	55
552	0	595	7	638	11	681	23	724	26	767	43
553	3	596	7	639	10	682	10	725	27	768	63
554	1	597	4	640	12	683	21	726	44	769	46
555	2	598	1	641	9	684	16	727	39	770	52
556	2	599	3	642	9	685	17	728	34	771	41
557	1	600	5	643	10	686	17	729	43	772	47
558	1	601	7	644	11	687	11	730	33	773	48
559	1	602	9	645	11	688	21	731	48	774	72

Table A18. Continued.

Channel #	*f*	Channel #	*f*	Channel #	*f*	Channel #	*f*	Channel #	*f*	Channel #	*f*
775	49	818	56	861	35	904	13	947	1	990	0
776	38	819	60	862	38	905	20	948	3	991	0
777	58	820	48	863	25	906	9	949	2	992	0
778	50	821	43	864	27	907	7	950	1	993	0
779	64	822	69	865	38	908	10	951	1	994	0
780	47	823	59	866	32	909	15	952	2	995	0
781	50	824	47	867	39	910	16	953	1	996	0
782	59	825	46	868	38	911	8	954	2	997	0
783	52	826	44	869	33	912	4	955	0	998	0
784	63	827	52	870	33	913	13	956	1	999	0
785	76	828	47	871	27	914	10	957	1	1000	0
786	58	829	38	872	20	915	8	958	1	1001	1
787	78	830	56	873	32	916	13	959	2	1002	2
788	58	831	50	874	34	917	7	960	4	1003	0
789	53	832	52	875	20	918	8	961	3	1004	0
790	74	833	46	876	27	919	7	962	2	1005	0
791	62	834	45	877	23	920	7	963	0	1006	0
792	56	835	59	878	37	921	7	964	4	1007	0
793	47	836	40	879	27	922	9	965	0	1008	0
794	51	837	39	880	28	923	13	966	4	1009	0
795	66	838	42	881	29	924	7	967	1	1010	0
796	43	839	38	882	23	925	7	968	3	1011	0
797	60	840	50	883	24	926	5	969	0	1012	0
798	59	841	36	884	21	927	4	970	1	1013	0
799	72	842	42	885	19	928	9	971	2	1014	0
800	60	843	55	886	29	929	4	972	1	1015	0
801	67	844	35	887	11	930	5	973	1	1016	0
802	69	845	37	888	15	931	11	974	0	1017	0
803	66	846	54	889	23	932	1	975	0	1018	0
804	57	847	41	890	15	933	3	976	0	1019	0
805	51	848	35	891	22	934	2	977	0	1020	0
806	64	849	42	892	20	935	4	978	0	1021	0
807	48	850	35	893	19	936	3	979	0	1022	0
808	50	851	37	894	14	937	4	980	0	1023	0
809	55	852	40	895	17	938	2	981	0	1024	0
810	54	853	32	896	15	939	4	982	0		
811	60	854	40	897	11	940	7	983	0		
812	55	855	41	898	10	941	8	984	0		
813	47	856	33	899	11	942	4	985	0		
814	67	857	38	900	10	943	3	986	0		
815	53	858	25	901	10	944	3	987	0		
816	48	859	39	902	14	945	1	988	1		
817	46	860	30	903	9	946	1	989	0		

Table A19. Raw flow cytometry data for differentiating IMR-32 (Day 14, 1st replicate) used to generate Figure 3.2.

Channel #	*f*	Channel #	*f*	Channel #	*f*	Channel #	*f*	Channel #	*f*	Channel #	*f*
1	0	44	0	87	0	130	0	173	1	216	2
2	0	45	1	88	0	131	1	174	1	217	0
3	0	46	2	89	1	132	2	175	1	218	0
4	8	47	0	90	0	133	0	176	1	219	1
5	167	48	1	91	0	134	0	177	0	220	2
6	22	49	1	92	0	135	0	178	2	221	0
7	1	50	1	93	0	136	0	179	1	222	2
8	0	51	1	94	0	137	0	180	0	223	0
9	2	52	1	95	1	138	0	181	1	224	1
10	0	53	0	96	0	139	0	182	1	225	0
11	0	54	1	97	0	140	1	183	0	226	1
12	0	55	0	98	0	141	0	184	2	227	0
13	0	56	0	99	1	142	2	185	1	228	0
14	1	57	1	100	1	143	0	186	1	229	1
15	0	58	0	101	1	144	0	187	0	230	1
16	0	59	0	102	1	145	2	188	2	231	1
17	0	60	0	103	0	146	0	189	0	232	2
18	0	61	0	104	0	147	1	190	1	233	0
19	0	62	2	105	0	148	1	191	0	234	1
20	0	63	1	106	1	149	0	192	1	235	2
21	1	64	1	107	1	150	0	193	0	236	0
22	0	65	1	108	1	151	0	194	0	237	1
23	0	66	0	109	2	152	0	195	1	238	1
24	0	67	0	110	0	153	1	196	1	239	2
25	0	68	0	111	1	154	2	197	0	240	1
26	1	69	0	112	0	155	1	198	0	241	2
27	0	70	0	113	2	156	0	199	1	242	1
28	0	71	0	114	0	157	0	200	2	243	0
29	0	72	2	115	0	158	0	201	2	244	3
30	1	73	0	116	2	159	2	202	0	245	1
31	0	74	2	117	0	160	0	203	1	246	0
32	0	75	0	118	1	161	1	204	1	247	0
33	1	76	0	119	0	162	0	205	1	248	3
34	0	77	0	120	1	163	0	206	1	249	4
35	0	78	0	121	1	164	1	207	3	250	2
36	1	79	0	122	2	165	2	208	1	251	0
37	0	80	1	123	0	166	1	209	0	252	2
38	0	81	0	124	2	167	1	210	2	253	3
39	0	82	0	125	1	168	1	211	0	254	0
40	0	83	0	126	0	169	2	212	1	255	1
41	1	84	0	127	2	170	0	213	1	256	1
42	1	85	0	128	0	171	1	214	0	257	1
43	0	86	0	129	0	172	2	215	0	258	0

* Channel # and *f* represent oxonol fluorescence and frequency respectively.

Table A19. Continued.

Channel #	*f*	Channel #	*f*	Channel #	*f*	Channel #	*f*	Channel #	*f*	Channel #	*f*
259	0	302	0	345	2	388	1	431	0	474	4
260	3	303	1	346	1	389	2	432	4	475	4
261	1	304	1	347	2	390	0	433	1	476	2
262	1	305	2	348	0	391	3	434	2	477	1
263	0	306	2	349	2	392	1	435	2	478	3
264	1	307	2	350	3	393	2	436	1	479	1
265	1	308	1	351	0	394	2	437	3	480	2
266	2	309	1	352	1	395	2	438	5	481	1
267	3	310	0	353	2	396	5	439	1	482	4
268	0	311	2	354	2	397	2	440	3	483	6
269	0	312	2	355	1	398	1	441	2	484	3
270	0	313	1	356	1	399	2	442	6	485	0
271	0	314	2	357	2	400	2	443	0	486	1
272	0	315	1	358	2	401	4	444	0	487	4
273	3	316	1	359	0	402	1	445	2	488	4
274	0	317	1	360	1	403	1	446	2	489	5
275	0	318	5	361	1	404	1	447	3	490	0
276	0	319	2	362	2	405	2	448	3	491	4
277	1	320	2	363	1	406	7	449	6	492	2
278	1	321	0	364	3	407	0	450	3	493	4
279	0	322	1	365	4	408	2	451	1	494	2
280	0	323	2	366	3	409	0	452	1	495	4
281	1	324	0	367	2	410	2	453	3	496	2
282	2	325	5	368	2	411	0	454	0	497	2
283	1	326	2	369	1	412	3	455	3	498	1
284	2	327	0	370	1	413	1	456	2	499	4
285	0	328	1	371	4	414	6	457	4	500	2
286	1	329	3	372	1	415	1	458	4	501	1
287	0	330	3	373	1	416	1	459	0	502	1
288	0	331	1	374	2	417	1	460	5	503	1
289	1	332	2	375	2	418	0	461	4	504	4
290	1	333	2	376	1	419	0	462	1	505	5
291	0	334	0	377	2	420	1	463	4	506	2
292	4	335	3	378	1	421	3	464	2	507	2
293	2	336	0	379	0	422	1	465	1	508	4
294	3	337	1	380	3	423	1	466	2	509	3
295	1	338	0	381	2	424	2	467	1	510	1
296	1	339	5	382	5	425	1	468	0	511	1
297	0	340	2	383	1	426	0	469	3	512	4
298	1	341	0	384	2	427	4	470	2	513	0
299	2	342	4	385	1	428	2	471	2	514	3
300	0	343	0	386	1	429	3	472	4	515	2
301	0	344	2	387	3	430	0	473	0	516	2

Table A19. Continued.

Channel #	*f*	Channel #	*f*	Channel #	*f*	Channel #	*f*	Channel #	*f*	Channel #	*f*
517	2	560	2	603	6	646	1	689	4	732	5
518	1	561	2	604	6	647	6	690	7	733	12
519	0	562	2	605	3	648	5	691	6	734	11
520	6	563	8	606	4	649	4	692	10	735	9
521	2	564	2	607	2	650	3	693	4	736	13
522	5	565	4	608	2	651	3	694	6	737	6
523	2	566	6	609	2	652	8	695	8	738	12
524	1	567	7	610	1	653	4	696	3	739	8
525	4	568	2	611	0	654	4	697	6	740	11
526	3	569	5	612	3	655	2	698	8	741	10
527	1	570	3	613	1	656	8	699	12	742	16
528	3	571	3	614	1	657	6	700	10	743	9
529	4	572	2	615	5	658	7	701	7	744	14
530	4	573	3	616	0	659	5	702	8	745	13
531	1	574	4	617	2	660	5	703	9	746	17
532	1	575	2	618	2	661	2	704	6	747	12
533	4	576	4	619	6	662	5	705	5	748	7
534	1	577	4	620	6	663	4	706	11	749	16
535	3	578	5	621	3	664	6	707	7	750	15
536	3	579	4	622	1	665	6	708	4	751	15
537	1	580	3	623	8	666	3	709	5	752	19
538	3	581	4	624	2	667	3	710	8	753	25
539	1	582	2	625	3	668	6	711	8	754	17
540	2	583	2	626	3	669	8	712	6	755	14
541	4	584	2	627	9	670	5	713	6	756	17
542	2	585	2	628	4	671	7	714	8	757	12
543	3	586	0	629	3	672	5	715	6	758	15
544	4	587	3	630	2	673	5	716	6	759	14
545	3	588	6	631	5	674	9	717	10	760	17
546	7	589	2	632	2	675	5	718	7	761	13
547	1	590	6	633	7	676	7	719	10	762	16
548	0	591	5	634	5	677	7	720	10	763	17
549	1	592	2	635	7	678	5	721	12	764	13
550	0	593	4	636	4	679	4	722	7	765	19
551	2	594	4	637	2	680	4	723	9	766	23
552	1	595	4	638	4	681	6	724	8	767	22
553	0	596	7	639	2	682	15	725	7	768	15
554	5	597	2	640	3	683	6	726	11	769	16
555	4	598	2	641	6	684	5	727	7	770	19
556	1	599	1	642	5	685	10	728	14	771	25
557	1	600	5	643	4	686	4	729	9	772	22
558	0	601	1	644	5	687	8	730	4	773	12
559	0	602	3	645	3	688	4	731	5	774	22

Table A19. Continued.

Channel #	*f*	Channel #	*f*	Channel #	*f*	Channel #	*f*	Channel #	*f*	Channel #	*f*
775	13	818	50	861	45	904	49	947	19	990	2
776	14	819	39	862	63	905	51	948	15	991	2
777	18	820	43	863	52	906	45	949	16	992	3
778	23	821	34	864	56	907	57	950	17	993	3
779	21	822	45	865	46	908	41	951	10	994	3
780	26	823	38	866	38	909	50	952	15	995	1
781	22	824	39	867	57	910	54	953	16	996	3
782	19	825	42	868	56	911	30	954	10	997	1
783	21	826	44	869	60	912	32	955	11	998	2
784	20	827	63	870	63	913	50	956	15	999	5
785	20	828	41	871	49	914	52	957	8	1000	2
786	19	829	47	872	69	915	38	958	8	1001	2
787	26	830	51	873	74	916	36	959	6	1002	5
788	27	831	34	874	53	917	40	960	9	1003	2
789	24	832	43	875	63	918	32	961	6	1004	1
790	23	833	55	876	43	919	35	962	11	1005	2
791	22	834	38	877	59	920	33	963	12	1006	3
792	28	835	43	878	62	921	38	964	9	1007	2
793	34	836	37	879	46	922	28	965	7	1008	0
794	31	837	37	880	59	923	33	966	16	1009	1
795	25	838	47	881	54	924	34	967	8	1010	0
796	36	839	48	882	70	925	28	968	9	1011	0
797	35	840	46	883	54	926	32	969	9	1012	0
798	25	841	43	884	70	927	21	970	9	1013	0
799	23	842	46	885	64	928	26	971	7	1014	1
800	31	843	55	886	54	929	26	972	10	1015	0
801	40	844	67	887	47	930	32	973	11	1016	0
802	37	845	63	888	57	931	42	974	12	1017	0
803	40	846	50	889	69	932	24	975	9	1018	0
804	33	847	56	890	63	933	22	976	4	1019	0
805	28	848	67	891	49	934	28	977	2	1020	0
806	43	849	63	892	50	935	25	978	2	1021	0
807	34	850	43	893	53	936	24	979	6	1022	0
808	34	851	64	894	49	937	20	980	2	1023	0
809	51	852	56	895	58	938	21	981	4	1024	0
810	28	853	52	896	45	939	22	982	2		
811	51	854	59	897	63	940	20	983	3		
812	37	855	47	898	67	941	17	984	4		
813	31	856	44	899	67	942	30	985	5		
814	41	857	53	900	57	943	23	986	5		
815	41	858	54	901	49	944	13	987	4		
816	27	859	71	902	43	945	21	988	3		
817	36	860	54	903	36	946	20	989	4		

Table A20. Raw flow cytometry data for differentiating IMR-32 (Day 14, 2nd replicate) used to generate Figure 3.2.

Channel #	*f*	Channel #	*f*	Channel #	*f*	Channel #	*f*	Channel #	*f*	Channel #	*f*
1	0	44	0	87	0	130	0	173	0	216	0
2	0	45	0	88	0	131	0	174	0	217	0
3	0	46	0	89	0	132	0	175	0	218	0
4	0	47	0	90	0	133	0	176	0	219	0
5	12	48	0	91	0	134	0	177	0	220	0
6	4	49	0	92	0	135	0	178	0	221	0
7	3	50	0	93	0	136	0	179	0	222	0
8	0	51	0	94	0	137	0	180	0	223	0
9	0	52	0	95	0	138	0	181	0	224	0
10	1	53	0	96	0	139	0	182	0	225	0
11	0	54	0	97	0	140	0	183	0	226	0
12	0	55	0	98	0	141	0	184	0	227	0
13	0	56	0	99	1	142	0	185	0	228	0
14	0	57	0	100	0	143	1	186	0	229	0
15	0	58	0	101	0	144	0	187	0	230	0
16	0	59	0	102	0	145	0	188	0	231	0
17	0	60	0	103	0	146	0	189	0	232	0
18	0	61	0	104	0	147	0	190	0	233	0
19	0	62	0	105	0	148	0	191	1	234	0
20	0	63	0	106	0	149	0	192	0	235	0
21	0	64	0	107	0	150	1	193	0	236	0
22	1	65	0	108	0	151	0	194	0	237	0
23	0	66	0	109	0	152	0	195	0	238	0
24	0	67	0	110	0	153	0	196	0	239	0
25	0	68	0	111	0	154	0	197	0	240	0
26	0	69	0	112	0	155	0	198	0	241	1
27	0	70	0	113	0	156	0	199	0	242	0
28	0	71	0	114	0	157	0	200	0	243	0
29	0	72	0	115	0	158	0	201	0	244	0
30	0	73	0	116	0	159	0	202	0	245	0
31	0	74	0	117	0	160	0	203	0	246	0
32	0	75	0	118	0	161	0	204	0	247	0
33	0	76	0	119	0	162	0	205	0	248	0
34	0	77	1	120	0	163	0	206	0	249	0
35	0	78	0	121	0	164	0	207	0	250	0
36	0	79	0	122	0	165	0	208	0	251	0
37	0	80	0	123	0	166	0	209	0	252	0
38	0	81	0	124	0	167	0	210	0	253	0
39	0	82	1	125	0	168	0	211	0	254	0
40	0	83	0	126	0	169	0	212	0	255	0
41	0	84	0	127	0	170	1	213	0	256	1
42	0	85	0	128	0	171	0	214	0	257	0
43	0	86	0	129	0	172	0	215	0	258	0

* Channel # and *f* represent oxonol fluorescence and frequency respectively.

Table A20. Continued.

Channel #	*f*	Channel #	*f*	Channel #	*f*	Channel #	*f*	Channel #	*f*	Channel #	*f*
259	0	302	0	345	0	388	0	431	1	474	1
260	0	303	0	346	0	389	0	432	2	475	1
261	0	304	0	347	0	390	0	433	2	476	0
262	0	305	0	348	0	391	0	434	1	477	0
263	0	306	0	349	0	392	0	435	2	478	0
264	0	307	0	350	0	393	0	436	1	479	1
265	0	308	0	351	0	394	0	437	1	480	0
266	0	309	0	352	0	395	1	438	1	481	1
267	0	310	0	353	0	396	0	439	0	482	1
268	0	311	0	354	0	397	2	440	0	483	1
269	0	312	0	355	0	398	1	441	0	484	2
270	0	313	1	356	0	399	0	442	0	485	1
271	0	314	0	357	0	400	0	443	0	486	1
272	0	315	1	358	0	401	1	444	0	487	0
273	0	316	0	359	0	402	1	445	0	488	2
274	0	317	0	360	0	403	0	446	1	489	1
275	0	318	2	361	1	404	0	447	0	490	0
276	0	319	0	362	1	405	0	448	0	491	1
277	0	320	0	363	0	406	1	449	1	492	3
278	0	321	0	364	1	407	0	450	1	493	0
279	0	322	0	365	0	408	0	451	0	494	0
280	0	323	0	366	0	409	1	452	0	495	0
281	0	324	0	367	0	410	1	453	0	496	2
282	0	325	0	368	0	411	0	454	0	497	1
283	0	326	0	369	0	412	0	455	0	498	0
284	0	327	0	370	0	413	1	456	1	499	0
285	0	328	0	371	0	414	0	457	1	500	1
286	0	329	0	372	0	415	0	458	0	501	1
287	0	330	0	373	0	416	0	459	2	502	2
288	0	331	0	374	0	417	0	460	1	503	0
289	0	332	0	375	0	418	0	461	0	504	1
290	0	333	0	376	0	419	0	462	0	505	1
291	0	334	0	377	0	420	0	463	0	506	1
292	0	335	0	378	0	421	0	464	0	507	2
293	0	336	1	379	0	422	0	465	1	508	1
294	0	337	1	380	1	423	0	466	0	509	0
295	0	338	0	381	0	424	1	467	0	510	3
296	0	339	0	382	0	425	0	468	0	511	1
297	0	340	0	383	2	426	0	469	1	512	2
298	0	341	0	384	1	427	1	470	0	513	2
299	0	342	1	385	0	428	1	471	0	514	2
300	0	343	0	386	1	429	0	472	1	515	0
301	0	344	0	387	0	430	0	473	1	516	1

Table A20. Continued.

Channel #	*f*	Channel #	*f*	Channel #	*f*	Channel #	*f*	Channel #	*f*	Channel #	*f*
517	3	560	4	603	10	646	12	689	27	732	40
518	1	561	1	604	5	647	7	690	25	733	30
519	0	562	3	605	9	648	6	691	17	734	47
520	2	563	3	606	1	649	17	692	26	735	31
521	1	564	4	607	3	650	16	693	26	736	29
522	1	565	2	608	4	651	14	694	29	737	41
523	2	566	1	609	6	652	8	695	17	738	28
524	1	567	3	610	1	653	16	696	18	739	37
525	1	568	3	611	5	654	17	697	28	740	36
526	0	569	4	612	6	655	16	698	28	741	35
527	1	570	2	613	3	656	12	699	20	742	36
528	1	571	2	614	8	657	15	700	32	743	33
529	2	572	6	615	8	658	17	701	19	744	33
530	2	573	0	616	5	659	16	702	21	745	41
531	4	574	1	617	6	660	15	703	30	746	30
532	2	575	5	618	8	661	9	704	22	747	55
533	1	576	2	619	5	662	13	705	33	748	31
534	2	577	6	620	5	663	18	706	31	749	30
535	1	578	3	621	5	664	18	707	33	750	37
536	4	579	4	622	7	665	13	708	27	751	39
537	2	580	4	623	9	666	23	709	21	752	33
538	0	581	1	624	6	667	16	710	26	753	31
539	3	582	2	625	11	668	20	711	34	754	44
540	3	583	5	626	8	669	18	712	28	755	46
541	2	584	3	627	3	670	14	713	23	756	31
542	0	585	2	628	8	671	20	714	41	757	33
543	1	586	2	629	9	672	10	715	28	758	51
544	3	587	2	630	5	673	12	716	32	759	33
545	7	588	2	631	8	674	13	717	26	760	36
546	0	589	1	632	2	675	16	718	42	761	54
547	3	590	0	633	9	676	13	719	37	762	41
548	0	591	1	634	6	677	27	720	26	763	50
549	5	592	5	635	9	678	21	721	40	764	47
550	5	593	3	636	4	679	29	722	38	765	41
551	2	594	3	637	8	680	15	723	29	766	46
552	2	595	1	638	11	681	23	724	40	767	30
553	4	596	2	639	8	682	23	725	32	768	37
554	2	597	3	640	5	683	17	726	38	769	40
555	3	598	6	641	4	684	16	727	24	770	46
556	4	599	6	642	15	685	27	728	32	771	56
557	4	600	5	643	11	686	22	729	33	772	36
558	0	601	5	644	8	687	19	730	36	773	35
559	0	602	4	645	9	688	22	731	35	774	38

Table A20. Continued.

Channel #	*f*	Channel #	*f*	Channel #	*f*	Channel #	*f*	Channel #	*f*	Channel #	*f*
775	49	818	46	861	38	904	7	947	4	990	1
776	40	819	50	862	37	905	13	948	2	991	0
777	58	820	70	863	28	906	17	949	2	992	0
778	48	821	60	864	39	907	14	950	3	993	0
779	49	822	64	865	34	908	7	951	2	994	0
780	40	823	44	866	33	909	8	952	1	995	0
781	44	824	67	867	36	910	12	953	0	996	1
782	52	825	65	868	27	911	9	954	2	997	0
783	44	826	52	869	37	912	6	955	1	998	0
784	51	827	57	870	39	913	15	956	3	999	0
785	51	828	55	871	26	914	8	957	0	1000	0
786	46	829	59	872	25	915	13	958	2	1001	0
787	48	830	54	873	27	916	7	959	0	1002	1
788	48	831	62	874	26	917	2	960	0	1003	0
789	52	832	53	875	33	918	9	961	3	1004	1
790	61	833	60	876	30	919	9	962	1	1005	0
791	40	834	57	877	34	920	9	963	3	1006	0
792	47	835	67	878	27	921	6	964	0	1007	0
793	60	836	52	879	25	922	8	965	0	1008	0
794	52	837	54	880	21	923	5	966	0	1009	0
795	46	838	59	881	17	924	7	967	2	1010	0
796	43	839	54	882	26	925	7	968	2	1011	0
797	53	840	47	883	21	926	6	969	1	1012	0
798	65	841	49	884	17	927	7	970	1	1013	0
799	55	842	44	885	17	928	2	971	1	1014	0
800	51	843	63	886	22	929	3	972	0	1015	0
801	44	844	37	887	19	930	5	973	1	1016	0
802	63	845	48	888	9	931	2	974	0	1017	0
803	46	846	59	889	26	932	2	975	0	1018	0
804	56	847	47	890	16	933	6	976	0	1019	0
805	38	848	54	891	22	934	2	977	2	1020	0
806	72	849	52	892	10	935	2	978	0	1021	0
807	48	850	43	893	22	936	3	979	0	1022	0
808	47	851	45	894	21	937	5	980	1	1023	0
809	47	852	46	895	19	938	3	981	1	1024	0
810	59	853	41	896	19	939	5	982	1		
811	66	854	42	897	15	940	6	983	1		
812	57	855	46	898	18	941	1	984	0		
813	51	856	41	899	15	942	2	985	0		
814	53	857	37	900	23	943	1	986	1		
815	57	858	32	901	13	944	1	987	1		
816	52	859	47	902	8	945	3	988	0		
817	49	860	33	903	14	946	5	989	1		

Table A21. Confocal microscopy data from differentiating (Day 2) IMR-32 cells used to generate Figure 3.4.

CELL#	Fl(i)	Fl(o)	LOG(Fl(i)/Fl(o))	CELL#	Fl(i)	Fl(o)	LOG(Fl(i)/Fl(o))	CELL#	Fl(i)	Fl(o)	LOG(Fl(i)/Fl(o))
1	12.79	0.70	1.26	44	6.97	0.70	1.00	87	10.25	0.70	1.16
2	5.95	0.70	0.93	45	8.73	0.70	1.09	88	10.82	0.70	1.19
3	7.25	0.70	1.01	46	6.95	0.70	0.99	89	6.53	0.70	0.97
4	7.76	0.70	1.04	47	5.57	0.70	0.90	90	1.64	0.70	0.37
5	12.38	0.70	1.25	48	5.25	0.70	0.87	91	13.62	0.70	1.29
6	6.95	0.70	0.99	49	13.78	0.70	1.29	92	13.61	0.70	1.29
7	6.15	0.70	0.94	50	13.17	0.70	1.27	93	7.65	0.70	1.04
8	8.12	0.70	1.06	51	8.31	0.70	1.07	94	12.48	0.70	1.25
9	6.41	0.70	0.96	52	5.34	0.70	0.88	95	11.35	0.70	1.21
10	5.29	0.70	0.88	53	9.63	0.70	1.14	96	12.76	0.70	1.26
11	6.08	0.70	0.94	54	14.55	0.70	1.32	97	2.10	0.70	0.48
12	8.03	0.70	1.06	55	9.30	0.70	1.12	98	10.55	0.70	1.18
13	4.46	0.70	0.80	56	5.04	0.70	0.85	99	13.22	0.70	1.27
14	1.90	0.70	0.43	57	13.15	0.70	1.27	100	10.95	0.70	1.19
15	4.37	0.70	0.79	58	4.72	0.70	0.83	101	15.07	0.70	1.33
16	4.87	0.70	0.84	59	6.04	0.70	0.93	102	10.37	0.70	1.17
17	3.01	0.70	0.63	60	8.66	0.70	1.09	103	7.26	0.70	1.01
18	4.43	0.70	0.80	61	22.73	0.70	1.51	104	6.17	0.70	0.94
19	2.81	0.70	0.60	62	3.33	0.70	0.67	105	15.47	0.70	1.34
20	10.34	0.70	1.17	63	9.89	0.70	1.15	106	13.00	0.70	1.27
21	4.25	0.70	0.78	64	6.83	0.70	0.99	107	15.19	0.70	1.33
22	6.99	0.70	1.00	65	7.09	0.70	1.00	108	9.17	0.70	1.12
23	7.16	0.70	1.01	66	8.05	0.70	1.06	109	9.31	0.70	1.12
24	7.24	0.70	1.01	67	7.79	0.70	1.04	110	9.13	0.70	1.11
25	7.23	0.70	1.01	68	11.32	0.70	1.21	111	12.66	0.70	1.26
26	2.08	0.70	0.47	69	6.75	0.70	0.98	112	10.64	0.70	1.18
27	8.36	0.70	1.08	70	9.75	0.70	1.14	113	9.87	0.70	1.15
28	4.41	0.70	0.80	71	11.84	0.70	1.23	114	4.81	0.70	0.84
29	5.28	0.70	0.88	72	10.58	0.70	1.18	115	10.74	0.70	1.18
30	5.31	0.70	0.88	73	10.48	0.70	1.17	116	10.02	0.70	1.15
31	5.83	0.70	0.92	74	7.97	0.70	1.05	117	10.48	0.70	1.17
32	3.71	0.70	0.72	75	7.12	0.70	1.01	118	2.07	0.70	0.47
33	5.68	0.70	0.91	76	7.15	0.70	1.01	119	11.81	0.70	1.23
34	6.58	0.70	0.97	77	6.75	0.70	0.98	120	6.23	0.70	0.95
35	8.21	0.70	1.07	78	5.15	0.70	0.86	121	11.91	0.70	1.23
36	7.18	0.70	1.01	79	17.44	0.70	1.39	122	4.83	0.70	0.84
37	4.78	0.70	0.83	80	9.39	0.70	1.13	123	6.40	0.70	0.96
38	5.60	0.70	0.90	81	10.00	0.70	1.15	124	5.31	0.70	0.88
39	5.66	0.70	0.91	82	12.20	0.70	1.24	125	6.71	0.70	0.98
40	6.77	0.70	0.98	83	17.54	0.70	1.40	126	13.15	0.70	1.27
41	5.92	0.70	0.92	84	6.78	0.70	0.98	127	11.30	0.70	1.21
42	5.42	0.70	0.89	85	8.31	0.70	1.07	128	7.22	0.70	1.01
43	19.69	0.70	1.45	86	6.89	0.70	0.99	129	8.54	0.70	1.08

* Fl(i) and Fl(o) – Fluorescence intensities inside and outside the cell, respectively.

Table A21. Continued.

CELL#	Fl(i)	Fl(o)	LOG(Fl(i)/Fl(o))	CELL#	Fl(i)	Fl(o)	LOG(Fl(i)/Fl(o))	CELL#	Fl(i)	Fl(o)	LOG(Fl(i)/Fl(o))
130	10.47	0.70	1.17	173	9.93	0.70	1.15	216	5.50	0.70	0.89
131	8.39	0.70	1.08	174	14.57	0.70	1.32	217	3.39	0.70	0.68
132	8.33	0.70	1.07	175	6.44	0.70	0.96	218	6.22	0.70	0.95
133	9.22	0.70	1.12	176	17.01	0.70	1.38	219	8.68	0.70	1.09
134	5.14	0.70	0.86	177	12.76	0.70	1.26	220	4.74	0.70	0.83
135	21.75	0.70	1.49	178	6.36	0.70	0.96	221	4.67	0.70	0.82
136	16.64	0.70	1.37	179	11.20	0.70	1.20	222	4.64	0.70	0.82
137	15.95	0.70	1.36	180	11.27	0.70	1.20	223	5.11	0.70	0.86
138	7.92	0.70	1.05	181	6.18	0.70	0.94	224	2.55	0.70	0.56
139	10.12	0.70	1.16	182	8.89	0.70	1.10	225	5.00	0.70	0.85
140	8.56	0.70	1.09	183	6.72	0.70	0.98	226	10.54	0.70	1.18
141	10.03	0.70	1.15	184	7.34	0.70	1.02	227	8.47	0.70	1.08
142	9.16	0.70	1.11	185	5.85	0.70	0.92	228	6.49	0.70	0.96
143	11.83	0.70	1.23	186	11.84	0.70	1.23	229	2.72	0.70	0.59
144	15.35	0.70	1.34	187	11.23	0.70	1.20	230	3.62	0.70	0.71
145	10.02	0.70	1.15	188	17.72	0.70	1.40	231	4.91	0.70	0.84
146	6.93	0.70	0.99	189	17.68	0.70	1.40	232	4.31	0.70	0.79
147	22.02	0.70	1.50	190	11.15	0.70	1.20	233	3.49	0.70	0.70
148	11.61	0.70	1.22	191	14.07	0.70	1.30	234	2.34	0.70	0.52
149	8.78	0.70	1.10	192	17.77	0.70	1.40				
150	10.04	0.70	1.15	193	9.62	0.70	1.14				
151	8.94	0.70	1.10	194	13.20	0.70	1.27				
152	10.65	0.70	1.18	195	11.62	0.70	1.22				
153	3.29	0.70	0.67	196	11.59	0.70	1.22				
154	9.52	0.70	1.13	197	1.86	0.70	0.42				
155	11.40	0.70	1.21	198	5.58	0.70	0.90				
156	11.90	0.70	1.23	199	15.92	0.70	1.35				
157	12.84	0.70	1.26	200	18.52	0.70	1.42				
158	9.28	0.70	1.12	201	11.71	0.70	1.22				
159	15.55	0.70	1.34	202	6.42	0.70	0.96				
160	18.44	0.70	1.42	203	5.47	0.70	0.89				
161	12.93	0.70	1.26	204	2.14	0.70	0.48				
162	11.04	0.70	1.20	205	5.98	0.70	0.93				
163	12.90	0.70	1.26	206	2.40	0.70	0.53				
164	7.58	0.70	1.03	207	5.23	0.70	0.87				
165	10.42	0.70	1.17	208	3.60	0.70	0.71				
166	17.06	0.70	1.38	209	4.75	0.70	0.83				
167	12.17	0.70	1.24	210	10.34	0.70	1.17				
168	9.13	0.70	1.11	211	3.73	0.70	0.72				
169	12.46	0.70	1.25	212	2.85	0.70	0.61				
170	20.20	0.70	1.46	213	7.16	0.70	1.01				
171	15.73	0.70	1.35	214	3.86	0.70	0.74				
172	9.42	0.70	1.13	215	4.24	0.70	0.78				

Table A22. Confocal microscopy data from differentiating (Day 16) IMR-32 cells used to generate Figure 3.4.

CELL#	Fl(i)	Fl(o)	LOG(Fl(i)/Fl(o))	CELL#	Fl(i)	Fl(o)	LOG(Fl(i)/Fl(o))	CELL#	Fl(i)	Fl(o)	LOG(Fl(i)/Fl(o))	CELL#	Fl(i)	Fl(o)	LOG(Fl(i)/Fl(o))
1	8.74	1.27	0.84	25	15.87	1.27	1.10	49	9.19	1.27	0.86	73	9.45	1.27	0.87
2	10.56	1.27	0.92	26	9.11	1.27	0.85	50	5.59	1.27	0.64	74	8.85	1.27	0.84
3	17.57	1.27	1.14	27	9.10	1.27	0.85	51	9.21	1.27	0.86	75	14.44	1.27	1.05
4	13.23	1.27	1.02	28	5.46	1.27	0.63	52	13.06	1.27	1.01	76	28.06	1.27	1.34
5	6.57	1.27	0.71	29	13.16	1.27	1.01	53	11.28	1.27	0.95	77	11.83	1.27	0.97
6	4.88	1.27	0.58	30	15.15	1.27	1.08	54	12.34	1.27	0.99	78	16.34	1.27	1.11
7	14.69	1.27	1.06	31	7.11	1.27	0.75	55	10.31	1.27	0.91	79	16.53	1.27	1.11
8	8.70	1.27	0.83	32	9.74	1.27	0.88	56	10.75	1.27	0.93	80	18.84	1.27	1.17
9	8.84	1.27	0.84	33	4.65	1.27	0.56	57	11.98	1.27	0.97	81	12.22	1.27	0.98
10	3.90	1.27	0.49	34	7.74	1.27	0.78	58	11.52	1.27	0.96	82	20.83	1.27	1.21
11	8.66	1.27	0.83	35	8.18	1.27	0.81	59	7.17	1.27	0.75	83	9.72	1.27	0.88
12	9.78	1.27	0.89	36	8.24	1.27	0.81	60	17.17	1.27	1.13	84	17.96	1.27	1.15
13	7.56	1.27	0.77	37	4.09	1.27	0.51	61	10.71	1.27	0.93	85	12.23	1.27	0.98
14	7.97	1.27	0.80	38	9.46	1.27	0.87	62	10.58	1.27	0.92	86	11.85	1.27	0.97
15	8.31	1.27	0.81	39	9.68	1.27	0.88	63	13.39	1.27	1.02	87	9.57	1.27	0.88
16	4.79	1.27	0.58	40	10.22	1.27	0.90	64	11.70	1.27	0.96	88	32.23	1.27	1.40
17	5.63	1.27	0.65	41	9.41	1.27	0.87	65	15.32	1.27	1.08	89	14.78	1.27	1.06
18	6.85	1.27	0.73	42	10.65	1.27	0.92	66	10.87	1.27	0.93	90	11.14	1.27	0.94
19	11.98	1.27	0.97	43	12.12	1.27	0.98	67	15.17	1.27	1.08	91	11.94	1.27	0.97
20	6.49	1.27	0.71	44	12.37	1.27	0.99	68	8.80	1.27	0.84	92	11.40	1.27	0.95
21	14.29	1.27	1.05	45	10.92	1.27	0.93	69	15.28	1.27	1.08	93	17.67	1.27	1.14
22	4.84	1.27	0.58	46	13.03	1.27	1.01	70	13.86	1.27	1.04	94	7.60	1.27	0.78
23	22.24	1.27	1.24	47	3.36	1.27	0.42	71	16.99	1.27	1.13	95	11.64	1.27	0.96
24	12.19	1.27	0.98	48	12.56	1.27	0.99	72	16.91	1.27	1.12	96	7.55	1.27	0.77

* Fl(i) and Fl(o) – Fluorescence intensity inside and outside the cell, respectively.

Table A22. Continued.

CELL#	Fl(i)	Fl(o)	LOG(Fl(I)/Fl(o))	CELL#	Fl(i)	Fl(o)	LOG(Fl(i)/Fl(o))	CELL#	Fl(i)	Fl(o)	LOG(Fl(i)/Fl(o))	CELL#	Fl(i)	Fl(o)	LOG(Fl(i)/Fl(o))
97	9.49	1.27	0.87	121	15.74	1.27	1.09	145	24.61	1.27	1.29	169	16.63	1.27	1.12
98	20.26	1.27	1.20	122	7.73	1.27	0.78	146	34.27	1.27	1.43	170	27.82	1.27	1.34
99	19.86	1.27	1.19	123	10.61	1.27	0.92	147	15.28	1.27	1.08	171	22.46	1.27	1.25
100	3.42	1.27	0.43	124	18.27	1.27	1.16	148	17.13	1.27	1.13	172	18.21	1.27	1.16
101	11.15	1.27	0.94	125	11.19	1.27	0.94	149	20.23	1.27	1.20	173	25.27	1.27	1.30
102	17.79	1.27	1.15	126	12.97	1.27	1.01	150	19.19	1.27	1.18	174	21.22	1.27	1.22
103	8.40	1.27	0.82	127	5.80	1.27	0.66	151	18.28	1.27	1.16	175	24.65	1.27	1.29
104	8.91	1.27	0.85	128	20.64	1.27	1.21	152	10.64	1.27	0.92	176	14.08	1.27	1.04
105	11.49	1.27	0.96	129	13.71	1.27	1.03	153	22.90	1.27	1.25	177	13.53	1.27	1.03
106	19.71	1.27	1.19	130	14.36	1.27	1.05	154	18.74	1.27	1.17	178	36.36	1.27	1.46
107	20.90	1.27	1.22	131	21.04	1.27	1.22	155	27.27	1.27	1.33	179	21.69	1.27	1.23
108	13.88	1.27	1.04	132	14.07	1.27	1.04	156	29.37	1.27	1.36	180	18.58	1.27	1.16
109	15.74	1.27	1.09	133	15.88	1.27	1.10	157	17.47	1.27	1.14	181	30.33	1.27	1.38
110	13.16	1.27	1.01	134	20.22	1.27	1.20	158	12.94	1.27	1.01	182	12.46	1.27	0.99
111	19.21	1.27	1.18	135	17.62	1.27	1.14	159	27.07	1.27	1.33	183	19.09	1.27	1.18
112	18.60	1.27	1.16	136	11.89	1.27	0.97	160	18.87	1.27	1.17	184	27.85	1.27	1.34
113	9.76	1.27	0.88	137	7.50	1.27	0.77	161	17.52	1.27	1.14	185	20.94	1.27	1.22
114	8.34	1.27	0.82	138	50.05	1.27	1.59	162	19.75	1.27	1.19	186	16.51	1.27	1.11
115	20.24	1.27	1.20	139	16.24	1.27	1.11	163	30.98	1.27	1.39	187	26.35	1.27	1.32
116	13.62	1.27	1.03	140	14.95	1.27	1.07	164	28.69	1.27	1.35				
117	14.22	1.27	1.05	141	29.31	1.27	1.36	165	50.87	1.27	1.60				
118	11.68	1.27	0.96	142	14.21	1.27	1.05	166	28.32	1.27	1.35				
119	14.87	1.27	1.07	143	21.37	1.27	1.22	167	17.27	1.27	1.13				
120	9.56	1.27	0.88	144	22.14	1.27	1.24	168	22.16	1.27	1.24				

Table A23. Statistical comparison between Day 2 and Day 16 differentiating IMR32 cells (with respect to LOG(Fl(i)/Fl(o)) histograms) using Mann-Whitney U-test. Raw data used for comparison was obtained from Table A21 and A22.

Ranks

	DAY_DIFF	N	Mean Rank	Sum of Ranks
LOG(Fl(i)/Fl(o))	2.00	234	220.26	51541.00
	16.00	187	199.41	37290.00
	Total	421		

Test Statistics[a]

	LOG(Fl(i)/Fl(o))
Mann-Whitney U	19712.000
Z	-1.747
P-VALUE	.081

a. Grouping Variable: DAY_DIFF

TABLE A24. Results of enolase assay for 50 chromatographic fractions obtained from differentiating IMR-32 (Day 2) cells used to generate Figure 3.6.

FRACTION #	SV	AV	TV	OD/MIN	EU/ML	TEU	FRACTION #	SV	AV	TV	OD/MIN	EU/ML	TEU	FRACTION #	SV	AV	TV	OD/MIN	EU/ML	TEU
1	0.5	1	1	0	0	0	21	0.5	1	1	0	0	0	41	0.5	1	1	0	0	0
2	0.5	1	1	0	0	0	22	0.5	1	1	0	0	0	42	0.5	1	1	0	0	0
3	0.5	1	1	0.0047	0.0212	0.0212	23	0.5	1	1	0	0	0	43	0.5	1	1	0	0	0
4	0.5	1	1	0.045	0.2034	0.2034	24	0.5	1	1	0	0	0	44	0.5	1	1	0	0	0
5	0.5	1	1	0.1446	0.6536	0.6536	25	0.5	1	1	0	0	0	45	0.5	1	1	0	0	0
6	0.5	1	1	0.2023	0.9144	0.9144	26	0.5	1	1	0	0	0	46	0.5	1	1	0	0	0
7	0.5	1	1	0.1974	0.8922	0.8922	27	0.5	1	1	0	0	0	47	0.5	1	1	0	0	0
8	0.5	1	1	0.1366	0.6174	0.6174	28	0.5	1	1	0	0	0	48	0.5	1	1	0	0	0
9	0.5	1	1	0.0864	0.3905	0.3905	29	0.5	1	1	0.0099	0.0447	0.0447	49	0.5	1	1	0	0	0
10	0.5	1	1	0.0508	0.2296	0.2296	30	0.5	1	1	0.0134	0.0606	0.0606	50	0.5	1	1	0	0	0
11	0.5	1	1	0.0221	0.0999	0.0999	31	0.5	1	1	0.0196	0.0886	0.0886							
12	0.5	1	1	0.0091	0.0411	0.0411	32	0.5	1	1	0.0189	0.0854	0.0854							
13	0.5	1	1	0	0	0	33	0.5	1	1	0.0127	0.0574	0.0574							
14	0.5	1	1	0	0	0	34	0.5	1	1	0.006	0.0271	0.0271							
15	0.5	1	1	0	0	0	35	0.5	1	1	0	0	0							
16	0.5	1	1	0	0	0	36	0.5	1	1	0	0	0							
17	0.5	1	1	0	0	0	37	0.5	1	1	0	0	0							
18	0.5	1	1	0	0	0	38	0.5	1	1	0	0	0							
19	0.5	1	1	0	0	0	39	0.5	1	1	0	0	0							
20	0.5	1	1	0	0	0	40	0.5	1	1	0	0	0							

TEU after chromatography	**4.43**
TEU before chromatography	**5.28**
Yield of enolase activity	**83.86**
TEU (NSE)	**0.36**
TEU (NNSE)	**4.06**
% NSE activity	**8.22**

* SV- sample volume (ml); AV- assay volume (ml); TV- total volume (ml); EU/ML- enzyme units: ((OD/MIN*2.26)/SV); TEU- total enzyme units (EU/ML*TV). The calculated NSE value is given in % of total enolase activity.

TABLE A25. Results of enolase assay for 50 chromatographic fractions obtained from differentiating IMR-32 (Day 4, 1st replicate) cells used to generate Figure 3.6.

FRACTION #	SV	AV	TV	OD/MIN	EU/ML	TEU	FRACTION #	SV	AV	TV	OD/MIN	EU/ML	TEU	FRACTION #	SV	AV	TV	OD/MIN	EU/ML	TEU
1	0.5	1	1	0	0	0	21	0.5	1	1	0	0	0	41	0.5	1	1	0	0	0
2	0.5	1	1	0	0	0	22	0.5	1	1	0	0	0	42	0.5	1	1	0	0	0
3	0.5	1	1	0.0042	0.0190	0.0190	23	0.5	1	1	0	0	0	43	0.5	1	1	0	0	0
4	0.5	1	1	0.0248	0.1121	0.1121	24	0.5	1	1	0	0	0	44	0.5	1	1	0	0	0
5	0.5	1	1	0.0864	0.3905	0.3905	25	0.5	1	1	0	0	0	45	0.5	1	1	0	0	0
6	0.5	1	1	0.1355	0.6125	0.6125	26	0.5	1	1	0	0	0	46	0.5	1	1	0	0	0
7	0.5	1	1	0.1464	0.6617	0.6617	27	0.5	1	1	0	0	0	47	0.5	1	1	0	0	0
8	0.5	1	1	0.1175	0.5311	0.5311	28	0.5	1	1	0	0	0	48	0.5	1	1	0	0	0
9	0.5	1	1	0.0746	0.3372	0.3372	29	0.5	1	1	0	0	0	49	0.5	1	1	0	0	0
10	0.5	1	1	0.0455	0.2057	0.2057	30	0.5	1	1	0	0	0	50	0.5	1	1	0	0	0
11	0.5	1	1	0.025	0.1130	0.1130	31	0.5	1	1	0.0059	0.0267	0.0267							
12	0.5	1	1	0.0096	0.0434	0.0434	32	0.5	1	1	0.0108	0.0488	0.0488							
13	0.5	1	1	0.0047	0.0212	0.0212	33	0.5	1	1	0.0116	0.0524	0.0524							
14	0.5	1	1	0	0	0	34	0.5	1	1	0.0177	0.0800	0.0800							
15	0.5	1	1	0	0	0	35	0.5	1	1	0.0115	0.0520	0.0520							
16	0.5	1	1	0	0	0	36	0.5	1	1	0.0116	0.0524	0.0524							
17	0.5	1	1	0	0	0	37	0.5	1	1	0.0082	0.0371	0.0371							
18	0.5	1	1	0	0	0	38	0.5	1	1	0	0	0							
19	0.5	1	1	0	0	0	39	0.5	1	1	0	0	0							
20	0.5	1	1	0	0	0	40	0.5	1	1	0	0	0							

TEU after chromatography	**3.40**
TEU before chromatography	**3.99**
Yield of enolase activity	**85.20**
TEU (NSE)	**0.35**
TEU (NNSE)	**3.05**
% NSE activity	**10.29**

* SV- sample volume (ml); AV- assay volume (ml); TV- total volume (ml); EU/ML- enzyme units: ((OD/MIN*2.26)/SV); TEU- total enzyme units (EU/ML*TV). The calculated NSE value is given in % of total enolase activity.

TABLE A26. Results of enolase assay for 50 chromatographic fractions obtained from differentiating IMR-32 (Day 4, 2nd replicate) cells used to generate Figure 3.6.

FRACTION #	SV	AV	TV	OD/MIN	EU/ML	TEU	FRACTION #	SV	AV	TV	OD/MIN	EU/ML	TEU	FRACTION #	SV	AV	TV	OD/MIN	EU/ML	TEU
1	0.5	1	1	0	0	0	21	0.5	1	1	0	0	0	41	0.5	1	1	0	0	0
2	0.5	1	1	0	0	0	22	0.5	1	1	0	0	0	42	0.5	1	1	0	0	0
3	0.5	1	1	0.0042	0.0190	0.0190	23	0.5	1	1	0	0	0	43	0.5	1	1	0	0	0
4	0.5	1	1	0.0085	0.0384	0.0384	24	0.5	1	1	0	0	0	44	0.5	1	1	0	0	0
5	0.5	1	1	0.0448	0.2025	0.2025	25	0.5	1	1	0	0	0	45	0.5	1	1	0	0	0
6	0.5	1	1	0.072	0.3254	0.3254	26	0.5	1	1	0	0	0	46	0.5	1	1	0	0	0
7	0.5	1	1	0.071	0.3209	0.3209	27	0.5	1	1	0	0	0	47	0.5	1	1	0	0	0
8	0.5	1	1	0.0464	0.2097	0.2097	28	0.5	1	1	0	0	0	48	0.5	1	1	0	0	0
9	0.5	1	1	0.0321	0.1451	0.1451	29	0.5	1	1	0	0	0	49	0.5	1	1	0	0	0
10	0.5	1	1	0.0156	0.0705	0.0705	30	0.5	1	1	0	0	0	50	0.5	1	1	0	0	0
11	0.5	1	1	0.008	0.0362	0.0362	31	0.5	1	1	0.0036	0.0163	0.0163							
12	0.5	1	1	0.0034	0.0154	0.0154	32	0.5	1	1	0.0054	0.0244	0.0244							
13	0.5	1	1	0	0	0	33	0.5	1	1	0.0072	0.0325	0.0325							
14	0.5	1	1	0	0	0	34	0.5	1	1	0.0108	0.0488	0.0488							
15	0.5	1	1	0	0	0	35	0.5	1	1	0.0083	0.0375	0.0375							
16	0.5	1	1	0	0	0	36	0.5	1	1	0.0056	0.0253	0.0253							
17	0.5	1	1	0	0	0	37	0.5	1	1	0.0034	0.0154	0.0154							
18	0.5	1	1	0	0	0	38	0.5	1	1	0	0	0							
19	0.5	1	1	0	0	0	39	0.5	1	1	0	0	0							
20	0.5	1	1	0	0	0	40	0.5	1	1	0	0	0							

TEU after chromatography	**1.58**
TEU before chromatography	**1.84**
Yield of enolase activity	**86.28**
TEU (NSE)	**0.20**
TEU (NNSE)	**1.38**
% NSE activity	**12.65**

* SV- sample volume (ml); AV- assay volume (ml); TV- total volume (ml); EU/ML- enzyme units: ((OD/MIN*2.26)/SV); TEU- total enzyme units (EU/ML*TV). The calculated NSE value is given in % of total enolase activity.

TABLE A27. Results of enolase assay for 50 chromatographic fractions obtained from differentiating IMR-32 (Day 4, 3rd replicate) cells used to generate Figure 3.6.

FRACTION #	SV	AV	TV	OD/MIN	EU/ML	TEU	FRACTION #	SV	AV	TV	OD/MIN	EU/ML	TEU	FRACTION #	SV	AV	TV	OD/MIN	EU/ML	TEU
1	0.5	1	1	0	0	0	21	0.5	1	1	0	0	0	41	0.5	1	1	0	0	0
2	0.5	1	1	0	0	0	22	0.5	1	1	0	0	0	42	0.5	1	1	0	0	0
3	0.5	1	1	0.0042	0.0190	0.0190	23	0.5	1	1	0	0	0	43	0.5	1	1	0	0	0
4	0.5	1	1	0.0072	0.0325	0.0325	24	0.5	1	1	0	0	0	44	0.5	1	1	0	0	0
5	0.5	1	1	0.0272	0.1229	0.1229	25	0.5	1	1	0	0	0	45	0.5	1	1	0	0	0
6	0.5	1	1	0.078	0.3526	0.3526	26	0.5	1	1	0	0	0	46	0.5	1	1	0	0	0
7	0.5	1	1	0.0716	0.3236	0.3236	27	0.5	1	1	0	0	0	47	0.5	1	1	0	0	0
8	0.5	1	1	0.0606	0.2739	0.2739	28	0.5	1	1	0	0	0	48	0.5	1	1	0	0	0
9	0.5	1	1	0.044	0.1989	0.1989	29	0.5	1	1	0	0	0	49	0.5	1	1	0	0	0
10	0.5	1	1	0.0264	0.1193	0.1193	30	0.5	1	1	0	0	0	50	0.5	1	1	0	0	0
11	0.5	1	1	0.008	0.0362	0.0362	31	0.5	1	1	0.0037	0.0167	0.0167							
12	0.5	1	1	0.0034	0.0154	0.0154	32	0.5	1	1	0.0057	0.0258	0.0258							
13	0.5	1	1	0	0	0	33	0.5	1	1	0.0072	0.0325	0.0325							
14	0.5	1	1	0	0	0	34	0.5	1	1	0.011	0.0497	0.0497							
15	0.5	1	1	0	0	0	35	0.5	1	1	0.0087	0.0393	0.0393							
16	0.5	1	1	0	0	0	36	0.5	1	1	0.0053	0.0240	0.0240							
17	0.5	1	1	0	0	0	37	0.5	1	1	0.0035	0.0158	0.0158							
18	0.5	1	1	0	0	0	38	0.5	1	1	0	0	0							
19	0.5	1	1	0	0	0	39	0.5	1	1	0	0	0							
20	0.5	1	1	0	0	0	40	0.5	1	1	0	0	0							

TEU after chromatography	**1.70**
TEU before chromatography	**1.96**
Yield of enolase activity	**86.57**
TEU (NSE)	**0.20**
TEU (NNSE)	**1.49**
% NSE activity	**12.00**

* SV- sample volume (ml); AV- assay volume (ml); TV- total volume (ml); EU/ML- enzyme units: ((OD/MIN*2.26)/SV); TEU- total enzyme units (EU/ML*TV). The calculated NSE value is given in % of total enolase activity.

TABLE A28. Results of enolase assay for 50 chromatographic fractions obtained from differentiating IMR-32 (Day 6) cells used to generate Figure 3.6.

FRACTION #	SV	AV	TV	OD/MIN	EU/ML	TEU	FRACTION #	SV	AV	TV	OD/MIN	EU/ML	TEU	FRACTION #	SV	AV	TV	OD/MIN	EU/ML	TEU
1	0.5	1	1	0	0	0	21	0.5	1	1	0	0	0	41	0.5	1	1	0	0	0
2	0.5	1	1	0	0	0	22	0.5	1	1	0	0	0	42	0.5	1	1	0	0	0
3	0.5	1	1	0.0045	0.0203	0.0203	23	0.5	1	1	0	0	0	43	0.5	1	1	0	0	0
4	0.5	1	1	0.024	0.1085	0.1085	24	0.5	1	1	0	0	0	44	0.5	1	1	0	0	0
5	0.5	1	1	0.1215	0.5492	0.5492	25	0.5	1	1	0	0	0	45	0.5	1	1	0	0	0
6	0.5	1	1	0.1519	0.6866	0.6866	26	0.5	1	1	0	0	0	46	0.5	1	1	0	0	0
7	0.5	1	1	0.1643	0.7426	0.7426	27	0.5	1	1	0	0	0	47	0.5	1	1	0	0	0
8	0.5	1	1	0.1156	0.5225	0.5225	28	0.5	1	1	0.0067	0.0303	0.0303	48	0.5	1	1	0	0	0
9	0.5	1	1	0.0763	0.3449	0.3449	29	0.5	1	1	0.0151	0.0683	0.0683	49	0.5	1	1	0	0	0
10	0.5	1	1	0.0432	0.1953	0.1953	30	0.5	1	1	0.0141	0.0637	0.0637	50	0.5	1	1	0	0	0
11	0.5	1	1	0.0205	0.0927	0.0927	31	0.5	1	1	0.0198	0.0895	0.0895							
12	0.5	1	1	0.0151	0.0682	0.0682	32	0.5	1	1	0.0168	0.0759	0.0759							
13	0.5	1	1	0.0079	0.0357	0.0357	33	0.5	1	1	0.0151	0.0683	0.0683							
14	0.5	1	1	0	0	0	34	0.5	1	1	0.0123	0.0556	0.0556							
15	0.5	1	1	0	0	0	35	0.5	1	1	0.0106	0.0479	0.0479							
16	0.5	1	1	0	0	0	36	0.5	1	1	0.0075	0.0339	0.0339							
17	0.5	1	1	0	0	0	37	0.5	1	1	0	0	0							
18	0.5	1	1	0	0	0	38	0.5	1	1	0	0	0							
19	0.5	1	1	0	0	0	39	0.5	1	1	0	0	0							
20	0.5	1	1	0	0	0	40	0.5	1	1	0	0	0							

TEU after chromatography	**3.90**
TEU before chromatography	**4.68**
Yield of enolase activity	**83.40**
TEU (NSE)	**0.53**
TEU (NNSE)	**3.37**
% NSE activity	**13.68**

* SV- sample volume (ml); AV- assay volume (ml); TV- total volume (ml); EU/ML- enzyme units: ((OD/MIN*2.26)/SV); TEU- total enzyme units (EU/ML*TV). The calculated NSE value is given in % of total enolase activity.

TABLE A29. Results of enolase assay for 50 chromatographic fractions obtained from differentiating IMR-32 (Day 8, 1st replicate) cells used to generate Figure 3.6.

FRACTION #	SV	AV	TV	OD/MIN	EU/ML	TEU	FRACTION #	SV	AV	TV	OD/MIN	EU/ML	TEU	FRACTION #	SV	AV	TV	OD/MIN	EU/ML	TEU
1	0.5	1	1	0	0	0	21	0.5	1	1	0	0	0	41	0.5	1	1	0	0	0
2	0.5	1	1	0	0	0	22	0.5	1	1	0	0	0	42	0.5	1	1	0	0	0
3	0.5	1	1	0	0	0	23	0.5	1	1	0	0	0	43	0.5	1	1	0	0	0
4	0.5	1	1	0.0274	0.1238	0.1238	24	0.5	1	1	0	0	0	44	0.5	1	1	0	0	0
5	0.5	1	1	0.0556	0.2513	0.2513	25	0.5	1	1	0	0	0	45	0.5	1	1	0	0	0
6	0.5	1	1	0.0589	0.2662	0.2662	26	0.5	1	1	0	0	0	46	0.5	1	1	0	0	0
7	0.5	1	1	0.0573	0.2590	0.2590	27	0.5	1	1	0	0	0	47	0.5	1	1	0	0	0
8	0.5	1	1	0.0543	0.2454	0.2454	28	0.5	1	1	0	0	0	48	0.5	1	1	0	0	0
9	0.5	1	1	0.0489	0.2210	0.2210	29	0.5	1	1	0	0	0	49	0.5	1	1	0	0	0
10	0.5	1	1	0.0486	0.2197	0.2197	30	0.5	1	1	0.0047	0.0212	0.0212	50	0.5	1	1	0	0	0
11	0.5	1	1	0.0431	0.1948	0.1948	31	0.5	1	1	0.0128	0.0579	0.0579							
12	0.5	1	1	0.0349	0.1577	0.1577	32	0.5	1	1	0.0151	0.0683	0.0683							
13	0.5	1	1	0.0318	0.1437	0.1437	33	0.5	1	1	0.0203	0.0918	0.0918							
14	0.5	1	1	0.0268	0.1211	0.1211	34	0.5	1	1	0.0252	0.1139	0.1139							
15	0.5	1	1	0.0206	0.0931	0.0931	35	0.5	1	1	0.018	0.0814	0.0814							
16	0.5	1	1	0.0211	0.0954	0.0954	36	0.5	1	1	0.0141	0.0637	0.0637							
17	0.5	1	1	0.0204	0.0922	0.0922	37	0.5	1	1	0.0063	0.0285	0.0285							
18	0.5	1	1	0.0151	0.0683	0.0683	38	0.5	1	1	0	0	0							
19	0.5	1	1	0.012	0.0542	0.0542	39	0.5	1	1	0	0	0							
20	0.5	1	1	0.0078	0.0353	0.0353	40	0.5	1	1	0	0	0							

TEU after chromatography	**3.17**
TEU before chromatography	**3.83**
Yield of enolase activity	**82.68**
TEU (NSE)	**0.53**
TEU (NNSE)	**2.64**
% NSE activity	**16.62**

* SV- sample volume (ml); AV- assay volume (ml); TV- total volume (ml); EU/ML- enzyme units: ((OD/MIN*2.26)/SV); TEU- total enzyme units (EU/ML*TV). The calculated NSE value is given in % of total enolase activity.

TABLE A30. Results of enolase assay for 50 chromatographic fractions obtained from differentiating IMR-32 (Day 8, 2nd replicate) cells used to generate Figure 3.6.

FRACTION #	SV	AV	TV	OD/MIN	EU/ML	TEU	FRACTION #	SV	AV	TV	OD/MIN	EU/ML	TEU	FRACTION #	SV	AV	TV	OD/MIN	EU/ML	TEU
1	0.5	1	1	0	0	0	21	0.5	1	1	0	0	0	41	0.5	1	1	0	0	0
2	0.5	1	1	0	0	0	22	0.5	1	1	0	0	0	42	0.5	1	1	0	0	0
3	0.5	1	1	0.0074	0.0334	0.0334	23	0.5	1	1	0	0	0	43	0.5	1	1	0	0	0
4	0.5	1	1	0.0204	0.0922	0.0922	24	0.5	1	1	0	0	0	44	0.5	1	1	0	0	0
5	0.5	1	1	0.0823	0.372	0.372	25	0.5	1	1	0	0	0	45	0.5	1	1	0	0	0
6	0.5	1	1	0.1065	0.4814	0.4814	26	0.5	1	1	0	0	0	46	0.5	1	1	0	0	0
7	0.5	1	1	0.0977	0.4416	0.4416	27	0.5	1	1	0	0	0	47	0.5	1	1	0	0	0
8	0.5	1	1	0.0608	0.2748	0.2748	28	0.5	1	1	0	0	0	48	0.5	1	1	0	0	0
9	0.5	1	1	0.0466	0.2106	0.2106	29	0.5	1	1	0	0	0	49	0.5	1	1	0	0	0
10	0.5	1	1	0.0307	0.1388	0.1388	30	0.5	1	1	0	0	0	50	0.5	1	1	0	0	0
11	0.5	1	1	0.0155	0.0701	0.0701	31	0.5	1	1	0.0037	0.0167	0.0167							
12	0.5	1	1	0.0072	0.0325	0.0325	32	0.5	1	1	0.0052	0.0235	0.0235							
13	0.5	1	1	0	0	0	33	0.5	1	1	0.009	0.0407	0.0407							
14	0.5	1	1	0	0	0	34	0.5	1	1	0.0117	0.0529	0.0529							
15	0.5	1	1	0	0	0	35	0.5	1	1	0.0148	0.0669	0.0669							
16	0.5	1	1	0	0	0	36	0.5	1	1	0.0147	0.0664	0.0664							
17	0.5	1	1	0	0	0	37	0.5	1	1	0.0102	0.0461	0.0461							
18	0.5	1	1	0	0	0	38	0.5	1	1	0.0071	0.0321	0.0321							
19	0.5	1	1	0	0	0	39	0.5	1	1	0.0036	0.0163	0.0163							
20	0.5	1	1	0	0	0	40	0.5	1	1	0	0	0							

TEU after chromatography	**2.51**
TEU before chromatography	**2.97**
Yield of enolase activity	**84.6**
TEU (NSE)	**0.36**
TEU (NNSE)	**2.15**
% NSE activity	**14.4**

* SV- sample volume (ml); AV- assay volume (ml); TV- total volume (ml); EU/ML- enzyme units: ((OD/MIN*2.26)/SV); TEU- total enzyme units (EU/ML*TV). The calculated NSE value is given in % of total enolase activity.

TABLE A31. Results of enolase assay for 50 chromatographic fractions obtained from differentiating IMR-32 (Day 8, 3rd replicate) cells used to generate Figure 3.6.

FRACTION #	SV	AV	TV	OD/MIN	EU/ML	TEU	FRACTION #	SV	AV	TV	OD/MIN	EU/ML	TEU	FRACTION #	SV	AV	TV	OD/MIN	EU/ML	TEU
1	0.5	1	1	0	0	0	21	0.5	1	1	0	0	0	41	0.5	1	1	0	0	0
2	0.5	1	1	0	0	0	22	0.5	1	1	0	0	0	42	0.5	1	1	0	0	0
3	0.5	1	1	0.0072	0.0325	0.0325	23	0.5	1	1	0	0	0	43	0.5	1	1	0	0	0
4	0.5	1	1	0.0134	0.0606	0.0606	24	0.5	1	1	0	0	0	44	0.5	1	1	0	0	0
5	0.5	1	1	0.0765	0.3458	0.3458	25	0.5	1	1	0	0	0	45	0.5	1	1	0	0	0
6	0.5	1	1	0.0989	0.4470	0.4470	26	0.5	1	1	0	0	0	46	0.5	1	1	0	0	0
7	0.5	1	1	0.0854	0.3860	0.3860	27	0.5	1	1	0	0	0	47	0.5	1	1	0	0	0
8	0.5	1	1	0.0712	0.3218	0.3218	28	0.5	1	1	0	0	0	48	0.5	1	1	0	0	0
9	0.5	1	1	0.0452	0.2043	0.2043	29	0.5	1	1	0	0	0	49	0.5	1	1	0	0	0
10	0.5	1	1	0.0297	0.1342	0.1342	30	0.5	1	1	0	0	0	50	0.5	1	1	0	0	0
11	0.5	1	1	0.0145	0.0655	0.0655	31	0.5	1	1	0.0041	0.0185	0.0185							
12	0.5	1	1	0.0067	0.0303	0.0303	32	0.5	1	1	0.0054	0.0244	0.0244							
13	0.5	1	1	0	0	0	33	0.5	1	1	0.0088	0.0398	0.0398							
14	0.5	1	1	0	0	0	34	0.5	1	1	0.0115	0.0520	0.0520							
15	0.5	1	1	0	0	0	35	0.5	1	1	0.0151	0.0683	0.0683							
16	0.5	1	1	0	0	0	36	0.5	1	1	0.0141	0.0637	0.0637							
17	0.5	1	1	0	0	0	37	0.5	1	1	0.0112	0.0506	0.0506							
18	0.5	1	1	0	0	0	38	0.5	1	1	0.0073	0.0330	0.0330							
19	0.5	1	1	0	0	0	39	0.5	1	1	0.0039	0.0176	0.0176							
20	0.5	1	1	0	0	0	40	0.5	1	1	0	0	0							

TEU after chromatography	**2.40**
TEU before chromatography	**2.75**
Yield of enolase activity	**87.19**
TEU (NSE)	**0.37**
TEU (NNSE)	**2.03**
% NSE activity	**15.36**

* SV- sample volume (ml); AV- assay volume (ml); TV- total volume (ml); EU/ML- enzyme units: ((OD/MIN*2.26)/SV); TEU- total enzyme units (EU/ML*TV). The calculated NSE value is given in % of total enolase activity.

TABLE A32. Results of enolase assay for 50 chromatographic fractions obtained from differentiating IMR-32 (Day 10) cells used to generate Figure 3.6.

FRACTION #	SV	AV	TV	OD/MIN	EU/ML	TEU	FRACTION #	SV	AV	TV	OD/MIN	EU/ML	TEU	FRACTION #	SV	AV	TV	OD/MIN	EU/ML	TEU
1	0.5	1	1	0	0	0	21	0.5	1	1	0	0	0	41	0.5	1	1	0	0	0
2	0.5	1	1	0	0	0	22	0.5	1	1	0	0	0	42	0.5	1	1	0	0	0
3	0.5	1	1	0.0065	0.0294	0.0294	23	0.5	1	1	0	0	0	43	0.5	1	1	0	0	0
4	0.5	1	1	0.0325	0.1469	0.1469	24	0.5	1	1	0	0	0	44	0.5	1	1	0	0	0
5	0.5	1	1	0.0999	0.4515	0.4515	25	0.5	1	1	0	0	0	45	0.5	1	1	0	0	0
6	0.5	1	1	0.1265	0.5718	0.5718	26	0.5	1	1	0	0	0	46	0.5	1	1	0	0	0
7	0.5	1	1	0.1196	0.5406	0.5406	27	0.5	1	1	0	0	0	47	0.5	1	1	0	0	0
8	0.5	1	1	0.0913	0.4127	0.4127	28	0.5	1	1	0.0041	0.0185	0.0185	48	0.5	1	1	0	0	0
9	0.5	1	1	0.056	0.2531	0.2531	29	0.5	1	1	0.0154	0.0696	0.0696	49	0.5	1	1	0	0	0
10	0.5	1	1	0.031	0.1401	0.1401	30	0.5	1	1	0.0186	0.0841	0.0841	50	0.5	1	1	0	0	0
11	0.5	1	1	0.0177	0.0800	0.0800	31	0.5	1	1	0.0234	0.1058	0.1058							
12	0.5	1	1	0.0087	0.0393	0.0393	32	0.5	1	1	0.0251	0.1135	0.1135							
13	0.5	1	1	0	0	0	33	0.5	1	1	0.0253	0.1144	0.1144							
14	0.5	1	1	0	0	0	34	0.5	1	1	0.0213	0.0963	0.0963							
15	0.5	1	1	0	0	0	35	0.5	1	1	0.02	0.0904	0.0904							
16	0.5	1	1	0	0	0	36	0.5	1	1	0.0172	0.0777	0.0777							
17	0.5	1	1	0	0	0	37	0.5	1	1	0.0142	0.0642	0.0642							
18	0.5	1	1	0	0	0	38	0.5	1	1	0.0098	0.0443	0.0443							
19	0.5	1	1	0	0	0	39	0.5	1	1	0.0076	0.0344	0.0344							
20	0.5	1	1	0	0	0	40	0.5	1	1	0	0	0							

TEU after chromatography	**3.58**
TEU before chromatography	**4.27**
Yield of enolase activity	**83.87**
TEU (NSE)	**0.91**
TEU (NNSE)	**2.67**
% NSE activity	**25.51**

* SV- sample volume (ml); AV- assay volume (ml); TV- total volume (ml); EU/ML- enzyme units: ((OD/MIN*2.26)/SV); TEU- total enzyme units (EU/ML*TV). The calculated NSE value is given in % of total enolase activity.

TABLE A33. Results of enolase assay for 50 chromatographic fractions obtained from differentiating IMR-32 (Day 12, 1st replicate) cells used to generate Figure 3.6.

FRACTION #	SV	AV	TV	OD/MIN	EU/ML	TEU	FRACTION #	SV	AV	TV	OD/MIN	EU/ML	TEU	FRACTION #	SV	AV	TV	OD/MIN	EU/ML	TEU
1	0.5	1	1	0	0	0	21	0.5	1	1	0	0	0	41	0.5	1	1	0	0	0
2	0.5	1	1	0	0	0	22	0.5	1	1	0	0	0	42	0.5	1	1	0	0	0
3	0.5	1	1	0.0065	0.0294	0.0294	23	0.5	1	1	0	0	0	43	0.5	1	1	0	0	0
4	0.5	1	1	0.019	0.0859	0.0859	24	0.5	1	1	0	0	0	44	0.5	1	1	0	0	0
5	0.5	1	1	0.0656	0.2965	0.2965	25	0.5	1	1	0	0	0	45	0.5	1	1	0	0	0
6	0.5	1	1	0.0899	0.4063	0.4063	26	0.5	1	1	0	0	0	46	0.5	1	1	0	0	0
7	0.5	1	1	0.1001	0.4525	0.4525	27	0.5	1	1	0	0	0	47	0.5	1	1	0	0	0
8	0.5	1	1	0.0773	0.3494	0.3494	28	0.5	1	1	0.0058	0.0262	0.0262	48	0.5	1	1	0	0	0
9	0.5	1	1	0.0566	0.2558	0.2558	29	0.5	1	1	0.0141	0.0637	0.0637	49	0.5	1	1	0	0	0
10	0.5	1	1	0.0332	0.1501	0.1501	30	0.5	1	1	0.0185	0.0836	0.0836	50	0.5	1	1	0	0	0
11	0.5	1	1	0.0187	0.0845	0.0845	31	0.5	1	1	0.0213	0.0963	0.0963							
12	0.5	1	1	0.0104	0.0470	0.0470	32	0.5	1	1	0.0241	0.1089	0.1089							
13	0.5	1	1	0.0059	0.0267	0.0267	33	0.5	1	1	0.032	0.1446	0.1446							
14	0.5	1	1	0	0	0	34	0.5	1	1	0.0229	0.1035	0.1035							
15	0.5	1	1	0	0	0	35	0.5	1	1	0.0151	0.0683	0.0683							
16	0.5	1	1	0	0	0	36	0.5	1	1	0.0149	0.0673	0.0673							
17	0.5	1	1	0	0	0	37	0.5	1	1	0.0109	0.0493	0.0493							
18	0.5	1	1	0	0	0	38	0.5	1	1	0.0068	0.0307	0.0307							
19	0.5	1	1	0	0	0	39	0.5	1	1	0	0	0							
20	0.5	1	1	0	0	0	40	0.5	1	1	0	0	0							

TEU after chromatography	**3.03**
TEU before chromatography	**3.69**
Yield of enolase activity	**82.06**
TEU (NSE)	**0.84**
TEU (NNSE)	**2.18**
% NSE activity	**27.84**

* SV- sample volume (ml); AV- assay volume (ml); TV- total volume (ml); EU/ML- enzyme units: ((OD/MIN*2.26)/SV); TEU- total enzyme units (EU/ML*TV). The calculated NSE value is given in % of total enolase activity.

TABLE A34. Results of enolase assay for 50 chromatographic fractions obtained from differentiating IMR-32 (Day 12, 2nd replicate) cells used to generate Figure 3.6.

FRACTION #	SV	AV	TV	OD/MIN	EU/ML	TEU	FRACTION #	SV	AV	TV	OD/MIN	EU/ML	TEU	FRACTION #	SV	AV	TV	OD/MIN	EU/ML	TEU
1	0.5	1	1	0	0	0	21	0.5	1	1	0	0	0	41	0.5	1	1	0	0	0
2	0.5	1	1	0	0	0	22	0.5	1	1	0	0	0	42	0.5	1	1	0	0	0
3	0.5	1	1	0	0	0	23	0.5	1	1	0	0	0	43	0.5	1	1	0	0	0
4	0.5	1	1	0.0045	0.0203	0.0203	24	0.5	1	1	0	0	0	44	0.5	1	1	0	0	0
5	0.5	1	1	0.0453	0.2048	0.2048	25	0.5	1	1	0	0	0	45	0.5	1	1	0	0	0
6	0.5	1	1	0.07	0.3164	0.3164	26	0.5	1	1	0	0	0	46	0.5	1	1	0	0	0
7	0.5	1	1	0.0722	0.3263	0.3263	27	0.5	1	1	0	0	0	47	0.5	1	1	0	0	0
8	0.5	1	1	0.0581	0.2626	0.2626	28	0.5	1	1	0	0	0	48	0.5	1	1	0	0	0
9	0.5	1	1	0.0349	0.1577	0.1577	29	0.5	1	1	0	0	0	49	0.5	1	1	0	0	0
10	0.5	1	1	0.0231	0.1044	0.1044	30	0.5	1	1	0.0063	0.0285	0.0285	50	0.5	1	1	0	0	0
11	0.5	1	1	0.0107	0.0484	0.0484	31	0.5	1	1	0.0105	0.0475	0.0475							
12	0.5	1	1	0.0063	0.0285	0.0285	32	0.5	1	1	0.0155	0.0701	0.0701							
13	0.5	1	1	0.0047	0.0212	0.0212	33	0.5	1	1	0.0156	0.0705	0.0705							
14	0.5	1	1	0	0	0	34	0.5	1	1	0.0164	0.0741	0.0741							
15	0.5	1	1	0	0	0	35	0.5	1	1	0.0155	0.0701	0.0701							
16	0.5	1	1	0	0	0	36	0.5	1	1	0.0153	0.0692	0.0692							
17	0.5	1	1	0	0	0	37	0.5	1	1	0.0112	0.0506	0.0506							
18	0.5	1	1	0	0	0	38	0.5	1	1	0.0068	0.0308	0.0308							
19	0.5	1	1	0	0	0	39	0.5	1	1	0	0	0							
20	0.5	1	1	0	0	0	40	0.5	1	1	0	0	0							

TEU after chromatography	**2.00**
TEU before chromatography	**2.39**
Yield of enolase activity	**83.88**
TEU (NSE)	**0.51**
TEU (NNSE)	**1.49**
% NSE activity	**25.54**

* SV- sample volume (ml); AV- assay volume (ml); TV- total volume (ml); EU/ML- enzyme units: ((OD/MIN*2.26)/SV); TEU- total enzyme units (EU/ML*TV). The calculated NSE value is given in % of total enolase activity.

TABLE A35. Results of enolase assay for 50 chromatographic fractions obtained from differentiating IMR-32 (Day 12, 3rd replicate) cells used to generate Figure 3.6.

FRACTION #	SV	AV	TV	OD/MIN	EU/ML	TEU	FRACTION #	SV	AV	TV	OD/MIN	EU/ML	TEU	FRACTION #	SV	AV	TV	OD/MIN	EU/ML	TEU
1	0.5	1	1	0	0	0	21	0.5	1	1	0	0	0	41	0.5	1	1	0	0	0
2	0.5	1	1	0	0	0	22	0.5	1	1	0	0	0	42	0.5	1	1	0	0	0
3	0.5	1	1	0	0	0	23	0.5	1	1	0	0	0	43	0.5	1	1	0	0	0
4	0.5	1	1	0.0052	0.0235	0.0235	24	0.5	1	1	0	0	0	44	0.5	1	1	0	0	0
5	0.5	1	1	0.0462	0.2088	0.2088	25	0.5	1	1	0	0	0	45	0.5	1	1	0	0	0
6	0.5	1	1	0.0689	0.3114	0.3114	26	0.5	1	1	0	0	0	46	0.5	1	1	0	0	0
7	0.5	1	1	0.0731	0.3304	0.3304	27	0.5	1	1	0	0	0	47	0.5	1	1	0	0	0
8	0.5	1	1	0.0577	0.2608	0.2608	28	0.5	1	1	0	0	0	48	0.5	1	1	0	0	0
9	0.5	1	1	0.0363	0.1641	0.1641	29	0.5	1	1	0	0	0	49	0.5	1	1	0	0	0
10	0.5	1	1	0.0221	0.0999	0.0999	30	0.5	1	1	0.0067	0.0303	0.0303	50	0.5	1	1	0	0	0
11	0.5	1	1	0.0113	0.0511	0.0511	31	0.5	1	1	0.0112	0.0506	0.0506							
12	0.5	1	1	0.0067	0.0303	0.0303	32	0.5	1	1	0.0147	0.0664	0.0664							
13	0.5	1	1	0.0056	0.0253	0.0253	33	0.5	1	1	0.0152	0.0687	0.0687							
14	0.5	1	1	0	0	0	34	0.5	1	1	0.0159	0.0719	0.0719							
15	0.5	1	1	0	0	0	35	0.5	1	1	0.0146	0.0660	0.0660							
16	0.5	1	1	0	0	0	36	0.5	1	1	0.0139	0.0628	0.0628							
17	0.5	1	1	0	0	0	37	0.5	1	1	0.0121	0.05470	0.05470							
18	0.5	1	1	0	0	0	38	0.5	1	1	0.0056	0.0253	0.0253							
19	0.5	1	1	0	0	0	39	0.5	1	1	0	0	0							
20	0.5	1	1	0	0	0	40	0.5	1	1	0	0	0							

TEU after chromatography	**2.00**
TEU before chromatography	**2.38**
Yield of enolase activity	**83.90**
TEU (NSE)	**0.49**
TEU (NNSE)	**1.51**
% NSE activity	**24.80**

* SV- sample volume (ml); AV- assay volume (ml); TV- total volume (ml); EU/ML- enzyme units: ((OD/MIN*2.26)/SV); TEU- total enzyme units (EU/ML*TV). The calculated NSE value is given in % of total enolase activity.

TABLE A36. Results of enolase assay for 50 chromatographic fractions obtained from differentiating IMR-32 (Day 14) cells used to generate Figure 3.6.

FRACTION #	SV	AV	TV	OD/MIN	EU/ML	TEU	FRACTION #	SV	AV	TV	OD/MIN	EU/ML	TEU	FRACTION #	SV	AV	TV	OD/MIN	EU/ML	TEU
1	0.5	1	1	0	0	0	21	0.5	1	1	0	0	0	41	0.5	1	1	0	0	0
2	0.5	1	1	0	0	0	22	0.5	1	1	0	0	0	42	0.5	1	1	0	0	0
3	0.5	1	1	0.0075	0.0339	0.0339	23	0.5	1	1	0	0	0	43	0.5	1	1	0	0	0
4	0.5	1	1	0.0271	0.1225	0.1225	24	0.5	1	1	0	0	0	44	0.5	1	1	0	0	0
5	0.5	1	1	0.0592	0.2676	0.2676	25	0.5	1	1	0	0	0	45	0.5	1	1	0	0	0
6	0.5	1	1	0.0881	0.3982	0.3982	26	0.5	1	1	0	0	0	46	0.5	1	1	0	0	0
7	0.5	1	1	0.0804	0.3634	0.3634	27	0.5	1	1	0	0	0	47	0.5	1	1	0	0	0
8	0.5	1	1	0.0595	0.2689	0.2689	28	0.5	1	1	0.0062	0.0280	0.0280	48	0.5	1	1	0	0	0
9	0.5	1	1	0.0445	0.2011	0.2011	29	0.5	1	1	0.009	0.0407	0.0407	49	0.5	1	1	0	0	0
10	0.5	1	1	0.0316	0.1428	0.1428	30	0.5	1	1	0.0141	0.0637	0.0637	50	0.5	1	1	0	0	0
11	0.5	1	1	0.0194	0.0877	0.0877	31	0.5	1	1	0.0218	0.0985	0.0985							
12	0.5	1	1	0.0113	0.0511	0.0511	32	0.5	1	1	0.0246	0.1112	0.1112							
13	0.5	1	1	0.0061	0.0276	0.0276	33	0.5	1	1	0.0275	0.1243	0.1243							
14	0.5	1	1	0	0	0	34	0.5	1	1	0.0247	0.1116	0.1116							
15	0.5	1	1	0	0	0	35	0.5	1	1	0.0223	0.1008	0.1008							
16	0.5	1	1	0	0	0	36	0.5	1	1	0.0136	0.0615	0.0615							
17	0.5	1	1	0	0	0	37	0.5	1	1	0.0127	0.0574	0.0574							
18	0.5	1	1	0	0	0	38	0.5	1	1	0.0106	0.0479	0.0479							
19	0.5	1	1	0	0	0	39	0.5	1	1	0.0063	0.0285	0.0285							
20	0.5	1	1	0	0	0	40	0.5	1	1	0	0	0							

TEU after chromatography	**2.84**
TEU before chromatography	**3.33**
Yield of enolase activity	**85.34**
TEU (NSE)	**0.87**
TEU (NNSE)	**1.96**
% NSE activity	**30.79**

* SV- sample volume (ml); AV- assay volume (ml); TV- total volume (ml); EU/ML- enzyme units: ((OD/MIN*2.26)/SV); TEU- total enzyme units (EU/ML*TV). The calculated NSE value is given in % of total enolase activity.

TABLE A37. Results of enolase assay for 50 chromatographic fractions obtained from differentiating IMR-32 (Day 16, 1st replicate) cells used to generate Figure 3.6.

FRACTION #	SV	AV	TV	OD/MIN	EU/ML	TEU	FRACTION #	SV	AV	TV	OD/MIN	EU/ML	TEU	FRACTION #	SV	AV	TV	OD/MIN	EU/ML	TEU
1	0.5	1	1	0	0	0	21	0.5	1	1	0	0	0	41	0.5	1	1	0	0	0
2	0.5	1	1	0	0	0	22	0.5	1	1	0	0	0	42	0.5	1	1	0	0	0
3	0.5	1	1	0.0065	0.0294	0.0294	23	0.5	1	1	0	0	0	43	0.5	1	1	0	0	0
4	0.5	1	1	0.0265	0.1198	0.1198	24	0.5	1	1	0	0	0	44	0.5	1	1	0	0	0
5	0.5	1	1	0.0601	0.2717	0.2717	25	0.5	1	1	0	0	0	45	0.5	1	1	0	0	0
6	0.5	1	1	0.0865	0.3910	0.3910	26	0.5	1	1	0	0	0	46	0.5	1	1	0	0	0
7	0.5	1	1	0.0793	0.3584	0.3584	27	0.5	1	1	0	0	0	47	0.5	1	1	0	0	0
8	0.5	1	1	0.0605	0.2735	0.2735	28	0.5	1	1	0.0061	0.0276	0.0276	48	0.5	1	1	0	0	0
9	0.5	1	1	0.0465	0.2102	0.2102	29	0.5	1	1	0.0095	0.0429	0.0429	49	0.5	1	1	0	0	0
10	0.5	1	1	0.0305	0.1379	0.1379	30	0.5	1	1	0.0152	0.0687	0.0687	50	0.5	1	1	0	0	0
11	0.5	1	1	0.0206	0.0931	0.0931	31	0.5	1	1	0.0236	0.1067	0.1067							
12	0.5	1	1	0.0124	0.0560	0.0560	32	0.5	1	1	0.0254	0.1148	0.1148							
13	0.5	1	1	0.0075	0.0339	0.0339	33	0.5	1	1	0.0286	0.1293	0.1293							
14	0.5	1	1	0	0	0	34	0.5	1	1	0.0257	0.1162	0.1162							
15	0.5	1	1	0	0	0	35	0.5	1	1	0.0232	0.1049	0.1049							
16	0.5	1	1	0	0	0	36	0.5	1	1	0.0143	0.0647	0.0647							
17	0.5	1	1	0	0	0	37	0.5	1	1	0.0128	0.0579	0.0579							
18	0.5	1	1	0	0	0	38	0.5	1	1	0.0108	0.0488	0.0488							
19	0.5	1	1	0	0	0	39	0.5	1	1	0.0063	0.0285	0.0285							
20	0.5	1	1	0	0	0	40	0.5	1	1	0	0	0							

TEU after chromatography	**2.89**
TEU before chromatography	**3.33**
Yield of enolase activity	**86.74**
TEU (NSE)	**0.91**
TEU (NNSE)	**1.97**
% NSE activity	**31.56**

* SV- sample volume (ml); AV- assay volume (ml); TV- total volume (ml); EU/ML- enzyme units: ((OD/MIN*2.26)/SV); TEU- total enzyme units (EU/ML*TV). The calculated NSE value is given in % of total enolase activity.

TABLE A38. Results of enolase assay for 50 chromatographic fractions obtained from differentiating IMR-32 (Day 16, 2nd replicate) cells used to generate Figure 3.6.

FRACTION #	SV	AV	TV	OD/MIN	EU/ML	TEU	FRACTION #	SV	AV	TV	OD/MIN	EU/ML	TEU	FRACTION #	SV	AV	TV	OD/MIN	EU/ML	TEU
1	0.5	1	1	0	0	0	21	0.5	1	1	0	0	0	41	0.5	1	1	0	0	0
2	0.5	1	1	0	0	0	22	0.5	1	1	0	0	0	42	0.5	1	1	0	0	0
3	0.5	1	1	0.0063	0.0285	0.0285	23	0.5	1	1	0	0	0	43	0.5	1	1	0	0	0
4	0.5	1	1	0.0347	0.1568	0.1568	24	0.5	1	1	0	0	0	44	0.5	1	1	0	0	0
5	0.5	1	1	0.0596	0.2694	0.2694	25	0.5	1	1	0	0	0	45	0.5	1	1	0	0	0
6	0.5	1	1	0.0853	0.3856	0.3856	26	0.5	1	1	0	0	0	46	0.5	1	1	0	0	0
7	0.5	1	1	0.0781	0.3530	0.3530	27	0.5	1	1	0	0	0	47	0.5	1	1	0	0	0
8	0.5	1	1	0.0565	0.2554	0.2554	28	0.5	1	1	0	0	0	48	0.5	1	1	0	0	0
9	0.5	1	1	0.0473	0.2138	0.2138	29	0.5	1	1	0.0061	0.0276	0.0276	49	0.5	1	1	0	0	0
10	0.5	1	1	0.0312	0.1410	0.1410	30	0.5	1	1	0.0155	0.0701	0.0701	50	0.5	1	1	0	0	0
11	0.5	1	1	0.0211	0.0954	0.0954	31	0.5	1	1	0.0237	0.1071	0.1071							
12	0.5	1	1	0.0123	0.0556	0.0556	32	0.5	1	1	0.0238	0.1076	0.1076							
13	0.5	1	1	0.0071	0.0321	0.0321	33	0.5	1	1	0.0277	0.1252	0.1252							
14	0.5	1	1	0	0	0	34	0.5	1	1	0.0254	0.1148	0.1148							
15	0.5	1	1	0	0	0	35	0.5	1	1	0.0216	0.0976	0.0976							
16	0.5	1	1	0	0	0	36	0.5	1	1	0.0153	0.0692	0.0692							
17	0.5	1	1	0	0	0	37	0.5	1	1	0.0136	0.0615	0.0615							
18	0.5	1	1	0	0	0	38	0.5	1	1	0.0071	0.0321	0.0321							
19	0.5	1	1	0	0	0	39	0.5	1	1	0	0	0							
20	0.5	1	1	0	0	0	40	0.5	1	1	0	0	0							

TEU after chromatography	**2.80**
TEU before chromatography	**3.40**
Yield of enolase activity	**82.35**
TEU (NSE)	**0.81**
TEU (NNSE)	**1.99**
% NSE activity	**29.03**

* SV- sample volume (ml); AV- assay volume (ml); TV- total volume (ml); EU/ML- enzyme units: ((OD/MIN*2.26)/SV); TEU- total enzyme units (EU/ML*TV). The calculated NSE value is given in % of total enolase activity.

TABLE A39. Results of enolase assay for 50 chromatographic fractions obtained from differentiating IMR-32 (Day 16, 3rd replicate) cells used to generate Figure 3.6.

FRACTION #	SV	AV	TV	OD/MIN	EU/ML	TEU	FRACTION #	SV	AV	TV	OD/MIN	EU/ML	TEU	FRACTION #	SV	AV	TV	OD/MIN	EU/ML	TEU
1	0.5	1	1	0	0	0	21	0.5	1	1	0	0	0	41	0.5	1	1	0	0	0
2	0.5	1	1	0	0	0	22	0.5	1	1	0	0	0	42	0.5	1	1	0	0	0
3	0.5	1	1	0.0066	0.0298	0.0298	23	0.5	1	1	0	0	0	43	0.5	1	1	0	0	0
4	0.5	1	1	0.0336	0.1519	0.1519	24	0.5	1	1	0	0	0	44	0.5	1	1	0	0	0
5	0.5	1	1	0.0587	0.2653	0.2653	25	0.5	1	1	0	0	0	45	0.5	1	1	0	0	0
6	0.5	1	1	0.0865	0.3910	0.3910	26	0.5	1	1	0	0	0	46	0.5	1	1	0	0	0
7	0.5	1	1	0.0773	0.3494	0.3494	27	0.5	1	1	0	0	0	47	0.5	1	1	0	0	0
8	0.5	1	1	0.0543	0.2454	0.2454	28	0.5	1	1	0	0	0	48	0.5	1	1	0	0	0
9	0.5	1	1	0.0497	0.2246	0.2246	29	0.5	1	1	0.0063	0.0285	0.0285	49	0.5	1	1	0	0	0
10	0.5	1	1	0.0323	0.1460	0.1460	30	0.5	1	1	0.0149	0.0673	0.0673	50	0.5	1	1	0	0	0
11	0.5	1	1	0.0217	0.0981	0.0981	31	0.5	1	1	0.0216	0.0976	0.0976							
12	0.5	1	1	0.0131	0.0592	0.0592	32	0.5	1	1	0.0245	0.1107	0.1107							
13	0.5	1	1	0.0067	0.0303	0.0303	33	0.5	1	1	0.0267	0.1207	0.1207							
14	0.5	1	1	0	0	0	34	0.5	1	1	0.0243	0.1098	0.1098							
15	0.5	1	1	0	0	0	35	0.5	1	1	0.0221	0.0999	0.0999							
16	0.5	1	1	0	0	0	36	0.5	1	1	0.0149	0.0673	0.0673							
17	0.5	1	1	0	0	0	37	0.5	1	1	0.0123	0.0556	0.0556							
18	0.5	1	1	0	0	0	38	0.5	1	1	0.0067	0.0303	0.0303							
19	0.5	1	1	0	0	0	39	0.5	1	1	0	0	0							
20	0.5	1	1	0	0	0	40	0.5	1	1	0	0	0							

TEU after chromatography	**2.78**
TEU before chromatography	**3.33**
Yield of enolase activity	**83.53**
TEU (NSE)	**0.79**
TEU (NNSE)	**1.99**
% NSE activity	**28.35**

* SV- sample volume (ml); AV- assay volume (ml); TV- total volume (ml); EU/ML- enzyme units: ((OD/MIN*2.26)/SV); TEU- total enzyme units (EU/ML*TV). The calculated NSE value is given in % of total enolase activity.

APPENDIX B

RAW DATA FOR CHAPTER 4

Table B1. Linear mapping across the circular coil setup at an input current of 50 mA[1].

Position (in.)	MFI (mT)* Off the microscope			MFI (mT) On the microscope		
	REP#1	REP#2	REP#3	REP#1	REP#2	REP#3
-1.00	0.2357	0.2359	0.2361	0.2281	0.2275	0.2283
-0.75	0.2155	0.2149	0.2159	0.2134	0.2129	0.2127
-0.50	0.1921	0.1909	0.1916	0.1917	0.1924	0.1911
-0.25	0.1837	0.1822	0.1846	0.1731	0.1735	0.1728
0.00	0.1764	0.1771	0.176	0.164	0.1641	0.1634
0.25	0.1846	0.1812	0.1846	0.1729	0.1735	0.1721
0.50	0.1935	0.1918	0.1906	0.1923	0.1909	0.1923
0.75	0.2165	0.2147	0.2167	0.2123	0.2122	0.2126
1.00	0.2355	0.2356	0.2355	0.2275	0.2268	0.227

[1] Data used for Figure 4.4. * MFI- Magnetic field intensity

Table B2. Linear mapping across the circular coil setup at an input current of 100 mA.[1]

Position (in.)	MFI (mT)* Off the microscope			MFI (mT) On the microscope		
	REP#1	REP#2	REP#3	REP#1	REP#2	REP#3
-1.00	0.5028	0.5023	0.5024	0.472	0.4693	0.4732
-0.75	0.4715	0.4721	0.4719	0.4531	0.4524	0.4527
-0.50	0.4234	0.4226	0.4237	0.4136	0.4129	0.4143
-0.25	0.3973	0.3961	0.3986	0.3789	0.3802	0.3793
0.00	0.3875	0.3881	0.3876	0.3718	0.3718	0.3698
0.25	0.3973	0.3992	0.3994	0.3793	0.3787	0.3801
0.50	0.4216	0.4222	0.4248	0.4127	0.4149	0.4105
0.75	0.4723	0.471	0.4719	0.4523	0.4507	0.4519
1.00	0.5026	0.5022	0.5022	0.4733	0.4742	0.4699

[1] Data used for Figure 4.4. * MFI- Magnetic field intensity

Table B3. Linear mapping across the circular coil setup at an input current of 200 mA.[1]

Position (in.)	MFI (mT)* Off the microscope			MFI (mT) On the microscope		
	REP#1	REP#2	REP#3	REP#1	REP#2	REP#3
-1.00	1.03	1.027	1.029	0.9651	0.9666	0.9644
-0.75	0.967	0.9661	0.9669	0.9306	0.9321	0.9319
-0.50	0.8769	0.8776	0.8786	0.8506	0.8491	0.8508
-0.25	0.8241	0.8237	0.8239	0.7792	0.7779	0.7783
0.00	0.8081	0.8061	0.8052	0.7639	0.7649	0.7628
0.25	0.8237	0.8262	0.8265	0.7779	0.7781	0.7801
0.50	0.8755	0.8767	0.8795	0.8516	0.8487	0.851
0.75	0.966	0.9653	0.9667	0.9312	0.9305	0.9298
1.00	1.031	1.031	1.027	0.9645	0.964	0.9667

[1] Data used for Figure 4.4. * MFI- Magnetic field intensity

Table B4. Linear mapping across the circular coil setup at an input current of 300 mA.[1]

Position (in.)	MFI (mT)* Off the microscope			MFI (mT) On the microscope		
	REP#1	REP#2	REP#3	REP#1	REP#2	REP#3
-1.00	1.554	1.556	1.553	1.468	1.47	1.467
-0.75	1.468	1.466	1.468	1.397	1.401	1.398
-0.50	1.331	1.332	1.329	1.291	1.293	1.291
-0.25	1.248	1.249	1.248	1.187	1.186	1.188
0.00	1.224	1.221	1.221	1.163	1.161	1.161
0.25	1.249	1.25	1.247	1.186	1.185	1.186
0.50	1.33	1.329	1.332	1.292	1.291	1.29
0.75	1.465	1.467	1.469	1.396	1.4	1.399
1.00	1.552	1.552	1.555	1.464	1.467	1.468

[1] Data used for Figure 4.4. * MFI- Magnetic field intensity

Table B5. Linear mapping across the circular coil setup at an input current of 500 mA.[1]

Position (in.)	MFI (mT)* Off the microscope			MFI (mT) On the microscope		
	REP#1	REP#2	REP#3	REP#1	REP#2	REP#3
-1.00	2.613	2.604	2.608	2.446	2.449	2.447
-0.75	2.471	2.469	2.472	2.362	2.364	2.361
-0.50	2.237	2.239	2.236	2.175	2.176	2.173
-0.25	2.108	2.109	2.107	2.003	2.001	2
0.00	2.053	2.053	2.054	1.955	1.956	1.954
0.25	2.11	2.11	2.107	2.002	2	2.002
0.50	2.236	2.238	2.234	2.172	2.174	2.173
0.75	2.47	2.468	2.471	2.36	2.362	2.359
1.00	2.615	2.606	2.603	2.444	2.448	2.446

[1] Data used for Figure 4.4. * MFI- Magnetic field intensity

Table B6. Coils temperature data at 50 mA and a constant frequency of 60 Hz over a 4 hour time period at three positions from the center of the coil.

Time (min)	Position (in.)					
	0		0.5		1	
	T1	T2	T1	T2	T1	T2
0	68.1	68.1	68.1	68.1	65.7	65.7
10	68.1	68.1	68.1	68.1	65.9	65.7
20	68.3	68.1	68.2	68.1	65.9	65.8
30	68.1	68.1	68.1	68.1	65.9	66
40	68.3	68.2	68.3	68.2	65.9	65.7
50	68.3	68.4	68.4	68.4	65.9	66
60	68.6	67.9	68.4	68.2	65.7	65.9
70	68.6	68.3	68.6	68.3	65.9	65.8
80	68.4	68.4	68.4	68.4	65.8	65.8
90	68.4	68.2	68.4	68.2	65.5	65.7
100	68.4	68.2	68.2	68.2	65.9	66
110	68.4	68.2	68.4	68.2	66	66.3
120	68.4	68.4	68.4	68.4	66	66.3
130	68.4	68.4	68.2	68.4	66	66.2
140	68.6	68.5	68.6	68.5	66	66.2
150	68.6	68.5	68.6	68.5	66	66.2
160	68.9	68.8	68.7	68.8	66.2	66.3
170	68.9	69.3	68.2	68.3	66.2	66.3
180	69	69.3	69	69	66.2	66.3
190	69.1	69	69.1	69	66.2	66.5
200	69.1	69.2	69.1	69.2	66.2	66.3
210	69.2	69.5	69.2	69.3	66.2	66.3
220	69.2	69.8	69.2	69.4	66.2	66.3
230	69.2	69.8	69.2	69.3	66.2	66.3
240	69.4	69.6	69.4	69.3	66.2	66.1

T1- Temperature on the coil; T2- Ambient temperature.
Data for Figure 4.6.

Table B7. Coils temperature data at 100 mA and a constant frequency of 60 Hz over a 4 hour time period at three positions from the center of the coil.

Time (min)	Position (in.)					
	0		0.5		1	
	T1	T2	T1	T2	T1	T2
0	70.1	70.1	67.6	67.6	66.5	66.5
10	70.3	69.8	68	67.4	66.8	66.3
20	70.3	69.5	68.5	67.9	67.1	66.8
30	70.1	69.6	68.6	67.7	67.4	66.6
40	70.3	69.5	68.7	68	67.4	66.9
50	70.1	69.3	68.8	68	67.4	66.9
60	70.1	69.4	68.8	67.9	67.6	66.8
70	70.1	69.1	68.7	67.9	67.6	66.8
80	70	69	68.8	67.9	67.6	66.8
90	70.1	68.8	68.7	67.7	67.6	66.6
100	70	68.8	68.7	67.6	67.6	66.5
110	70	68.8	68.6	67.7	67.4	66.6
120	69.8	69	68.8	68	67.4	66.9
130	69.8	68.7	68.7	67.7	67.6	66.6
140	69.8	69	68.7	67.9	67.6	66.8
150	69.7	68.5	68.7	67.9	67.6	66.8
160	69.8	68.5	68.7	67.9	67.6	66.8
170	69.5	68.5	68.7	67.9	67.6	66.8
180	69.3	68.4	68.7	67.9	67.6	66.8
190	69.5	68.2	68.7	67.9	67.8	66.9
200	69.5	68.2	68.9	68.2	67.6	67.1
210	69.3	68.2	68.8	68	67.6	66.9
220	69.5	68.2	68.9	67.9	67.6	66.8
230	69.4	68.2	68.9	67.9	67.8	66.8
240	69.3	68.2	68.8	67.9	67.6	66.8

T1- Temperature on the coil; T2- Ambient temperature.
Data for Figure 4.6.

Table B8. Coils temperature data at 300 mA and a constant frequency of 60 Hz over a 4 hour time period at three positions from the center of the coil.

Time (min)	Position (in.)					
	0		0.5		1	
	T1	T2	T1	T2	T1	T2
0	67.3	67.3	66.5	66.5	66.9	66.9
10	69.7	67.1	69.1	66.4	69.5	66.9
20	71.8	66.9	71	66.1	71.6	66.6
30	73.1	66.9	72.2	66.2	72.9	66.6
40	73.4	67	72.5	66.2	73.2	66.9
50	73.8	67.1	73.1	66.3	73.7	66.9
60	73.6	67	72.8	66.2	73.7	67.1
70	74	67.2	73.3	66.3	74.1	67.1
80	74.3	67	73.5	66.3	74.1	67.1
90	74.2	67.1	73.3	66.4	74.3	67.1
100	74.2	67.2	73.2	66.5	74.3	67.3
110	74.4	67	73.3	66.3	74.2	67.1
120	74.2	66.8	73.3	66	74.3	66.8
130	73.9	66.9	73.3	66.1	74.3	66.8
140	73.9	66.8	73.1	66	74	66.8
150	74.4	67.1	72.9	66.4	74	66.6
160	73.9	66.6	73.2	66	74	66.6
170	74	66.9	73.2	66.2	73.8	66.6
180	73.7	67	73	66.3	73.8	66.8
190	74.1	67	73.3	66.4	73.8	66.6
200	74.3	67	73.2	66.3	73.6	66.8
210	73.9	67	73.3	66.3	74	66.3
220	73.7	66.9	72.9	66	73.8	66.6
230	73.6	66.9	72.8	66.1	73.7	66.6
240	74	66.9	73.2	66.1	73.7	66.6

T1- Temperature on the coil; T2- Ambient temperature.
Data for Figure 4.6.

Table B9. Coils temperature data at 500 mA and a constant frequency of 60 Hz over a 4 hour time period at three positions from the center of the coil.

Time (min)	Position (in.)					
	0		0.5		1	
	T1	T2	T1	T2	T1	T2
0	66.9	66.9	67.6	67.6	66.6	66.6
10	74.1	67	75	67.7	73.5	67
20	80.2	67.3	81.1	68.1	79.5	67.3
30	82.4	66.8	83.3	67.5	82.1	66.8
40	84	67.1	84.9	67.8	83.6	67.1
50	84.2	67.3	85.3	68	84.1	67.3
60	84.3	67.4	85.4	68.1	84.3	67.4
70	85.2	67.3	86.1	68	85.1	67.3
80	85.3	67.3	86.2	67.9	85	67.3
90	85.5	67.3	86.4	68	85	67.3
100	85.7	67.4	86.6	68.1	85.2	67.4
110	85.6	67.3	86.5	68	85.1	67.3
120	85.8	66.9	86.7	67.6	85	66.9
130	86.4	67.4	87.3	68.1	85.1	67.4
140	86.3	67.1	87.2	67.8	85.9	67.1
150	86.4	67.3	87.3	68	85.8	67.3
160	86.6	67.6	87.7	68.3	86.2	67.6
170	86.5	67.4	87.4	68.1	86	67.4
180	86.3	67.1	87.2	67.8	86	67.1
190	86.8	67.6	87.7	68.3	86.4	67.6
200	87.1	67.6	87.8	68.3	86.9	67.6
210	87.1	67.7	88	68.4	86.8	67.7
220	86.8	67.3	87.7	68	86.8	67.3
230	87.2	67.9	88.1	68.6	86.8	67.9
240	86.8	67.4	87.8	68.1	86.6	67.4

T1- Temperature on the coil; T2- Ambient temperature.
Data for Figure 4.6.

Table B10. Raw confocal microscopy data obtained from IMR-32 cells in depolarizing buffer (High $[K^+]_o$/valinomycin). Average (D_o/D_i) obtained were used to calculate V_m values for different experimental conditions.

	D_i							D_i						
#	T10	T20	T30	T40	T50	T60	#	T10	T20	T30	T40	T50	T60
1	24.5	26.4	25.8	27.4	30.1	25.3	**30**	21.4	27.5	27.6	31.0	32.8	28.7
2	18.8	21.8	22.8	22.2	23.3	28.1	**31**	28.1	29.7	37.3	33.0	30.4	39.1
3	28.1	23.7	28.1	27.0	29.7	27.4	**32**	35.0	34.6	36.5	37.4	39.8	40.4
4	29.8	27.2	31.0	31.6	37.7	42.1	**33**	28.5	32.5	33.7	37.5	36.7	36.5
5	22.3	22.0	24.8	25.6	26.7	25.3	**34**	29.8	30.4	33.6	32.9	36.4	35.8
6	24.8	21.9	24.7	25.5	27.8	26.6	**35**	32.0	35.2	36.9	37.2	42.2	48.9
7	29.9	28.3	32.5	39.2	44.4	48.8	**36**	30.3	33.4	33.7	37.9	40.3	37.0
8	25.8	26.0	25.3	27.9	28.3	32.5	**37**	29.1	31.2	33.4	30.2	34.7	32.3
9	29.7	27.7	26.6	29.2	40.9	51.5	**38**	35.4	38.9	35.5	39.8	40.1	43.4
10	30.8	30.2	27.2	33.4	34.2	39.8	**39**	33.7	40.9	35.5	40.0	46.7	42.9
11	21.3	25.6	21.7	24.5	24.8	31.1	**40**	28.1	29.2	31.3	36.1	40.9	44.1
12	27.4	31.0	33.0	31.5	41.9	46.0	**41**	29.7	33.1	35.8	37.4	39.1	43.6
13	25.4	26.1	25.6	29.3	34.1	36.7	**42**	32.0	33.6	38.1	40.3	41.6	41.6
14	22.1	23.8	25.6	26.1	28.6	29.7	**43**	27.5	29.3	29.4	30.6	33.2	33.9
15	22.2	24.6	22.9	23.0	24.6	28.8	**44**	33.7	33.9	32.8	34.0	42.3	38.9
16	26.0	27.0	26.6	28.7	34.5	36.8	**45**	35.8	42.3	41.4	42.6	46.3	45.9
17	32.9	29.8	34.2	34.1	36.4	37.8	**46**	30.1	33.6	36.2	31.9	41.6	38.6
18	25.0	25.6	24.0	27.1	26.8	30.2	**47**	31.2	37.3	32.7	38.6	41.4	41.5
19	20.9	21.0	20.4	27.1	24.5	23.6	**48**	29.0	30.2	31.6	34.2	35.9	32.2
20	34.0	33.6	35.8	39.6	37.5	42.8	**49**	23.8	29.5	27.2	30.8	35.8	34.4
21	32.6	30.1	32.8	30.9	34.5	37.0	**50**	32.4	31.3	35.8	33.6	36.4	37.8
22	23.9	23.8	25.7	33.0	29.7	37.7	**51**	53.2	52.3	50.4	48.5	46.6	43.6
23	24.8	27.4	28.7	29.1	30.5	32.4	**52**	23.6	23.2	23.8	26.3	28.5	30.9
24	22.2	23.8	28.3	26.8	27.7	28.5	**53**	29.1	34.2	30.2	30.8	37.2	31.3
25	32.6	33.1	34.1	38.8	39.0	45.3	**54**	29.6	31.5	32.4	30.5	29.0	29.9
26	26.2	29.0	31.5	34.2	34.3	35.2	**55**	22.5	31.2	26.4	34.2	40.4	40.2
27	33.2	32.3	35.2	34.2	38.3	38.2	**56**	25.8	30.1	28.0	38.9	48.2	58.2
28	30.2	27.7	32.1	35.2	37.9	43.1	**57**	34.4	36.7	33.6	36.3	39.4	39.7
29	26.9	30.1	31.5	31.5	34.2	34.8							

D_o					
T10	T20	T30	T40	T50	T60
8.2	8.3	7.7	8.6	10.3	10.4

Average D_o/D_i					
T10	T20	T30	T40	T50	T60
0.3	0.3	0.3	0.3	0.3	0.3

D_o-Fluorescence intensity outside the cell

D_I- Fluorescence intensity inside the cell

Table B11. Raw confocal microscopy data obtained from unexposed IMR-32 cells in normal HEPES buffer.

	Fl_i							Fl_i					
#	T10	T20	T30	T40	T50	T60	#	T10	T20	T30	T40	T50	T60
1	17.9	17.8	22.8	22.0	25.7	23.1	**28**	7.9	10.8	13.1	13.8	16.2	17.5
2	15.4	18.3	21.7	21.5	23.5	18.8	**29**	13.2	12.9	9.8	10.1	7.9	10.9
3	9.4	10.1	12.3	11.3	14.2	16.7	**30**	10.5	15.3	20.3	18.7	22.0	21.4
4	10.3	14.6	13.7	16.9	21.5	23.7	**31**	14.0	34.0	20.7	18.9	14.2	13.6
5	11.9	11.3	15.2	13.5	15.8	15.9	**32**	12.7	15.1	17.3	22.2	27.1	34.9
6	13.5	18.1	18.5	23.2	32.5	34.4	**33**	11.0	12.6	12.2	15.5	20.5	22.0
7	16.0	16.9	19.1	18.9	20.1	17.7	**34**	10.4	11.0	10.0	13.1	14.6	24.7
8	10.2	9.7	10.6	12.2	14.3	14.1	**35**	11.5	14.2	14.8	18.6	17.6	20.7
9	13.3	16.6	18.7	17.7	20.8	29.4	**36**	12.4	11.4	12.9	21.9	15.2	21.0
10	12.9	14.0	14.4	14.3	15.9	16.7	**37**	8.0	10.0	9.3	11.8	13.7	18.5
11	16.3	11.5	12.9	21.8	32.5	26.1	**38**	14.9	18.4	19.8	20.6	27.6	34.0
12	12.8	17.6	32.5	18.3	16.8	19.5	**39**	9.8	11.2	7.1	6.8	7.5	5.7
13	18.5	20.7	77.4	45.5	29.5	10.0	**40**	12.8	20.6	15.5	22.6	32.5	41.7
14	14.6	18.0	18.4	24.2	30.8	35.2	**41**	16.5	27.1	10.3	13.7	10.6	9.8
15	16.8	12.4	17.5	19.3	24.5	55.0	**42**	30.4	25.6	14.2	18.2	18.9	28.5
16	14.5	18.1	32.6	23.4	26.1	29.6	**43**	10.5	10.5	13.3	13.4	23.1	30.6
17	9.7	12.5	15.6	16.5	18.8	32.8	**44**	7.2	8.5	8.2	9.0	10.8	10.9
18	19.6	17.0	19.8	22.0	27.8	38.5	**45**	14.7	19.4	19.3	22.5	28.2	50.0
19	10.6	10.1	12.7	12.4	16.3	22.9	**46**	18.1	18.8	19.2	22.2	31.7	53.6
20	14.4	18.9	21.8	20.8	23.2	41.3	**47**	19.9	15.5	20.6	18.4	10.5	11.0
21	12.6	13.4	14.6	16.8	19.6	24.9	**48**	12.9	15.4	17.1	17.0	32.0	26.1
22	14.2	15.5	17.4	16.4	17.9	23.6	**49**	19.6	17.7	17.5	9.6	12.5	12.8
23	12.2	25.2	25.8	34.6	13.9	46.1	**50**	12.1	30.8	11.7	9.6	11.9	11.4
24	11.2	16.2	15.7	15.6	17.9	16.1	**51**	11.7	12.7	15.6	12.1	16.2	19.1
25	10.1	16.6	13.0	10.2	8.3	8.2	**52**	7.5	8.8	9.1	10.0	8.8	12.9
26	8.5	11.6	12.0	15.6	20.2	21.6	**53**	12.1	14.0	17.4	19.8	14.5	20.3
27	11.0	13.3	11.8	12.1	13.8	13.8	**54**	14.6	15.3	17.7	19.0	21.0	24.7

Fl_o					
T10	T20	T30	T40	T50	T60
4.6	4.6	4.9	4.5	4.4	4.7

Data for Figure 4.8.
T(n) – Time at n^{th} minute. # - cell number
Fl_o-Fluorescence intensity outside the cell
Fl_i- Fluorescence intensity inside the cell

Table B12. Raw confocal microscopy data obtained from exposed (200 μT, 60 Hz) IMR-32 cells in normal HEPES buffer.

	Fl_i							Fl_i					
#	T10	T20	T30	T40	T50	T60	#	T10	T20	T30	T40	T50	T60
1	7.6	8.9	9.6	10.3	13.6	16.1	**41**	13.2	15.9	23.6	32.7	55.9	37.7
2	9.8	9.7	12.0	13.7	14.5	17.0	**42**	20.1	23.2	26.6	25.8	31.6	22.1
3	8.7	8.7	9.6	13.8	15.0	17.8	**43**	13.8	14.5	18.6	21.7	19.9	20.4
4	8.0	9.0	10.0	12.1	15.0	17.1	**44**	10.1	11.0	11.8	17.1	15.4	17.9
5	8.6	9.0	8.8	8.3	8.7	9.1	**45**	18.5	24.1	35.1	45.1	47.8	47.0
6	9.4	11.4	11.2	11.0	10.4	12.3	**46**	10.0	10.2	9.5	13.1	10.0	12.0
7	10.1	12.3	12.5	11.9	15.1	16.2	**47**	9.7	13.3	15.9	41.6	40.3	34.2
8	17.7	18.6	18.1	23.4	23.5	25.0	**48**	13.1	12.5	14.2	23.0	18.1	21.3
9	7.2	7.4	8.2	11.3	9.1	13.0	**49**	13.0	16.1	21.8	18.5	16.9	18.5
10	10.3	11.7	13.7	14.5	16.8	26.5	**50**	9.7	10.3	9.8	10.8	11.0	10.5
11	6.8	8.1	7.1	9.2	10.1	33.2	**51**	18.9	18.0	20.8	24.6	28.4	40.6
12	10.1	10.2	9.1	9.5	10.9	13.5	**52**	12.3	18.1	42.0	46.8	35.8	34.2
13	10.6	12.7	12.1	13.3	14.2	16.0	**53**	21.2	16.3	13.9	16.7	14.3	14.1
14	7.5	8.2	9.6	11.2	14.5	15.7	**54**	10.4	10.0	10.0	10.3	10.6	13.0
15	8.7	9.0	12.7	15.8	22.5	36.7	**55**	10.7	13.4	11.2	12.3	13.3	16.6
16	7.6	6.4	7.0	9.5	9.8	11.6	**56**	12.7	14.8	16.2	18.7	12.1	12.1
17	7.0	7.0	9.6	8.9	17.7	12.5	**57**	8.1	9.0	12.3	13.1	14.5	13.0
18	12.2	13.5	14.3	15.5	18.3	19.4	**58**	7.9	9.5	9.9	12.9	13.3	14.0
19	13.1	14.1	15.7	17.0	20.4	24.1	**59**	9.5	11.8	11.7	15.0	18.1	19.7
20	7.5	5.9	6.6	8.0	8.3	8.8	**60**	6.4	8.6	10.5	9.4	18.0	55.3
21	11.1	10.3	12.1	11.7	14.1	14.2	**61**	23.9	20.9	22.8	19.1	29.3	41.5
22	10.7	8.7	11.1	11.5	9.8	15.4	**62**	15.0	14.7	13.7	13.7	13.8	19.3
23	6.7	8.4	8.3	11.3	13.7	11.8	**63**	12.2	13.0	11.8	13.3	12.1	12.7
24	8.3	6.9	10.5	9.7	11.6	11.7	**64**	11.5	11.4	16.7	15.0	17.4	32.6
25	9.2	11.9	11.3	11.7	13.3	12.0	**65**	11.3	14.9	20.0	24.0	23.1	27.1
26	12.6	14.1	14.7	17.4	16.6	19.6	**66**	8.2	9.2	10.2	10.2	10.7	13.3
27	11.9	11.6	9.7	9.9	10.7	8.1	**67**	11.4	13.5	13.0	14.0	14.6	15.7
28	8.0	9.2	8.1	10.8	10.0	10.2	**68**	25.2	15.9	15.9	18.5	19.9	22.2
29	12.3	10.1	13.9	12.2	15.8	16.4	**69**	13.3	13.4	14.7	14.2	15.1	15.9
30	7.9	9.6	11.9	16.0	19.9	20.2	**70**	8.4	9.0	10.0	12.2	13.1	13.5
31	13.2	11.1	15.4	18.7	22.0	20.5	**71**	9.8	10.5	11.3	12.2	13.5	13.4
32	10.6	14.5	15.7	17.7	17.5	18.6	**72**	10.7	13.6	15.9	16.2	18.0	20.5
33	8.9	7.4	12.6	11.5	11.7	13.9	**73**	11.5	12.6	12.6	15.3	16.1	13.9
34	7.7	9.5	12.2	12.5	13.3	13.7	**74**	10.4	14.0	14.8	13.7	14.9	20.2
35	19.6	19.3	25.1	26.2	32.6	29.1	**75**	13.2	16.9	20.6	20.4	17.6	20.7
36	9.9	12.0	13.2	15.3	14.3	16.4	**76**	19.6	20.7	23.4	25.8	24.6	25.8
37	12.2	10.5	12.4	25.6	32.6	30.6	**77**	9.1	9.0	10.3	15.5	14.0	15.2
38	12.4	15.5	20.2	22.2	21.3	21.6	**78**	26.5	14.8	13.0	15.7	18.1	19.3
39	12.0	12.2	15.4	18.7	19.9	19.5	**79**	7.1	7.1	8.2	8.6	9.5	10.4
40	15.6	16.9	17.4	22.2	23.9	20.5	**80**	9.6	13.1	12.1	14.4	16.0	15.1

Fl_o					
T10	T20	T30	T40	T50	T60
4.3	4.1	4.0	4.0	4.1	4.0

Data for Figure 4.8.
T(n) – Time at n^{th} minute. # - cell number
Fl_o-Fluorescence intensity outside the cell
Fl_i- Fluorescence intensity inside the cell

Table B13. Raw confocal microscopy data obtained from unexposed IMR-32 cells in HEPES buffer (K^+ replaced with Cs^+).

	Fl_i							Fl_i					
#	T10	T20	T30	T40	T50	T60	#	T10	T20	T30	T40	T50	T60
1	11.0	12.1	15.2	21.3	22.2	32.7	**33**	12.8	11.3	13.3	18.6	34.8	50.1
2	15.2	13.7	15.0	19.0	19.0	19.9	**34**	9.1	13.4	15.7	17.6	24.1	23.5
3	7.2	12.9	16.7	17.6	13.6	13.5	**35**	12.1	16.6	19.0	19.4	20.3	22.5
4	8.8	11.0	11.4	13.3	17.2	22.0	**36**	10.3	11.7	17.7	16.3	26.0	28.7
5	9.7	13.6	16.2	19.7	25.7	16.8	**37**	9.2	11.8	14.5	20.4	22.6	24.7
6	13.9	16.7	19.6	21.5	31.7	29.4	**38**	15.6	16.3	18.5	17.1	19.9	20.8
7	8.2	8.9	11.9	14.8	16.2	21.4	**39**	18.1	32.5	30.0	32.6	54.5	108.2
8	10.5	10.8	16.0	17.5	16.7	10.2	**40**	9.8	12.0	18.9	18.3	19.9	21.8
9	14.8	14.9	16.7	20.4	21.2	20.2	**41**	10.1	12.8	18.9	20.8	54.0	73.9
10	12.6	15.0	20.5	21.2	30.9	15.1	**42**	14.5	17.7	23.7	32.7	70.1	88.2
11	12.2	18.3	17.5	19.2	25.0	11.8	**43**	10.9	14.2	13.5	19.4	18.7	11.4
12	15.9	15.3	17.7	18.8	18.9	16.5	**44**	11.5	11.6	13.9	12.5	18.9	17.8
13	8.1	10.4	14.1	19.2	23.8	22.9	**45**	19.3	26.9	32.9	34.2	23.6	15.3
14	8.3	9.2	10.6	15.0	15.2	16.7	**46**	26.0	22.4	17.1	21.3	31.7	37.0
15	18.5	27.8	28.3	25.9	18.8	14.5	**47**	8.6	10.3	12.9	13.8	17.6	19.2
16	8.9	14.8	17.2	35.4	36.8	86.1	**48**	4.9	8.2	9.1	8.1	11.0	10.6
17	9.6	10.5	14.9	19.1	21.6	25.4	**49**	11.7	21.9	26.6	21.1	18.3	20.0
18	12.6	16.5	27.9	46.5	62.9	69.7	**50**	29.9	13.7	20.0	34.3	39.5	65.9
19	20.9	25.9	30.9	39.0	61.0	75.7	**51**	7.6	9.1	11.1	12.0	14.8	15.9
20	15.4	21.1	24.0	28.0	28.2	24.7	**52**	8.1	11.7	19.6	18.7	22.6	22.8
21	13.6	21.1	24.1	35.1	41.6	34.9	**53**	15.4	21.3	29.7	29.7	25.3	23.9
22	12.5	20.5	34.4	33.7	17.8	18.4	**54**	13.3	22.2	27.7	25.2	20.1	19.8
23	12.1	21.2	26.9	27.1	25.8	24.5	**55**	5.9	6.9	6.3	8.6	11.2	16.5
24	7.1	12.3	15.1	25.1	27.0	24.2	**56**	17.6	22.0	28.0	26.0	42.6	62.6
25	14.3	14.7	22.2	32.8	41.1	48.3	**57**	10.8	13.7	16.9	18.8	20.8	23.2
26	10.8	13.7	15.5	21.7	33.6	52.7	**58**	14.7	8.5	8.9	11.0	19.6	54.9
27	13.2	17.9	17.2	17.9	22.6	23.2	**59**	6.6	9.9	10.1	12.2	12.8	13.5
28	11.0	15.0	21.3	27.7	31.0	27.2	**60**	7.5	9.8	13.0	14.9	17.2	25.9
29	28.5	37.9	37.9	35.4	35.7	28.2	**61**	7.4	9.5	14.3	14.7	13.7	15.0
30	21.6	28.6	40.6	47.3	37.1	36.4	**62**	9.2	12.9	24.1	18.9	18.1	17.9
31	7.9	8.9	9.7	13.8	19.8	36.6	**63**	9.7	13.3	16.7	15.9	21.7	21.5
32	25.0	28.8	30.3	43.2	76.9	93.2	**64**	11.7	15.5	24.2	24.2	20.1	26.3

Fl_o					
T10	T20	T30	T40	T50	T60
7.0	6.9	6.7	6.1	6.7	6.7

Data for Figure 4.8.
T(n) – Time at n^{th} minute. # - cell number
Fl_o-Fluorescence intensity outside the cell
Fl_i- Fluorescence intensity inside the cell

Table B14. Raw confocal microscopy data obtained from exposed (200 μT, 60 Hz) IMR-32 cells in HEPES buffer (K^+ replaced with Cs^+).

	Fl_i							Fl_i						
#	T10	T20	T30	T40	T50	T60	#	T10	T20	T30	T40	T50	T60
1	8.5	9.3	11.7	13.4	16.6	15.3	**31**	10.2	12.4	10.9	10.1	11.0	16.6
2	6.5	9.2	11.7	14.1	19.1	29.0	**32**	7.0	9.4	11.0	9.4	7.0	5.5
3	6.0	7.0	12.7	21.7	26.3	32.0	**33**	7.1	7.7	9.2	9.1	10.1	9.0
4	14.5	14.9	10.8	10.4	9.5	7.5	**34**	7.9	6.3	7.4	9.2	9.8	14.5
5	7.7	8.9	9.0	12.3	13.3	13.8	**35**	7.3	7.5	9.0	8.6	11.8	8.2
6	11.2	15.6	36.2	25.8	17.5	15.1	**36**	7.9	8.1	12.2	22.7	23.7	16.1
7	7.5	6.9	9.8	14.1	29.5	34.8	**37**	5.7	8.6	8.0	10.3	11.6	13.0
8	6.7	8.0	8.6	11.7	10.1	7.6	**38**	8.1	9.6	16.2	15.1	29.9	24.1
9	5.5	6.2	7.2	6.7	10.4	10.9	**39**	7.9	10.7	10.8	16.6	16.1	8.6
10	11.2	15.6	12.3	14.6	16.1	23.3	**40**	9.2	8.9	11.5	17.0	27.9	42.5
11	7.1	6.3	9.2	14.1	44.5	45.1	**41**	8.3	8.2	9.9	15.5	11.8	9.5
12	4.8	5.8	7.6	8.0	10.1	8.4	**42**	5.1	6.1	7.3	9.2	16.8	25.1
13	6.4	7.2	8.8	15.2	21.8	10.1	**43**	3.6	7.3	8.6	13.1	17.4	22.3
14	6.1	6.9	7.8	8.6	33.4	35.4	**44**	9.9	9.9	11.0	24.1	29.9	30.2
15	11.6	10.2	13.6	12.7	15.4	16.2	**45**	5.7	8.5	9.6	13.7	14.3	11.9
16	4.8	5.7	8.1	7.8	10.3	7.1	**46**	5.7	5.4	5.9	7.3	10.6	72.1
17	6.7	8.0	8.9	8.8	12.3	11.9	**47**	5.6	5.4	6.0	6.2	6.8	7.6
18	8.3	8.6	11.3	9.2	9.9	10.3	**48**	10.6	20.0	21.5	22.2	20.0	24.8
19	6.9	7.0	6.6	9.9	11.6	13.1	**49**	6.6	7.5	10.4	13.1	15.2	15.6
20	7.2	7.5	7.3	8.3	7.3	8.0	**50**	7.0	10.3	13.7	48.6	41.0	52.8
21	8.3	10.9	14.7	15.5	12.6	16.6	**51**	6.8	7.6	9.4	10.4	10.6	11.1
22	8.4	9.4	7.6	14.2	14.5	19.3	**52**	6.7	7.6	7.0	10.2	13.0	12.6
23	7.5	6.4	7.6	12.8	19.1	20.6	**53**	5.3	5.7	6.3	6.3	6.8	7.7
24	8.6	9.1	11.1	13.9	16.5	18.3	**54**	7.6	8.0	11.2	13.1	16.8	24.3
25	7.2	8.9	11.1	13.3	11.8	12.2	**55**	5.3	5.7	7.5	8.3	12.0	15.3
26	8.6	8.8	10.7	15.4	17.1	19.8	**56**	6.7	5.3	8.2	11.9	30.3	45.6
27	7.8	8.9	11.1	27.0	36.0	43.4	**57**	8.5	8.2	7.4	7.9	9.5	14.3
28	6.8	8.1	9.6	11.5	12.0	10.3	**58**	5.8	7.3	7.5	10.8	14.3	22.1
29	6.8	9.0	13.4	20.1	27.7	25.4	**59**	5.8	7.0	7.5	7.3	9.4	8.0
30	5.3	9.9	17.4	24.8	39.5	34.0	**60**	5.3	6.2	6.6	7.9	10.6	12.2

Fl_o					
T10	T20	T30	T40	T50	T60
5.1	5.1	5.3	5.2	5.0	4.7

Data for Figure 4.8.
T(n) – Time at n^{th} minute. # - cell number
Fl_o-Fluorescence intensity outside the cell
Fl_i- Fluorescence intensity inside the cell

Table B15. Raw confocal microscopy data obtained from unexposed IMR-32 cells in HEPES buffer (100 mM TEA-Cl).

	Fl_i							Fl_i					
#	T10	T20	T30	T40	T50	T60	#	T10	T20	T30	T40	T50	T60
1	33.5	37.2	42.0	47.7	44.4	51.0	**29**	24.3	30.0	33.0	22.6	24.3	41.0
2	35.7	28.8	23.3	30.3	41.9	46.1	**30**	16.2	15.3	19.8	22.7	26.7	24.4
3	27.9	31.7	35.3	40.6	37.4	46.4	**31**	12.2	19.5	22.4	33.9	58.9	50.9
4	14.1	15.9	20.5	21.9	26.5	31.0	**32**	15.3	16.2	17.6	20.5	27.2	29.2
5	36.3	43.0	54.3	47.0	47.8	55.9	**33**	16.6	15.6	16.0	16.2	22.3	39.0
6	23.4	30.1	27.5	32.8	34.2	36.0	**34**	21.6	21.4	27.3	26.2	34.6	39.3
7	30.9	37.1	38.0	37.4	34.3	42.6	**35**	27.8	20.7	19.8	23.3	26.1	26.5
8	22.7	22.5	28.5	21.5	36.5	26.5	**36**	25.0	28.5	27.7	36.7	40.9	34.0
9	25.0	22.3	21.3	24.0	26.9	28.0	**37**	21.9	23.1	26.8	33.5	48.0	40.9
10	27.2	26.0	25.1	25.6	28.0	25.3	**38**	21.5	20.3	28.8	20.8	25.5	39.9
11	27.0	23.1	29.4	38.3	34.9	53.0	**39**	10.3	9.8	12.9	12.0	16.9	18.7
12	45.3	41.4	62.7	59.9	42.3	57.1	**40**	17.7	19.9	25.6	24.4	23.5	24.6
13	25.9	26.1	53.7	59.3	62.8	71.2	**41**	23.6	26.5	32.7	32.6	32.2	32.6
14	69.8	47.2	30.3	27.0	31.9	34.2	**42**	13.9	16.1	17.2	16.6	19.1	20.7
15	33.5	41.8	41.7	48.2	47.4	56.8	**43**	23.5	28.3	39.5	46.7	65.1	58.3
16	27.9	32.1	38.9	55.7	50.3	68.5	**44**	16.8	24.0	22.1	10.7	11.5	10.2
17	17.0	18.3	11.8	14.7	29.0	25.7	**45**	20.1	22.2	26.9	30.8	38.3	33.9
18	38.6	19.9	20.1	14.8	33.2	23.5	**46**	15.0	16.4	16.6	19.4	20.5	22.9
19	31.0	31.2	35.0	39.5	40.3	47.0	**47**	17.4	20.8	25.9	25.6	37.1	45.7
20	19.0	14.6	24.1	9.8	13.6	23.9	**48**	24.0	25.0	26.9	33.4	36.8	36.8
21	24.3	27.5	29.9	34.5	39.4	49.1	**49**	16.4	17.1	17.9	19.3	25.0	48.5
22	21.0	22.7	29.2	34.0	43.5	42.7	**50**	10.2	14.5	15.5	15.1	18.1	19.0
23	13.9	21.6	20.7	29.6	31.0	31.5	**51**	19.0	21.3	28.0	34.6	37.8	33.0
24	15.8	15.8	21.8	24.8	26.9	28.2	**52**	24.7	27.2	32.2	30.0	33.2	34.0
25	16.1	20.3	24.2	28.0	30.9	32.2	**53**	15.9	16.0	19.8	23.2	31.2	31.1
26	12.9	14.4	16.8	14.8	18.7	18.7	**54**	32.9	35.8	37.3	41.8	49.9	52.2
27	15.6	16.7	19.9	21.2	23.5	29.9	**55**	16.2	19.7	21.5	24.2	24.1	28.5
28	24.5	28.6	28.8	31.1	36.1	32.0	**56**	25.4	21.9	19.0	17.3	23.5	24.2

Fl_o					
T10	T20	T30	T40	T50	T60
4.9	4.8	5.1	4.9	4.9	4.3

Data for Figure 4.8.
T(n) – Time at n^{th} minute. # - cell number
Fl_o-Fluorescence intensity outside the cell
Fl_i- Fluorescence intensity inside the cell

Table B16. Raw confocal microscopy data obtained from exposed (200 μT, 60 Hz) IMR-32 cells in HEPES buffer (100 mM TEA-Cl).

	Fl_i							Fl_i					
#	T10	T20	T30	T40	T50	T60	**#**	T10	T20	T30	T40	T50	T60
1	9.2	11.8	13.9	13.9	17.8	16.7	**34**	10.3	11.7	14.0	12.3	14.8	14.3
2	16.5	16.4	17.5	20.1	20.6	20.8	**35**	23.9	36.5	28.9	44.9	44.6	32.4
3	13.5	17.7	21.6	20.5	25.9	35.2	**36**	12.8	12.0	13.8	12.6	17.9	24.8
4	15.1	15.5	15.4	16.4	10.4	8.2	**37**	14.6	19.3	30.0	37.5	40.6	46.7
5	18.0	18.5	19.1	19.8	22.2	23.7	**38**	14.2	15.3	15.5	18.6	18.5	21.9
6	28.4	24.6	27.1	36.5	41.8	47.1	**39**	30.4	39.2	44.3	42.5	39.8	70.7
7	14.8	13.4	17.1	15.7	19.6	20.3	**40**	12.9	19.1	19.9	20.3	19.9	21.2
8	13.1	16.4	15.5	19.9	20.3	25.2	**41**	9.4	12.0	11.6	13.6	15.6	16.2
9	8.8	9.7	12.5	11.6	13.3	15.6	**42**	20.0	24.1	24.6	26.3	27.1	29.5
10	10.2	10.9	12.8	13.8	13.5	13.1	**43**	18.7	23.8	26.6	29.0	27.3	33.5
11	15.3	17.3	16.7	21.3	24.1	27.9	**44**	11.5	14.5	19.4	21.6	20.9	20.0
12	23.0	26.9	32.5	32.1	33.6	30.3	**45**	15.4	17.9	12.3	15.0	14.5	14.4
13	12.4	14.1	16.0	18.7	20.6	19.7	**46**	10.5	12.8	15.6	21.0	17.0	19.5
14	8.2	10.5	11.7	17.5	19.1	22.5	**47**	20.2	21.5	26.7	25.8	27.1	29.2
15	7.8	8.2	6.9	6.7	6.8	8.0	**48**	12.2	13.9	13.5	13.5	12.8	13.9
16	8.9	11.0	11.4	10.8	12.5	12.6	**49**	12.8	11.3	10.9	11.8	13.8	13.1
17	11.6	13.2	14.9	20.2	23.7	22.2	**50**	19.5	28.1	28.2	43.4	27.6	27.6
18	19.2	18.0	15.5	18.3	20.0	24.7	**51**	15.3	15.4	15.9	19.0	20.9	20.8
19	14.5	18.2	28.5	30.8	36.7	35.8	**52**	13.4	13.3	16.0	15.4	18.6	22.6
20	9.2	11.7	13.9	14.8	16.4	16.0	**53**	17.3	23.0	24.5	25.6	31.4	24.0
21	20.2	22.9	29.1	33.6	36.9	42.7	**54**	22.5	23.7	23.4	25.4	23.8	25.5
22	11.6	12.0	15.3	16.6	15.7	21.2	**55**	11.0	15.2	26.8	28.1	33.7	19.1
23	15.0	16.1	17.1	18.3	23.4	21.5	**56**	13.0	14.0	14.7	15.2	23.8	23.0
24	9.8	13.6	12.7	14.5	15.8	20.8	**57**	18.7	20.9	15.8	17.9	21.1	19.5
25	15.5	21.2	19.2	19.1	22.2	27.1	**58**	16.0	17.4	17.3	17.8	22.7	27.7
26	11.6	16.3	14.8	14.8	16.8	19.5	**59**	18.6	14.5	14.1	12.3	16.9	13.7
27	26.8	25.8	30.9	35.0	29.5	21.9	**60**	11.1	11.7	13.4	21.9	16.0	14.2
28	7.9	10.2	9.9	10.6	14.2	15.2	**61**	9.1	11.0	12.2	13.7	18.9	14.6
29	22.2	27.3	30.1	28.3	29.3	31.3	**62**	12.0	12.2	18.8	18.8	21.8	21.9
30	11.5	13.9	17.7	24.3	25.3	16.9	**63**	12.5	13.6	16.4	16.7	17.0	18.9
31	9.2	11.0	10.9	12.3	13.3	15.8	**64**	19.1	18.8	21.6	18.5	16.9	41.3
32	12.8	13.6	11.3	12.9	15.1	18.2	**65**	20.2	21.5	19.9	22.4	22.2	25.6
33	13.9	18.2	20.6	25.7	36.3	38.1	**66**	16.7	20.3	24.4	28.5	27.4	28.2

Fl_o					
T10	T20	T30	T40	T50	T60
4.0	3.7	3.5	3.6	3.7	3.4

Data for Figure 4.8.
T(n) – Time at n^{th} minute. # - cell number
Fl_o-Fluorescence intensity outside the cell
Fl_i- Fluorescence intensity inside the cell

Table B17. Raw confocal microscopy data obtained from unexposed IMR-32 cells in HEPES buffer (50 mM $[K^+]_o$, 70 mM $[Na^+]_o$).

	Fl_i							Fl_i					
#	T10	T20	T30	T40	T50	T60	**#**	T10	T20	T30	T40	T50	T60
1	32.1	31.2	37.0	40.2	47.3	46.6	**28**	38.9	41.0	45.3	41.2	46.0	44.1
2	21.1	25.0	29.2	53.0	37.0	31.9	**29**	31.8	41.3	49.6	53.6	49.1	65.8
3	38.4	36.6	46.3	52.5	37.2	52.4	**30**	37.1	42.9	40.6	43.1	40.3	38.5
4	41.9	40.7	43.3	44.2	49.3	56.1	**31**	40.9	39.3	35.9	31.5	30.1	32.1
5	20.7	23.9	28.6	36.1	39.7	36.1	**32**	30.7	37.5	39.0	39.8	35.4	54.0
6	29.4	33.1	33.4	36.9	34.5	40.9	**33**	48.7	57.9	59.8	61.6	68.0	64.7
7	23.6	28.7	30.3	38.0	48.8	46.6	**34**	56.6	59.7	64.0	66.1	72.1	67.5
8	36.0	29.8	36.2	36.3	42.0	46.1	**35**	51.5	65.8	74.0	62.3	67.7	73.0
9	31.8	36.2	44.4	46.9	44.1	43.9	**36**	52.5	54.2	51.1	60.6	63.6	68.2
10	29.6	31.2	32.7	35.8	33.5	28.9	**37**	55.9	59.9	60.8	55.5	55.9	62.0
11	29.8	37.0	44.7	41.5	53.8	52.9	**38**	52.2	49.6	48.2	51.5	52.0	58.1
12	31.5	31.1	46.1	41.0	47.4	49.0	**39**	48.4	55.1	60.7	61.9	66.1	68.1
13	33.7	36.4	40.7	41.1	47.0	45.0	**40**	56.3	58.3	60.3	62.8	66.3	70.2
14	29.9	30.5	42.6	47.5	39.6	37.2	**41**	59.0	56.9	54.4	60.1	58.2	58.1
15	34.0	34.7	41.9	39.0	45.5	39.9	**42**	45.8	49.5	46.2	48.5	46.0	54.4
16	28.4	29.3	32.9	32.4	29.3	32.0	**43**	45.9	46.2	49.7	53.1	57.0	56.8
17	27.2	28.3	37.4	36.1	37.8	39.3	**44**	50.1	52.4	55.8	54.0	52.9	53.7
18	29.5	29.7	29.9	26.9	26.5	30.6	**45**	57.2	59.4	69.3	75.8	70.4	78.6
19	26.8	31.4	37.8	34.4	30.8	36.6	**46**	39.8	40.6	42.5	42.9	51.9	53.8
20	32.1	32.8	29.5	31.5	29.3	32.7	**47**	46.6	52.3	65.2	71.6	76.3	74.2
21	28.2	25.1	23.3	20.4	20.2	21.2	**48**	58.4	61.1	61.7	66.6	68.4	70.5
22	27.2	27.3	28.4	37.0	37.9	45.9	**49**	43.3	48.9	48.6	47.2	48.4	54.3
23	23.7	23.9	28.3	25.9	29.7	31.5	**50**	38.5	44.1	41.1	42.0	53.5	49.1
24	26.9	30.0	28.9	30.6	30.3	31.3	**51**	50.6	55.8	57.9	61.8	68.0	68.6
25	31.8	31.7	34.8	33.5	30.4	34.8	**52**	46.9	53.7	54.3	50.5	52.6	52.6
26	38.9	40.6	42.5	45.2	43.3	49.4	**53**	47.0	49.3	71.4	70.2	61.6	56.5
27	33.9	33.1	33.9	31.4	30.0	34.8							

Fl_o					
T10	T20	T30	T40	T50	T60
4.7	4.3	4.7	5.0	4.6	5.1

Data for Figure 4.8.
T(n) – Time at n^{th} minute. # - cell number
Fl_o-Fluorescence intensity outside the cell
Fl_i- Fluorescence intensity inside the cell

Table B18. Raw confocal microscopy data obtained from exposed (200 μT, 60 Hz) IMR-32 cells in HEPES buffer (50 mM K^+, 70 mM Na^+).

	Fl_i							Fl_i						
#	T10	T20	T30	T40	T50	T60	**#**	T10	T20	T30	T40	T50	T60
1	51.7	50.1	52.1	57.9	55.6	61.7	**32**	49.2	52.2	51.7	50.8	51.9	64.3
2	62.1	60.9	58.9	72.5	74.2	78.7	**33**	52.1	56.6	53.1	53.4	56.6	62.8
3	50.1	50.2	52.2	60.6	57.8	57.6	**34**	67.7	68.2	63.3	57.4	55.3	65.2
4	54.7	62.0	63.7	65.7	68.6	64.2	**35**	38.3	45.4	49.0	52.5	55.2	61.4
5	54.1	56.0	54.6	62.6	56.6	62.7	**36**	37.5	44.5	46.1	44.1	43.8	56.2
6	57.4	58.1	61.0	67.7	72.5	65.7	**37**	47.2	47.5	52.6	48.0	52.0	63.1
7	64.8	63.8	64.1	67.8	61.8	65.2	**38**	48.2	53.8	56.1	59.0	59.7	68.3
8	54.0	62.0	58.6	67.8	74.0	76.5	**39**	37.6	42.6	45.0	44.7	42.9	49.5
9	46.8	52.1	50.8	54.6	57.0	51.5	**40**	52.6	54.0	57.5	50.3	53.8	57.7
10	41.6	46.7	44.9	55.9	62.3	54.0	**41**	46.4	48.9	51.4	51.0	49.2	62.9
11	59.0	62.5	59.8	64.6	70.1	73.1	**42**	56.5	61.8	61.6	59.5	59.9	66.9
12	53.6	53.7	57.6	60.6	62.2	60.8	**43**	53.1	60.1	58.6	60.8	62.4	60.1
13	71.8	66.9	65.5	74.2	71.1	75.4	**44**	60.2	55.8	65.3	64.3	64.2	67.5
14	64.3	63.9	61.0	64.1	70.4	73.7	**45**	66.2	75.4	67.8	66.1	66.9	71.5
15	58.3	56.5	57.1	61.9	63.8	61.4	**46**	70.3	75.5	75.8	75.8	77.1	82.8
16	56.3	59.3	55.2	64.6	68.0	68.1	**47**	61.8	63.4	64.6	65.7	63.6	68.8
17	67.3	66.4	59.7	55.6	54.7	51.1	**48**	45.9	47.2	51.9	54.6	52.7	61.3
18	52.3	61.9	56.0	67.4	75.4	70.1	**49**	61.1	63.2	62.7	61.2	65.6	68.1
19	65.2	61.0	64.9	70.6	69.9	69.5	**50**	69.3	71.1	73.9	75.8	78.9	80.2
20	57.4	55.5	59.8	60.9	59.6	62.1	**51**	53.1	59.2	63.1	63.2	63.7	70.3
21	54.8	58.1	57.1	66.6	65.4	59.9	**52**	47.0	47.7	51.8	55.7	54.0	52.7
22	41.9	46.9	53.2	52.7	56.7	62.0	**53**	61.9	61.3	65.6	64.9	65.8	70.9
23	46.1	50.6	51.7	51.4	47.7	64.5	**54**	63.5	64.5	65.3	70.8	66.0	73.8
24	42.4	46.6	51.5	50.5	52.5	59.2	**55**	60.4	66.5	68.5	76.3	74.5	83.3
25	42.7	48.0	47.8	44.2	45.9	56.2	**56**	66.0	68.3	63.0	72.8	68.6	76.1
26	38.4	45.9	50.0	46.0	48.0	61.8	**57**	62.1	66.2	61.2	66.6	66.3	69.6
27	48.6	54.3	53.3	56.7	55.0	63.7	**58**	68.6	78.6	78.4	77.4	77.3	82.1
28	44.0	48.7	46.8	51.6	51.2	59.6	**59**	68.3	69.7	64.3	69.8	65.6	82.4
29	42.0	44.2	49.2	47.5	44.2	49.1	**60**	78.5	78.9	85.2	77.5	80.5	88.0
30	43.3	42.2	47.4	48.5	48.5	49.7	**61**	63.1	66.2	65.0	66.5	69.1	68.6
31	45.3	51.8	54.1	49.6	57.6	61.4							

Fl_o					
T10	T20	T30	T40	T50	T60
8.5	7.5	7.0	7.7	7.6	6.8

Data for Figure 4.8.
T(n) – Time at n^{th} minute. # - cell number
Fl_o-Fluorescence intensity outside the cell
Fl_i- Fluorescence intensity inside the cell

APPENDIX C

RAW DATA FOR CHAPTER 5

Figure C1. Sequencing results of the RT-PCR (Reverse Transcriptase- Polymerase Chain Reaction) APP695 product obtained from IMR32 cells. GENBANK analysis showed 98% homology with existing APP695 human mRNA sequence.

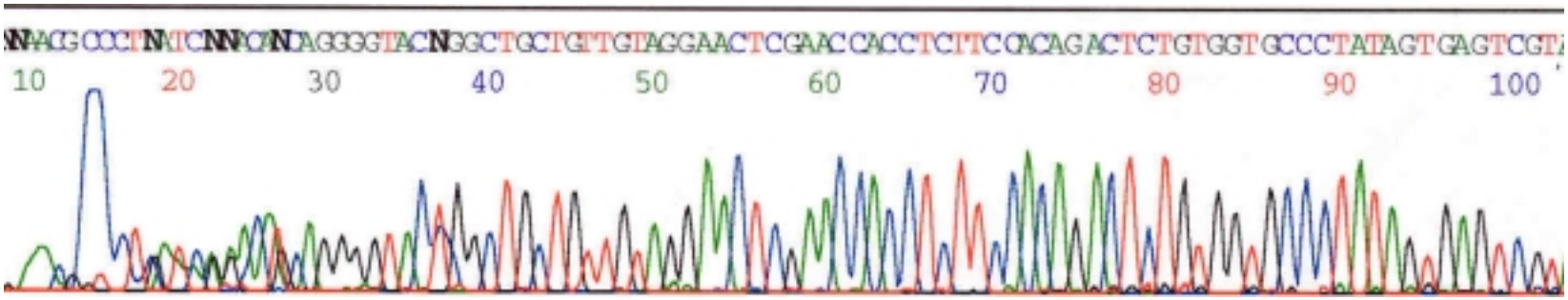

TABLE C1. Chemiluminescent signal intensities obtained from RNA from differentiating (Day 2) IMR32 cells exposed to a magnetic field (60Hz, 50 μT, 4h).

	REPLICATION 1			
CONDITION	Actin	APP695	APP695/Actin	EX/CO
CO1	819.05	466.56	0.57	1.00
A1	1082.09	714.84	0.66	1.16
B1	1036.53	615.85	0.59	1.04
C1	1177.09	787.95	0.67	1.18
	REPLICATION 2			
CO2	1117.31	770.93	0.69	1.00
A2	1178.83	971.49	0.82	1.19
B2	1175.82	979.06	0.83	1.21
C2	1103.22	932.28	0.85	1.22
	REPLICATION 3			
CO3	943.10	877.10	0.93	1.00
A3	1089.63	983.04	0.90	0.97
B3	991.86	854.16	0.86	0.93
C3	847.48	805.86	0.95	1.02

EX- Experimental Condition:
(CO- Control; A- Exposed; B- External coil; C- Sham)

TABLE C2. Chemiluminescent signal intensities obtained from RNA from differentiating (Day 2) IMR32 cells exposed to a magnetic field (60Hz, 100 μT, 4h).

	REPLICATION 1			
CONDITION	Actin	APP695	APP695/Actin	EX/CO
CO1	1210.69	652.51	0.54	1.00
A1	1298.85	671.29	0.52	0.96
B1	1488.90	748.60	0.50	0.93
C1	1891.15	896.08	0.47	0.88
	REPLICATION 2			
CO2	1790.65	1002.27	0.56	1.00
A2	1791.06	934.10	0.52	0.93
B2	1570.70	739.61	0.47	0.84
C2	1685.07	878.72	0.52	0.93
	REPLICATION 3			
CO3	2010.60	1072.90	0.53	1.00
A3	1871.28	1065.19	0.57	1.07
B3	1853.50	941.72	0.51	0.95
C3	2252.28	1196.99	0.53	1.00

EX- Experimental Condition:
(CO- Control; A- Exposed; B- External coil; C- Sham)

TABLE C3. Chemiluminescent signal intensities obtained from RNA from differentiating (Day 2) IMR32 cells exposed to a magnetic field (60Hz, 200 μT, 4h).

	REPLICATION 1			
CONDITION	Actin	APP695	APP695/Actin	EX/CO
CO1	834.04	363.57	0.44	1.00
A1	916.27	375.45	0.41	0.94
B1	1046.93	453.51	0.43	0.99
C1	911.18	372.97	0.41	0.94
	REPLICATION 2			
CO2	925.04	491.99	0.53	1.00
A2	954.12	540.13	0.57	1.06
B2	961.99	546.59	0.57	1.07
C2	1034.11	593.54	0.57	1.08
	REPLICATION 3			
CO3	1045.25	527.42	0.50	1.00
A3	1045.01	493.60	0.47	0.94
B3	954.07	418.15	0.44	0.87
C3	1155.92	519.33	0.45	0.89

EX- Experimental Condition:
(CO- Control; A- Exposed; B- External coil; C- Sham)

TABLE C4. Chemiluminescent signal intensities obtained from RNA from differentiating (Day 10) IMR32 cells exposed to a magnetic field (60Hz, 50 μT, 4h).

	REPLICATION 1			
CONDITION	Actin	APP695	APP695/Actin	EX/CO
CO1	2056.61	911.21	0.44	1.00
A1	2056.84	398.46	0.19	0.44
B1	2334.15	737.49	0.32	0.71
C1	2411.98	696.30	0.29	0.65
	REPLICATION 2			
CO2	2578.77	1245.50	0.48	1.00
A2	3366.47	1771.99	0.53	1.09
B2	2545.63	1557.16	0.61	1.27
C2	2617.48	2178.91	0.83	1.72
	REPLICATION 3			
CO3	2181.28	1079.20	0.49	1
A3	2098.37	828.97	0.40	0.80
B3	1681.51	834.78	0.50	1.00
C3	1528.54	623.78	0.41	0.82

EX- Experimental Condition:
(CO- Control; A- Exposed; B- External coil; C- Sham)

TABLE C5. Chemiluminescent signal intensities obtained from RNA from differentiating (Day 10) IMR32 cells exposed to a magnetic field (60Hz, 100 μT, 4h).

	REPLICATION 1			
CONDITION	Actin	APP695	APP695/Actin	EX/CO
CO1	827.91	464.25	0.56	1.00
A1	922.31	542.04	0.59	1.05
B1	974.65	655.52	0.67	1.20
C1	1002.43	639.28	0.64	1.14
	REPLICATION 2			
CO2	1105.54	732.44	0.66	1.00
A2	1160.72	807.38	0.70	1.05
B2	1107.40	773.35	0.70	1.05
C2	1069.50	715.97	0.67	1.01
	REPLICATION 3			
CO3	954.44	692.40	0.73	1.00
A3	736.28	606.40	0.82	1.14
B3	927.82	692.72	0.75	1.03
C3	967.09	711.76	0.74	1.01

EX- Experimental Condition:
(CO- Control; A- Exposed; B- External coil; C- Sham)

TABLE C6. Chemiluminescent signal intensities obtained from RNA from differentiating (Day 10) IMR32 cells exposed to a magnetic field (60Hz, 200 μT, 4h).

	REPLICATION 1			
CONDITION	Actin	APP695	APP695/Actin	EX/CO
CO1	1392.97	590.34	0.42	1.00
A1	1377.85	601.29	0.44	1.03
B1	1540.17	681.47	0.44	1.04
C1	1552.98	714.76	0.46	1.09
	REPLICATION 2			
CO2	1454.84	1015.71	0.70	1.00
A2	1877.70	689.86	0.37	0.53
B2	1831.53	904.76	0.49	0.71
C2	1787.88	1083.79	0.61	0.87
	REPLICATION 3			
CO3	1778.25	1143.34	0.64	1.00
A3	1747.63	881.10	0.50	0.78
B3	1532.58	674.31	0.44	0.68
C3	1489.42	720.18	0.48	0.75

EX- Experimental Condition:
(CO- Control; A- Exposed; B- External coil; C- Sham)

TABLE C7. Chemiluminescent signal intensities obtained from RNA from differentiating (Day 16) IMR32 cells exposed to a magnetic field (60Hz, 50 μT, 4h).

	REPLICATION 1			
CONDITION	Actin	APP695	APP695/Actin	EX/CO
CO1	2543.28	474.44	0.19	1.00
A1	2904.69	503.57	0.17	0.93
B1	2723.33	561.04	0.21	1.10
C1	2727.33	589.91	0.22	1.16
	REPLICATION 2			
CO2	2843.65	902.01	0.32	1.00
A2	2848.90	960.19	0.34	1.06
B2	2797.44	908.54	0.32	1.02
C2	2781.60	1000.82	0.36	1.13
	REPLICATION 3			
CO3	2043.48	398.88	0.20	1.00
A3	2399.34	496.85	0.21	1.06
B3	2282.83	420.19	0.18	0.94
C3	2017.47	399.93	0.19	1.02

EX- Experimental Condition:
(CO- Control; A- Exposed; B- External coil; C- Sham)

TABLE C8. Chemiluminescent signal intensities obtained from RNA from differentiating (Day 16) IMR32 cells exposed to a magnetic field (60Hz, 100 μT, 4h).

	REPLICATION 1			
CONDITION	Actin	APP695	APP695/Actin	EX/CO
CO1	937.83	417.86	0.44	1.00
A1	1042.69	482.53	0.46	1.04
B1	1176.91	532.23	0.45	1.01
C1	950.66	438.19	0.46	1.03
	REPLICATION 2			
CO2	814.14	408.59	0.50	1.00
A2	826.42	392.84	0.48	0.95
B2	807.92	353.07	0.44	0.87
C2	874.15	362.01	0.41	0.83
	REPLICATION 3			
CO3	1019.80	392.17	0.38	1.00
A3	806.89	295.88	0.37	0.95
B3	785.01	242.05	0.31	0.80
C3	837.67	241.26	0.29	0.75

EX- Experimental Condition:
(CO- Control; A- Exposed; B- External coil; C- Sham)

TABLE C9. Chemiluminescent signal intensities obtained from RNA from differentiating (Day 16) IMR32 cells exposed to a magnetic field (60Hz, 200 μT, 4h).

	REPLICATION 1			
CONDITION	Actin	APP695	APP695/Actin	EX/CO
CO1	1005.79	483.51	0.48	1.00
A1	1183.71	538.50	0.45	0.95
B1	1327.48	654.55	0.49	1.03
C1	1088.75	613.07	0.56	1.17
	REPLICATION 2			
CO2	852.94	587.06	0.69	1.00
A2	817.19	530.95	0.65	0.94
B2	816.80	599.97	0.73	1.07
C2	994.78	668.23	0.67	0.98
	REPLICATION 3			
CO3	1025.66	556.29	0.54	1.00
A3	827.48	394.46	0.48	0.88
B3	741.77	385.54	0.52	0.96
C3	679.01	372.57	0.55	1.01

EX- Experimental Condition:
(CO- Control; A- Exposed; B- External coil; C- Sham)

APPENDIX D

LABORATORY PROTOCOLS

D.1 MEDIUM FORMULATIONS FOR IMR-32 GROWTH AND DIFFERENTIATION

Basic MEM: (1 liter)

MEM (Sigma-M3024) - 9.4 gm

Phenol Red - 5 mg

Sodium Bicarbonate - 2.2 gm

Add above components to 800 ml of nanopure water and adjust pH to 7.2. Make up volume to 1L and sterilize using 0.2 μm filters into bottles accordingly.

Growth medium: (500 ml)

Basic MEM - 440 ml

Fetal Bovine Serum (Hyclone) - 50 ml

Sodium Pyruvate (100 mM) - 5 ml

L-glutamine (200 mM) - 5 ml

Differentiation medium: (500 ml)

Basic MEM - 460 ml

Fetal Bovine Serum (Hyclone) - 25 ml

Sodium Pyruvate (100 mM) - 5 ml

L- glutamine (200 mM) - 5 ml

5-Bromodeoxyuridine (1 mM) - 5 ml

D.2 PROTOCOLS FOR FLOW CYTOMETRY:

Saline solution:

Potassium Chloride	5 mM
Sodium Chloride	140 mM
Magnesium Chloride	1 mM
Calcium Chloride	1.8 mM
HEPES	10 mM
D- Glucose	10 mM

Adjust pH to 7.3.

Procedure for cell suspension

1. Remove all media from 60mm tissue culture plates
2. Add 5 ml of saline solution to the plate
3. Dislodge cells by mechanical dispersion using a pasteur pipette
4. Spin down cells and remove saline by vacuum aspiration
5. Resuspend cells in 5 ml of saline solution
6. Count cells using a hemocytometer
7. Distribute 0.5 x 10^6 cells/ml accordingly for the experiment
8. Add 20 µl of Propidium Iodide (Molecular Probes) and 20 µl of 1X Oxonol dye (Molecular Probes) accordingly for the experiment and incubate at 37^{o}C for 30 min
9. Place tubes on ice and transport to Cell Analysis Facility for flow cytometry analysis

Schematic of the flow cytometry setup

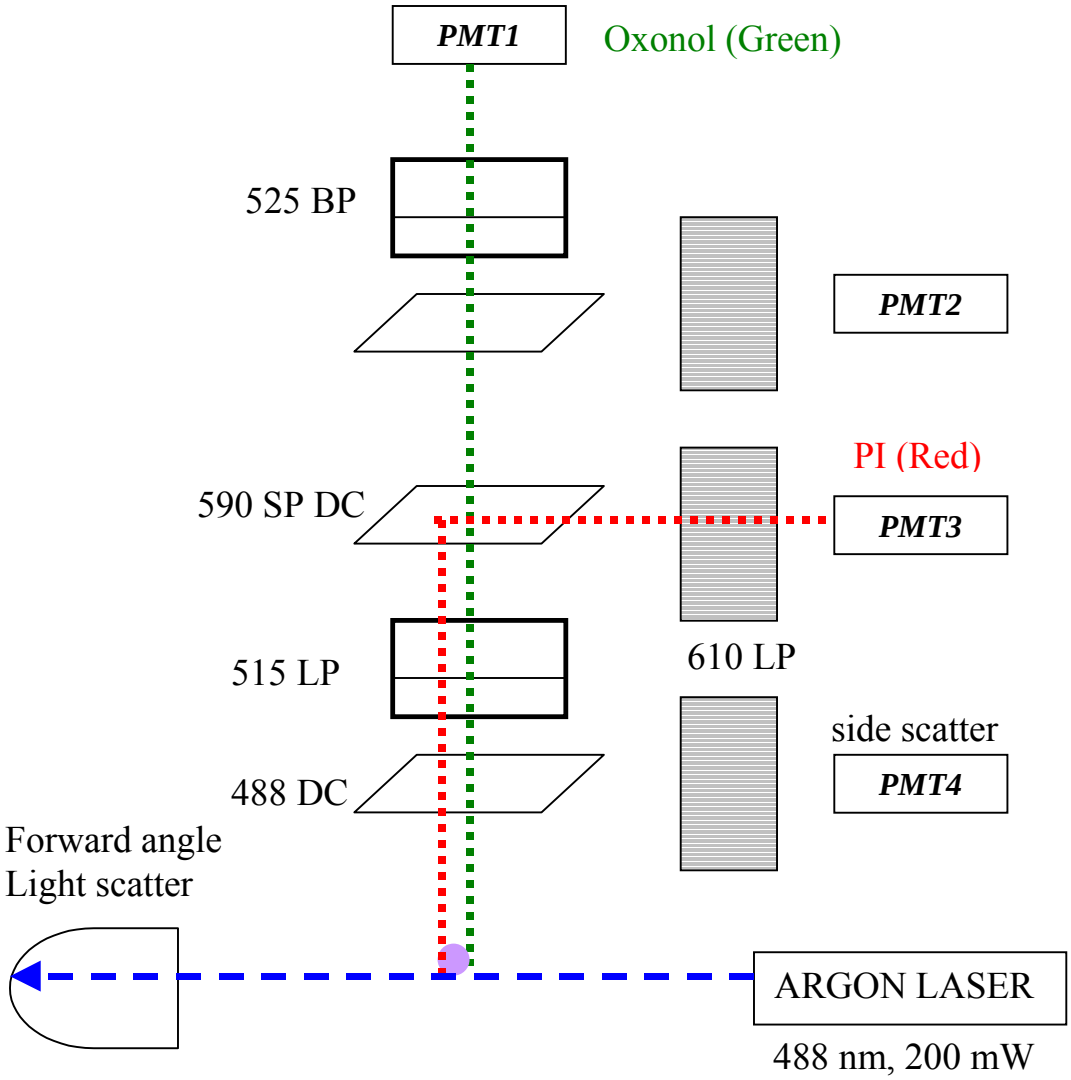

D.3 CONFOCAL MICROSCOPY PROTOCOLS

Confocal imaging system startup and shutdown

To turn on PCM-2000:

1. Turn on laser fan rocker switch (labeled #1)
2. Turn key to Argon laser (labeled #2)
3. Turn on power strip on the laser bench (labeled #3)
4. For epi-fluorescence, push ignition button to ignite the mercury vapor lamp (labeled #4)
5. Turn on power strip below the confocal bench (labeled #5). Make sure that all 6 plugs are plugged in to receive power
6. Write date, initials, and time on in the Nikon PCM-2000 log
7. Log onto Windows NT using your network ID and network password

To turn off PCM-2000

1. Logoff Windows NT. Shut down computer. Wait for message "It is now safe to turn off the computer"
2. Turn off power strip below the confocal bench (labeled #5)
3. Turn off power strip on the laser bench (labeled #3)
4. Turn key off to Argon laser (labeled #2)
5. Leave fan on until air is cool. Turn off fan rocker switch (labeled #1)
6. Write time off and total time in the Nikon PCM-2000 log
7. Use lens tissue and lens cleaner to clean any immersion oil from the objective
8. Put cover back on microscope, being careful to keep it from touching the hot lamp housing

C-Imaging system positions

Once you are logged onto Windows NT

1. Double-click on Simple PCI shortcut on desktop. (Also in Start Menu ➔ Programs ➔ C-Imaging Systems➔Simple PCI)
2. Check to make sure you are using the desired profile. File➔Manage Profiles ➔highlight desired profile➔Close. Desired workfile should be opened if profile is set up correctly
3. Check to make sure all sliders and shutters are in desired positions

DEFAULT POSITIONS

LASER	Argon (in standby)	Exciter filter	DOWN
	488nm line	Neutral density	UP
		down	0%
		1 click up	3%
		2 clicks up	10%
		up	100%
	GheNe	Filter slider	2 CLICKS UP
	543nm line		

SCANHEAD	Excitation filter (EX)	DOWN
	Neutral density (ND)	UP
	down	0%
	1 click up	3%
	2 clicks up	10%
	up	100%
	Dichroic #1	DOWN (RGB)
	Pinhole	DOWN (Small)
	Dichroic #2	1 CLICK UP (565)
	BA1 (PMT1)	DOWN (515/30HQ)
	BA2 (PMT2)	DOWN (EM565LP)

4. Find and focus the specimen using the eyepieces. Remember:

	Fluorescence (IN) vs.	Confocal (OUT)
Beam splitter dial	A	C
Fluorescent Lamphouse shutter	In	Out
Fluorescence Filter shutter	G, B2, UV (depends on dye)	Out (far right)

5. Use Fastscan and stage controls/focus drive to locate the area of interest. Click Abort when done.
6. Click Capture1 to capture an image.
7. Toggle Image Profile and Profile Positioning buttons on. Drag red line through horizontal region of interest. Drag green line through vertical region or interest.
8. Look at scale in bottom left corner. You want to minimize saturated pixels. Big changes in gain are 10%. Small changes in gain are 5%.
9. Use Image Profile and Capture1 to set the gain levels. Set black levels to 250 if the background is not too noticeable. Background can be processed out later.

Acquisition for V_m measurement

Time Scan (X-Y-T):

1. A frame size (normally 1024x1024) is selected
2. In the image window, click ROI. Maximize window
3. Click on appropriate shape and trace ROIs inside the cell to get internal fluorescence (in our case, ~ 2μm in length). A background ROI is also included to measure external fluorescence. To delete ROIs, right click on them to highlight, and press Delete key.
4. When done drawing ROIs, right click on window and save ROIs to a file in home directory as an *.roi file. Click OK
5. Click on Sequence in acquisition window. Choose Time Scan and Intensity Monitor. Click Finish
6. In Display Setup tab,
    - Setup 2 ROIs to monitor
    - Change x axis to field time instead of field number
    - Select Intensity Measurement to add, define or change measurements
    - Display full graph
    - Let y axis autoscale
7. Adjust speed and resource tab as necessary
8. Click thin line
9. Save intensity measurement data after experiment is over
10. For experiment in: (CHAPTER III)
    - Choose frame size of 1024x1024
    - Choose maximum speed and write to memory
    - Click M:0
    - Click Stop collection after 3 frames
11. For experiment in: (CHAPTER IV)

- Choose frame size of 1024x1024
- Choose Delay time of 600 sec/frame
- Click D:0
- Click stop collection after 7 frames

Schematic of the confocal system (Laserhead)

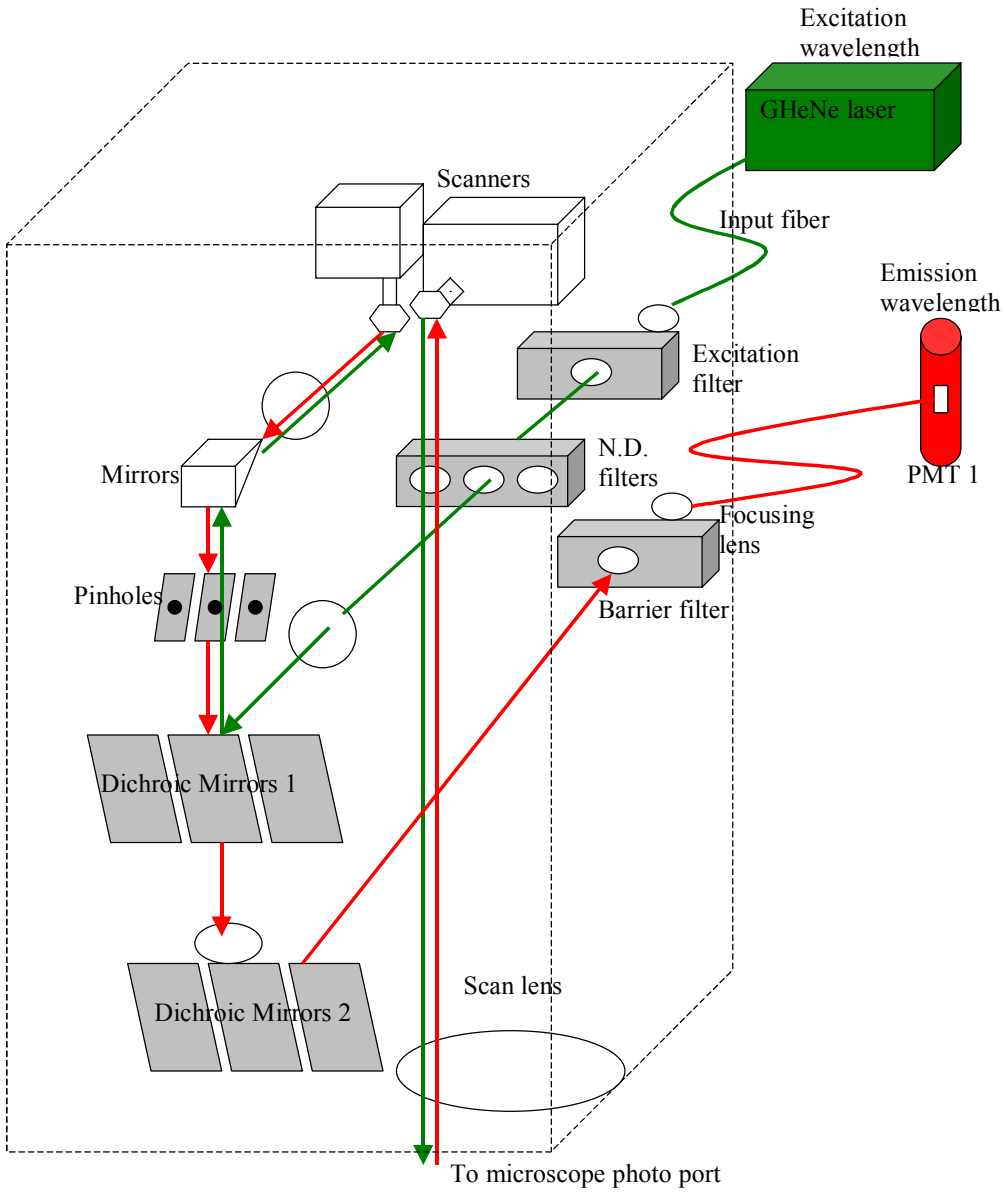

PMT- photomultiplier tube; ND- neutral density; GheNe- green helium neon

D.4 PROTOCOLS FOR COLUMN CHROMATOGRAPHY

***Column buffer* (10X)**

100 mM Tris HCl

10 mM $MgSO_4$

Adjust pH to 7.4

1M KCl

Potassium chloride - 37.28 gm

10X Column Buffer- 50 ml

Adjust to 500 ml with deionized water

***Enzyme assay buffer* (10 ml)**

10X Column Buffer – 5 ml

1M KCl- 0.5 ml

Adjust to 10 ml with deionized water

Schematic of the chromatography setup

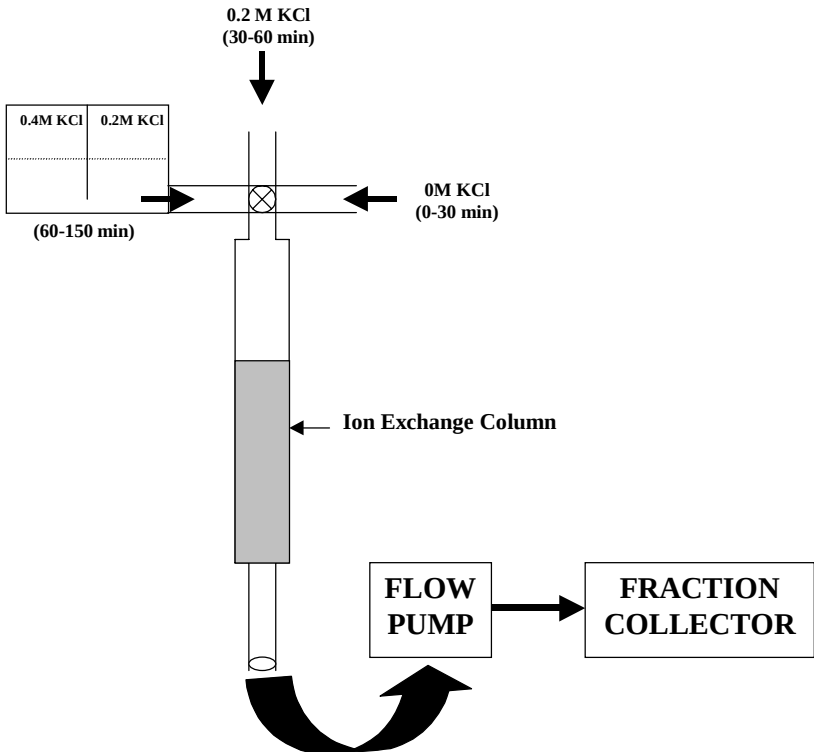

D.5 ENOLASE ENZYME ASSAY USING THE BECKMAN DU-600 SPECTROPHOTOMETER

1. After chromatography run, all 50 fractions were collected and stored on ice
2. The UV lamp on the Beckman DU-600 Spectrophotometer was turned on and let to warm up for at least 30 min
3. The quartz cuvette that was used was washed thoroughly with 70% ethanol in between experiments
4. An absorbance value of zero was set using deionized water as the blank
5. For each experiment, a control experiment was run with 10 µl (1.2 U) of pure enolase enzyme and activity was compared with manufacturer's value. (0.5 ml of enzyme solution [10 µl of enzyme + 490 µl of 1X column buffer] + 0.5 ml of assay buffer)
6. Assay for the sample included 2 runs simultaneously: (a) 0.5 ml of sample from fraction + 0.5 ml of assay buffer. (b) 0.5 ml of sample from fraction + 0.5 ml of Assay buffer. The solutions were let to equilibrate to RT for 30 seconds
7. 20 µl of PGA (final concentration – 1mM) was added only to (b) and the reaction was started. The absorbance increase was measured until 5 min
8. A linear absorbance increase of 0.1 at 240 nm was equivalent to the formation of 0.226 µM of phosphoenolpyruvate. The activity was expressed in enzyme units per ml of sample

D.6 RNA EXTRACTION FROM SAMPLES

1. To cell pellet, add 1 ml of TRIZOL reagent. Vortex and let stay at RT for 5 min
2. Add 200 µl of chloroform. Shake tubes vigorously for 15 seconds and incubate at RT for 3 min
3. Transfer contents to a 1.5 ml microcentrifuge tube
4. Centrifuge contents at 14,000 rpm for 15 min at 4^{o}C
5. Transfer the top phase (containing the RNA) to a fresh microcentrifuge tube
6. Add 500 µl of isopropanol and incubate at RT for 10 min
7. Centrifuge at 14,000 rpm for 10 min at 4^{o}C
8. Remove supernatant and look out for white pellet at bottom of tube
9. Wash pellet with 75% ethanol in DEPC-treated water
10. Mix by vortexing and centrifuge at 8000 rpm for 5 min at 4^{o}C
11. Air-dry the RNA pellet for 10 min
12. Dissolve the RNA in 50 µl of RNAse-free water
13. Incubate for 10 min at 55-60^{o}C
14. Store at –70^{o}C until further use

D.7 DOT BLOT TO CHECK FOR DIG INCORPORATION

Maleate Buffer:(10 mM sodium maleate pH 7.5; 150 mM NaCl)

1M Sodium Maleate pH 7.5 -50 ml

3M Sodium Chloride – 25 ml

Adjust to 500 ml with nanopure water and autoclave or filter sterilize

100 mM Sodium Maleate pH 7.5

Maleic Acid (disodium salt) – 4 gm

Add 225 ml of nanopure water and adjust pH to 7.5. Then adjust to 250 ml with nanopure water Filter sterilize or autoclave

Northern Blocking agent: (10% blocking reagent stock solution diluted 1:5 in maleate buffer)

Blocking reagent – 1 gm

Maleate Buffer- 50 ml

Heat and stir to dissolve completely and store at 4^{o}C

Procedure

1. Prepare dilutions of control dig-RNA and dig-labeled probes (ten-fold dilutions, five times) in DEPC-treated water. Therefore for each probe tested (and for the control), there will be five tubes, each with 9 µl, add 1 µl to the first tube then take 1 µl from that and add to second tube, etc. NOTE: The control dilutions as spotted on the membrane are 10 ng/µl, 1 ng/µl, 100 pg/µl, 10 pg/µl, 1 pg/µl
2. Mark concave side of nylon membrane, dot 1 µl of probe onto each designated spot. (Note: put a piece of filter paper underneath, it makes for a much better defined dot)
3. Auto- cross link membrane twice using UV crosslinker
4. Wash membrane briefly in maleate buffer for 5 min
5. Incubate membrane with northern blocking solution for 5 min at RT
6. Incubate membrane with anti-dig-AP in northern blocking solution (1:5000) for 5 min at RT. Agitate regularly
7. Wash membrane with maleate buffer, twice for 5 min at RT
8. Wash membrane in Buffer 2 (Detection Buffer) for 2 min at RT
9. Add substrate solution (10 ml of Buffer 2, 200 µl of NBT/BCIP stock). Incubate in dark at RT. According to directions from Roche, the #4 dot of the control should be visible at 30 min. (this amount is equal to 10 pg/µl)

D.8 NORTHERN BLOTTING PROTOCOL

Solutions required

1. 10X MOPS running buffer

   800 ml H_2O (DEPC treated)

   41.8 MOPS (3-[N-Morpholino]propane-sulfonic acid)

   adjust to pH 7.0 with NaOH

   16.6 ml 3M DEPC-treated NaAcetate

   20.0 ml 0.5M DEPC-treated EDTA (pH8.0)

   bring to 1L, filter sterilize

2. 20X SSC, autoclaved

   175.3 gm NaCl

   88.2 gm Sodium citrate

   800 ml of DEPC-H_2O.

   Adjust pH to 7.0 with NaOH

   Bring to 1L and autoclave

3. EtBR, DEPC treated (10mg/ml)

4. Formaldehyde loading buffer (1ml)

   1mM EDTA, pH8 (5µl)

   0.25% Bromophenol blue (2.5 mg)

   0.25% xylene cyanol (2.5 mg)

   50% glycerol (500µl)

   DEPC H_2O (495µl)

5. 2X SSC + 0.1% SDS (500ml)

   50 ml 20X SSC

   5 ml 10% SDS

   445 ml DEPC-H_2O Autoclave

6. 0.1X SSC + 0.1% SDS (500ml)

   2.5 ml 20X SSC

   5 ml 10% SDS

   adjust to 1L. autoclave

7. Maleic Acid Buffer

   11.61 gm Maleic acid

   8.77 gm NaCl

   800 ml of DEPC-H_2O

   Adjust pH to 7.5

   Bring to 1L and autoclave

8. Detection Buffer (BUFFER II)

   11.61 gm Maleic acid

   8.77 gm NaCl

   800 ml of DEPC-H_2O

   Adjust pH to 7.5

   Bring to 1L and autoclave

NOTE: Electrophoresis tanks used for RNA work should be cleaned with detergent solution, rinsed in water, dried with EtOH and then filled with a solution of 3% H_2O_2. After 10 min at RT, the tank should be rinsed thoroughly with H_2O that has been DEPC treated.

Electrophoresis of RNA through gel containing formaldehyde

Prepare 0.7% agarose gel: (for the medium tray)

Melt 1.4 g agarose in 46 ml DEPC-H_2O

Cool it to 60^oC

Add 12 ml of 5X MOPS (heating to 60^oC)

Add 3.7 ml formaldehyde (37%)

Cast the gel in a chemical hood and allow the gel to set for at least 30 min at RT

Running buffer: 1X MOPS (800 ml for the medium box)

Prepare RNA samples

RNA (upto 30 µg)	5 µl
5X MOPS buffer	2 µl
Formaldehyde	3.5 µl
Formamide	10 µl

Incubate the samples for 15 min at 65°C, and the chill them on ice. Centrifuge the samples for 5 sec to deposit all of the fluid at the bottom of tube. Add 2 µl of sterile formaldehyde gel-loading buffer (fridge –20°C). to each sample.

Before loading the samples, prerun the gel for 5 min at 5V/cm. Immediately load the samples into the lanes of the gel.

Run the gel submerged in 1X MOPS buffer at 40V for 20 min & 60V for 2 hrs.

At the end of the run (when bromophenol blue has migrated approx 8 cm, stain with EtBr (0.5 µg/ml in 0.1M ammonium acetate) for 30-45 min or 20 µl EB/200 ml water.

Destain twice in 200 ml of deionized water for 10 min each.

Photograph the gel (28S-5000bp; 18S-2000bp; 5.8S-160bp).

Blotting gel

Soak the gel in 200 ml 10XSSC for 10 min to remove formaldehyde from the gel.

Fill the tray with 300 ml 10XSSC.

Soak the nylon membrane in deionized water and 10XSSC for 10 min each.

Place gel face down on blotting paper and place nylon membrane on top of gel.

Place filter paper on top and wet with 10XSSC. Place 3in thick brown paper & place weight.

Check every 5 hours & remove brown paper and replenish with fresh paper.

After RNA was transferred to nylon membrane for ~24hrs, paper towels & filter paper was removed from above gel. Turn over the gel and nylon membrane and lay them, gel side up on a dry sheet of filter paper. Mark the position of gel slots on the nylon membrane with left side cut.

Soak nylon membrane in 6XSSC for 5 min at RT. This removes pieces of agarose sticking to the filter (9ml 20XSSC + 21 ml DEPC water).

Remove membrane from 6XSSC and allow excess fluid to drain away. Place the membrane flat on a paper towel to dry for @ least 30 min at RT.

Auto cross-link twice in UV crosslinker.

Prehybridization

60°C for 2hrs in 2 ml Prehybridization buffer

Hybridization

60°C for 21 hrs in 2ml hyb buffer + 5 µl probe

prehyb & hyb buffer (100ml)

10 ml Denhradt 50X

33 ml 20X SSC

50 ml formamide

0.5 ml salmon sperm DNA (10mg/ml, denatured, Sigma)

1.0 ml 10% SDS

5.5 ml H_2O

(may add 1.5-3.0 mg/ml yeast RNA to achieve better background)

Denhardt 50X (stored at –20°C)

5g Ficoll (type 400, Pharmacia)

5 g polyvinylpyrolidone

5g BSA (fraction V, sigma)

bring to 500 ml

Wash

2X SSC + 0.1% SDS, RT, 15 min

0.1X SSC + 0.1% SDS, RT, 15 min

0.1X SSC + 0.1% SDS, 60°C, 15 min

Blocking

3ml of 10% blocking solution is added to 27 ml of Maleic Acid Buffer (30 min)

Antibody binding

6µl of anti-dig AP + 2ml of 10X Blocking Solution is added to 30 ml of Maleic Acid Buffer. (30 min)

Wash

Maleic acid buffer - 15 min x 2 RT

Buffer II (10 ml) 15 min

Detection

2 ml buffer II + 20 µl CSPD stock. Incubate in dark for 30 min

D.9 QUANTIFICATION OF RNA TRANSCRIPT LEVELS USING QUANTITY-ONE SOFTWARE.

1. Scan x-ray images in adobe photoshop
2. Change image format from color to grayscale
3. Save image as a *.tiff file
4. In Quantity One open the *.tiff file
5. GO TO → view → transform (This checks for saturation)
6. Highlight "saturated pixels". If no red spots are evident on the RNA bands then hit OK; else reduce the maximum value below 255 and then hit OK
7. Click on "volume quick guide"
8. Click on "volume rectangle tool"
9. Draw boxes around the bands of interest
10. Select an area for background (Make sure that you double click on this box and indicate that it is the background)
11. GO TO → REPORTS→ volume analysis report
12. Select parameters of interest (e.g., mean, area)
13. Output is expressed as a table with all values corresponding to band intensities
14. Click on "Export" icon at bottom of the table
15. Click "Go" → Save as *.out file. (*.out is recognized by Microsoft Excel)
16. Open the data in Microsoft Excel
17. Save data as an Excel spreadsheet for further analysis